and Demixing
in Multiphase
With Application
pulsion Systems

Mixing and Demixing Processes in Multiphase Flows With Application to Propulsion Systems

Edited by
Rand Decker and Charles F. Schafer
George C. Marshall Space Flight Center
Marshall Space Flight Center, Alabama

NASA

National Aeronautics
and Space Administration

Scientific and Technical
Information Division

TABLE OF CONTENTS

Mixing and Demixing Processes in Multiphase Flows
With Applications to Propulsion Systems

February 25 & 26, 1988

NASA: Marshall Space Flight Center
Conference Room 3053
Building 4610

Sponsored by: Fluid Dynamics Branch
Structures and Dynamics Laboratory
and
University Space Research Associates
Huntsville, Alabama

Thursday, February, 25th:

8:30am: Welcome, *Fred Leslie*, Chief, Fluid Dynamics Branch, NASA: MSFC

9:00: The Application of Single Particle Hydrodynamics in Continuum Models of Multiphase Flow, *Rand Decker*, NRC Associate at NASA: MSFC

9:30: Continuum Theories for Fluid-Particle Mixtures: Some Aspects of Lift Forces and Turbulence, *David F. McTigue* (presenting), *Richard C. Givler, Jace W. Nunziato*, Sandia National Laboratories

10:00: Turbulence Modeling of Gas-Solid Suspension Flows, *C.P. Chen*, University of Alabama at Huntsville

10:30: Break

10:50: Confined Turbulent Fluid-Particle Flow Modeling Using Multiple Realization Particle Trajectory Schemes, *A.A. Adeniji-Fashola*, NRC Associate at NASA: MSFC

11:20: Numerical Models for Particle Dispersion in Turbulent Flow, *Clayton T. Crowe*, Washington State University

11:50: Lunch

1:30pm: Migration Arising From Gradients in Shear Stress in Concentrated Suspensions, *David Leighton,* Notre Dame University

2:00: Observations of Break-up Processes of Liquid Jets Using Real-Time X-Ray Radiography, *Kenneth K. Kuo,* The Penn State University

2:30: Break

2:50: Round-Table Discussion: Physical, Model, Numerical and Experimental Aspects of Mixing and Demixing Processes in Multiphase Flows Chairman: *Rand Decker,* NRC Associate at NASA: MSFC

4:50: Administrative and Social Announcements

Friday, February 26th:

9:00am: Non-Gradient Diffusion in Pre-Mixed, Turbulent Flames, *Paul A. Libby,* University of California at San Diego

9:30: Turbulent Heat Flux in Low Mach Number Flows with Large Density Variations, *Peter O'Rourke* (presenting), *Lance R. Collins,* Los Alamos National Laboratory

10:00: Two-Phase Combustion Processes of Mobile Stick Propellant Bundles *Kenneth K. Kuo,* The Penn State University

10:30: Break

10:50: Round-Table Discussion: Propulsion Applications of Mixing and Demixing Processes of Multiphase Flows, Chairman: *Charles Schafer* Fluid Dynamics Branch, NASA: MSFC

12:50pm: Closing Remarks, *Charles Schafer,* Fluid Dynamics Branch, NASA: MSFC

2:00: Tour of facilities at the Marshall Space Flight Center &/or the Alabama Space and Rocket Center Museum, (optional)

2

The Application of Single Particle Hydrodynamics in Continuum Models of Multiphase Flow

Rand Decker

National Research Council Associate, Fluid Dynamics Branch
Structures and Dynamics Laboratory
NASA: Marshall Space Flight Center
Huntsville, Alabama, 35812

Abstract: A review of the application of single particle hydrodynamics in models for the exchange of interphase momentum in continuum models of multiphase flow is presented. Considered are the equations of motion for a laminar, mechanical two phase flow. Inherent to this theory is a model for the interphase exchange of momentum due to drag between the dispersed particulate and continuous fluid phases. In addition, applications of two phase flow theory to de-mixing flows require the modelling of interphase momentum exchange due to lift forces. The applications of single particle analysis in deriving models for drag and lift are examined.

3

I. Introduction

Before the advent of numerical approximation techniques, coupled with large computational facilities the study of single particle hydrodynamics was popular. Following the early conceptual efforts on theories of multiphase flow [1],[2] investigations into the form of certain classes of phenomena were undertaken. Specifically, those investigating the form for models of interphase momentum exchange found a wealth of information by evoking the arguments once used in single particle hydrodynamics. As an example, consider the following quote [3], used in a context specific to arguments relating to forms of momentum exchange models in continuum theories of multiphase flows:

"On the other hand, the terms ... and ... have no analogs in single particle calculations and will be neglected."

It would appear that the application of single particle hydrodynamics in continuum models of multiphase flow has received a degree of acceptance.

II. Continuum Theories of Multiphase Flow

Continuum theories of multiphase flow have developed along parallel lines: Mixture Theory and the Theory of Interpenetrating Media with Moving Interfaces. Both approaches are rooted in the same fundamental assumption, namely: That both the dispersed and continuous phases of the flow can be treated as and described within an Eulerian kinematic framework by the conservation equations of a macro-continua. Implicit in this assumption is that the variable fields of each phase are unique and continuous over the flow domain. The limits of this assumption for the case of dilute concentrations of the dispersed phase have been explored [4] and the alternative of a Lagrangian or 'particle tracking' kinematic scheme for the dispersed phase forwarded. In addition, continuum models have been adapted to granular material flows [5] where the dispersed phase concentration approaches a maximum.

Mixture theories arise from the specialization of the classical field theory requirements of internally consistent thermodynamic arguments [6],[7]. In contrast, the theories of interpenetrating media address more directly modifications to the classical transport equations due to discontinuous or 'jump' conditions at moving phase boundaries [8],[9],[10],[11]. To reduce to a local form, the conservation equations resulting from the theories of interpenetrating media must be averaged in either space or time. In fact, the key difference between the mixture theory formulation for multiphase flows and the averaged conservation equations for interpenetrating media is that; while the averaging process is implicit in the mixture theory approach it is an explicit operation in the course of writing the conservation equations from the interpenetrating, moving phase boundary approach.

With few exceptions, it is reassuring to note both approaches result in the same set of conservation equations.

Consider a simple two phase flow. That is one in which the dispersed phase is a dilute, mono-dispersed suspension of non-reacting, smooth, rigid, spherical particles in an incompressible, linearly viscous fluid. Both phases and the surroundings are thermally equilibrated. Laminar flow conditions prevail.

4

Regardless of the method of formulation, the conservation equations reduce to the expressions for continuity and balance of momentum [10],[12] and constitute the continuum equations of motion of the mechanical theory of two phase flow.

CONTINUITY: $\dfrac{\partial \phi^\alpha \rho^\alpha}{\partial t} + \underline{\nabla} \cdot \phi^\alpha \rho^\alpha \underline{V}^\alpha$, α = D (DISPERSED), C (CONTINUOUS) $\hspace{2cm}$ (1)

SATURATION: $\phi^D + \phi^C = 1$ $\hspace{6cm}$ (2)

BALANCE OF MOMENTUM: $\phi^\alpha \rho^\alpha \left(\dfrac{\partial \underline{V}^\alpha}{\partial t} + \underline{V}^\alpha \cdot \underline{\nabla}\, \underline{V}^\alpha \right) = -\phi^\alpha \underline{\nabla} p^\alpha + \underline{\nabla} \cdot \underline{T}^\alpha + \phi^\alpha \rho^\alpha \underline{b}^\alpha + \hat{\underline{M}}^\alpha + \left(\lambda - p^\alpha \right) \underline{\nabla} \phi^\alpha$ $\hspace{1cm}$ (3)

WHERE $\phi\,(\underline{x},t)$: CONCENTRATION

ρ $\hspace{1cm}$: MATERIAL DENSITY

$\underline{V}\,(\underline{x},t)$: VELOCITY

$p\,(\underline{x},t)$: SPHERICAL STRESS (PRESSURE)

$\underline{T}\,(\underline{x},t)$: DEVIATORIC STRESS

$\hat{\underline{M}}\,(\underline{x},t)$: INTERPHASE MOMENTUM EXCHANGE

$\lambda\,(\underline{x},t)$: SATURATION (CONTACT) PRESSURE

The flow has two velocity fields and two concentration fields. Each phase has a unique, constant material density and may be acted upon by a set of external potentials or body forces. In addition, there exists unique expressions for the spherical and deviatoric elements of the dispersed and continuous phase stress tensors. Lastly, under the assumption that the flow is saturated, i.e. no phaseless voids may develop, the phases are coupled by an interface "saturation" pressure and momentum exchange or transfer between the phases.

If the external potentials are specified, the momentum exchange terms modeled and the deviatoric elements of the stress tensors specified by constitutive assumption or neglected via arguments with respect to magnitude, the resulting is the unclosed system of 9 equations in 10 unknown fields; velocity, concentration and spherical stress or pressure, for each phase. Commonly, the assumption of equal phase pressures is used in an effort to create a closed determinant system of fields and conservation equations [1],[11]. However, in should be noted that the wisdom of this assumption has been challenged on both physical and mathematical grounds [12],[13],[14].

III. Models of Momentum Exchange in Two Phase Flow

As a common denominator, all theories of two phase flow embody some model for the exchange of momentum between phases. For simple, mechanical two phase flow it can be demonstrated rigorously that the sum of the interphase momentum transfer must be conservative, i.e. the sum of all momentum transfer terms is zero. Those exceptions to this "summing rule" are more a matter of bookkeeping than conceptual difference [15].

In addition, the degree of coupling between the phases of the flow , both in a physical and mathematical sense is controlled by the momentum transfer model. Two way coupling, i.e. momentum transfer from one phase to the other and vice versa is implicit in the requirement of conservative transfer of momentum. In attempts to simplify the computational complexities associated with applying continuum theories of two phase flow the assumption of one way coupling is often evoked [16]. One way coupling allows for the transfer of momentum from the continuous to the dispersed phase, but not vice versa. In this case the process of momentum exchange is not conservative. Within this context, one way coupling is synonymous with the statement that the velocity field of the continuous phase is unchanged due to the presence of the dispersed phase within the flow. The computational simplifications result from the fact that it is no longer necessary to solve the conservation equations for the continuous phase field variables simultaneously with the conservation equations of the dispersed phase. Given a solution to the continuous phase variable fields, perhaps generated by single phase analysis or experimental techniques, the uncoupled conservation equations can be solved for the dispersed phase variable fields.

The use of a step function to describe the "effectiveness" of momentum transfer has been proposed and applied to the problem of laminar two phase jet flows [1],[17]. This approach allows the degree of coupling to vary, step-wise from uncoupled to one way coupled. The arguments raised are: that in flows where interparticle spacing in large relative to the sum of the particle diameter and twice the fluid boundary layer thickness on the surface of the particles no net momentum transfer between the phases occurs. It is argued that when the interparticle spacings are large and the suspension is dilute, the slip between the phases results only in unrecoverable dissipation in the particle wakes. However, if the multitude of efforts in the analysis of two way coupled, dilute two phase flows can be used as an indication, then it would appear that the "ineffectiveness" of interphase momentum transfer in dilute two phase flows is not generally accepted.

Arguments have been presented for the set of variables which constitute the general class of admissible momentum exchange functions [3],[18].

$$\underline{M}^{\alpha} \cdot \phi^D S \left(\underline{V}^D - \underline{V}^C \right) + \phi^D B \, \vec{\nabla} \cdot \vec{\nabla} \, \underline{V}^C + C \, \vec{\nabla} \left(\vec{\nabla} \cdot \underline{V}^C \right) + L \left(\underline{V}^D - \underline{V}^C \right) \cdot \underline{D}^C + \cdots$$

$$\text{(4)}$$

$$\text{WHERE:} \quad \underline{D}^C \left(\underline{x}, t \right) = 1/2 \left(\vec{\nabla} \underline{V}^C + \underline{V}^C \, \vec{\nabla} \right), \quad \text{RATE AT DEFORMATION TENSOR}$$

where ... indicates that additional functions, of higher order in gradient, do exist. S,B,C and L are constructed from the scalar invariants of the admissible vector and tensor fields. In addition, owing to the discrete nature of the dispersed phase, the admissibility, as a class of momentum exchange function of gradients of dispersed phase field variables is still debated [11]. If the existence of smooth, continuous first partials derivatives to the dispersed phase variables is at question, consider: Implicit in the assumption of the continuum model of two phase flow was that the dispersed phase could be treated as a macro-continua, i.e. that the dispersed phase field variables are smooth and continuous.

In fact, the use of Divergence (Gauss') theorem in the process of reducing the global conservation equations to the local form requires the existence of continuous first partial derivatives of dispersed phase velocity and concentration fields.

The appropriateness of using phenomenologically based arguments for the purpose of identifying the specific forms of the momentum exchange models from the general admissible class is justified [19]. In fact, more often than not it is the lack of a phenomenological or physical analogue that results in the neglect of a class of the admissible momentum exchange functions.

Depending on the purpose of the analysis, four generic categories of momentum exchange processes and models are identifiable:

-Drag Forces
-Lift Forces
-Inertial Coupling or Virtual Mass Effects
-Inertial History Effects

The arguments for the inclusion of the inertial coupling/virtual mass effects and inertial history effects are raised during the construction of models for momentum exchange in two phase flows [1],[20],[21]. The analogous single particle hydrodynamic forces have been investigated and debated [22],[23],[24],[25]. Inertial coupling stems from the analysis of the forces required to displace a given volume of fluid during the acceleration of a particle through it. Likewise, the inertial history or Basset force is linked with the acceleration history of a particle moving through a quiescent fluid. However, the lack of complete agreement on the single particle hydrodynamic analysis of these effects and the lack of agreement on the forms or even the necessity for retaining these effects [12] in models of momentum exchange in two phase flows precludes them from additional discussion at this point.

Drag Forces

Common to all theories of two phase flow is a model for momentum exchange due to drag between the fluid phase and the particles of the dispersed phase [11],[12],[26],[27],[28]. Intrinsic to each of these models is the existence of a slip velocity between the phases. The result being a net drag force on each phase:

$$\underline{M}^D_{drg} = -\underline{M}^C_{drg} = S(\underline{V}^D - \underline{V}^C) \qquad (5)$$

where the factor of proportionality; S is derived from arguments which are rooted in single particle analysis.

The most sophisticated models for S are derived from an analysis of the mean, terminal sedimentation velocities of a dispersion of spheres falling through a quiescent Newtonian fluid under gravity [11],[12],[29]. The analysis is limited to flows, about any one single sphere in the Stokesian regime, where the Reynolds number between the fluid and the sphere is of order unity or smaller. This implies either very small slip velocities and/or a very viscous fluid. The net result being that the inertia of the fluid phase is neglected.

Equilibrium between the force on a single sphere due to the gravitational potential and the terminal or steady state sedimentation velocity drag can be given as:

$$u_o = \frac{2a^2}{9\mu}(\rho^D - \rho^C)\underline{g}$$ (6)

WHERE: a: PARTICLE RADIUS

μ: FLUID VISCOSITY

$\underline{g}$: GRAVITATIONAL POTENTIAL

This sedimentation velocity potential is modified by the probability of hydrodynamic interaction with the next closest sphere, where the distance separating these spheres is defined probabilistically for a uniform dispersion. The result is the mean sedimentation velocity potential, corrected by the presence of a dispersion of other spheres of a given concentration:

$$\underline{u} = u_o(1 - 6.55\,\phi^D)$$ (7)

The incorporation of this result into a form for the interphase momentum exchange in two phase flow due to drag requires the suppositions that: At a given slip velocity the potentials acting on each phase due to drag are equal and opposite, i.e. momentum exchange is conserved. The slip velocity of two phase flow is then equated with the modified mean sedimentation velocity due to gravity. Resulting in, for a single spherical particle:

$$\frac{9\mu}{2a^2}(1 - 6.55\,\phi^D)(\underline{V}^D - \underline{V}^C) = (\rho^D - \rho^C)\underline{g}$$ (8)

This result is then further generalized with the assumption that if this is the potential for interphase momentum exchange due to drag on a single sphere, then the drag force per unit volume of mixed flow should be simply this potential normalized by the local volume fraction or concentration of the particulate phase:

$$\underline{\hat{M}}_{drg}^D = -\underline{\hat{M}}_{drg}^C = \frac{9\mu}{2a^2}\phi^D(1 + 6.55\,\phi^D)(\underline{V}^D - \underline{V}^C)$$ (9)

The caveats are obvious: The single particle analysis is grounded in the assumption of Stokes flow for the motion or slip of the dispersed phase relative to the continuous phase. Unlike the slip velocity of two phase flow, the sedimentation velocity at a given concentration is a constant, being the result of a constant potential; gravity. The modification to the mean sedimentation velocity by the hydrodynamic interactions with the other particles of the dispersion has presupposed that the dispersion is uniform, i.e. gradients of dispersed phase concentration are not present.

8

Lift Forces

It is observed that certain classes of laminar shear flows will result in demixing of the dispersed phase [30],[31], i.e. the dispersed phase will become distributed in a non-uniform manner, despite the fact that initially the flow may have been homogeneous with respect to dispersed phase concentration. Analysis of these phenomena have been made using single particle hydrodynamics [32] and using continuum two phase flow theory with the inclusion of lift forces in the description of the interphase momentum exchange [11],[12],[15],[16],[33]. It is generally accepted that the lift forces are those potentials, accounted for within the interphase momentum exchange which produce dispersed phase motions or migrations transverse to the slip or velocity difference between the phases. These lift forces arise through the interaction of the slip velocity, the rotation or spin of the particles of the dispersed phase and the shearing or gradients of the continuous phase velocity. If the exchange of momentum between the dispersed and continuous phase is conserved, then the lift force potentials act equally and in opposite sense on both phases.

A variety of single particle analysis, with the resulting identification of certain lift forces have been performed [23],[34],[35],[36],[37],[38]. The lift force on a single particle, as outlined by Saffman, [35] is the most commonly used in models of momentum exchange due to lift forces in continuum theories of demixing two phase flow. Saffman's analysis identifies the lift force:

$$L = \frac{K\mu a^2}{\nu^{1/2}} \underline{u}(y) \left(\frac{\partial u(y)}{\partial y} \right)^{1/2} \tag{10}$$

WHERE ν :   FLUID KINEMATIC VISCOSITY

$u(y)$:   FLUID VELOCITY (IN PARALLEL FLOW)

Unlike the assumption of Stokes flow used in the analysis of and subsequent application to momentum exchange due to drag, Saffman's lift analysis begins with the Navier-Stokes equations. However, the Reynolds numbers for the slip velocity, the particle spin and the fluid shear are all constrained to order unity or smaller. Hence, even though the Saffman's analysis retains the inertial terms of the Navier-Stokes equations, the flow is not inertially dominated. The solution requires the matching of the "inner" and "outer" asymptotic expansions of the flow equations in an analysis technique pioneered before numerical approximation coupled with computational methods became available [39]. In Saffman's analysis the field variables for the flow about a single sphere are expanded about the radial position from the sphere center. The inner expansion has as a boundary condition the no slip requirement at the sphere surface. Since the sphere is spinning, the no slip boundary condition constrains the fluid to have the angular velocity of the sphere surface. Hence, the particle spin enters the calculation implicitly, despite the fact that due to the level of truncation, it does not appear explicitly in the expression for lift. The necessity for an outer expansion results from the non-convergent nature of the solutions to the inner expansion as the distance from the sphere center approaches the infinite.

The outer expansion embodies a second boundary condition, at a some large distance from the sphere center; namely, the undisturbed (by particles) velocity field as radial position approaches the infinite. In fact the primary difference in most single particle analysis of lift is whether the boundary condition for the fluid velocity field in the outer expansion is constrained by a wall condition [32], a quiescent fluid [34] or by the rate of fluid strain [35]. The assumptions implicit in Saffman's analysis of the lift force on a single sphere include: the flow is uniform and parallel, the slip velocity is parallel to the plane of the fluid shear, the shear or velocity gradients of the fluid are linear and the particle spin vector lies in the plane of the fluid shear, but is normal to the slip vector. The resulting force is normal to the plane of the fluid shear (and slip vector) as well as being normal to the spin vector of the particle. If, in terms of the slip velocity, the particle lags behind the fluid the lift will produce a migration of the particle into the faster, adjacent fluid and vice versa if the particle leads the fluid. In other words, the sense of the lift force depends on the sense of both the gradients of the fluid velocity and the slip velocity.

Saffman's result for the lift on a single spherical particle has been generalized for the analysis of the momentum exchange due to lift forces in continuum theories of de-mixing two phase flow [11],[12],[15]. The lift force on the dispersed phase is normalized by the number of particles in a unit volume of two phase flow. The resulting generalized form of the momentum exchange due to lift being written:

$$\underline{M}^D_{lft} = -\underline{M}^C_{lft} = \frac{3K(\rho^C \mu)^{1/2}}{4\pi a} \phi^D \underline{D}^C |\underline{D}^C|^{-1/2} \cdot (\underline{V}^D - \underline{V}^C) \tag{11}$$

This form of the momentum exchange due to lift has been used in calculations of parallel, de-mixing two phase flows using continuum theories. However, it is not clear that this general form will reduce directly to Saffman's result for a one dimensional, parallel flow, both in terms of magnitude and the directional nature of the lift force. In addition, despite the fact that the intentions are well motivated, the meaning of operations such as absolute value, square root and division by a second order tensor valued variable is not clear.

IV. Summary

In conclusion, it has been shown that single particle hydrodynamics is the only source presently used to derive and justify forms for the interphase momentum exchange models within continuum theories of laminar multiphase.

Four generic classes of momentum exchange models can be identified: Drag, Lift, Inertial or Virtual Mass effects and Inertial History or Basset forces. The latter two categories are still advent in nature and have not yet assumed a role in the models of interphase momentum exchange in applications of continuum theories of two phase flow. On the other hand, examples of Drag and Lift forces in applied momentum exchange models are numerous, though not without obvious caveats and inconsistencies.

It is encouraging that the requirements of emerging technologies based on an understanding of multiphase flow processes has motivated such a great deal of work on generalized models for interphase momentum exchange.

10

References

1. Soo, S.L., 1967: Fluid Dynamics of Multiphase Systems, Blaisdell

2. Marble, F.E., 1970: Dynamics of Dusty Gases, in: Annual Reviews of Fluid Mechanics, Vol. 2

3. Drew, D.A. and Lahey, R.T., 1979: Application of General Constitutive Principles to the Derivation of Multidimensional Two-Phase Flow Equations, Int. J. Multiphase Flow, Vol. 5

4. Crowe, C.T., 1986: Two-Fluid vs. Trajectory Models; Range of Applicability, in: Gas/Solid Flows, ASME/FED Vol. 35

5. Haff, P.K., 1983: Grain Flow as a fluid-mechanical phenomenon, J. Fluid Mech., Vol. 134

6. Bowen, R.M., 1976: Theory of Mixtures, in: Continuum Physics, Vol. III, A.C. Eringen, ed., Academic Press

7. Passman, S.L., Nunziato, J.W. and Walsh, E.K., 1984: A Theory for Multiphase Mixtures, in: Rational Thermodynamics, C. Truesdell, ed., Springer

8. Drew, D.A. and Segel, L.A., 1971: Averaged Equations for Two-Phase Flows, Studies in Applied Mathematics, Vol.1, no. 3

9. Slattery, J.C., 1972: Momentum, Energy and Mass Transfer in Continua, McGraw-Hill

10. Ishii, M., 1975: Thermo-Fluid Dynamic Theory of Two-Phase Flow, Eyrolles

11. Drew, D.A., 1976: Two-Phase Flows: Constitutive Equations for Lift and Brownian Motion and Some Basic Flows, Arch. of Rat. Mech., Vol. 62

12. Nunziato, J.W., 1983: A Multiphase Mixture Theory for Fluid-Particle Flows, in: Theory of Dispersed Multiphase Flow, R.E. Meyer, ed., Academic Press

13. Stuhmiller, J.H., 1977: The Influence of Interfacial Pressure Forces on the Character of Two-Phase Flow Model Equations, Int. J. Multiphase Flow, Vol. 3

14. Givler, R.C., 1987: An Interpretation for the Solid-Phase Pressure in Slow, Fluid-Particle Flows, Int. J. Multiphase Flow, Vol. 13, no. 5

15. McTigue, D.F., Givler, R.C. and Nunziato, J.W., 1986: Rheological Effects of Non-Uniform Particle Distributions in Dilute Suspensions, J. Rheol., Vol. 30, no. 5

16. Soo, S.L., 1984: Development of Theories on Liquad-Solid Flows, Journal of Pipelines, Vol. 4

17. Elghobashi, S.E. and Megahed, I.E.A., 1981: Mass and Momentum Transport in a Laminar Isothermal Two-Phase Round Jet, Numerical Heat Transfer, Vol.4

18. Nunziato, J.W. and Walsh, E.K., 1980: On Ideal Multiphase Mixtures with Chemical Reaction, Arch. of Rat. Mech., Vol. 73

19. Hinch., E.J. and Leal, L.G., 1975: Constitutive Equations in Suspension Mechanics. Part 1. General Formulation, J. Fluid Mech., Vol. 71

20. Drew, D., Cheng, L. and Lahey, R.T., 1979: The Analysis of Virtual Mass Effects in Two-Phase Flow, Int. J. Multiphase Flow, Vol. 5

21. Drew, D.A. and Lahey, R.T., 1987: The Virtual Mass and Lift Force on a Sphere in Rotating and Straining Inviscid Flow, Int. J. Multiphase Flow, Vol. 13

22. Tchen, C.M., 1947: Mean Value and Correlation Problems connected with the Motion of Small Particles Suspended in a Turbulent Fluid, Ph.D. Thesis, Delft

23. Happel J. and Brenner H., 1973: Low Reynolds Number Hydrodynamics, Noordhoff

24. Gouesbet, A., Berlemont, A. and Picart, A., 1982: On the Tchen's Theory of Discrete Particle Dispersion: Can Dense Particles Disperse Faster Than Fluid Particles?, Heat and Mass Transfer, Vol. 9

25. Maxey, M.R. and Riley, J.J., 1983: Equation of Motion for a Small Rigid Sphere in a Nonuniform Flow, Phys. Fluids, Vol. 26

26. Harlow, F.H. and Amsden, A.A., 1975: Numerical Calculation of Multiphase Fluid Flow, Journal of Computational Physics, Vol. 17

27. Zuber, N. and Ishii, M., 1978: Relative Motion and Interfacial Drag Coefficient in Dispersed Two-Phase Flow of Bubbles, Drops and Particles. AIChE Jl., Vol. 25

28. Ahmadi, G., 1982: A Continuum Theory for Two Phase Media, Acta Mechanica, Vol. 44

29. Batchelor, G.K., 1972: Sedimentation in a Dilute Dispersion of Spheres, J. Fluid Mech., Vol. 52

30. Segre', G. and Silberberg, A., 1962: Behaviour of Macroscopic Rigid Spheres Poiseuille Flow, J. Fluid Mech., Vol. 14

31. Aoki, H., Kurosaki, Y. and Anzai, H., 1979: Study on the Tubular Pinch Effect in a Pipe Flow I. Lateral Migration of a Single Particle in Laminar Poiseuille Flow, Bull. of the JSME, Vol. 22, no. 164

32. Ho. B.P. and Leal, L.G., 1974: Inertial Migration of Rigid Spheres in Two-Dimensional Unidirectional Flows, J. Fluid Mech., Vol. 65

33. Hamed, A. and Tabakoff, W., 1975: Solid Particle Demixing in a Suspension Flow of Viscous Gas, Transactions of the ASME, March, 1975

34. Rubinow, S.I. and Keller, J.B., 1961: The Transverse Force on a Spinning Sphere Moving in a Viscous Fluid, J. Fluid Mech., Vol. 11

35. Saffman, P.G., 1965: The Lift on a Small Sphere in a Slow Shear Flow, J. Fluid Mech., Vol. 22

36. Drew, D.A., 1978: The Force on a Small Sphere in a Slow Viscous Flow, J. Fluid Mech., Vol. 88

37. Leal, L.G., 1980: Particle Motions in a Viscous Fluid, in: Annual Reviews of Fluid Mechanics, Vol. 12

38. Auton, T.R., 1987: The Lift Force on a Spherical Body in a Rotational Flow, J. Fluid Mech., Vol. 183

39. Lamb, H., 1932: Hydrodynamics, Cambridge

Continuum Theories for Fluid–Particle Flows: Some Aspects of Lift Forces and Turbulence [1]

David F. McTigue, Richard C. Givler, Jace W. Nunziato

Fluid and Thermal Sciences Department
Sandia National Laboratories
Albuquerque, NM 87185

Abstract

A general framework is outlined for the modeling of fluid-particle flows. The momentum exchange between the constituents embodies both lift and drag forces, constitutive equations for which can be made explicit with reference to known single-particle analyses. Relevant results for lift are reviewed, and invariant representations are posed. The fluid and particle velocities and the particle volume fraction are then decomposed into mean and fluctuating parts to characterize turbulent motions, and the equations of motion are averaged. In addition to the Reynolds stresses, further correlations between concentration and velocity fluctuations appear. These can be identified with turbulent transport processes such as "eddy diffusion" of the particles. When the drag force is dominant, the classical convection–dispersion model for turbulent transport of particles is recovered. When other interaction forces enter, particle segregation effects can arise. This is illustrated qualitatively by consideration of turbulent channel flow with lift effects included.

Introduction

Flow of an incompressible, single-phase fluid is fully characterized by a single kinematic field, the velocity. The kinematics of a fluid-particle mixture involves the velocity of each constituent, and an additional scalar field representing the particle volume fraction, or concentration. In some flows, the latter can be quite critical. For example, since the effective viscosity of a suspension is a strong function of the concentration, particle segregation in a viscometer will violate the assumption of homogeneity required to interpret measurements. Furthermore, if the distribution of particles is in part determined by the shear *rate* (*e.g.*, Ho and Leal, 1974; McTigue, *et al.*, 1986), the apparent viscosity will be rate-dependent, and the mixture will appear to be non-Newtonian even when this may not be so locally.

A great deal of work has been done on the dynamics of a single particle in a viscous fluid; reviews are given by Happel and Brenner (1965), Goldsmith and Mason (1967), Brenner (1966, 1970), and Leal (1980). In many applications, however, it is neither practical nor even of interest to track individual particles. Rather, the

---

15

primary concern is more often for some average characteristics of the flow. The objective of a continuum mixture theory is to provide governing equations for these average kinematic fields. Ideally, one would like to draw upon knowledge gained from single-particle analyses to guide the development of the constitutive models required by the continuum theory. As a practical matter, this process relies heavily upon empirical input as well.

This paper is intended to illustrate by example the construction of a two-phase flow model for turbulent mixtures. It is highly idealized and far from complete, but captures some interesting phenomenology. We first outline the general mechanical balance laws for a mixture. We then review in detail results from the literature on lift forces in viscous and inviscid flows. Generalizations in forms appropriate for the exchange of momentum between the constituents in a mixture are then discussed. "Exact" equations of motion are posed for the simplest forms for lift and drag interactions. Turbulent decomposition and averaging yields not only Reynolds stress terms, but other correlations of velocity and concentration fluctuations as well. Simple "eddy viscosity" and "eddy diffusivity" closure schemes are adopted to model the correlations. We then show that the classical convection-diffusion model for turbulent transport emerges naturally for the case when the drag term dominates the disperse phase momentum balance. Finally, we consider channel flow with the lift force present, and identify an equilibrium particle segregation due to a balance of lift and turbulent diffusion.

Balance Laws

The balance equations for the mass and momentum of constituent α are given by:

$$\frac{\partial \rho_\alpha}{\partial t} + \nabla \cdot (\rho_\alpha \mathbf{v}_\alpha) = 0, \tag{1}$$

$$\rho_\alpha \left(\frac{\partial \mathbf{v}_\alpha}{\partial t} + \mathbf{v}_\alpha \cdot \nabla \mathbf{v}_\alpha \right) = \nabla \cdot \mathbf{T}_\alpha + \rho_\alpha \mathbf{g} + \mathbf{m}_\alpha, \tag{2}$$

where ρ_α is the density (mass of constituent α per unit volume of the mixture), $\mathbf{v}_\alpha$ is the velocity, $\mathbf{T}_\alpha$ is the stress, $\mathbf{g}$ is the acceleration due to gravity, and $\mathbf{m}_\alpha$ is a body force due to the interaction of constituent α with the other constituents present. Equations (1) and (2) take the form of the classical balance laws for a single-phase continuum, with the exception of the interaction force, or momentum exchange, $\mathbf{m}_\alpha$. Equation (1) neglects chemical interactions or phase changes, which would be embodied in mass exchange terms (cf, Passman, et al., 1984).

We anticipate that the mixture can be represented as a single continuum, so that:

$$\frac{\partial \rho}{\partial t} + \nabla \cdot (\rho \mathbf{v}) = 0, \tag{3}$$

$$\rho \left(\frac{\partial \mathbf{v}}{\partial t} + \mathbf{v} \cdot \nabla \mathbf{v} \right) = \nabla \cdot \mathbf{T} + \rho \mathbf{g}, \tag{4}$$

where ρ, $\mathbf{v}$, and $\mathbf{T}$ are the density, velocity, and stress for the mixture. Comparison of (1)–(4) shows that the mixture quantities are related to the constituent quantities by the *summation rules*:

$$\rho = \Sigma \rho_\alpha \tag{5}$$

$$\rho \mathbf{v} = \Sigma \rho_\alpha \mathbf{v}_\alpha \tag{6}$$

$$\mathbf{T} = \Sigma [\mathbf{T}_\alpha - \rho_\alpha (\mathbf{v} - \mathbf{v}_\alpha)(\mathbf{v} - \mathbf{v}_\alpha)], \tag{7}$$

$$\Sigma \mathbf{m}_\alpha = \mathbf{0}, \tag{8}$$

where Σ indicates the summation over all constituents present. Equation (8) shows that whatever momentum is lost from one constituent is gained by the other(s).

The density fields, ρ_α, can vary due to changes in both the volume fraction, ϕ_α, and the local density (mass of constituent α per unit volume of that constituent), γ_α. Thus, it is convenient to introduce the decomposition:

$$\rho_\alpha = \phi_\alpha \gamma_\alpha. \tag{9}$$

Finally, we consider only *saturated* mixtures, in which all space is occupied, which imposes the requirement:

$$\Sigma \phi_\alpha = 1. \tag{10}$$

Equations (1)–(10) hold for multiphase systems with any number of constituents. For present purposes, we specialize to the case of two, a continuous fluid ($\alpha = f$) and a dispersed particulate solid ($\alpha = s$). In this case, we let

$$\phi = \phi_s = 1 - \phi_f. \tag{11}$$

We also restrict attention to mixtures comprised of incompressible constituents (γ_f and γ_s constant).

Without loss of generality, it is convenient to decompose the stresses, $\mathbf{T}_\alpha$, into an isotropic pressure, p_α, and an *extra stress*, $\mathbf{T}_\alpha^*$:

$$\mathbf{T}_\alpha = -\phi_\alpha p_\alpha \mathbf{1} + \mathbf{T}_\alpha^*. \tag{12}$$

There is substantial motivation to include in the momentum exchange a buoyancy force, $p_f \nabla \phi$, due to the fluid pressure acting over the interfacial surfaces (*e.g.*, Passman, *et al.*, 1984). Thus, we also define an *extra momentum exchange*, $\mathbf{m}_s^*$, such that

$$\mathbf{m}_s = p_f \nabla \phi + \mathbf{m}_s^* \tag{13}$$

Finally, equations (1)–(13) can be combined in the form:

$$-\frac{\partial \phi}{\partial t} + \nabla \cdot [(1 - \phi)\mathbf{v}_f] = 0, \tag{14}$$

$$\frac{\partial \phi}{\partial t} + \nabla \cdot (\phi \mathbf{v}_s) = 0, \tag{15}$$

$$\rho_f \left(\frac{\partial \mathbf{v}_f}{\partial t} + \mathbf{v}_f \cdot \nabla \mathbf{v}_f \right) = -(1 - \phi)\nabla p_f + \nabla \cdot \mathbf{T}_f^* + \rho_f \mathbf{g} - \mathbf{m}_s^*, \qquad (16)$$

$$\rho_s \left(\frac{\partial \mathbf{v}_s}{\partial t} + \mathbf{v}_s \cdot \nabla \mathbf{v}_s \right) = -\phi \nabla p_f - \nabla[\phi(p_s - p_f)] + \nabla \cdot \mathbf{T}_s^* + \rho_s \mathbf{g} + \mathbf{m}_s^*, \qquad (17)$$

Note from (14) and (15) that, even though the constituents are taken to be incompressible, neither velocity field is, in general, divergence-free.

Lift Forces

Particle segregation has been observed experimentally in Poiseuille flow by a number of investigators; results have been summarized by Brenner (1966), Cox and Mason (1971), Goldsmith and Mason (1967), and Leal (1980). In general, these studies show that particles lagging the fluid motion tend to migrate toward the centerline, or region of minimum shear rate, and particles leading the fluid migrate toward the wall. Segré and Silberberg (1962) found that, for a small range of mean flow Reynolds number, neutrally buoyant particles can achieve an equilibrium position at a dimensionless radius of about 0.6.

Saffman (1956) and Bretherton (1962) have shown that a particle embedded in a steady, rectilinear Stokes flow, i.e. at zero Reynolds number, cannot experience a net force normal to the unperturbed fluid streamlines. Thus, any analysis for the cross-stream lift on a particle in a steady, rectilinear flow must take inertia into account. One approach is to introduce small inertial effects through a perturbation of the Stokes flow problem, and a number of such analyses are in the literature. Both unbounded and bounded domains have been addressed. The analyses for the former assume that the boundaries of the unperturbed flow are sufficiently far away that they do not interact with the disturbance due to the particle. Boundaries play an indirect role in this type of problem, of course, insofar as their presence may be required to establish the velocity gradient or curvature with which the particle interacts. Two well-known analyses for unbounded flows are those by Rubinow and Keller (1961) and Saffman (1968), which are summarized briefly below.

Analyses for bounded flows address configurations in which, say, a fixed wall lies within the disturbance field of the particle. Examples include the work of Ho and Leal (1974) and Vasseur and Cox (1976). It is not immediately apparent how one might adopt analyses of this type in the formulation of a continuum model. Although we have attempted previously to do so (McTigue, et al., 1986) using the results of Ho and Leal, the result is not very satisfactory. The indication of difficulty is the appearance of the channel width in the expression for the lift. It would seem that this should enter through boundary conditions rather than through a constitutive equation. Obviously, this arises because the bounded-flow analyses are geometry-specific. For this reason, we consider in more detail generalizations only of lift forces in unbounded flows.

Rubinow and Keller (1961) consider a sphere spinning with angular velocity $\mathbf{\Omega}$ and translating at velocity $\mathbf{V}'$ through an incompressible viscous fluid. The fluid is

assumed to be static far from the sphere. The solution takes the form of a Stokes expansion in the near field that satisfies boundary conditions at the particle, but fails far away, and an Oseen expansion in the far field that exhibits the converse behavior. An asymptotic match is performed in order to calculate the forces on the sphere. The expansions are in powers of the particle Reynolds number,

$$R_V = \frac{\gamma_f a V}{\mu},\tag{18}$$

where a is the particle radius, V is the magnitude of the translation velocity, and μ is the fluid viscosity. The result of interest here is that for the lift force normal to the direction of translation, $\mathbf{f}_L^{(RK)}$:

$$\mathbf{f}_L^{(RK)} = \pi a^3 \gamma_f \mathbf{\Omega} \times \mathbf{V}'[1 + O(R_V)].\tag{19}$$

Consider a rectilinear shearing flow, $v_{f1}(x_2)$. A force-free particle spins with the angular velocity of the fluid, so that $\Omega_3 = -\kappa/2$, where $\kappa = \partial v_{f1}/\partial x_2$ is the shear rate, and $V_1' = -V = -(v_{f1} - v_{s2})$. The "slip–spin" lift force (19) is then

$$f_{L2}^{(RK)} = \frac{1}{2}\pi a^3 \gamma_f \kappa V.\tag{20}$$

It is interesting to note that, although Rubinow and Keller's analysis is for a small inertial correction to the Stokes flow problem, the lift force is, to leading order, independent of viscosity.

Saffman (1968) considers a sphere in a simple shear flow, translating parallel to the undisturbed streamlines with a relative velocity of magnitude V'. The analysis again is based on matched asymptotic expansions. In addition to (18), two other Reynolds numbers enter the problem:

$$R_\kappa = \frac{\gamma_f a^2 \kappa}{\mu}, \quad R_\Omega = \frac{\gamma_f a \Omega}{\mu},\tag{21}$$

and the conditions under which the analysis holds are

$$R_V \ll R_\kappa^{1/2}, \quad R_V \ll 1, \quad R_\Omega \ll 1.\tag{22}$$

For a simple shear flow given by $v_{f1} = v_0 + \kappa x_2$, Saffman obtained a "slip–shear" lift force in the form:

$$\mathbf{f}_{L2}^{(S)} = 6.46 a^2 \gamma_f^{1/2} \mu^{1/2} (\mathrm{sgn}\kappa)|\kappa|^{1/2} V.\tag{23}$$

Equation (23) indicates that a particle lagging the fluid ($V > 0$) migrates toward higher-velocity streamlines, and a particle leading the fluid ($V < 0$) migrates in the direction of decreasing fluid velocity. This qualitative behavior is in accord with experimental observations. In the rectilinear shearing flow, the ratio of the "slip–spin" lift (20) found by Rubinow and Keller to the "slip–shear" lift (23) treated by Saffman, then, scales like $R_\kappa^{1/2}$.

In a more general flow field, the applicability of the "slip-shear" analysis requires that the characteristic length scale for the disturbance field is much less than that for the variation in shear rate. Saffman (1968) suggested, from dimensional reasoning, that the lift due to interaction of the particle disturbance field with the mean-flow *curvature* takes the form

$$\mathbf{f}_{L2}^{(SC)} = ca^4 \gamma_f^{2/3} \mu^{1/3} \kappa (\text{sgn}\varsigma)|\varsigma|^{2/3},\tag{24}$$

where ς is the curvature (*e.g.*, for an undisturbed mean flow $v_{f1} = v_0 + \kappa x_2 + \varsigma x_2^2/2$). Saffman noted that determination of both the sign and the magnitude of the constant c await more complete analysis. In this unbounded flow, one may define a curvature Reynolds number $R_\varsigma = \gamma_f a^3 \varsigma/\mu$, in terms of which the ratio of the "shear-curvature" lift (24) to the "slip-shear" lift (23) scales like $R_\kappa^{1/2} R_\varsigma^{2/3} R_V^{-1}$. It is interesting to speculate upon the possibility that these two forces oppose one another in certain flows. Consider, for example, plane Poiseuille flow carrying a neutrally buoyant particle. The particle slips relative to the fluid due to the Faxén effect only. Thus, for symmetric flow in a channel of half-width d, the shear rate is $\kappa = -3\bar{v}x_2/d^2$, the curvature is $\varsigma = -3\bar{v}/d^2$, and the slip is $V = a^2\bar{v}/2d^2$, where $\bar{v}$ is the mean velocity. The "slip-shear" and "shear-curvature" forces are then balanced where

$$\left|\frac{x_2}{d}\right| = 0.80c^{-2}\overline{R}^{-1/3},\tag{25}$$

where $\overline{R} = \gamma_f \bar{v} d/\mu$ is the channel Reynolds number. Segré and Silberberg (1962) observed an off-axis peak in particle concentration in flows of dilute suspensions in circular tubes. The peak occurred at a dimensionless radius of about 0.6, and was manifest in flows characterized by $\overline{R}$ of order 10. If these conditions apply to a plane geometry, the constant c would be of order 0.8. The ratio of the "slip-shear" (23) to the "shear-curvature" (24) lifts in Poiseuille flow scales like $\overline{R}^{-1/6}$. Ho and Leal (1974) also considered interaction with the mean flow curvature, but in a bounded flow. The ratio of the curvature effect discussed by Saffman in an unbounded flow (24) to that found by Ho and Leal scales like $\overline{R}^{-1/3}$.

Both Rubinow and Keller and Saffman studied small Reynolds number effects. In the other limit, Drew and Lahey (1987) have recently considered *inviscid* rotational flow past a sphere. They obtain a lift force of exactly the same form as that found by Rubinow and Keller (19), but multiplied by a factor 4/3. The same result was obtained independently by Auton (1987). This is essentially like the classical Kutta-Joukowski lift on a two-dimensional body in a plane flow, which is just $\gamma_f U \Gamma$, where U is the velocity of the body and Γ is the circulation.

Invariant Forms for the Lift Force

The momentum exchange, $\mathbf{m}_s^*$, includes fluid-particle interaction forces such as lift and drag. For brevity, let us decompose $\mathbf{m}_s^*$ into drag, $\mathbf{m}_D^*$, lift, $\mathbf{m}_L^*$, and other components:

$$\mathbf{m}_s^* = \mathbf{m}_D^* + \mathbf{m}_L^* + \ldots.\tag{26}$$

20

It has been suggested previously (Drew, 1976; McTigue, *et al.*, 1986; Passman, 1986) that the lift might include terms of the form

$$\mathbf{m}_L^{\star} = 2\alpha_2\phi\mathbf{D}_f \cdot (\mathbf{v}_f - \mathbf{v}_s) + 4\beta_2\phi\mathbf{D}_f \cdot (\nabla \cdot \mathbf{D}_f), \tag{27}$$

where $\mathbf{D}_\alpha = \text{sym}\nabla\mathbf{v}_\alpha$. It is expected that α_2 and β_2 may be a functions of the particle volume fraction, ϕ, the relative speed, $|\mathbf{v}_f - \mathbf{v}_s|$, and the invariants of $\mathbf{D}_f$, $\mathbf{D}_s$, and their higher-order derivatives. In particular, if we assume that, for dilute suspensions, we should recover the single-particle results discussed in the foregoing section,[2] this function can be made explicit. For example, Saffman's result for the "slip-shear" lift (23) is recovered for the choice

$$\alpha_2 = \frac{3(6.46)}{4\pi a}\left(\frac{\gamma_f^2\mu^2}{2\text{tr}\mathbf{D}_f^2}\right)^{1/4}. \tag{28}$$

The "shear-curvature" lift (24) is recovered for the choice

$$\beta_2 = \frac{3ca\gamma_f^{2/3}\mu^{1/3}}{4\pi|2\nabla \cdot \mathbf{D}_f|^{1/3}}. \tag{29}$$

Generalization of a "slip–spin" lift of the form found by Rubinow and Keller (20) poses some difficulty. It would appear that such a lift is proportional to $2\mathbf{W}_f \cdot (\mathbf{v}_f - \mathbf{v}_s)$, where $\mathbf{W}_f = \text{skw}\nabla\mathbf{v}_f$ is the skew-symmetric part of the fluid velocity gradient. However, $\mathbf{W}_f$ is not invariant (*e.g.*, Truesdell, 1977, p. 115). Drew and Lahey (1987) have suggested that this dilemma can be resolved by simultaneous consideration of the virtual mass effect. The virtual mass, too, when generalized from the classical expression, is not easily put into an invariant form. However, the *combination* of the virtual mass and lift forces posed by Drew and Lahey is invariant:

$$\mathbf{m}_{VM}^{\star} + \mathbf{m}_L^{\star} = \frac{1}{2}\gamma_f\phi\left[\left(\frac{D_f\mathbf{v}_f}{Dt} - \frac{D_s\mathbf{v}_s}{Dt}\right) - 2\mathbf{W}_f \cdot (\mathbf{v}_f - \mathbf{v}_s)\right], \tag{30}$$

where $\mathbf{m}_{VM}^{\star}$ is the momentum exchange due to the virtual mass effect, and the substantial derivative is defined by $D_\alpha/Dt \equiv \partial/\partial t + \mathbf{v}_\alpha \cdot \nabla$. In (30), neither the virtual mass, represented by the difference in convective accelerations, nor the lift, in the form $2\mathbf{W}_f \cdot (\mathbf{v}_f - \mathbf{v}_s)$, is invariant, while their sum is. This depends upon the remarkable result that the coefficient $\gamma_f/2$ is the same for both the virtual mass and the lift. That (30) embodies the classical virtual mass effect is easily seen by specializing to an unsteady, uniform flow. That it embodies the result of Drew and Lahey for the lift can be demonstrated by specializing to steady, rectilinear shearing flow. Drew and Lahey point out that a simple regrouping of terms can yield an invariant form for the virtual mass:

$$\mathbf{m}_{VM}^{\star} = \frac{1}{2}\gamma_f\phi\left[\left(\frac{D_s\mathbf{v}_f}{Dt} - \frac{D_f\mathbf{v}_s}{Dt}\right) - (\mathbf{v}_f - \mathbf{v}_s) \cdot \nabla(\mathbf{v}_f - \mathbf{v}_s)\right], \tag{31}$$

and a lift in the form of the first term in (27) with $\alpha_2 = \gamma_f/2$. Equations (31) and the lift sum to recover (30).

---

[2]This assumption was stated by Drew (1976) as the *principle of correct low concentration limits.*

Turbulent Decomposition and Averaging

It is evident from the foregoing discussion concerning lift forces that the formulation of the necessary constitutive models necessary to complete the equations of motion (14–17) is quite formidable. It remains to specify relationships for the stresses, $\mathbf{T}_f^*$ and $\mathbf{T}_s^*$, the pressure difference, $p_s - p_f$, and momentum exchanges such as that due to drag, $\mathbf{m}_D^*$. Each of these raises subtle and complex modeling issues. For present purposes, we skirt these difficulties in order to isolate phenomena associated with the lift and drag. In particular, we assume

$$\mathbf{T}_f^* = 0, \tag{32}$$

$$\mathbf{T}_s^* = 0, \tag{33}$$

$$p_f = p_s = p, \tag{34}$$

$$\mathbf{m}_D^* = \alpha_1 \phi (\mathbf{v}_f - \mathbf{v}_s), \tag{35}$$

$$\mathbf{m}_L^* = 2\alpha_2 \phi \mathbf{D}_f \cdot (\mathbf{v}_f - \mathbf{v}_s). \tag{36}$$

We rationalize neglect of the fluid extra stress, $\mathbf{T}_f^*$ (32), by confining attention to inertially-dominated flows.[3] In a dilute suspension, it is easy to imagine that the disperse-phase extra stress, $\mathbf{T}_s^*$, vanishes (33), implying that there is no direct exchange of momentum between particles. The assumption of equal pressures (34) implies that Brownian motion (Nunziato, 1983) and certain inertial effects at the particle scale (Givler, 1987) are negligible. The drag force, $\mathbf{m}_D^*$, is written in its familiar form (35), proportional to the relative velocity. The coefficient α_1 is, in general, expected to depend upon ϕ and $|\mathbf{v}_f - \mathbf{v}_s|$, accounting for the effects of particle interference at high concentration and inertia at high relative velocity, respectively. The choice $\alpha_1 = 9\mu/2a^2$ corresponds to the classical result for Stokes drag on a single particle, and is adopted here. Finally, we take the lift in the form of (36), with α_2 assumed to be constant for simplicity. Neglect of inertial effects in the drag (35) while retaining those giving rise to the lift (36) is justified if $R_V R_\kappa^{-n} \ll 1$, where $n = 1$ for the "slip-spin" lift of Rubinow and Keller (20) and $n = 1/2$ for the "slip-shear" lift of Saffman (23).

Under these assumptions, the momentum equations (16–17) reduce to:

$$\rho_f \left(\frac{\partial \mathbf{v}_f}{\partial t} + \mathbf{v}_f \cdot \nabla \mathbf{v}_f \right) = -(1 - \phi)\nabla p + \rho_f \mathbf{g}$$

$$-\alpha_1 \phi (\mathbf{v}_f - \mathbf{v}_s) - 2\alpha_2 \phi \mathbf{D}_f \cdot (\mathbf{v}_f - \mathbf{v}_s), \tag{37}$$

$$\rho_s \left(\frac{\partial \mathbf{v}_s}{\partial t} + \mathbf{v}_s \cdot \nabla \mathbf{v}_s \right) = -\phi \nabla p + \rho_s \mathbf{g}$$

$$+\alpha_1 \phi (\mathbf{v}_f - \mathbf{v}_s) + 2\alpha_2 \phi \mathbf{D}_f \cdot (\mathbf{v}_f - \mathbf{v}_s), \tag{38}$$

---

[3]The dissipative, viscous terms represented by $\mathbf{T}_f^*$ are critical, of course, to the extension of this discussion to the kinetic energy balances.

Note that these "exact" equations of motion do not contain interaction terms representing diffusive forces.

The independent field variables in (37) and (38) are each decomposed according to:

$$\mathbf{v}_a = \overline{\mathbf{v}}_a + \mathbf{v}'_a, \tag{39}$$

$$\phi = \overline{\phi} + \phi', \tag{40}$$

$$p = \overline{p} + p', \tag{41}$$

where overbars indicate mean quantities and primes indicate fluctuating quantities. By definition, $\overline{\phi'} = 0$ and $\overline{p'} = 0$. However, the averaging scheme chosen here defines the mean velocities in terms of mean *momenta*, an approach introduced originally for compressible, single-phase flows (Favre, 1965), and suggested in the multiphase context by Drew (1975):

$$\overline{\rho}_\alpha \overline{\mathbf{v}}_\alpha = \overline{\rho_\alpha \mathbf{v}_\alpha}. \tag{42}$$

Note that $\overline{\rho}_a = \gamma_a \overline{\phi}_a$ for incompressible constituents. Note also that the averages of the velocity fluctuations do not vanish, but $\overline{(1 - \phi)\mathbf{v}'_f} = 0$ and $\overline{\phi \mathbf{v}'_s} = 0$.

Substitution of (39)–(41) into (14), (15), (37), and (38) and averaging yields:

$$-\frac{\partial \overline{\phi}}{\partial t} + \nabla \cdot [(1 - \overline{\phi})\overline{\mathbf{v}}_f] = 0, \tag{43}$$

$$\frac{\partial \overline{\phi}}{\partial t} + \nabla \cdot (\overline{\phi}\overline{\mathbf{v}}_s) = 0, \tag{44}$$

$$\overline{\rho}_f \left(\frac{\partial \overline{\mathbf{v}}_f}{\partial t} + \overline{\mathbf{v}}_f \cdot \nabla \overline{\mathbf{v}}_f \right) = -(1 - \overline{\phi})\nabla \overline{p} + \overline{\phi' \nabla p'} + \nabla \cdot \mathbf{T}'_f + \overline{\rho}_f \mathbf{g}$$
$$-\alpha_1 \left[\overline{\phi}(\overline{\mathbf{v}}_f - \overline{\mathbf{v}}_s) + \overline{\phi \mathbf{v}'_f} \right]$$
$$-2\alpha_2 \left[\overline{\phi} \, \overline{\mathbf{D}}_f \cdot (\overline{\mathbf{v}}_f - \overline{\mathbf{v}}_s) + \overline{\mathbf{D}}_f \cdot \overline{\phi \mathbf{v}'_f} + \overline{\phi \mathbf{D}'_f} \cdot (\overline{\mathbf{v}}_f - \overline{\mathbf{v}}_s) \right] \tag{45}$$

$$\overline{\rho}_s \left(\frac{\partial \overline{\mathbf{v}}_s}{\partial t} + \overline{\mathbf{v}}_s \cdot \nabla \overline{\mathbf{v}}_s \right) = -\overline{\phi}\nabla \overline{p} - \overline{\phi' \nabla p'} + \nabla \cdot \mathbf{T}'_s + \overline{\rho}_s \mathbf{g}$$
$$+\alpha_1 \left[\overline{\phi}(\overline{\mathbf{v}}_f - \overline{\mathbf{v}}_s) + \overline{\phi \mathbf{v}'_f} \right]$$
$$+2\alpha_2 \left[\overline{\phi} \, \overline{\mathbf{D}}_f \cdot (\overline{\mathbf{v}}_f - \overline{\mathbf{v}}_s) + \overline{\mathbf{D}}_f \cdot \overline{\phi \mathbf{v}'_f} + \overline{\phi \mathbf{D}'_f} \cdot (\overline{\mathbf{v}}_f - \overline{\mathbf{v}}_s) \right] \tag{46}$$

where $\mathbf{T}'_\alpha = -\overline{\rho_\alpha \mathbf{v}'_\alpha \mathbf{v}'_\alpha}$ is a Reynolds stress for constituent α, and triple correlations have been omitted.

Constitutive Models for Turbulent Correlations

The averaged mass balances (43–44) appear in forms identical to the exact equations (14–15), in part as a consequence of the definition of average velocity (42). Averaging the momentum balances, however, yields a number of correlations of fluctuating quantities. The Reynolds stress terms are familiar from single-phase turbulence, but several additional correlations arise here that are a direct consequence of the fluctuations in the particle concentration field, ϕ. Of special note is the correlation of particle concentration and fluid velocity fluctuations, $\overline{\phi \mathbf{v}'_f}$, which represents a flux of particles due to the fluid turbulence. In all subsequent developments, we neglect the pressure–concentration correlations appearing in (45) and (46).

For the present discussion, it suffices to adopt the simplest possible closure scheme, following essentially the classical "eddy viscosity" argument. That is, a correlation of some fluctuating quantity with $\mathbf{v}'_\alpha$ is taken to be proportional to the gradient of the mean of that quantity:

$$- \overline{\rho_\alpha \mathbf{v}'_\alpha \mathbf{v}'_\alpha} = u_\alpha l_{1\alpha} [\nabla \cdot (\bar{\rho}_\alpha \bar{\mathbf{v}}_\alpha)] \mathbf{1} + 2 u_\alpha l_{2\alpha} \mathrm{sym} \nabla (\bar{\rho}_\alpha \bar{\mathbf{v}}_\alpha), \tag{47}$$

$$\overline{\phi \mathbf{v}'_f} = -u_f l_3 \nabla \bar{\phi}, \tag{48}$$

$$2 \overline{\phi \mathbf{D}'_f} = -u_f l_4 \nabla (\nabla \bar{\phi}), \tag{49}$$

where u_α is an appropriate velocity scale for constituent α, and the ls are appropriate length scales ("mixing lengths").

Turbulent Convection and Dispersion of Particles

A commonly encountered situation for which modeling capabilities are well developed is that for particles fully entrained in the fluid. In this case, the particles are essentially "passive" tracers for the fluid, and are transported by the mean convective motion and by turbulent diffusion. It is worth considering briefly where this classical model is embedded in the mixture theory outlined here.

For $\bar{\phi} \ll 1$, the fluid mass and momentum balances (43 and 45) are approximately those for the fluid alone:

$$\nabla \cdot \bar{\mathbf{v}}_f = 0, \tag{50}$$

$$\bar{\gamma}_f \left(\frac{\partial \bar{\mathbf{v}}_f}{\partial t} + \bar{\mathbf{v}}_f \cdot \nabla \bar{\mathbf{v}}_f \right) = -\nabla \bar{p} + \nabla \cdot \mathbf{T}'_f + \gamma_f \mathbf{g}. \tag{51}$$

In this approximation, the fluid motion is unaffected by the presence of the particles, and can be solved independently. The disperse-phase mass balance (44) remains in its exact form. Suppose the drag coefficient, α_1, is large, so that the dominant terms in (46) are simply those due to drag. This can always be realized for sufficiently

small particles; the ratio of the drag to lift forces discussed in the foregoing scales at least like a^{-1}. The disperse-phase momentum balance then reduces to:

$$\bar{\phi}(\bar{\mathbf{v}}_f - \bar{\mathbf{v}}_s) = -\overline{\phi \mathbf{v}'_f}, \tag{52}$$

i.e., the mean flux of particles relative to the fluid is balanced by the turbulent correlation $\overline{\phi \mathbf{v}'_f}$.

Equations (44), (50), and (52) combine to give:

$$\frac{\partial \bar{\phi}}{\partial t} + \bar{\mathbf{v}}_f \cdot \nabla \bar{\phi} = -\nabla \cdot (\overline{\phi \mathbf{v}'_f}). \tag{53}$$

Substitution of (48) into (53) yields:

$$\frac{\partial \bar{\phi}}{\partial t} + \bar{\mathbf{v}}_f \cdot \nabla \bar{\phi} = \nabla \cdot (\mathcal{D} \nabla \bar{\phi}), \tag{54}$$

where $\mathcal{D} = u_f l_3$. This recovers the classical result: the particle concentration field is governed by a convection–dispersion equation, with turbulent dispersion coefficient or "eddy diffusivity" $\mathcal{D}$. A similar discussion for the case when the gravitational body force is retained was presented by McTigue (1981, 1983).

Although this limiting case is relatively simple and quite well known, the present development is revealing. Many texts derive the turbulent diffusion equation solely from a statement of mass balance, a decomposition and averaging process, and a model for the correlation of concentration and velocity fluctuations. This tends to mask the fact that the turbulent diffusion is a *dynamic* process in response to fluid-particle interactions. Thus, the momentum equations must be considered. Indeed, it is worth reiterating here that the turbulent dispersive flux, $\overline{\phi \mathbf{v}'_f}$, appearing in in (53) arose from decomposing and averaging the drag force (35). Thus, the tendency for the particles to be convected with the mean fluid velocity and dispersed by the fluid velocity fluctuations is clearly identified with the drag. Analogous observations have been made previously with regard to molecular diffusion (*e.g.*, Müller, 1968).

We also note that the assumptions leading to (54) are quite special, and emphasize in particular the neglect of any interaction forces other than drag in writing (52). It is evident that much more complex phenomenology could be embedded in the general scheme outlined here if additional interaction forces come into play.

Channel Flow With Lift Effects

Particle segregation has been observed in turbulent jets (Laats and Frishman, 1970), and ascribed to the "Magnus" lift force (30). Here we consider plane channel flow in order to simplify the kinematics, and retain the cross-stream lift effects embodied in (46). The analysis is highly simplified and somewhat speculative, and is intended only to illustrate the type of phenomena that might be represented by a mixture model of the type sketched out here.

Consider a vertical channel, with steady upward flow. The flow is in the $+x_1$ direction, so that $\mathbf{g} = \{-g, 0, 0\}$, $x_2 = 0$ at the wall, and $x_2 = h$ at the centerline. We assume that $\gamma_s > \gamma_f$, so that gravitational settling will cause the disperse particulate phase to lag the fluid.

For a steady, rectilinear flow in the mean, the mass balances (43, 44) are identically satisfied. We expect again that, for $\bar{\phi} \ll 1$, the fluid momentum balance can be approximated by that for the fluid alone (51). Thus, in the streamwise direction, (51) becomes:

$$0 = -\frac{d\bar{p}}{dx_1} + \frac{d}{dx_2}T'_{f21} - \gamma_f g. \tag{55}$$

For a smooth-walled channel, familiar arguments for the mixing length l_{2f} (47) and the identity $u_f = u_\star = (\tau_0/\gamma_f)^{1/2}$, where τ_0 is the shear stress at the wall, lead to the usual logarithmic velocity profile:

$$\frac{\bar{v}_{f1}}{u_\star} = \frac{1}{\kappa}\ln\frac{u_\star x_2}{\nu} + 5.5, \tag{56}$$

where $\kappa \simeq 0.4$ is the Kármán constant, and $\nu = \mu/\gamma_f$ is the kinematic viscosity. The streamwise momentum balance for the particles, from (46) and (48), and neglecting T'_{s21}, becomes:

$$0 = -\bar{\phi}\frac{d\bar{p}}{dx_1} - \gamma_s\bar{\phi}g + \alpha_1\bar{\phi}(\bar{v}_{f1} - \bar{v}_{s1}) - \alpha_2 u_\star\kappa_s x_2\frac{d\bar{v}_{f1}}{dx_2}\frac{d\bar{\phi}}{dx_2}, \tag{57}$$

where we have assumed $u_f l_3 = u_\star\kappa_s x_2$. Substituting from (55) for the mean pressure gradient in (57), and noting that the fluid shear stress gradient is simply $-\gamma_f u_\star^2/h$, (57) becomes:

$$0 = \frac{\gamma_f u_\star^2}{h} - (\gamma_s - \gamma_f)g + \alpha_1(\bar{v}_{f1} - \bar{v}_{s1}) - \alpha_2 u_\star\kappa_s x_2\frac{d\bar{v}_{f1}}{dx_2}\left(\frac{1}{\bar{\phi}}\frac{d\bar{\phi}}{dx_2}\right). \tag{58}$$

Let us suppose, again for simplicity, that the second and third terms in (58) dominate. In this case, we are left with a balance between the buoyant weight and the drag, giving

$$\bar{v}_{f1} - \bar{v}_{s1} = V_\infty, \tag{59}$$

where $V_\infty = 2a^2(\gamma_s - \gamma_f)g/9\mu$ is the Stokes settling velocity.

The cross-stream momentum balance for the disperse phase is

$$0 = -\alpha_1 u_\star\kappa_s x_2\left(\frac{1}{\bar{\phi}}\frac{d\bar{\phi}}{dx_2}\right) + \alpha_2\frac{d\bar{v}_{f1}}{dx_2}(\bar{v}_{f1} - \bar{v}_{s1}), \tag{60}$$

which is simply a balance between turbulent diffusion and the lift due to the mean flow. Note from (60) that the gradient of $\bar{\phi}$ vanishes at the centerline if the fluid velocity gradient vanishes there. According to the eddy viscosity model adopted for the Reynolds stress (47), the latter is in fact required by symmetry. However, of

26

course, the logarithmic velocity profile (56) does not satisfy this condition. There-fore, we can anticipate a similar failing in the solution for $\bar{\phi}$. Substitution of (56) and (59) into (60) and integration gives

$$\bar{\phi} = \bar{\phi}(h) \exp\left[-\frac{\alpha_2 V_\infty u_*}{\alpha_1 \kappa \mathcal{D}_h} \left(\frac{1 - \eta}{\eta} \right) \right], \tag{61}$$

where $\eta = x_2/h$, and a diffusivity, $\mathcal{D}_h = u_* \kappa_s h$ has been introduced. This profile has some of the expected characteristics: the particles are concentrated toward the center of the channel by the lift; the central peak is flattened by diffusion; and the channel margins, where the fluid velocity gradient is steepest, can be essentially clear of particles. That (61) indicates $\bar{\phi}(0) = 0$ is a result of using the logarithmic fluid velocity profile (56), which is not valid in the limit $x_2 \rightarrow 0$, in (60).

Lee and Durst (1982) conducted experiments in this configuration using glass beads in an air stream. Some of their results are in qualitative agreement with those found here: the air velocity profile (56) is little affected by the presence of the particles (at less than 0.5% mean volume fraction); the particles lag the fluid approximately by their fall velocity (59); and there is a particle-free zone near the wall. However, important phenomena are missed by this simple analysis. In particular, Lee and Durst observed that the velocity difference (59) is not uniform across the channel, but typically decreases toward zero near the wall. The particle velocity profiles, then, are more nearly uniform across the channel, suggesting that the turbulent mixing brings high-momentum particles from the core of the flow toward the boundary. For the smaller particles examined, the profiles actually cross near the wall; *i.e.*, the particles *lead* the fluid, so that the momentum exchange due to drag (35) changes sign. These phenomena are clearly not embodied in the model analysis outlined here. The limitation is most likely in the simple, Boussinesq closure scheme adopted (47–49). Kashiwa (1987) has modeled these experiments using a higher-order ($k - \epsilon$) closure, and is able to represent the cross-stream transport of streamwise particle momentum into the near-wall region.

Summary and Discussion

Treatment of turbulent suspensions in the context of the continuum theory of mixtures is currently in its most rudimentary stages. The appeal of the overall approach is that it provides an axiomatic framework on which to build. In practice, of course, one is quickly confronted with the difficulty of posing specific constitutive equations for the stresses and momentum exchange that embody the phenomena of interest. This is only compounded in the case of turbulent mixtures, in which correlations between the three kinematic fields, $\mathbf{v}_f$, $\mathbf{v}_s$, and ϕ proliferate. The intent of this paper is not to lay out a definitive set of equations of motion for such a system. Rather, we have attempted only to sketch the general spirit of the approach, and to illustrate by means of the simplest possible example. The sequence is familiar from its antecedents in classical, single-fluid flow: state balance laws, pose constitutive

equations, construct "exact" equations of motion, introduce a decomposition and averaging scheme, model the resulting correlations, and, finally, solve boundary value problems. The channel flow problem considered here, exhibiting particle segregation effects, only hints at the rich and complex phenomenology that could be embedded in such a model.

Each section of the paper encounters challenges. Exact forms for lift forces, even from single-particle analyses, are not well established; those that are known are complex; and their generalizations are not immediately obvious. We emphasize in particular that *bounded* flows have been analyzed (*e.g.*, Vasseur and Cox, 1976) in which wall effects are critical, and it is not clear how one might adopt such results in a continuum model. Many of these remarks carry over to other interaction forces, as well, such as the "Basset" term (*e.g.*, Hinze, 1975, p. 463), which accounts for the history of the particle acceleration. Because no universally valid expressions for lift, drag, or other forces are available, considerable judgement is required in selecting the forms appropriate to a particular application. Constitutive equations for any concentration beyond the dilute limit are especially difficult to define; few analytical results are available (*e.g.*, Batchelor's (1972) work on "hindered settling") and resort is usually made to empiricism.

Perhaps the greatest challenge encountered in constructing a model for turbulent mixtures is the "closure" problem, familiar from single-phase turbulence, but magnified here by the presence of additional fluctuating fields. As in single-phase problems, some simple configurations can be addressed through classical Boussinesq models (*e.g.*, 47–49) and simple scaling arguments. However, it is also clear, even from the highly idealized channel flow problem addressed here, that such an approach is severely limited. For example, the Boussinesq model for the Reynolds stresses (47) does not embody normal stress effects in rectilinear flows, while one might easily imagine that such effects could be important. Higher-order closure schemes are obviously called for, and steps in this direction have been taken with some success. Scheiwiller (1986) has developed a $k - \epsilon$ model to represent snow avalanches, and has achieved excellent agreement with laboratory experiments. Kashiwa (1987) has used a similar approach, and successfully captures some of the unusual phenomena observed by Lee and Durst (1982) in the vertical channel flow discussed in the foregoing section.

References

Auton, T. R., The lift force on a spherical body in a rotational flow *Journal of Fluid Mechanics*, **183** (1987), 199–218.

Batchelor, G. K., Sedimentation in a dilute dispersion of spheres, *Journal of Fluid Mechanics*, **52** (1972), 245–268.

Brenner, H., Hydrodynamic resistance of particles at small Reynolds numbers, *Ad-*

vances in *Chemical Engineering*, **6** (1966), 287–438.

Brenner, H., Dynamics of neutrally buoyant particles in low Reynolds number flows, *Progress in Heat and Mass Transfer*, **6** (1970), 509–574.

Bretherton, F. P., The motion of rigid particles in a shear flow at low Reynolds number, *Journal of Fluid Mechanics*, **14** (1962), 284–304.

Cox, R. G., and S. G. Mason, Suspended particles in fluid flow through tubes, *Annual Reviews of Fluid Mechanics*, **3** (1971), 291–316.

Drew, D. A., Turbulent sediment transport over a flat bottom using momentum balance, *Journal of Applied Mechanics*, **42** (1975), 38–44.

Drew, D. A., Two-phase flows: constitutive equations for lift and Brownian motion and some basic flows, *Archive for Rational Mechanics and Analysis*, **62** (1976), 149–163.

Drew, D. A., and R. T. Lahey, Jr., The virtual mass and lift force on a sphere in rotating and straining inviscid flow, *International Journal of Multiphase Flow*, **13** (1987), 113–121.

Favre, A., Équations des gaz turbulents compressibles, I. – Formes générales, *Journal de Méchanique*, **4** (1965), 361–390.

Givler, R. C., An interpretation of the solid phase pressure in slow, fluid-particle flows, *International Journal of Multiphase Flow*, **13** (1987), 717–722.

Goldsmith, H. L., and S. G. Mason, The microrheology of dispersions, *Rheology, Theory and Applications*, F. R. Eirich, ed., Academic, New York, **4** (1967), 85–250.

Hinze, J. O., *Turbulence*, McGraw-Hill, New York, 1975.

Ho, B. P., and L. G. Leal, Inertial migration of rigid spheres in two-dimensional unidirectional flows, *Journal of Fluid Mechanics*, **65** (1974), 365–400.

Kashiwa, B., Statistical theory of turbulent incompressible multimaterial flow, Ph. D. Thesis, Department of Mechanical Engineering, University of Washington, Seattle, printed as *Los Alamos National Laboratories Technical Report*, **LA–11088–T**, October 1987.

Laats, M. K., and F. A. Frishman, Assumptions used in calculating the two-phase jet, *Fluid Dynamics*, **5** (1970), 333–338.

Leal, L. G., Particle motions in a viscous fluid, *Annual Reviews of Fluid Mechanics*, **12** (1980), 435–476.

Lee, S. L., and F. Durst, On the motion of particles in turbulent duct flows, *International Journal of Multiphase Flow*, **8** (1982), 125–146.

McTigue, D. F., Mixture theory for suspended sediment transport, *ASCE Journal of the Hydraulics Division*, **107**, HY6 (1981), 659–673.

McTigue, D. F., Mixture theory for turbulent diffusion of heavy particles, *Theory of Dispersed Multiphase Flow*, R. E. Meyer, ed., Academic Press, New York, 1983, 227–250.

McTigue, D. F., R. C. Givler, and J. W. Nunziato, Rheological effects of non-uniform particle distributions in dilute suspensions, *Journal of Rheology*, **30** (1986), 1053–1076.

Müller, I., A thermodynamic theory of mixtures of fluids, *Archive for Rational Mechanics*, **28** (1968), 1–39.

Nunziato, J. W., A multiphase mixture theory for fluid-particle flows, *Theory of Dispersed Multiphase Flow*, R. E. Meyer, ed., Academic Press, New York, 1983, 191–226.

Passman, S. L., Forces on the solid constituent in a multiphase flow, *Journal of Rheology*, **30** (1986), 1077–1083.

Passman, S. L., J. W. Nunziato, and E. K. Walsh, A theory for multiphase mixtures, *Rational Thermodynamics*, C. Truesdell, ed., Second Edition, Springer-Verlag, 1984, New York, 286–325.

Rubinow, S. I., and J. B. Keller, The transverse force on a spinning sphere moving in a viscous fluid, *Journal of Fluid Mechanics*, **11** (1961), 447–459.

Saffman, P. G., On the motion of small spherical particles in a viscous liquid, *Journal of Fluid Mechanics*, **1** (1956), 540–553.

Saffman, P. G., The lift of a small sphere in a slow shear flow, *Journal of Fluid Mechanics*, **22** (1965), 385–400; Corrigendum, **31** (1968), 624.

Scheiwiller, Thomas, Dynamics of powder snow avalanches, *Mitteilungen der Versuchsanstalt für Wasserbau, Hydrologie und Glaziologie*, no. 81, ETH, Zürich, 1986.

Segré, G., and A. Silberberg, Behaviour of macroscopic rigid spheres in poiseuille flow, part 2. Experimental results and interpretation, *Journal of Fluid Mechanics*, **14** (1962), 136–157.

Truesdell, C., Sulle basi della termomeccanica, *Accademia Nazionale dei Lincei, Rendiconti della Classe de Scienze Fisiche, Matematiche e Naturali*, **22** (1957), 33–88, 158–166.

Truesdell, C., *A First Course in Rational Continuum Mechanics*, Vol. 1, Academic, New York, 1977.

Truesdell, C., *Rational Thermodynamics*, Second Edition, Springer-Verlag, New York, 1984.

Vasseur, P. and R. G. Cox, The lateral migration of a spherical particle in two-dimensional shear flows, *Journal of Fluid Mechanics*, **78** (1976), 385–413.

TURBULENCE MODELING OF GAS-SOLID SUSPENSION FLOWS *

C. P. Chen

Department of Mechanical Engineering
The University of Alabama in Huntsville
Huntsville, Alabama

INTRODUCTION

Gas-solid two-phase flows occur commonly in many natural and industrial situations. Examples are blood flows, rocket exhaust plumes, pulverized coal gasification and combustion, and sediment transport by air and water. These flows are invariably turbulent and are characterized by the mutual coupling between the solid particles and the gas phase. Contrary to passive additives in a single-phase flow, the particles will change the flow structure of the carrying fluid. Globally, metering and heat transfer data [1,2,3] of two-phase flows shows discrepancy from the single-phase data. Further, small scale turbulence structures are also affected. Solid particles may attenuate the spreading rate and damp the turbulance intensity in a jet flow [5,6]. The alternation of the turbulence structure was found to depend on the particle size, the solid loading ratio as well as the physical properties of the different existing phases.

In general, a complete theoretical treatment of two-phase flows is not possible because of the lack of detailed understanding of the physical processes involved [7]. Previous analytical studies have not been very successful, due in part to a lack of knowledge about the turbulent flow field of the conveying gas which is a prerequisite to the solution of the two-phase flow problem. Difficulties in theoretical analysis also arise from the coupling between the two phases, i.e., the exchange of momentum, mass and energy between phases. These coupling phenomena comprise a very complex interaction which affects both the gas and particulate phases. Consideration of the infinite variety of interfacial geometries and flow regimes, various forms of non-equilibrium, and aggregation of particles complicates the problem even further.

The inability of the theoretical analysis to account for all the complicated interactions in two-phase flows is similar in the study of single-phase turbulent flows two decades or so ago. An exact theory of turbulence did not (and still does not) exist; however, using a combination of theoretical equations, modeling assumptions, and experimental evidence, mathematical models describing certain features of the flow were developed. The field of turbulence modeling has subsequently been developed to the point where single-phase turbulent flow fields can be predicted rather well using a variety of turbulence models of varying complexity [8,9]. These advances suggest that a similar combination of theory, experiment, and modeling could be used to develop computational models capable of predicting two-phase flows. However, extra sets of equations and correlations need to be formulated and modeled for turbulent gas-solid flows. The purpose of this

paper is to discuss and review the recent advances in two-phase turbulence modeling techniques and their applications in various gas-solid suspension flow situations. In addition to the turbulence closures, heat transfer effect, particle dispersion and wall effects are partially covered here.

APPROACHES AND GOVERNING EQUATIONS

Because of the intrinsic, complex coupling between different species in two-phase flows, there seems to be no "unified" set of governing equations that can completely describe the flow field of two-phase media. However, there are quite a number of different formulations in the literature from which to begin. One approach, the so called "discrete" or "tracking" approach, starts with an equation of motion for a single discrete particle in a turbulent fluid flow field and the particle's trajectory is calculated. For particles much smaller than the smallest scales (say Kolmogorov's microscale) of turbulent motion and for which the solid's material density is much greater than the conveying gas, the BBO equation (Basset, Boussinesq, Oseen), which is the momentum equation of a single particle, can be reduced to [10]:

$$\frac{d}{dt} v_i = \frac{1}{t_*} (u_i - v_i) + g_i \qquad (1)$$

Because the Eulerian velocity u_i is a stochastic quantity when the conveying gas flow is turbulent, this simple looking ODE cannot be solved analytically due to its inherent nonlinearity.

However, progress has been made using this approach in conjunction with the turbulence closure models which have been developed for single phase flows. The basic strategy is to use the turbulence model to calculate the fluid flow field assuming that no particles are present. This calculation is used to generate the velocity in equation (1) after making suitable assumptions regarding turbulent time scales, length scales and isotropy. To account for the mutual coupling (or the "two-way" coupling [11]) of mass, momentum, and energy between phases, the extra source terms generated by particles must be included in the Eulerian sets of governing equations for the gas phase. In the mean flow fields, this can be achieved by the iterative PSIC (particle-source-in-cell) technique developed by Crowe and co-workers [12,13] or by the non-iterative, transient numerical scheme of Dukowicz [14]. The discrete particle approach can also be extended to account for the particle-turbulence interactions which have two aspects -- the turbulent particle dispersion (the influence of fluid turbulence on the particles), and the "modulation" effect [15] (the effect of particles on fluid flow turbulence). These will be discussed in further detail in the next section.

In the non-discrete (continuum) approaches, two formulations are commonly used; the first considers the gas-solid suspension to be represented as a single inhomogeneous medium. The interactive forces between the phases are taken account of by internal stresses which must be related by constitutive equations to the bulk properties of the medium. Sets of governing equations for this approach were first formulated by

34

Barenblett [16] and described in detail in Monin and Yaglom [17]. This approach was also used recently in heat transfer analysis of a gas-particle pipe flow [18].

The other approach is the so-called "two-fluid" approach. This approach regards the gas and particles as two inter-penetrating continua in much the same way as the two species of a flowing binary mixture, for example. Here, the cloud of particles is regarded as a continuum and the governing equations are obtained by properly averaging the conservation equations over a volume and expressing the equations in differential forms. Many authors, namely Murray [19], Drew [20], Marble [21] and Ahmadi [22], have described the two-phase flow based on the two-fluid formulation and applied it to some physical processes. It is often not possible to formulate a general set of governing equations for gas-solid two-phase turbulent flows due to the lack of understanding and differences in interpretation of the physical processes involved (for example, the "solid-phase pressure" term [23]). In order to obtain theoretical relations of two-phase turbulent flows, several assumptions have to be invoked to simplify the formulation. These are:

1. The particle phase is dilute (volume fraction of particles, $\phi \ll 1$) and is made up of particles spherical in shape and uniform in size. The particle material density $\rho_s \gg \rho$, so that the model is valid when $\rho_p = \mathcal{O}(\rho)$. This assumption is required because we ignore particle-particle collisions, the frequency of which increase quadratically with loading. The uniformity of particle size reduces the book-keeping in the formulation; extension to poly-dispersed non-uniform size distribution is a straight forward matter for dilute suspensions.

2. Both the particulate and fluid phases behave macroscopically as continua. The fluid phase is Newtonian and both phases have constant physical properties and do not undergo any phase change. The continuum hypothesis assumes that the mathematical "points" are large enough to contain many particles and fluid molecules to ensure a stationary average. In order to satisfy the "dilute suspension" and continuum assumptions simultaneously for particle phases, some stringent restrictions regarding the number of particles in a smallest control volume made up of Kolmogorov microscale, the distance between particles to avoid direct inter-particle interactions, have been discussed [10,24,25]. However, the continuum approach has proven to be applicable also to situations which do not strictly meet such conditions [26].

3. The mean flow is steady and incompressible. Molecular diffusion, Brownian motion and gravity effects on the particulate phase are negligible compared with turbulent diffusion. Electrical and magnetic forces are not considered here.

With the above assumptions, we may adopt the governing equations developed by Marble [21,27] and Hinze [25] which are applicable to dilute gas-particle flows. Marble used statistical averages for the particle cloud and postulated the macroscopic governing equation for the gas phase. Continuity equations are written for each phase:

$$\frac{\partial \rho}{\partial t} + \frac{\partial}{\partial x_i} (\rho u_i) = 0 \qquad (2)$$

35

$$\frac{\partial \rho_p}{\partial t} + \frac{\partial}{\partial x_i}\left(\rho_p v_i\right) = 0 \tag{3}$$

Here ρ_p is the mass of particles per unit volume of mixture (or "density" of the particulate phase where $\rho_p = \rho_s \phi$, ϕ is the particulate phase volume fraction). The momentum conservation equations for each phase are:

$$\rho\,\frac{\partial u_i}{\partial t} + \rho u_j\,\frac{\partial u_i}{\partial x_j} = -\frac{\partial p}{\partial x_i} - \frac{\partial}{\partial x_j}\left(\tau_{ij}\right) + F_{pi} \tag{4}$$

$$\rho_p\,\frac{\partial v_i}{\partial t} + \rho_p v_j\,\frac{\partial v_i}{\partial x_j} = -F_{pi} \tag{5}$$

Here F_{pi} represents the force acting on the primary fluid per unit volume due to the presence of the particle. Note that due to dilute assumption, the multiplication of $(1 - \phi)$ by each term in equation (2) and (4) was replaced by 1. Of special note is that the values of u_i, ρ, P that appear in the continuum relations (2) and (4) are, in a sense, "smoothed" variables. The detailed gas disturbance caused by the particle motions are omitted from the instantaneous gas velocity vector u_i. Since the gas velocity varies strongly in the neighborhood of a particle that is moving through the gas, use of these smoothed variables in continuity, momentum and energy relations requires that all particle wakes or regions of immediate influence are dissipated very rapidly over the gas control volume. Hinze [25] treats this problem by attributing the forces around the particle as the external forces and disregarding the modified velocity field around the particles. If this external drag force follows Stokes law, then the fluid velocity u_i in the Stokes drag law is at "infinity", i.e., a large distance from the particle center so that the detailed fluid motion in the neighborhood of the particle is still not accounted for. However, the inadequacy of this model is not important for small volume fractions of particles having a not too large velocity relative to the gas. But for large volume fractions and cases in which particles may form into groups by trailing another in its wake, large regions of the flow may be inadequately modeled (c.f. [25] and [28]).

Several derivations concerning the two-fluid model equations have appeared in the literature. The derivations include those of Hinze [29], Soo [30], Drew and Segel [31], Ishii [32], Nunziato [33] and more recently, Roco and Shook [34]. The resulting equations differ in various ways such as the pressure gradient term for both gas and particulate phase, momentum source term, and shear stress tensor of the secondary phase although general constitutive equations relating stress and flow properties have not yet been developed. However, for the low concentration limit of suspension flows of small spherical particles, most of the derivations will recover similar forms. For example, the theory proposed by Ahmadi [35] which was general to the extent that it could be applied to both concentrated and dilute two-phase flows could be shown to recover the theory of dusty gas as derived by Saffman [36] in the low solid volume fraction range. The general expression for the internal forces between solid and continuous phase is discussed by Truesdell and Toupin [37] (also see [38]) and Drew and Segel [31]. The philosophical

reasons for using the two-fluid continuum approach and the common feature of dispersed two-phase flow systems can be seen in Drew's [20] review paper.

By performing the Reynolds decomposition and time averaging of equations (2) - (5), the following mean equations for statistically steady flows result.

$$\frac{\partial U_i}{\partial x_i} = 0 \tag{6}$$

$$\frac{\partial \bar{\rho_p} V_i}{\partial x_i} = - \frac{\partial}{\partial x_i} \overline{\rho_p' v_i'} \tag{7}$$

$$\rho U_j \frac{\partial U_i}{\partial x_j} = - \frac{\partial P}{\partial x_i} + \mu \frac{\partial^2 U_i}{\partial x_j \partial x_j} - \frac{1}{\rho} \frac{\partial}{\partial x_j} \overline{u_i' u_j'} + F_{pi} \tag{8}$$

$$\bar{\rho_p} V_j \frac{\partial V_i}{\partial x_j} = - \overline{\rho_p' v_j'} \frac{\partial V_i}{\partial x_j} - \frac{\partial}{\partial x_j} (\bar{\rho_p} \overline{v_i' v_j'}) - \frac{\partial}{\partial x_j} (V_j \overline{\rho_p' v_i'}) - F_{pi} \tag{9}$$

where some use of the continuity equations has been made in deriving equations (8) and (9). As a consequence of dilute suspension, triple correlations involving fluctuations in the particulate phase density are considered negligible. At this point the mean interaction term $\overline{F_{pi}}$ needs to be specified. Empirical expressions for the interaction terms have been summarized by [39] for low and moderate solids concentrations. The appropriate relationships are given by

$$\overline{F_{pi}} = \frac{1}{t_*} (1 + 0.179 \sqrt{Re_p} + 0.013 Re_p) \bar{\rho_p} (V_i - U_i) \tag{10}$$

$$+ \frac{1}{t_*} (1 + (^3/_2) 0.179 \sqrt{Re_p} + 0.113 \times 2 Re_p) \overline{\rho_p' (v_i' - u_i')}$$

where

$$Re_p = \frac{|U_i - V_i| \, d_p}{\nu} \tag{11}$$

and

$$t_* = d_p^2 \rho_s / 18 \rho \nu \tag{12}$$

We note that several turbulent correlations appear in equations (7) - (9) in addition to the conventional Reynolds stress $\overline{u_i' v_i'}$ for the single-phase flows. These terms arise from the velocity fluctuations and fluctuality volume fractions of the particulate phase and represent the turbulent momentum flux and mass flux of particles. To close the set of governing mean equations, models are required for these second order

correlations. The field of turbulence modeling for single-phase flows is a rapidly expanding one and will form the two-phase closure models described here.

TWO-PHASE TURBULENCE MODELING

The hierarchy of turbulence closure models has been received by Reynolds [40], and recently in [8,9]. The proposals range in complexity from zero equation models where the turbulent fluxes are modeled as if they were molecular fluxes, with an eddy diffusivity related to mean flow structures to Mean Reynolds Stress models where separate transport equations are solved for each component of the turbulent flux vectors and tensors. Most two-phase turbulence models follow the single-phase turbulence models for incompressible flows closely; their modeling is discussed in the following.

The most common and simplest modeling technique is to assume a Newtonian type constitutive equation for relating the turbulent fluxes to the mean field through an eddy viscosity. For gas phase Reynolds stresses,

$$\overline{u_i' v_j'} = - \nu_f S_{ij} + {}^2\!/_3\; \delta_{ij} k \tag{13}$$

where S_{ij} is the mean rate of strain tensor of gas flows $\dfrac{1}{2} \left(\dfrac{\partial U_i}{\partial x_j} + \dfrac{\partial U_j}{\partial x_i} \right)$

$k = {}^1\!/_2\; \overline{u_i' u_i'}$ and ν_f is the eddy viscosity.

Depending on the level of complexity employed, the eddy viscosity could be specified by zero-equation mixing length models, one-equation models or two-equation models. Due to the presence of solid particles, the eddy viscosity constructed by these models must take into account this effect.

ZERO-EQUATION MODELS

Early theoretical studies [41 - 43] indicate that the presence of solid particles decreases the eddy viscosity of the gas flows arising from dissipation of turbulence energy at the interface between solid particles and the fluid. These results lead several first-order closure schemes which modify the eddy viscosity for the clean gas flow without suspension of solid particles, ν_{f0}. For example, Owen [41] proposed

$$\frac{\nu_f}{\nu_{f0}} = \left(1 + \frac{\overline{\rho_p}}{\rho} \right)^{-\frac{1}{2}} \tag{14}$$

for the case $t_*/t_e \leq 1$ and

$$\frac{\nu_f}{\nu_{f0}} = \left[1 + \left(\frac{\overline{\rho_p}}{\rho} \right) \left(\frac{t_e}{t_*} \right) \right]^{-\frac{1}{2}} \tag{15}$$

for $t_e / t_* \geq 1$

This model has been used by Melville and Bray [44] for application in a turbulent free jet of dilute gas-particle mixture and has been further modified by Choi and Chung [45] and Chung et. al [46] for application in a wall-bounded shear flow. Most closure models developed at this level heavily involve empirical information and limiting case (loading ratio approaching zero) analysis and, in most cases, ignore the effect of particle size [47,48]. This level of models are very useful in engineering analysis because of their simple forms. However, they fail to handle some important effects, such as the "turbulence modulation", and besides, it is hard to prescribe the "mixing length" and the effect of particle on the mixing length scale. The next level of models, which incorporate a transport equation for the turbulence kinetic energy, and thus the velocity scale, were developed in the hope of providing additional generality and at the same time account for the effect of particles on the turbulence structure.

ONE-EQUATION MODEL

An equation describing the dynamics of the gas-phase turbulence kinetic energy can be derived from equations (4) and (8) by simple manipulations. For statistically steady, high Reynolds number flows it is given

$$U_i \frac{\partial k}{\partial x_i} = - \frac{\partial J_i}{\partial x_i} + P_k - \epsilon + \overline{u_i' F_{pi}} \qquad (16)$$

Here
$$P_k = - \overline{u_i' u_j'} \frac{\partial U_i}{\partial x_j}$$ is the rate of production of turbulence energy and

$$\epsilon = \nu \overline{\frac{\partial u_i'}{\partial x_j} \frac{\partial u_i'}{\partial x_j}}$$ is the rate of energy dissipation rate.

$$J_i = \frac{1}{2} \left(\overline{u_i' u_j' u_j'} + \frac{\overline{p' u_i'}}{\rho} - 2\nu \frac{\partial k}{\partial x_i} \right) \qquad \text{and}$$

$\overline{u_i' F_{pi}}$ the extra particle production (or dissipation) term, all per unit of mass. Probably the first attempt to use a one-equation turbulence model to study the two-phase flows is that of Dannon et. al [49]. They applied a k-ℓ closure model to a particle-laden axi-symmetric jet. The length scale ℓ was specified algebraically and was taken to be the same as that of a single-phase jet. For the k-equation (16), the diffusion term and production term were modeled following the conventional single-phase gradient-type modeling technique. In their study, quasi-equilibrium (i.e. $U_i \simeq V_i$) and mono-dispersed particles in Stokes regimes were assumed,

which simplify the interaction terms $F_{pi} = \dfrac{\rho_p(v_i - u_i)}{t_*}$ and the turbulence kinetic energy equation becomes

$$U_i \frac{\partial k}{\partial x_i} = \frac{\partial}{\partial x_i}\left(\frac{\nu_f}{\delta_k}\frac{\partial k}{\partial x_i}\right) + \nu_f \left(\frac{\partial U_i}{\partial x_j}\right)^2 - C_D \frac{k^{3/2}}{1}$$
$$+ \frac{\rho_p}{\rho}\frac{\overline{(u_i'v_i' - u_i'u_i')}}{t_*} + \frac{1}{\rho}\frac{\overline{\rho_p'u_i'(v_i' - u_i')}}{t_*} \qquad (17)$$

The triple correlation was neglected and the concern was the modeling of the additional dissipation term created by the particle slip velocity at the fluctuation level. This term is similar to the turbulence "modulation" effect attributed to the inability of dispersed-phase particles to completely follow turbulent eddy fluctuations at high frequency. This added dissipation mechanism has been experimentally observed [2,5,6,50,51] and has gained much attention in recent two-phase modeling studies.

The fluctuating velocity correlation of this term is bounded by

$$0 \leq -\overline{(u_i'v_i' - u_i'u_i')} \leq 2k \qquad (18)$$

where the two bounds represent the cases where particles completely follow the fluid $(u_i' = v_i')$ and stationary particles relative to the velocity fluctuation $(v_i' = 0)$. Dannon et. al [49] proposed a model that has the correct limiting behavior

$$-\overline{(u_i'v_i' - u_i'u_i')} = 2k\,[1 - \exp(-\beta(t_*/\tau))] \qquad (19)$$

where $\tau = (\nu/\epsilon)^{1/2}$ is the Kolmogorov time scale, and β is a model constant.

The use of the time scale τ was argued [52] to be inappropriate since the eddies contributing most to the correlation $\overline{u_i'u_i'}$ are the energetic eddies which have an integral time scale t_e. Dannon et. al [49] indicated that this model did not give good prediction due to a change in the structure of the turbulence and the structure was represented by the length scale. As a result, they had to arbitrarily modify the production and dissipation terms to reflect the structural variations. Due to the difficulty of specifying the length-scale distribution a priori in a flow and appropriate modeling for particle effect, most workers have abandoned one-equation models in favor of two-equation or even stress-equation models in which the length scale is computed from a transport equation.

40

TWO-EQUATION MODELS

Most studies in two-phase turbulence modeling utilizing a transport equation for the turbulence length scale ℓ' are based on a modeled equation of the isotropic dissipation rate ε; this equation can also be derived from equations (2), (4), (8) by appropriate differentiation, multiplication and averaging. The exact ε-equation consists of 67 terms with particle's effect accounted for [53]. For high Reynolds number flows and based on an order-of-magnitude analysis [54], the groups representing the production of ε by vortex stretching, the viscous destruction of ε, and the diffusive flux of ε in the X_i direction, which are not affected by particles, are usually modeled following the single-phase $k-\epsilon$ model of Jones and Launder [55]. The resulting modeled equation (except the extra particle destruction term) becomes

$$\frac{\partial}{\partial x_j} (U_j \epsilon) = \frac{\partial}{\partial x_j} \frac{\nu_t}{\delta_\epsilon} \frac{\partial \epsilon}{\partial x_j} - C_{\epsilon 1} \overline{u_i' u_j'} \frac{\partial U_i}{\partial x_j} \frac{\epsilon}{k} - C_{\epsilon 2} \frac{\epsilon^2}{k}$$

$$+ 2\nu \frac{\overline{\frac{\partial u_i'}{\partial x_k} \frac{\partial F_{pi}'}{\partial x_k}}}{} \frac{\overline{\rho_p}}{\rho} \qquad (20)$$

The last term in the RHS of the above equation is the contribution from interphase transport and is another main effort in two-phase modeling. This equation is solved simultaneous with the k-equation to estimate the eddy viscosity $\nu_t = C_\mu k^2/\epsilon$. Since the effects of particles are modeled through the k and ϵ equations, C_μ is assigned 0.09 same as the single phase flows.

In the two-equation model level, there have been several proposals for modeling the extra terms in the k and ϵ equation. Chen and Wood [52] basically followed [49] and proposed exponential forms for added dissipation terms in both the and equation. In the k equation, the correlation $\overline{u_i' v_i'}$ is modeled as

$$\overline{u_i' v_i'} = 2k \, \exp \, (-B_k \, t_*/t_e) \qquad (21)$$

where t_e is the time scale of the energetic eddies and in the context of the model is given by k and ϵ. t_e here has often been interpreted as the lifetime of a typical turbulence eddy by [56,57] in their Lagrangian calculations. The time ratio t_*/t_e is the Stokes number [12] measuring the response of how quick the particle responds to a typical eddy turnover. To generalize the model, the constant B_k was introduced and was determined by limiting behavior for small particles, which corresponded to the linear perturbation analysis with respect to a passive additive by [42]. A similar approach has been used by Pourahmadi and Humphrey [58] and Gavin et. al [59] in the k-equation. Their model for this term is summarized:

$$\overline{u_i' v_i'} = 2k \, / \, (1 + t_*/t_e) \qquad (22)$$

It can easily be shown, for small values of t_*/t_e, that this model yields the same results as equation (21), depending on the numerical value of B_k and the form assumed for t_e. Genchev and Karpuzov [60] assumed $t_* \gg t_e$ so that

$\overline{u_i'v_i'} = 0$ and no model was required. However they also assume that the particles will follow the mean fluid motion which implies $t_* << t_e$. This inconsistancy plus the lack of model comparisons with data in their paper casts doubt on their model.

The model of Elgobashi and Abou-Arab [53] for the correlation $\overline{u_i'v_i'}$ is based on Chao's [61] solution of the linearized Lagrangian equation of motion of a spherical particle in a turbulent flow. Their model, in its most general form, is extremely difficult to implement, especially for wall-bounded two-phase flows, owing to the necessity of computing definite integrals over all possible frequencies of fluid motion at every grid point. Given the uncertainties of the model it seems more appropriate to use a relatively simple model which exhibits the correct asymptotic behavior such as [52] and [58] (c.f. [62]).

As in modeling single-phase flows it is the ε-equation which provides the greatest uncertainty. In the model of Chen and Wood [26], particle-hydrodynamic drag force was assumed to follow Stokes law, thus the last term of equation (20) became

$$2\nu \, \frac{\overline{\rho_p}}{\rho} \, \overline{\frac{\partial u_i'}{\partial x_k} \frac{\partial F_{pi}'}{\partial x_k}} = \frac{2}{t_*} \frac{\overline{\rho_p}}{\rho} \left[\nu \, \overline{\frac{\partial u_i'}{\partial x_j} \left(\frac{\partial v_i'}{\partial x_j} - \frac{\partial u_i'}{\partial x_j} \right)} \right] \qquad (23)$$

A similar exponential model was proposed for this term as given by equation (19). A different time scale, i.e. Kolmogov's time scale τ, was used here in place of t_e since the eddies contributing most to the high frequency destruction mechanisms are the dissipative eddies which have a time scale $(\nu/\epsilon)^{1/2}$ [$\approx \tau$]. In [26] it was assumed that $\dfrac{\partial u_i'}{\partial x_j}$ and $\dfrac{\partial v_i'}{\partial x_j}$ are completely uncoupled on this time scale since $t_* >> \tau$ in most practical gas-solid turbulent flows. In this limit equation (23) becomes $(2\epsilon/t_*)(\overline{\rho_p}/\rho)$ Clearly this model is not correct for very small particles or if $t_* = \Theta(\tau)$ In the model of [58] an additional term is added but it assumes that the added sink of dissipation to be a function of the integral time scale t_e and hence does not seem to be particularly appropriate. The extra sink and destruction of ϵ are modeled collectively by [53] as $c_{\epsilon 2} \, \epsilon_t \, (\epsilon/t)$ in equation (20) where ϵ_t equals ϵ plus the extra dissipation terms appearing in the k-equation and $c_{\epsilon 2}$ is kept the same constant as in the single-phase flows.

DISPERSION OF SUSPENDED SOLID PARTICLES

Extremely small particles which behave like trace molecules can be treated as "passive" contaminants in the turbulent flow field. The behavior of clouds of particles may be extended from single-particle dynamics when the mixture is very dilute, say, the volume fraction of solid $< \Theta(10^{-2})$(c.f. [7]). The subject of passive additive transport has been treated extensively in the text of Monin and Yaglom [17]. See also the book by Hinze [63] and the review paper by Launder [64]. However, as the particle size increases, dispersion will be opposed by particle inertia and so once some critical particle size is exceeded, discrete particle dispersion must be treated in a different way from "passive" contaminant diffusion.

For dilute suspensions, the particle trajectories can be calculated by the tracking approach. In this approach, particle dispersion due to turbulence has been modeled by random walk [65] or a Monte-Carlo Stochastic method [14,66]. These methods usually require extensive computational storage and time to achieve a stationary average. In some Lagrangian approaches, certain types of diffusional velocity have been modeled for the particle motion which is usually proportional to the concentration gradient [67,68]. In the two-fluid approach, particle dispersion due to turbulence is represented by the correlations   and/or   . In lower level closures, these are usually modeled as a gradient type, Fickian diffusion process:

$$\overline{\rho_p{}'u_i{}'} = D_t \frac{\partial \overline{\rho_p}}{\partial x_i} \quad \text{and} \quad \overline{\rho_p{}'v_i{}'} = D_p \frac{\partial \overline{\rho_p}}{\partial x_i} \tag{24}$$

This constitutive equation is arbitrary at this point; however it may be justified theoretically under certain conditions [17].

Values of D_t and D_p are calculated by the value of eddy viscosity ν_f in most models by introducing the turbulent Schmidt numbers. Thus $D_t = \nu_f/Sc_t$ and $D_p = \nu_f/Sc_p$ or $D_p = \nu_p/Sc_p$, where ν_p is the effective eddy viscosity of the dispersed phase (to be discussed later). This type of phenomenological approach for diffusion process heavily relies on the classical theory of "fluid point" diffusion of Taylor (c.f. [63]). However, when particle size increases, discrete particle diffusion is opposed by particle inertia and the crossing-trajectories effect [69,70]. Since heavier particles have the tendency to "fall out" from one eddy to another, the correlations between particles and fluid velocities decrease. The effect is to decrease the particle dispersion. The effect of the particle inertia is not that clear. The inertia effect is characterized by the particle relaxation time t_*, which is controlled by the physical properties of particles and the fluid, and the flow characteristics. There have been arguments concerning the characteristic flow time scales [71,72,73] for turbulent dispersion, although it has been indicated that the diffusivity of the heavy particles is a little larger than that of the light particles. Higher-order modelings such as the one developed by [74] are able to predict this behavior. In the context of the lower-order phenomenological technique just mentioned, the Schmidt number should be modeled taking into account these effects. Recently one such model has been developed including a constant drift velocity [75]

$$D_p = 1 / (1 + 0.3 |U_i - V_i|^2 / \overline{V_j{}'V_j{}'})^{1/2} \tag{25}$$

in which the coefficient 0.3 was tuned based on the lateral dispersion of solid particles and measurements of [71,73].

However, in most models [26,53,58] the turbulent Schmidt number was simply set to some constant value following the turbulent mass transfer of a passive additive [76]. Some experimental data for gas-solid jets [77] however indicate that a constant value of Sc_t (i.e. independent of loading) is appropriate. For axi-symmetric flows, $Sc_t = Sc_p = 0.7$ is used [52,78]. In [53,58], the turbulent Schmidt number was simply chosen to be one.

Finally, due to the continuum formulation, the correlation $\overline{v_i'v_j'}$ has to be modeled. Following the gradient type model for the gas phase, this turbulent stress in the particulate phase is modeled from the Boussinesq assumption:

$$\overline{v_i'v_j'} = - \nu_p \left(\frac{\partial V_i}{\partial x_j} + \frac{\partial V_j}{\partial x_i} \right) + \frac{2}{3} \delta_{ij} \left(k_p + \nu_p \frac{\partial V}{\partial x} \right) \qquad (26)$$

Earlier analytical studies [79,80] have contributed to the understanding of some of the basic mechanisms of indirect interaction between particles through the surrounding particles. This has lead Melville and Bray [44] in their zero-equation modeling to propose

$$\frac{\nu_p}{\nu_t} = 1 / (1 + t_*/t_e) \qquad (27)$$

Similar models have been used by [46,52] although the evaluation of t_e is somewhat different. Alonso [81] reviewed some developments in determining ν_p and recommended the use of Peskins [82] formula

$$\frac{\nu_p}{\nu_t} = 1 - (T_L^2 \epsilon/15\nu) (3K^2 / (K + 2)) \qquad (28)$$

when $K = 2t_*/T_L$ and $T_L \simeq k/\epsilon$. This model has been used by [58,83]. Although this model recovers the correct form in the limit $t_* \to 0$ (i.e. $\nu_p = \nu_t$) as equation (27), it will yield negative value of ν_p for reasonable values of t_*, τ and T_L taken from pipe flow data. It is not likely that $\nu_p < 0$ is physically appropriate, casting doubt on this model.

The modeling technique discussed above based on the continuum approach, especially the modification of k and ϵ equation, has been extended and adopted in some Lagrangian formulations. It has been shown by Shuen et. al [6] that using the stochastic formulation instantaneous properties are known; therefore, the extra dissipation term due to particles in the k equation is exact and requires no modeling. This calculation is rather complex and recently Mostafa and Mongia [75,91] have utilized the continuum two-phase model of [58] to model this term in Lagrangian calculations. A similar approach has been taken by [84] which highly simplified the stochastic calculations. The extra sink term in the ϵ-equation is not closed in Monte-Carlo stochastic formulation and is modeled through a gradient type model in [6]. The sensitivity of this term has been tested recently [85] and it has been found that this term is important in conjunction with the modulation term in the k-equation. Incorporation of the effects of particle on turbulence scale and the response of the dispersed phase in two-phase turbulence models is essential for representing the structure of particle-laden turbulent flows.

44

For wall-bounded flows, boundary conditions for both gas and particulate phases are required. This is particularly important when other transport processes such as heat transfer and erosion are involved. The effect of particles on boundary layer and viscous sublayer flows has been studied analytically [10,86]. In most calculations, it is assumed that the influence of the particulate phase on the velocity defect law is to modify the logarithmic law in sublayer. Based on the Monin-Obakhov similarity analysis for the analogous stable stratified atmospheric boundary layer, a set of "wall functions" taking into account the effects of particle size and loading was used by Chen [87]. The logarithm profile was modified as

$$\frac{U}{U_*} = \frac{1}{\kappa} \ln [y^+] + \beta \frac{\overline{\rho_p}}{\rho} R_f \qquad (29)$$

with $\beta \simeq 5$ and particulate flux Richardson number

$$R_f = \overline{u_i{}'F_{pi}{}'} \Bigg/ \left(- \overline{u_i{}'u_j{}'} \frac{\partial U_i}{\partial x_j} \right) \qquad (30)$$

The wall shear stress of the two-phase flow is related to that of the single-phase flow by (c.f. [10]).

$$\frac{\tau_w}{\tau_{w0}} = 1 + \frac{\overline{\rho_p}}{\rho} \qquad (31)$$

The wall boundary conditions for particulate phase are complicated by the unsteady particle-wall interactions such as deposition of particles on the wall and re-entrainment mechanism. The resulting piece of information from a multitude of particle-wall interactions can be assessed as the slip velocity for the particulate phase at the wall [88,89]. An expression for the slip velocity and wall shear stress was suggested by Soo [88] based on rarefied gas-dynamics theories. The lack of particle-particle interaction, in accordance with the dilute suspension assumption gives a wall slip velocity:

$$V|_w = \ell_p \cdot \frac{\partial V}{\partial n} \bigg|_w \qquad (32)$$

and stress

$$\tau_p|_w = \frac{1}{2\sqrt{\pi}} \overline{\rho_p} V \frac{2}{3} (\overline{v_i{}'v_i{}'})^{1/2} \bigg|_w \qquad (33)$$

where the fluid-particle interaction length $\ell_p{}'$is given

$$\ell_p' = [\overline{(u_i' - v_i')^2}]^{1/2} t_*$$

and v_y is set to be zero at the wall following an impermeable wall condition for particles. These expressions have been utilized by [58,87] for their wall-bounded calculations. The effect of the walls on the particle drag coefficient, the particle turbulent intensity and the correlation $\overline{u_i'v_i'}$ and $\overline{u_i'(u_i' - v_i')}$, which represent the particle-gas interaction and contribute to the modulation of the wall turbulence structures, has been studied recently by Risk and Elghobashi [90] by including Magnus force and lifting force in the particle dynamic equation. Their analysis can be incorporated for detailed gas-particle wall function development.

SUMMARY AND DISCUSSION

Recent developments of two-phase turbulence models were reviewed. Most existing models are constructed following the familiar form of single-phase turbulence models. As in single-phase problems, most models are addressed through classical Boussinesq gradient-type diffusion processes and scaling arguments. Most models are also developed based on the treatment of turbulent suspensions in the context of the continuum, two-fluid theory of mixtures.

The appeal of the two-phase closure technique embedded in the two-fluid continuum formulation is that it provides an axiomatic approach on which the analogous single-phase turbulence models are built. In practice, one is confronted with the difficulty of constructing specific constitutive models for the stresses and momentum transfer, turbulent mass fluxes and mass transport in which additional fluctuating fields are magnified by the presence of solid particles. Following the modeling approach in single-phase flows, for simple flows (such as free shear flows) most two-phase models were addressed through classical Boussinesq assumptions and characteristic scaling arguments. Depending on the relaxation time scales, particles not only influence the higher wave number end of the gas-phase turbulence spectrum [10,25], but also the energy-containing range of the turbulence spectrum which is largely responsible for mixing [72,73]. Most proposals for treating turbulence modulations based on the two-equation $k-\epsilon$ model were not particularly successful for complex flows since they did not incorporate the turbulence scale effects and the response of the dispersed phase. Higher-order closure schemes or closures involving multiple-scale characterization of the gas turbulent spectrum are obviously called for, and some steps in this direction have been taken recently [74,87]. Additional measurements similar to that of [72,73] are also needed to gain a better understanding of particle-turbulence scale interactions and modulations in multiphase flows.

The real challenge and difficulty in developing a two-phase closure model for particle dispersion in connection with the two-fluid formulation is encountered in wall-bounded flows and poly-dispersed systems. Establishment of wall boundary conditions for the particle concentration and velocities depend on the interaction of particles with the wall. Particle-wall collisions are not always elastic and the phenomena is unsteady. The slip velocity boundary condition based on rarefied gas dynamics concepts is

probably not appropriate since the normal component of averaged velocity is not zero. Detailed measurements [92,93] and analysis [93,94] are needed. To extend the two-fluid continuum mixture theory for poly-dispersed situations, the continuous droplet models such as the one described in [95] can be used. The particles are represented by a statistical distribution function in a multi-dimensional space of droplet size, velocity location and time. The properties of particles are determined by solving the conservation of the distribution function.

One merit of the two-phase turbulence models developed on the continuum formulation is that they can be accommodated into the Lagrangian approach and do not require excessive computational storage and time [75,84]. Incorporation of more physics as turbulent combustion, evaporating sprays, boundary layer dust ingestion, poses no conceptual difficulties. Further testing and validation through well-defined experiments for more complex flows to establish the universality of the model constants are highly recommended.

REFERENCES

1. Lee, S.L. and Durst, F., "On the Motion of Particles in Turbulent Duct Flows," Int. J. Multiphase Flow, 8, 125, 1982.

2. Tsuji, Y., Morikawa, Y. and Shiomi, H., "LDV Measurements of an Air-Solid Two-Phase Flow in a Vertical Pipe," J. Fluid Mech., 139, 417, 1984.

3. Depew, C.A. and Kramer, T.J., "Heat Transfer to Flowing Gas-Solid Mixtures," Adv. Heat Transfer, 9, 113, 1973.

4. Hishida, K. et. al, "Heat Transfer to Plane Wall Jet in Gas-Solid Two-Phase Flow," Heat Transfer 1986, IHTC, 5, 2385, 1986.

5. Moderrass, D., Tan, H. and Elghobashi, S.E., "Two-Component LDA Measurement in a Two-Phase Turbulent Jet," AIAA J., 22, 624, 1984.

6. Shuen, J-S., et. al, "Structure of Particle-Laden Jets: Measurements and Predictions," AIAA J., 23, 396, 1985.

7. Soo, S.L., Fluid Dynamics of Multiphase Systems, Waltham, MA: Blaisdell Publishing Company, 1978.

8. Kline, S.J., Cantwell, B.J. and Lilley, G.M., eds., The 1980-1981 AFOSR-HTTM Stanford Conference on Complex Turbulent Flows, Stanford, California, 1981.

9. Lakshminarayana, B., "Turbulence Modeling for Complex Flows," AIAA J., 24, 1900, 1986.

10. Lumley, J.L., "Two-Phase and Non-Newtonian Flows," Chapter 7 in Turbulence, ed. P. Bradshaw, Berlin: Springer-Verlag, 1978.

11. Digiacinto, M., Sabetta, F. and Pira, F., "Two-Way Coupling Effects in Dilute Gas-Particle Flows," ASME-J. Fluid Eng., 104, 304, 1982.

12. Crowe, C.T., "Review - Numerical Models for Dilute Gas-Particle Flow," J. Fluid Eng., 104, 297, 1982.

13. Crowe, C.T., Sharma, M.P. and Stock, D.E., "The Particle-Source-in-Cell Method for Gas Droplet Flow," J. Fluid Eng., 99, 325, 1977.

14. Dukowicz, J.K., "A Particle-Fluid Numerical Model for Liquid Sprays," J. Comp. Physics, 35, 229, 1980.

15. AlTaweel, A.M. and Landau, J., "Turbulence Modulation in Two-Phase Jets," Int. J. Multiphase Flow, 3, 341, 1977.

16. Barenblett, G.I., "Motion of Suspended Particles in a Turbulent Flow," Prikl. Matem. Mekh., 17, 261, 1953.

17. Monin, A.S. and Yaglom, A.M., Statistical Fluid Mechanics: Mechanics of Turbulence, Vol. 1, Cambridge, MIT Press, 1971.

18. Michaelides, E.E., "Heat Transfer in Particulate Flows," Int. J. Heat Mass Transfer, 29, 265, 1986.

19. Murray, J.D., "On the Mathematics of Fluidization," J. Fluid Mech., 21, 3, 1965.

20. Drew, D.A., "Mathematical Modeling of Two-Phase Flow," Ann. Rev. Fluid Mech., 15, 261, 1983.

21. Marble, F.E., "Dynamics of a Gas Containing Small Solid Particles," Proc. 5th AGARD Combustion and Propulsion Symp., NY: Pergamon, 1963.

22. Ahmadi, G., "A Generalized Continuum Theory for Multiphase Suspension Flows," Int. J. Eng. Sci., 23, 1, 1985.

23. Givler, R.C., "An Interpretation for the Solid-Phase Pressure in Slow, Fluid-Particle Flows," Int. J. Multiphase Flow, 13, 717, 1987.

24. Reif, F., Fundamentals of Statistics and Thermal Physics, McGraw-Hill, 1965.

25. Hinze, J.O., "Turbulent Fluid and Particle Interaction," Prog. Heat Mass Transfer, 6, ed. G. Hestroni, Pergamon, 1972.

26. Chen, C.P. and Wood, P.E., "Turbulence Closure Modeling of Two-Phase Flows," Chem. Eng. Comm., 29, 291, 1984.

27. Marble, F.E., "Dynamics of Dusty Gases," Ann. Rev. Fluid Mech., 2, 397, 1970.

28. Abramovich, G.N., "Effect of Solid-Particles on Droplet Admixture on the Structure of a Turbulent Gas Jet," Int. J. Heat Mass Transfer, 14, 1039, 1971.

29. Hinze, J.O., "Momentum and Mechanical Energy Balance Equations for a Flowing Homogeneous Suspension with Slip Between the Two Phases," Appl. Sci. Res., 11A, 33, 1963.

30. Soo, S.L., "Equations of Multiphase Multidomain Mechanics," Multiphase Transport, ed. Veziroglu, Hemisphere, 1, 291, 1980.

31. Drew, D.A., and Segel, L.A., "Averaged Equation for Two-Phase Flows," Studies in Appl. Math, L, 205, 1971.

32. Ishii, M., Thermo-Fluid Dynamic Theory of Two Phase Flow, Eyrolles, France, 1975.

33. Nunziato, J.W., "A Multiphase Mixture Theory for Fluid-Particle Flows," Theory of Dispersed Multiphase Flow, R.E. Meyer ed., Academic Press, NY, 191, 1983.

34. Roco, M.C. and Shook, C.A., "Turbulent Flow of Incompressible Mixture," J. Fluids Eng., 107, 224, 1985.

35. Ahmadi, G., "A Continuum Theory for Two Phase Media," Acta Mechanica, 44, 299, 1982.

36. Saffman, P.G., "On the Stability of Laminar Flow of a Dusty Gas," J. Fluid Mech., 13, 120, 1962.

37. Truesdell, C. and Toupin, R., "The Classical Field Theories," in Encyclopedia of Physics, Vol. III/1, 226, Berlin: Springer-Verlag, 1960.

38. Truesdell, C., Rational Thermodynamics, 2nd ed., Springer-Verlag, 1984.

39. Clift, R., Grace, J.R. and Weber, M.E., Bubbles, Drops and Particles, Academic Press, 1978.

40. Reynolds, W.C., "Computation of Turbulent Flows," Ann. Rev. Fluid Mech., 8, 183, 1976.

41. Owen, P.R., "Pneumatic Transport," J. Fluid Mech., 39, 407, 1969.

42. Kuchanov, S.I. and Levich, V.G., "Energy Dissipation in a Turbulent Gas Containing Suspended Particles," Soviet Physics - Doklady, 12, 549, 1967.

43. Abramovich, G.N., "Effect of Solid-Particle or Droplet Admixture on the Structure of a Turbulent Gas Jet," Int. J. Heat Mass Transfer, 14, 1039, 1971.

44. Melville, W.K. and Bray, K.N.C., "A Model of the Two-Phase Turbulent Jet," Int. J. Heat Mass Transfer, 22, 647, 1979.

45. Choi, Y.D. and Chung, M.K., "Analysis of Turbulent Gas-Solid Suspension Flow in a Pipe," J. Fluid Eng., 105 329, 1983,

46. Chung, M.K., Sung, H.J. and Lee, K.B., "Computational Study of Turbulent Gas-Particle Flow in a Venturi," J. Fluid Eng., 108, 248, 1986.

47. Michaelides, E.E., "A Model for the Flow of Solid Particles in Gases," Int. J. Mult. Flow, 10, 61, 1984.

48. Lodes, A. and Mierka, D., "Local Phenomenological Properties of Turbulence in the Suspension Flow of Solid Particle-Gas System," ChE Sci, 42, 397, 1987.

49. Dannon, H., Wolfshtein, M. and Hestroni, G., "Numerical Calculations of Two-Phase Turbulent Round Jet," Int. J. Multiphase Flow, 3, 223, 1977.

50. Hestroni, G. and Sokolov, M., "Distribution of Mass, Velocity and Intensity of Turbulence in a Two-Phase Turbulent Jet," J. Applied Mech., 38, 315, 1971.

51. Fleckhaus, D., Hishida, K. and Maeda, M., "Effect of Laden Solid Particles on the Turbulent Flow Structure of a Round Free Jet," Exp. in Fluids, 5, 323, 1987.

52. Chen, C.P. and Wood, P.E., "A Turbulence Closure Modeling for Dilute Gas-Particle Flows," The Can. J. ChE, 63, 349, 1985.

53. Elghobashi, S.E. and Abou-Arab, T.W., "A Two-Equation Turbulence Closure for Two-Phase Flows," Phys. Fluids, 26, 931, 1983.

54. Tennekes, H. and Lumley, J.L., A First Course in Turbulence, Cambridge, MIT Press, 1972.

55. Jones, W.P. and Launder, B.E., "The Prediction of Laminarization with a Two-Equation Model of Turbulence," Int. J. Heat Mass Transfer, 15, 301, 1972.

56. Shuen, J.S., Chen L-D and Faeth, G.M., "Evaluation of a Stochastic Model of Particle Dispersion in a Turbulent Round Jet," AIChE J., 29, 167, 1983.

57. Weber, R., Boysan, F., Ayers, W.H., and Swithenbank, J., "Simulation of Dispersion of Heavy Particles in Confined Turbulent Flows," AIChE J., 30, 490, 1984.

58. Pourahmadi, F. and Humphrey, J.A.C., "Modeling Solid-Fluid Turbulent Flows . . .," Physico Chem. Hydro, 4, 141, 1983.

59. Gavin, L.B., Naumov, V.A. and Nikulin, N.M., "Use of an Equation Describing the Transport of the Energy . . .," Fluid Dynamics, $\underline{16}$, 34, 1983.

60. Genchev, Z.D. and Karpunov, D.S., "Effects of the Motion of Dust Particles on Turbulence Transport Equations," J. Fluid Mech., $\underline{101}$, 833, 1980.

61. Chao, B.T., "Turbulent Transport Behavior of Small Particles in Dilute Suspensions," Osterreich. Ing. - Archiv, $\underline{18}$, 1, 1964.

62. Mostafa, A.A. and Mongia, H.C., "On the Turbulence-Particles Interaction in Turbulent Two-Phase Flows," AIAA-86-0215, 1986.

63. Hinze, J.O., Turbulence, 2nd ed., McGraw-Hill, NY, 1975.

64. Launder, B., "Heat and Mass Transport," in Turbulence, ed. P. Bradshaw, 231, Springer-Verlag, 1978.

65. Hutchinson, P., Hewitt, G.F. and Dukler, A.E., "Deposition of Liquid or Solid Suspensions from Turbulent Gas Stream: A Stochastic Model," Chem. Eng. Sci., $\underline{26}$, 419, 1971.

66. Gosman, A.D. and Ioannides, E., "Aspects of Computer Simulation of Liquid Rocket Combustion Chamber," J. Energy, $\underline{7}$, 482, 1983.

67. Jurewicz, J.T. and Stock, D.E., "A Numerical Model for Turbulent Diffusion in Gas-Particle Flow," ASME, paper 76-WA/FE-33, 1976.

68. Smith, P.J., Fletcher, T.H. and Smoot, L.D., "Model for Pulverized Coal-Fired Reactors," 18th Sym. on Combustion, 1285, The Comb. Inst., 1981.

69. Yudine, M.I., "Physical Consideration of Heavy-Particle Diffusion," Advances in Geophysics, $\underline{6}$, 185, 1959.

70. Csanady, G.T., "Turbulent Diffusion of Heavy Particles in the Atmosphere," J. Atmosph. Sci., $\underline{20}$, 201, 1963.

71. Snyder, W.H. and Lumley, J.L., "Some Measurements of Particles Velocity Autocorrelation Function in Turbulent Flow," J. Fluid Mech., $\underline{48}$, 41, 1971.

72. Calabrese, R.V. and Middleman, S., "The Dispersion of Discrete Particles in a Turbulent Fluid Field," AIChE J., $\underline{25}$, 1025, 1979.

73. Wells, M.R. and Stock, D.E., "The Effect of Crossing Trajectories on the Dispersion of Particles in Turbulent Fluid," J. Fluid Mech., $\underline{136}$, 31, 1983.

74. Shih, T-H and Lumley, J.L., "Second-Order Modelling of Particle Dispersion in a Turbulent Flow," J. Fluid Mech., $\underline{163}$, 349, 1986.

75. Mostafa, A.A. and Mongia, H.C., "On the Modeling of Turbulent Evaporating Sprays: Eulerian Versus Lagrangian Approach," Int. J. Heat Mass Transfer, 30, 2583, 1987.

76. Reynolds, A.J., "The Variation of Turbulent Prandtl and Schmidt Numbers in Wakes and Jets," Int. J. Heat Mass Transfer, 19, 757, 1976.

77. Subramanian, V. and Ganesh, R., "Particle-Gas Dispersion Effects in a Round Jet," Can. J. Chem. Eng., 62, 161, 1984.

78. Lee, K.B. and Chung, M.K., "Refinement of the Mixing-Length Model for Prediction of Gas-Particle Flow in a Pipe," 13, 275, 1987.

79. Hjelmfelt, A.T. and Morkos, L.F., "Motion of Discrete Particles in a Turbulent Fluid," Appl. Sci. Res., 16, 149, 1966.

80. Meek, C.C. and Jones, B.G., "Studies of the Behavior of Heavy Particles in a Turbulent Fluid Flow," J. of Atmo. Sci., 30, 239, 1973.

81. Alonso, C.V., "Stochastic Models of Suspended Sediment Dispersion," J. Hydraulics Division - Proc. ASCE, 107, No. HY6, 733, 1981.

82. Peskin, R.L., "Stochastic Estimation Applications to Turbulent Diffusion," Int. Symp. on Stochastic Diffusion, ed. C.L. Chiu, 251, U. of Pittsburgh, 1971.

83. Elghobashi, S., Abou-Arab, T., Rizk, M. and Mostafa, A., "Prediction of the Particle-Laden Jet with a Two-Equation Turbulence Model," Int. J. Multiphase Flow, 10, 697, 1984.

84. Adenijo-Fashola, A.A. and Chen, C.P., "Comprehensive Modeling of Turbulent Particulate Flows Using Eulerian and Lagrangian Schemes," AIAA paper 87-1347, 1987.

85. Parthasarathy, R.N. and Faeth, G.M., "Structure of Particle-Laden Turbulent Water Jets in Still Water," Int. J. Multiphase Flow, 13, 699, 1987.

86. Boothroyd, R.G. and Walton, P.J., "Fully Developed Turbulent Boundary-Layer Flow of a Fine Particle Gaseous Suspension," Ind. Eng. ChE Fund., 12, 75, 1973.

87. Chen, C.P., "Numerical Analysis of Confined Recirculating Gas-Solid Turbulent Flows," Gas-Solid Flows - 1986, ASME FED, 35, 117, 1986.

88. Soo, S.L., "Development of Theories on Liquid Solid Flows," J. Pipeline, 4, 137, 1984.

89. Klinzing, G.E., "Particle-Wall Interactions as Related to Slip Velocties," Chem. Eng. Commun., 35, 223, 1985.

90. Rizk, M.A. and Elghobashi, S.E., "The Motion of a Spherical Particle Suspended in a Turbulent Flow Near a Plane Wall," Phys. Fluid, 23, 806, 1985.

91. Mostafa, A.A., Mongia, H.C., McDonell, V.G. and Samulsen, G.S., "On the Evolution of Particle-Laden Coaxial Jet Flows: A Theoretical and Experimental Study," AIAA paper 88-0239, 1988.

92. Chamberlain, A.C., Garland, J.A. and Wells, A.C., "Transport of Gases and Particles to Surfaces with Widely Spaced Roughness Elements," B-L Meteorology, 29, 343, 1984.

93. Papavergos, P.G. and Hedley, A.B., "Particle Deposition Behavior from Turbulent Flows," Chem. Eng. Rev. Dev., 62, 275, 1984.

94. Tsuji, Y., Morikawa, Y. et. al, "Numerical Simulation of Gas-Solid Two-Phase Flow in a Two-Dimensional Horizontal Channel," Int. J. Multiphase Flow, 13, 671, 1987.

95. Travis, J.R., Harlow, F.H. and Amsden, A.A., "Numerical Calculation of Two-Phase Flows," Nucl. Sci. and Eng., 61, 1, 1976.

CONFINED TURBULENT FLUID-PARTICLE FLOW MODELING USING MULTIPLE-REALIZATION PARTICLE TRAJECTORY SCHEMES

A. A. Adeniji - Fashola

NRC Research Associate
NASA - Marshall Space Flight Center
Huntsville, AL. 35812

ABSTRACT

A multiple-realization particle trajectory scheme has been developed and applied to the numerical prediction of confined turbulent fluid-particle flows. The example flows investigated include the vertical pipe upflow experimental data of Tsuji et al. and the experimental data of Leavitt for a coaxial jet flow, comprising a particle-laden central jet and a clean annular jet, into a large recirculation chamber. The results obtained from the numerical scheme agree well with the experimental data lending confidence to the modeling approach. The multiple-realization particle trajectory turbulent flow modeling scheme is believed to be a more elegant and accurate approach to the extension of single-particle hydrodynamics to dilute multi-particle systems than the more commonly employed two-fluid modeling approach. It is also better able to incorporate additional force terms such as lift, virtual mass and Bassett history terms directly into the particle equation of motion as appropriate. This makes it a suitable candidate for particle migration studies and an extension to situations involving liquid particulate phases with possible propulsion applications, such as in spray combustion, follows naturally.

INTRODUCTION

Turbulent fluid-particle flows are encountered in numerous technological applications such as fluidized-bed combustors and pulverized coal gasifiers and combustors as well as in atmospheric studies involving the dispersion of pollutants. The modeling of such turbulent flows involving the presence of a dispersed phase made up of small, light particles further complicates the already complex phenomena encountered in single phase turbulent flows. However, the need to optimize the design process in technological applications involving turbulent fluid-particle flows or enhance the prediction accuracy of atmospheric dispersion models makes it impossible to avoid the quest for a deeper understanding of the fundamental problems. Besides, the various interacting complex phenomena encountered in the modeling of this class of flows offer a very rich source of challenges to the fluid flow researcher.

The propulsion systems for space transportation vehicles, in particular the liquid-fueled variety, will benefit directly from an improvement in the modeling of turbulent fluid-particle flows. This is because such an improvement will translate to a better understanding of the mixing and combustion phenomena in spray combustion processes. Turbulent fluid-particle flows involving solid particles are simpler to model than fluid-droplet or fluid-bubble flows due to the added degrees of freedom in the latter associated with the deformation of the discrete entities of such a dispersed fluid phase. A study of turbulent fluid-solid particle flows is thus useful in eliminating the effects of the breakup or coalescence of droplets and bubbles from other particle-turbulence interactions encountered in such flows.

The two common approaches adopted in the literature for the modeling of two-phase flows are the homogeneous and the separated models. The former is applicable to situations in which the mean slip between the phases is small and the design parameters of interest are of the bulk variety such as the pressure drop or mass fluxes. In situations where more detailed information about intra- or inter-phase behavior is of interest, or where there is substantial segregation of the phases, the separated two-phase models are invariably preferred. For such flows, another major decision has to be made with regard to the scheme for the description of the dispersed phase - whether to adopt an Eulerian or a Lagrangian approach. Important considerations necessary for deciding which approach to adopt include the concentration of the dispersed phase which influences the mean separation distance between particles. The relative magnitudes of this length scale as well as the particle size and the microscale of the underlying turbulence in the continuous phase help to determine whether the dispersed phase can be treated as a continuum and thus described using the Eulerian approach or whether a Lagrangian description of the dispersed phase will be more appropriate.

In the following, we present a discussion of turbulent fluid-particle flow

modeling in which the continuous phase is described using the continuum Eulerian approach while a Lagrangian description is adopted for the dispersed phase. We shall restrict ourselves to confined flows and thus include a discussion of the treatment of solid boundaries using the Eulerian - Lagrangian scheme.

2. PARTICLE TRAJECTORY SCHEMES

In the Eulerian - Lagrangian modeling of two-phase flows, the continuous fluid phase is described using the standard single phase continuum equations. However, the dispersed phase is modeled by computing for individual particles the trajectories and temperature histories where appropriate. The dispersed phase velocity and temperature fields are subsequently obtained from information obtained from the realization of a sufficiently large ensemble of particle trajectories.

The use of a particle trajectory scheme in the modeling of turbulent fluid-particle flows represents only a subset in the field of computer simulation using particles as discussed by Hockney and Eastwood [1981]. Other important applications particle schemes discussed by Hockney and Eastwood include the modeling of covalent and ionic liquids, stellar and galaxy clusters, plasma and semiconductor devices.

In fluid dynamic applications, the Particle-In-Cell (PIC) method of Harlow [1964] and, later, the Particle-Source-In Cell (PSI-Cell) method of Crowe et al. [1977] have received considerable attention. In the present investigation, the PSI-Cell method has been adopted as the basis for the Eulerian - Lagrangian model developed.

The usual starting point for the development of fluid-particle flow theory is the consideration of the motion of a single particle in an infinite fluid. The nature of such a single-particle flow has been investigated by numerous researchers including Bassett [1888], Boussinesq [1903], Oseen [1927], Tchen [1947], Corrsin and Lumley [1956], Hjelmfelt and Mockros [1966] and Maxey and Riley [1983] and is relatively well understood for flows both within and outside of the Stokes flow regime. In the Eulerian treatment of the dispersed phase, the single particle flow theory is adopted directly to describe a multi-particle system and the validity of such a step is assumed. However, in the Lagrangian particle tracking approach, the focus remains on single particle hydrodynamics for obtaining an ensemble of statistical realizations, in this case the particle trajectories, which are then analyzed using the well established mathematical theory of statistics to extract the required phase information.

In the presence of turbulence, particle trajectories are not deterministic due to an imposition over the mean velocity of a rapidly fluctuating random velocity component. This additional velocity component due to turbulence enhances the

dispersion of the particles, in aggregate, while the presence of the particles in the continuous phase, even in relatively small concentrations [Al-Taweel and Landau 1977], does modify the underlying turbulence appreciably. This 'two-way coupling' between the turbulence and the particulate phase exercises considerable influence over the evolution of such flows. These important effects will be considered later.

3. GOVERNING EQUATIONS

The field equations for the continuous phase in the Eulerian - Lagrangian scheme are the same as those for single phase flows except for the addition of an extra 'source' term which accounts for the influence of the particulate phase on the continuous phase. The equations are written in a generalized form as

$$\frac{\partial}{\partial x_i}\left(\rho u_i \phi\right) = \frac{\partial}{\partial x_i}\left(\Gamma_{eff}\frac{\partial \phi}{\partial x_i}\right) + S + S_p \qquad (3.1)$$

where u_i are the instantaneous velocity components, Γ_{eff} the effective exchange coefficients, S the usual single-phase source terms, S_p the source terms due to the particulate phase and ϕ any of the field variables such as velocity component, temperature for flows involving energy exchange, turbulence kinetic energy or its dissipation rate.

The simplified form of the particle trajectory equation in which only the hydrodynamic drag term between the phases is retained [Adeniji-Fashola and Chen, 1987] is

$$\frac{dv_i}{dt} = \frac{(u_i - v_i)}{\tau_*} \qquad (3.2)$$

where, in general, the fluid and particle velocities, u_i and v_i respectively are made up of a mean and a fluctuating component and τ_* is a particle response time defined in terms of the particle relaxation time t_* which is valid for particle motion within the Stokes regime. Thus we have

$$u_i = U_i + u_i' \qquad (3.3)$$

$$v_i = V_i + v_i' \qquad (3.4)$$

$$\tau_* = t_*/f \tag{3.5}$$

where

$$t_* = \frac{\rho_s d_p^2}{18\,\mu} \tag{3.6}$$

and

$$f = \frac{C_D Re_p}{24} = \begin{cases} 1 & \text{FOR } Re_p = \dfrac{|U_i - V_i| d_p}{\nu} \le 1 \\[2mm] 1 + 0.15\, Re_p^{0.687} & \text{FOR } Re_p > 1 \end{cases} \tag{3.7}$$

An expression similar to equation (3.2) for the particle temperature history written for a particle thermal equilibration time t_{TH} can also be written for flows involving energy transfer [Chen and Adeniji-Fashola, 1987].

4. PARTICLE-TURBULENCE INTERACTION

A very important aspect of the modeling of turbulent fluid-particle flows is the particle-turbulence interaction problem. Turbulence kinetic energy extracted from the mean flow kinetic energy of the continuous phase is partly dissipated by the smallest eddies and partly imparted to the particles thus enhancing the dispersion of the particulate phase. This 'two-way coupling' referred to earlier - modulation of the kinetic energy of turbulence by the particles and enhanced dispersion of the particles by the turbulence will now be discussed in a little more detail. It is pertinent to point out at this point that the turbulent dispersion phenomenon is primarily responsible for the considerable enhancement in mixing observed for turbulent flows when compared with laminar flows.

TURBULENT DISPERSION

The turbulent dispersion phenomenon is very closely related to the interaction between individual particles and turbulent eddies. A particle normally interacts with a series of eddies as it moves through the fluid. The particle trajectory scheme attempts to simulate this interaction by tracking each repre-

59

sentative computational particle through a succession of turbulent eddies contained within the domain of interest. Figure 1 is a schematic illustration of this interaction between particle and eddies and in relation to the computational cells. As discussed by Gosman and Ioannides [1981], a particle interacts with a given eddy for a period of time which is the minimum between an estimated particle transit time within the eddy, t_{tr} and an eddy lifetime, t_e. The particle transit time is obtained as the solution of the linearized equation of motion of the particle while the Lagrangian time scale of the turbulent eddy is obtained from length and velocity scales of the turbulence which are extracted from a k- turbulence model. Thus,

$$t_{int} = Min\ [t_e, t_{tr}]$$

(4.1)

where

$$t_{tr} = -t_* ln\ [1.0 - l_e/t_* |u_i - v_i|]$$

(4.2)

and

$$t_e = l_e / (2k/3)^{1/2}$$

(4.3)

The eddy length macroscale, l_e is defined in terms of the kinetic energy of the turbulence, k and its dissipation rate, ε as

$$l_e = C_\mu^{3/4} k^{3/2}/\varepsilon$$

(4.4)

In a stochastic formulation of the particle trajectory scheme which is the case in the present study, the fluctuating component of the fluid velocity, u', is obtained from a Gaussian distribution of values having a zero mean and a standard deviation, σ_{ii} given by

$$\sigma_{ii} = (2k/3)^{1/2}$$

(4.5)

The Gaussian distribution is, however, not expected to be appropriate, in general, for describing non-homogeneous, non-turbulent flows.

TURBULENCE MODULATION

The presence of particles, even in very small concentrations, has the effect of modulating the turbulence intensity, the direction of modulation being influenced by the mean particle size and the level of modulation by the particle loading. This turbulence modulation effect was observed experimentally by Moderrass et al. [1984] and Tsuji et al. [1984] and attempts to mathematically characterize the phenomenon include those of Al-Taweel and Landau [1977] and Chen and Wood [1985]. The interphase interaction force terms between particles and the continuous phase are reflected as extra dissipation terms in the modeled equations for k and ϵ when the former are included in the derivation of the field equations for the latter. The earlier attempts to implement these turbulence modulation models have been mostly within a two-fluid formulation in which the two phases are described as two interpenetrating continua viewed from an Eulerian framework. Equations (4.6) and (4.7) from Chen and Wood [1986] show the extra dissipation terms due to the turbulence modulation effect of the particles for such a two-fluid formulation:

$$\frac{\partial}{\partial x_i}(U_i k) = \frac{\partial}{\partial x_i}\left(\frac{\nu_t}{\delta_K}\frac{\partial k}{\partial x_i}\right) + P_K - \epsilon - \underbrace{\frac{\overline{\rho_p u_i}}{\rho t_*}(1+0.15Re_p^{0.687})(U_i-V_i)}_{(TH1)}$$

$$\underbrace{-\frac{2k}{t_*}\frac{\overline{\rho_p}}{\rho}[1-\exp(-0.5\, t_*\epsilon/k)]}_{(TH2)} \tag{4.6}$$

$$\frac{\partial}{\partial x_i}(U_i \epsilon) = \frac{\partial}{\partial x_i}(\frac{\nu_t}{\delta_\epsilon}\frac{\partial \epsilon}{\partial x_i}) + \frac{\epsilon}{k}(C_1 P_K - C_2 \epsilon) - \underbrace{2\frac{\overline{\rho_p}}{\rho}\frac{\epsilon}{t_*}}_{(TH3)} \tag{4.7}$$

The term TH1 in equation (4.6) is the turbulence modulation term due to the mean slip while the terms TH2 and TH3 are due to the particle slip velocity at the fluctuating level. The model is valid for the situation

$$t_e > t_* > t_K \, , \qquad \text{where} \qquad t_K = (\nu/\epsilon)^{1/2} \tag{4.8}$$

is the Kolmogorov time scale. The model described above has been incorporated into the particle trajectory scheme of the present study.

5. NUMERICAL SCHEME

The set of governing differential equations describing the evolution of confined turbulent fluid particle flows cannot, in general, be solved analytically thus requiring the adoption of a numerical procedure. For the continuous phase, the governing Eulerian equation set is solved using the SIMPLE algorithm of Patankar and Spalding [1972] and Patankar [1980]. The overall scheme adopted for the solution of the governing equations is similar to that suggested by Crowe et al. [1977] and illustrated in Figure 2. An alternative scheme more suited to time-dependent flows was later presented by Dukowicz [1980] and further developed by Cloutman et al. [1982] and Amsden et al. [1985].

First, the "clean" fluid flow field is obtained by solving the continuous phase governing equations. This is done using a staggered grid distribution in which velocity cells are centered about the edges of the scalar cells. Next, particle trajectories are computed for a predetermined number of representative particles such that a statistically stationary solution is obtained for the overall particle flow field. The particle trajectories, and temperature history where appropriate, are obtained by solving for the particle the non-linear ordinary differential equations of motion and the energy equation subject to the currently existing continuous fluid flow and temperature fields. A fourth order Runge-Kutta algorithm is used for this purpose. During the calculation of a particle's trajectory and temperature history, the sources of momentum, energy, kinetic energy of turbulence and its dissipation rate, all due to the particle motion, are accumulated for each computational cell traversed. The form of the source terms have already been presented elsewhere [Adeniji-Fashola and Chen, 1987] and so will not be repeated here. These source terms are then used in the next global iteration on the continuous phase field equations until convergence is attained. It was found that source term relaxation was required to achieve stability of the global iteration scheme for some of the example flow problems studied.

PARTICLE SOURCE FIELD CONTINUITY

A necessary condition to obtain a globally converged solution is to ensure the continuity of the source fields as was also pointed out by Durst et al. [1984]. In order to ensure compliance with this important requirement, it is necessary to ensure the computation of source terms for each cell traversed by each computational particle through a judicious choice of the particle integration time step as well as have particles start from as many locations as is

practicable within the relevant portion of the inlet plane. In the present study, particles are uniformly distributed in physical space at the appropriate portion of the inlet plane of the computational domain in contrast to the scheme of Durst et al. [1984], in which particles are introduced only at grid nodes. The smooth profiles they obtained are very likely to be a consequence of the deterministic nature of the particle trajectories used in their study.

INTEGRATION TIME STEP

The choice of appropriate time steps for the integration of the particle equations of motion is very vital to obtaining a globally converged solution and smooth averaged particle flow fields. For the complex confined turbulent fluid-particle flow problems in general, some of the relevant time scales include the Lagrangian or macro time scale (eddy lifetime) of the turbulence, t_e; the Kolmogorov or the micro (dissipation) time scale of the turbulence, t_K; the particle relaxation time, $t*$; the particle residence time within a computational cell or the whole computational domain t_R. Also relevant to the stochastic determination of the particle turbulent intensity are the particle transit time within an eddy, t_{te} and the particle eddy interaction time, t_{int}. The integration time step is selected to ensure adequate resolution with regard to the trajectory and temperature evolution while ensuring computational efficiency by avoiding unnecessarily small time steps.

In the present study, a variable integration time step scheme was devised. An upper bound on the time step through any computational cell was imposed based on an estimated particle residence time for that cell and with the particle being constrained to undergo about four integration steps within the cell. Without this restriction, the possibility of a particle overshooting one or more cells, possibly due to a sudden reduction in cell dimensions in a non-uniform grid domain, exists. Such a situation will result in a failure to compute the relevant source term contributions for a cell that was actually traversed by the particle. The consequence will be a lack of smoothness in the particle source distribution and, possibly, divergence of the global iterations.

Also, for the reason of ensuring a smooth evolution of the particle trajectory and temperature history, a further restriction on the integration time step, $\Delta t < t*$, is made. The particle-eddy interaction time is determined and controlled independently of the integration time step.

PARTICLE AVERAGED PARAMETERS FROM PARTICLE TRAJECTORY STATISTICS

One of the problems associated with the use of the Lagrangian particle trajectory approach, highlighted by Smoot and Smith [1985], is the difficulty of extracting smooth mean particle flow and temperature fields from the statistics of trajectories and temperature histories obtained for representative computational particles. In the present study, the fluid properties utilized in the particle trajectory and temperature history calculations are the linearly interpolated values in which the four nearest neighbors regarding the particle's current location are used, resulting in second order accuracy [Sirigniano, 1983]. The details of the extraction of particle mean flow and temperature fields information from the particle trajectory and temperature history statistics are available in Adeniji-Fashola et al. [1988].

BOUNDARY CONDITIONS

The definition of a fluid flow problem becomes unique through the specification of the boundary conditions after the governing differential equations are outlined and an appropriate closure of these equations is effected. The example flow problems investigated in the present study include vertical pipe upflow and horizontal recirculation chamber flow. However, rather than define the boundary conditions specific to each flow problem separately, the more efficient approach of defining generic boundary condition types is adopted. It then becomes a straightforward exercise to construct the boundary conditions for these and other specific flow situations of interest.

Inlet Plane:

The specification of the inlet plane boundary conditions for fluid flow problems is very important, as was discussed by Sturgess et al. [1983] and Westphal and Johnston [1984], since this influences significantly the subsequent evolution of the flow, especially in the case of parabolic flows for which the inlet plane conditions constitute the initial conditions for the solution of the governing differential equations.

In order to correctly simulate a given fluid flow experiment numerically, the ideal specifications for the inlet flow variables are the actually measured values. The complete set of measured inlet flow variables is, however, hardly ever available. In the absence of such detailed experimental information, uniform profiles are commonly specified for the axial velocity and temperature profiles of the continuous phase flow at the inlet plane. The turbulent kinetic energy is usually assumed to be a percentage, between 3 and 20%, of the inlet flow mean kinetic energy. The kinetic energy dissipation rate at the inlet is then obtained as

$$\varepsilon = (C_\mu^{3/4} k^{3/2}) / l_d \qquad\qquad (5.1)$$

where l_d, the dissipation length scale, is specified as a fraction of the characteristic length scale at the inlet.

For the particle trajectory and temperature history calculations, the initial velocity and temperature slip values relevant to the particular flow problems are employed in setting the required inlet conditions.

Exit Plane:

At the exit plane, the usual boundary condition imposed for any flow variable, ϕ, is $\partial\phi/\partial n = 0$, where n is the normal to the exit plane. This condition is generally valid if the extent of the computational domain in the primary flow direction is sufficient to ensure fully-developed flow conditions for internal flows or self-similarity for jet flows at the exit plane. Particle trajectory and temperature history computations are discontinued for a computational particle once the particle exits from the computational domain through the exit plane or any other open boundary.

Solid Boundary:

The conventional wall functions approach is used to impose wall boundary conditions on the velocity and temperature as well as the turbulence kinetic energy and its dissipation rate. The presence of particles in a fluid flow has been experimentally observed to influence the boundary layer [Kramer and Depew, 1972] and, as a consequence, the nature of the wall function which is normally used to connect the actual value of a given variable at the wall to the value at the wall-adjacent grid node. During their trajectories, particles that reach the wall either adhere to it as observed in particle erosion problems [Dosanjh and Humphrey, 1984], or collide with the wall and get "reflected" back into the flow domain, usually with an accompanying loss of energy and momentum to the wall. In addition, the high level of shear in the wall vicinity coupled with a particle velocity slip introduces an additional transverse force on the particle which further modifies its subsequent trajectory and behavior in the near-wall region. These effects have not been included in the present study, in which perfectly reflecting boundary conditions have been adopted for the particle-wall interaction, but will be the subject of a future study.

Other generic boundary condition types include the symmetry axis, for which $\partial\phi/\partial n = 0$, where in this case, n is the normal to the symmetry axis, and the open boundary condition which has been used by Leschziner and Rodi [1984], Dosanjh and Humphrey [1984], Amano and Brandt [1984] and Chen and Adeniji-Fashola [1987] for modeling parabolic flows of free jets and wall jets using elliptic formulations. These are described in greater detail by Adeniji-Fashola et al. [1988].

6. EXAMPLE FLOWS

In order to illustrate the multiple-realization particle trajectory modeling scheme for confined turbulent fluid-particle flows described above, two example flow problems - vertical pipe upflow and horizontal coaxial jet flow in a recirculation chamber with a particle-laden central jet and a clean annular jet are examined. 1500 computational particles were found to be adequate in each example for obtaining statistically stationary solutions. Typically, global under-relaxation values of 0.50 were found adequate to ensure the stability of global iterations of which between five and seven were required to obtain globally converged solutions. The results obtained for the numerical simulation of these flows will now be discussed.

VERTICAL PIPE UPFLOW

The experimental data which served as the basis for this example numerical simulation are those of Tsuji et al. [1984] for the upflow of a particle-laden stream in a straight vertical pipe. The experimental flow within the test section is considered to be fully-developed after going through a riser that is 167.5 diameters long.

A 50 X 23 uniform grid distribution was used to discretize the computational domain which had an axial extent of 60 pipe diameters. Figure 3 shows both the experimental data and the numerical predictions of the radial profile of the slip in the axial velocity between the air and the particulate phase. The mean particle size and loading ratio are 200 μm and 1.0 respectively. The air velocity is slightly overpredicted in the 0.2R - 0.8R range where R is the pipe radius. However, the prediction accuracy is considered to be good for such a complex system. The radial profile of the axial velocity of the solid phase is particularly well predicted. The location of the cross-over in sign of the slip between the phases is predicted to be closer to the wall, less than 0.1R from the wall, than the 0.2R from the wall that was experimentally observed.

A similar picture obtained for the higher loading ratio of 2.1 is presented in Figure 4. The level of accuracy of the predictions is similar to that of the 1.0 loading ratio case. However, it is the air velocity profile that is better predicted in this case. The solid phase axial velocity is considerably underpredicted in the inner 60 percent of the wall region.

As pointed out earlier, the particulate phase has the effect of modulating

the level of the turbulence intensity. For smaller particle sizes this results in a decrease in the kinetic energy of turbulence. The experimentally observed and numerically predicted turbulence modulation effect for a loading ratio of 3.2 are illustrated in Figure 5. The solid line in the figure shows the predicted radial profile of the turbulence intensity for the corresponding "clean" flow. The predicted level of turbulence intensity is considerably higher than the level observed from experiment. Also, while a greater modulation effect was observed closer to the wall region, the predictions show a reversal in which the greater level of modulation is located closer to the pipe centerline. The imposed wall boundary conditions and wall functions in the numerical scheme are probably responsible for the suppression of the modulation effect in the near-wall region.

The development in the axial direction of the streamwise velocity of the particulate phase for an inlet velocity slip ratio of 0.10 is shown in the contour plot of Figure 6a and a corresponding surface plot in Figure 6b. The ability of the particle trajectory scheme to effectively handle extreme levels of velocity slip was tested by imposing an axial slip velocity of 0.10 at the pipe inlet plane. The figures indicate that a fully developed state was attained in the 60D extent of the computational domain.

HORIZONTAL COAXIAL JET FLOW IN RECIRCULATION CHAMBER

The experimental data of Leavitt [1980] serve as the basis for the numerical simulation of this example. The actual geometry studied is illustrated in the schematic of Figure 7. The primary jet air velocity at inlet is 33 m/s while the corresponding secondary jet air velocity is 42 m/s. Coal particles of a mass mean diameter of 43 μm were used to uniformly seed the primary jet and the particle loading ratio is 1.50. The estimated turbulence intensity levels at the inlet are 15 and 18% for the primary and secondary jets respectively. The primary and secondary jet diameters at inlet are 0.0255m and 0.127m respectively while the chamber diameter is 0.206m. The axial extent of the recirculation chamber is 0.926m (36.3 primary jet diameters or 4.5 chamber diameters).

A 41 X 41 non-uniform staggered grid distribution, shown in Figure 8, is used for the numerical study and the computational domain extended to 20D where D is the chamber diameter. The numerical prediction of the evolution of the axial velocity is shown in Figure 9. The corner recirculation zone is seen to extend to about 1.79D. No particles are predicted as reaching this recirculation zone and this is believed to be due to the high chamber-to-primary jet diameter ratio of 8.08 and the positive slope of the shear in the mixing layer between the primary and the secondary jets which will result in a slip-shear transverse force directed towards the centerline. Another interesting observation is that the particle axial velocity starts lo lead that of the fluid from

about the 0.80D axial location and this continues to about the 7.43D axial location downstream of which all axial velocity slip disappears. Particles are seen to have dispersed to the outer extremities of the recirculation chamber by the time the 12.0D axial location is reached. However, it should be remembered that this is only a hypothetical situation since the actual experimental investigation was limited to an axial extent of only 4.5D.

Figure 10 shows the axial evolution of the turbulence intensity. It is observed that up to about the 3.0D axial location, the turbulence intensity in the presence of particles (shown dotted) falls below that of the clean flow in the primary jet portion of the flow but is actually higher for the rest of the chamber in the radial direction. However, beyond the 3.0D axial location, the clean flow turbulence intensity uniformly lags the two-phase intensity at all radial locations for any given axial location. The kinetic energy of turbulence is essentially fully developed at the 5.15D axial location and only a radially uniform decrease in magnitude is observed for the rest of the flow in the axial direction. This is in contrast to the radial profile of the axial velocity which does not become fully developed for both phases until the 12.0 to 15.0 diameter range is reached.

The contour and surface plots of the particle axial velocity are shown in Figures 11a and 11b. These have been normalized with respect to the secondary jet gas velocity at inlet. Since, in contrast to the two-fluid scheme, non-zero values of the particle velocity are not returned for computational cells not visited by any particle during the trajectory calculations, the zero-velocity surface in the plots of Figure 11b also indicate the particle-deficient regions.

The comparison of the limited experimental data available from Leavitt [1980] is currently being undertaken.

7. CONCLUDING REMARKS AND RECOMMENDATIONS FOR FUTURE WORK

The numerical modeling of confined turbulent fluid-particle flows using the multiple-realization particle trajectory scheme has been presented. The performance of the numerical modeling scheme has been tested using data for the upward flow of a fluid-particle stream in a straight vertical pipe and for the horizontal coaxial jet flow in a large recirculation chamber for which the central jet is particle-laden.

The multiple-realization particle trajectory turbulent flow modeling scheme ...

68

is believed to be a more elegant and accurate approach to the extension of single-particle hydrodynamics to dilute multi-particle systems;

is better able to incorporate additional force terms such as lift, virtual mass and Bassett history terms in the particle equation of motion as appropriate;

needs further investigation in order to improve its computational efficiency and so reduce its huge CPU time requirements;

needs to have the particle-turbulence and particle-wall interactions further investigated to improve prediction accuracy.

ACKNOWLEDGEMENTS

REFERENCES

Adeniji-Fashola, A. A. and Chen, C. P., "Comprehensive Modeling of Turbulent Particulate Flows Using Eulerian and Lagrangian Schemes", AIAA Paper 87-1347, 1987.

Adeniji-Fashola, A. A., Chen, C. P. and Schafer, C. F., "Numerical Predictions of Two-Phase Gas-Particle Flows Using Eulerian and Lagrangian Schemes", NASA Technical Paper, in preparation, 1988.

Al-Taweel, A. M. and Landau, J., "Turbulence Modulation in Two-Phase Jets", Int. J. Multiphase Flows, 3, p. 341, 1977.

Amano, R. S. and Brandt, H., "Numerical Study of Turbulent Axisymmetric Jets Impinging on a Flat Plate and Flowing Into an Axisymmetric Cavity," J. Fluids Engrg., 106, p. 410, 1984.

Amsden, A. A., Ramshaw, J. D., O'Rourke, P. J. and Dukowicz, J. K. "KIVA: A Computer Program for Two- and Three-Dimensional Fluid Flows With Chemical Reactions and Fuel Sprays", Los Alamos National Laboratory Report LA-10245-MS, 1985.

Basset, A. B., Treatise on Hydrodynamics, Vol. 2, Ch. 22, p. 285, Deighton Bell, London, 1888.

Boussinesq, J., Theory Analytique de la Chaleur, Vol. 2, p. 224, L'Ecole Polytechnique, Paris, 1903.

Chen, C. P. and Wood, P. E., "A Turbulence Closure Model for Dilute Gas Particle Flows", Can. J. Ch. E. 63, p. 349, 1985.

Chen, C. P. and Adeniji-Fashola, A. A., "Heat Transfer in Turbulent Fluid-Solids Flows", 24th AIChE/ASME National Heat Transfer Conference, Pittsburgh, Aug. 9-12, 1987.

Cloutman, L. D., Dukowicz, J. K., Ramshaw, J. D. and Amsden, A. A. "CON-CHAS-SPRAY: A Computer Code for Reactive Flows with Fuel Sprays", Los Alamos National Laboratory Report LA-9294-MS, 1982.

Corrsin, S. and Lumley, J., "On the Equation of Motion for a Particle in Turbulent Fluid", App. Sci. Res. A, 6, p. 114, 1956.

Crowe, C. T., Sharma, M. P. and Stock, D. E., "The Particle-Source-In Cell (PSI-Cell) Model for Gas-Droplet Flows", J. Fluid Engrg. 99, p.325, 1977.

Depew, C. A. and Kramer, T. J., "Heat Transfer to Flowing Gas-Solid Mixtures", Adv. in Ht. Trans. 9, p. 113, 1973.

Dosanjh, S. and Humphrey, J. A. C., "The Influence of Turbulence on Erosion by a Particle-Laden Fluid Jet", LBL - 17247, Lawrence Berkeley Laboratory, U. Cal., 1984.

70

Dukowicz, J. K., "A Particle-Fluid Numerical Model for Liquid Sprays", J. Comp. Phys. 35, p. 229, 1980.

Durst, F., Milojevic, D. and Schonung, B., "Eulerian and Lagrangian Predictions of Particulate Two-Phase Flows: A Numerical Study" Appl. Math. Model., 8, p. 101, 1984.

Gosman, A. D. and Ioannides, E., "Aspects of Computer Simulation of Liquid Fueled Combustors", AIAA Paper 81-0323, 1981.

Harlow, F. H., "The Particle-in-Cell Computing Method in Fluid Dynamics", Methods Comput. Phys., 3, p. 319, 1964.

Hjelmfelt, Jr., A. T. and Mockros, L. F., "Motion of Discrete Particles in a Turbulent Fluid", Appl. Sci. Res., 16, p. 149, 1966.

Hockney, R. W. and Eastwood, J. W., Computer Simulation Using Particles, McGraw-Hill Intl. Book Co., 1981.

Leavitt, D. R. "Effects of Coal Dust and Secondary Swirl on Gas and Particle Mixing Rates in Confined Coaxial Jets", MS Thesis, Bringham Young University, 1980.

Maxey, M. R. and Riley, J. J., "Equation of Motion for a Small, Rigid Sphere in a Non-Uniform Flow", Phys. Fl., 26, p. 883, 1983.

Moderrass, D., Tan, H. and Elghobashi, S., "Two-Component LDA Measurement in a Two-Phase Turbulent Jet", AIAA J. 22, p. 624, 1984.

Oseen, C. W., Hydrodynamik, p. 132, Leipzig, 1927.

Patankar, S. V., Numerical Heat Transfer and Fluid Flow, Hemisphere Pub. Corp./McGraw-Hill Book Co., 1980.

Patankar, S. V. and Spalding, D. B.,"A Calculation Procedure for Heat, Mass and Momentum Transfer in Three-Dimensional Parabolic Flows", Int. J. Ht. Mass Trans., 15, p. 1787, 1972.

Sirignano, W. A., "Fuel Droplet Vaporization and Spray Combustion Theory", Prog. Energy. Comb. Sci., 9, p. 291, 1983.

Smoot, L. D. and Smith, P. J., Coal Combustion and Gasification, Plenum Press, New York, 1985.

Sturgess, G. J., Syed, S. A. and McManus, K. R., "Importance of Inlet Boundary Conditions for Numerical Simulation of Combustor Flows", AIAA Paper 83-1263, 1983.

Tchen, C. M., "Mean Value and Correlation Problems Connected With the Motion of Small Particles Suspended in a Turbulent Fluid", Ph.D. Thesis, Delft, 1947.

Tsuji,Y., Morikawa, Y. and Shiomi, H., "LDV Measurements of an Air-Solid Two-Phase Flow in a Vertical Pipe", J. Fl. Mech., 139, p. 417, 1984.

Westphal, R. V. and Johnston, J. P., "Effect of Initial Conditions on Turbulent Reattachment Downstream of a Backward-Facing Step", AIAA J., 22, p. 1727, 1984.

LIST OF FIGURES

PARTICLE TRAJECTORY THROUGH SUCCESSION OF
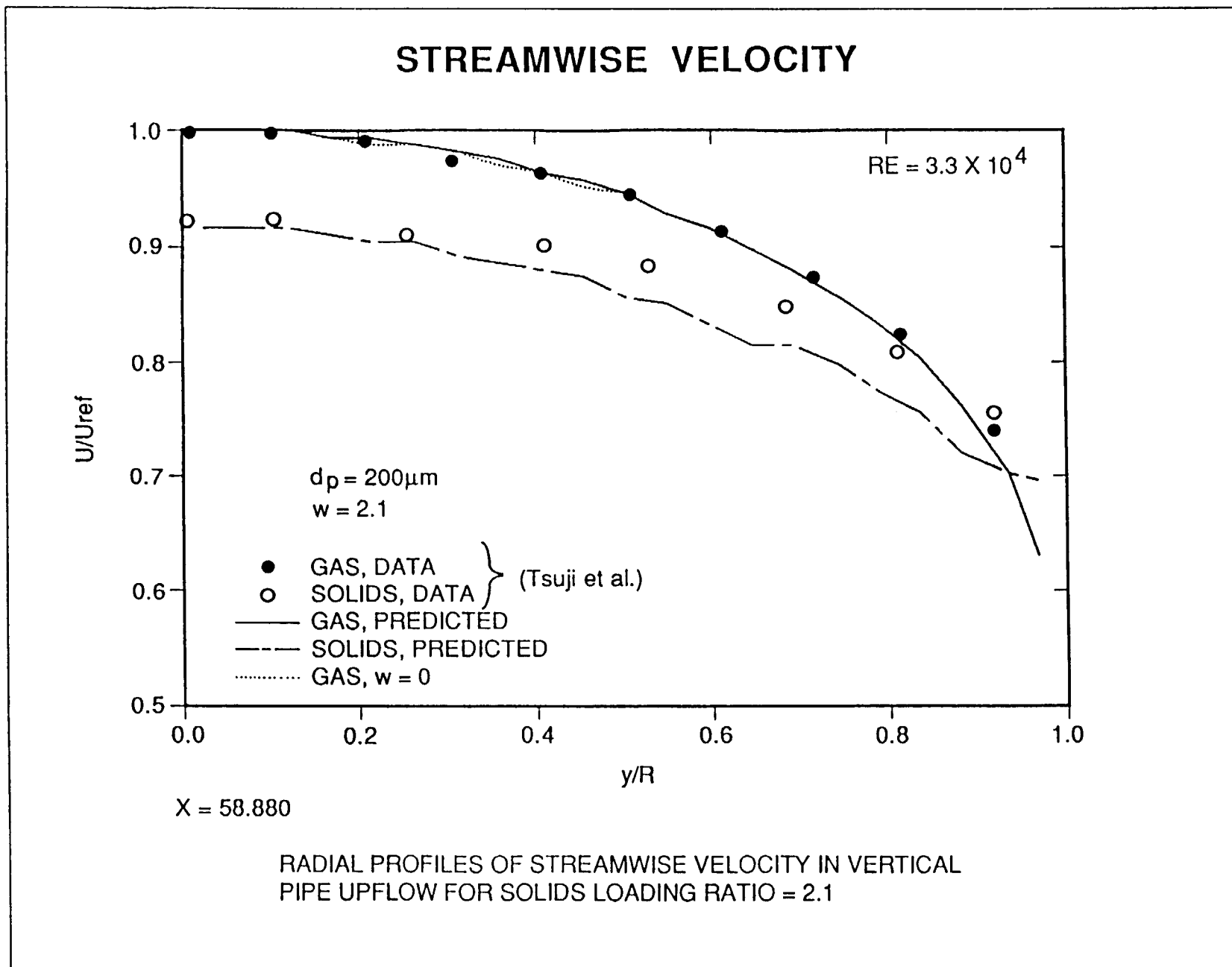TURBULENT EDDIES AND COMPUTATIONAL CELLS
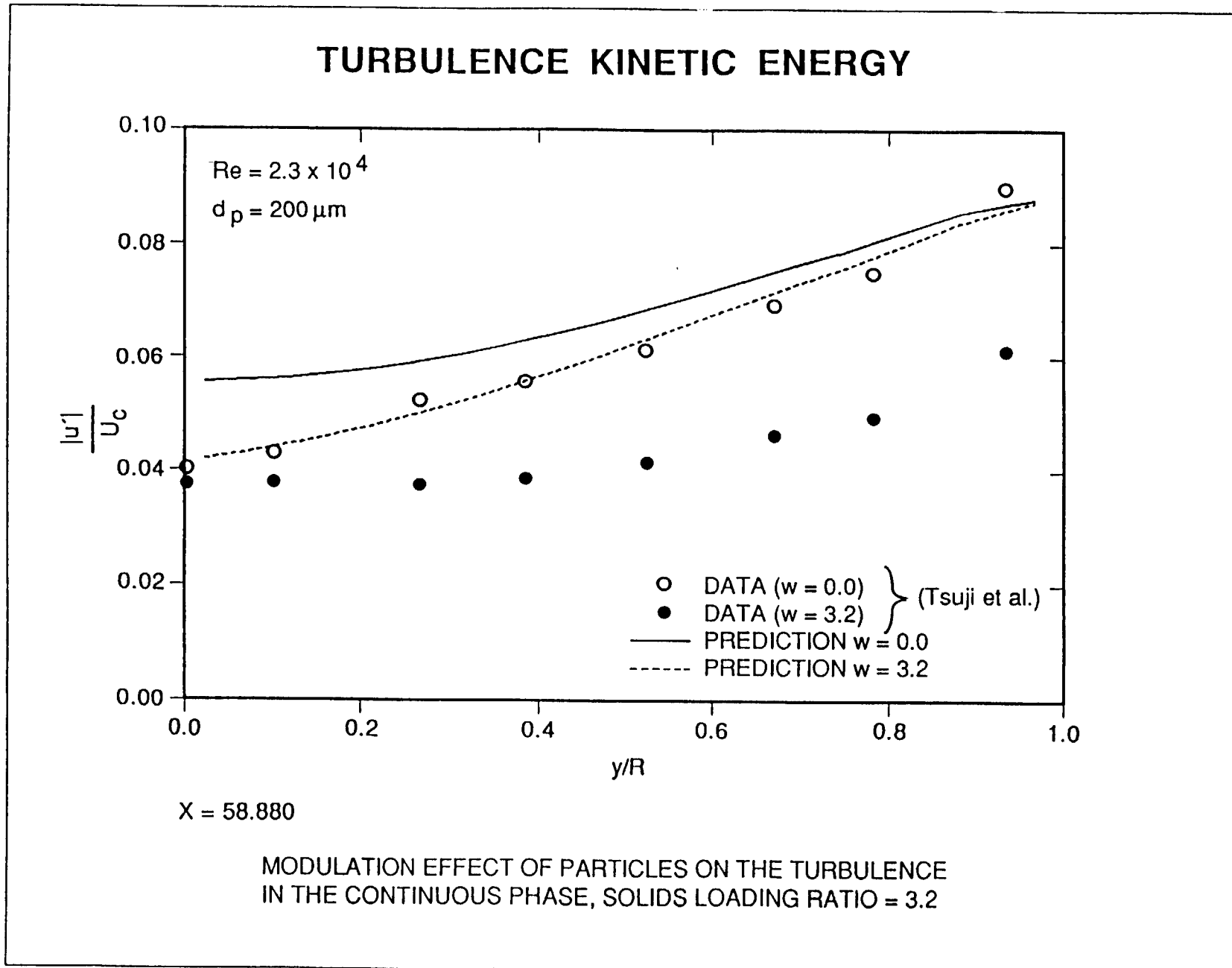
FIGURE 1.

FIGURE 2.

FIGURE 3.

STREAMWISE VELOCITY

RE = 3.3 X 10^4

d_p = 200μm
w = 2.1

● GAS, DATA ⎫
○ SOLIDS, DATA ⎰ (Tsuji et al.)
——— GAS, PREDICTED
—·—· SOLIDS, PREDICTED
·········· GAS, w = 0

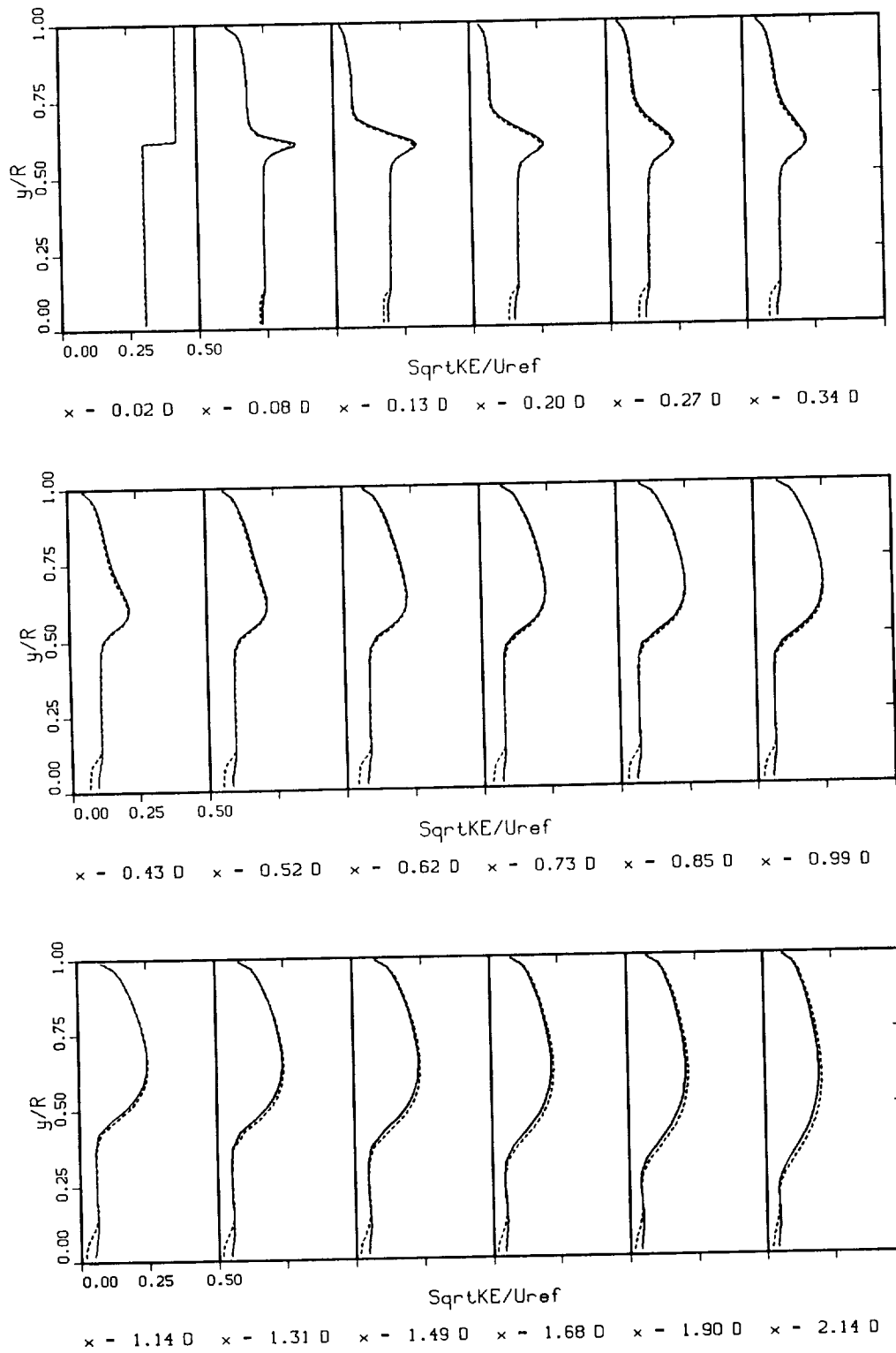X = 58.880

RADIAL PROFILES OF STREAMWISE VELOCITY IN VERTICAL
PIPE UPFLOW FOR SOLIDS LOADING RATIO = 2.1

FIGURE 4.

TURBULENCE KINETIC ENERGY

$Re = 2.3 \times 10^4$

$d_p = 200\,\mu m$

$\dfrac{|u'|}{U_c}$

○   DATA (w = 0.0) } (Tsuji et al.)
●   DATA (w = 3.2) }
—— PREDICTION w = 0.0
- - - - PREDICTION w = 3.2

y/R

X = 58.880

MODULATION EFFECT OF PARTICLES ON THE TURBULENCE
IN THE CONTINUOUS PHASE, SOLIDS LOADING RATIO = 3.2

FIGURE 5.

FIGURE 6.

PARTICLE STREAMWISE VELOCITY

0.6998

0.6998

0.7998

0.5999

0.6998

0.7998

0.7998

TRANSVERSE DIMENSION X 50

PARTICLE STREAMWISE VELOCITY DEVELOPMENT FOR AN INITIAL SLIP
RATIO = 0.1. PARTICLE LOADING = 3.2 AND REFERENCE VELOCITY IS THE
INLET GAS VELOCITY. DOMAIN LENGTH = 60D

(a)

Particle Streamwise Velocity

1.00

0.75

0.50

0.25

0.00

Up / Uref

0.39

30.39

60.39

90.39

Axial Distance - RAD

0.25

0.50

0.75

1.00

Radial Distance - RAD

(b)

PARTICLE-LADEN FLOW IN LARGE RECIRCULATION CHAMBER

FIGURE 7.

FIGURE 8.

Streamwise Velocity

FIGURE 9.

Streamwise Velocity

x = 2.27 D   x = 2.55 D   x = 2.85 D   x = 3.19 D   x = 3.56 D   x = 3.96 D

x = 4.41 D   x = 4.90 D   x = 5.44 D   x = 6.02 D   x = 6.70 D   x = 7.43 D

x = 8.20 D   x = 9.08 D   x = 10.000   x = 12.230   x = 14.900   x = 18.160

82

FIGURE 9. (cont.)

Turbulence Kinetic Energy

FIGURE 10.

Turbulence Kinetic Energy

SqrtKE/Uref

x - 2.40 D   x - 2.69 D   x - 3.01 D   x - 3.36 D   x - 3.75 D   x - 4.17 D

SqrtKE/Uref

x - 4.64 D   x - 5.15 D   x - 5.73 D   x - 6.36 D   x - 7.04 D   x - 7.77 D

SqrtKE/Uref

x - 8.59 D   x - 9.51 D   x - 10.53D   x - 12.82D   x - 15.63D   x - 19.03D

FIGURE 10. (cont.)

84

Particle Streamwise Velocity

TRANSVERSE DIMENSION X 50

COAXIAL JET INJECTION INTO LARGE RECIRCULATION CHAMBER WITH
PARTICLE-LADEN PRIMARY JET [LEAVITT, 1980]. PARTICLE LOADING RATIO = 1.50
AND U_{sec}/U_{pri} = 1.27. 43μ m MASS MEAN DIAMETER COAL PARTICLES
USED. DOMAIN LENGTH = 20D. REFERENCE VELOCITY IS THE SECONDARY
MEAN VELOCITY.

(a)

Particle Streamwise Velocity

(b)

FIGURE 11.

PARTICLE DISPERSION MODELS AND DRAG COEFFICIENTS FOR PARTICLES IN TURBULENT FLOWS*

by

C.T. Crowe, J.N. Chung and T.R. Troutt
Department of Mechanical and Materials Engineering
Washington State University
Pullman, WA 99164-2920

INTRODUCTION

The dispersion of particles in turbulence is fundamental to a variety of mass and energy transfer processes. The dispersion of particles in jets is important to the combustion process and the design of propulsion systems. The separation of particles by electrostatic precipitation is important in many applications from the power industry to clean-room technology. Understanding the basic phenomena underlying particle transport in turbulence and establishing viable models is important to the development of new technologies for advanced propulsion systems.

This paper reviews some the concepts underlying particle dispersion due to turbulence. The paper addresses the traditional approaches to particle dispersion in homogeneous, stationary turbulent fields and reviews recent work on particle dispersion in large scale turbulent structures. The paper also reviews the state of knowledge on particle drag coefficients in turbulent gas-particle flows.

MECHANISMS FOR PARTICLE DISPERSION

Basically two mechanisms have been used to physically model particle dispersion in turbulence. In homogeneous turbulent flows, the most common approach is to regard dispersion as a stochastic process. On the other hand, dispersion in large scale turbulent structures appears to be more influenced by the ordered motion. Both approaches are treated separately.

Particle Dispersion in Homogeneous, Stationary Turbulence

The traditional approach to treating particle dispersion is turbulence is to regard the process as a gradient diffusion (Fickian) process in which the diffusional velocities are proportional to the concentration gradient, the constant of proportionality being the diffusion coefficient.

$$V_F = -D\frac{\partial c}{\partial x_i} \qquad 1)$$

The earliest work that related the diffusion coefficient to properties in a homogeneous, stationary and isotropic flow was that of Taylor (1921) who provided the following relationship,

$$D = \overline{u'^2}T_L \qquad 2)$$

where $\overline{u'^2}$ is the mean square of the fluctuating velocity in the direction transverse to the main flow direction and T_L is the lagrangian integral time scale. Although Taylor's analysis was done for a fluid point, Synder and Lumley (1971) showed it was applicable to a particle provided the lagrangian time scale corresponded to the particle trajectory.

The earliest study of particle motion in a turbulent field was reported in a PhD thesis by Tchen (1947) who integrated the Basset, Boussinesq, Oseen equation for a particle in a homogeneous, stationary turbulent field. He assumed that the particle remained always in the same turbulent eddy. By so doing the long-time diffusion of the particle was equal to that of a fluid particle.

Many researchers after Tchen have strived to improve Tchen's model by relaxing the assumptions made by Tchen. Peskin (Soo, 1967) solved a nonlinear stochastic equation for the motion of a particle which did not deviate far from the initial coincident turbulent eddy. Unlike Tchen's analysis, Peskin assumed that only Stokes drag acted on the particle. He predicted that the diffusivity decreased uniformly with an inertial parameter which related the aerodynamic response time of the particle to the time scale for turbulence. The physical argument underlying this result was the larger the aerodynamic response time of the particle is compared to the eddy life time, the less a particle would respond to the unsteady turbulent field. Hinze (1972) used similar time-scale arguments for particle dispersion and concluded that if the particle density ratio is large, only those particles less than one tenth of the dissipation length scale will respond to the turbulent fluctuations.

A more general analysis of particle dispersion in homogeneous, isotropic stationary turbulence has been reported by Reeks (1977). He assumed a linear drag law and body force acted on the particle and obtained an expression for diffusion which depended on time, particle aerodynamic response time and the correlation function for the velocity field. He then utilized Phythian's model (1975) for the turbulent energy spectrum and predicted a particle diffusion coefficient. His results show that the diffusion coefficient for particles with no body force increases with increasing time and, at long times, approaches an asymptotic value. This long-time diffusion coefficient increases with increasing aerodynamic response time and can exceed that of a fluid particle. This result differed from Peskin's model. The reason underlying the trend predicted by Reeks is the fact that the diffusion is jointly dependent on the mean square of the particle velocity fluctuations and lagrangian integral time scale as shown by equation 2. Although the amplitude of the fluctuation velocity of the heavier particle is reduced, the lagrangian time scale is increased proportionately more giving rise to an increased diffusion coefficient.

Another factor controlling particle dispersion in homogeneous, stationary turbulence is the "crossing trajectory" effect first identified by Yudine (1959). If the mean velocity of the particles is different from that of the fluid, such as particles dropping at their terminal velocity through a turbulent field, the particles remain less time in a given eddy. The reduction in fluid-particle interaction time reduces the particle diffusion coefficient. Reeks also predicted a decrease in long-time diffusion coefficient by including a body force in the particle motion equation.

Thus there are two primary factors controlling particle dispersion in homogeneous turbulence, the inertial effect and the crossing trajectory effect. Experimentally it has been difficult to separate these effects since a heavy (not a fluid) particle will have both inertial and crossing trajectory effects. The most convincing experimental evidence that separates the two effects have been provided by Well and Stock (1983). They suspended

glass beads by Coulomb forces in a horizontal flow of near-homogeneous, grid-generated turbulence. The crossing trajectory effect was controlled by adjusting the field strength. Their data show that the inertial effects on particle diffusion coefficient are small compared the crossing trajectory effect. The small increase in diffusion with increasing inertial effects predicted by Reeks was not discernible because of the scatter in the experimental data.

Future developments in the analysis of stochastic turbulent flows will address departures from homogeneity and isotropy. Reeks (1981) has initiated work in this direction.

Particle Dispersion in Large Scale, Turbulent Structures

Large scale turbulent structures are encountered in flows generated by a large velocity gradient such as free shear layers and jets. Under these circumstances, large scale turbulent structures are formed which grow and pair with time. These structures were first identified by Brown and Roshko (1974) in flow visualization studies of mixing layers. A typical photograph of a large scale structure is shown in figure 1 . These turbulent flow fields are inhomogeneous, non-stationary and anisotropic but represent important, practical problems in industrial applications such as combustion systems.

Particle dispersion in turbulent flow characterized by large scale structures is mechanistically different than that in homogeneous flows. The particle motion is controlled by the moving structures and not by the fine scale turbulence. Thus, the dispersion process cannot be regarded as gradient transport.

A conceptual model for particle dispersion in large scale structures is the entrapment of particles in the structure and the subsequent centrifuging of the particles beyond the structures. This concept was first suggested by Singamsetti (1966) who observed, experimentally, that particles in a submerged jet could disperse more quickly than a fluid particle. The same trends have been observed by Lilly (1973), Householder 1968), Laats and Frishman (1970) and Subramanian and Ganesh (1984) in the experimental study of particle and droplet laden free jets. Lilly attributed his results to an increase lagrangian time scale but Yuu *et al.* (1978) claim Lilly's results were a manifestation of his experimental set-up. Laats and Frishman noticed this trend only in the early portion of the jet formation and surmised that it was due to a Magnus effect. Goldschmidt *et al.* (1972), in reviewing Householder's data, mentioned the possibility of particle centrifuging by large scale structures but concluded that the mechanism was not viable because it did not explain the observed trends in centrifuging bubbles.

Yule (1981) gave some credence to the mechanism when he observed droplets in jet flows being centrifuged toward the outer flow.

Crowe *et al.* (1985) report an effort to quantify those conditions under which the large scale structures are responsible for dispersing heavy particles beyond fluid particles. They proposed a time scaling argument similar to that used by Hinze (1972) for homogeneous turbulence. The aerodynamic response time of a particle is the time required for a particle released from rest in a uniform flow to accelerate to 63% of the flow velocity. For Stokes flow it is

$$\tau_A = \frac{\rho d^2}{18 \mu} \qquad \text{3)}$$

where ρ is the fluid density, d is the particle diameter and μ is the dynamic viscosity of the fluid. It is a measure of the responsiveness of a particle to changes in flow velocity. The characteristic time of the flow is given by

Figure 1. Shadowgraph Visualization of Large Scale Turbulent Structures in Plane
Mixing Layer (Brown and Roshko, 1974)

$$\tau_F = \frac{\delta}{\Delta U} \qquad\qquad 4)$$

where δ is the mixing layer thickness and ΔU is the velocity difference across the layer. Thus the scaling factor is

$$St = \frac{\tau_A}{\tau_F} = \frac{\rho d^2 \Delta U}{18\mu\delta} \qquad\qquad 5)$$

A schematic diagram showing the effect of Stokes number on particle dispersion is shown in figure 2. For small Stokes numbers, the particles are in near equilibrium with the conveying fluid and the particles will disperse as a fluid particle. At large Stokes numbers, the particles have insufficient time to respond to the structures and they disperse less than the fluid particle. However at intermediate Reynolds numbers, the particles are entrapped by the rotating structure and are centrifuged beyond the structures giving rise to a dispersion exceeding that of a fluid particle.

A preliminary numerical study (Crowe *et al.* 1985) using a simple vortex sheet model proposed by Stuart (1967) showed that particles could be centrifuged beyond the vortex at Stokes number between 0.1 and 1 as shown in figure 3. A subsequent study by Gore et al (1985) using pseudospectral direct simulation for modeling the vortex structures showed the same trend lending support to the model.

Recent experimental studies have shown the importance of large scale structures in the turbulent dispersion process. Kamalu *et al.* (1987) at Washington State University have reported on particle dispersion studies in horizontally oriented plane mixing layer. Both naturally evolving and subharmonically forced mixing layers were studied. The forced mixing layer was generated by a sound source, the effect of which was more ordered vortex structures. Particles, 40 microns in diameter, were released from a source upstream of the layer and photographed. A photograph of the particles in a subharmonically forced mixing layer is shown in figure 4. Shown in the same figure are streaklines generated by smoke with no particles in the flow. One notes the absence of particles in the vortex cores and the accumulation of particles near the edge of the vortex structures.

Laser Doppler measurements of particle velocities by Wen *et al.* (1987) lend more quantitative support on the role of large scale structures in particle dispersion. The measured lateral particle and fluid velocities taken in the same facility used by Kamalu *et al.* are shown in figure 5. The fluid velocities show the expected trend; negative on the top (high speed side) and positive on the bottom (low speed side) which indicates a motion of the fluid towards the mixing region. The particle velocities, on the other hand, are positive on the top and negative on the bottom indicating motion away from the mixing layer.

The importance of large scale structures in particle dispersion has also been verified in recent experimental studies by Kobayashi et al (1987) and Lazaro and Lasheras (1987).

The importance of large scale structures in turbulent dispersion of particles has been established. It represents a demarcation from particle dispersion in homogeneous turbulence because it is more deterministic than stochastic. Therefore it is not reasonable to model particle dispersion as a gradient transport process.

LARGE
PARTICLE
St >> 1

SMALL PARTICLE
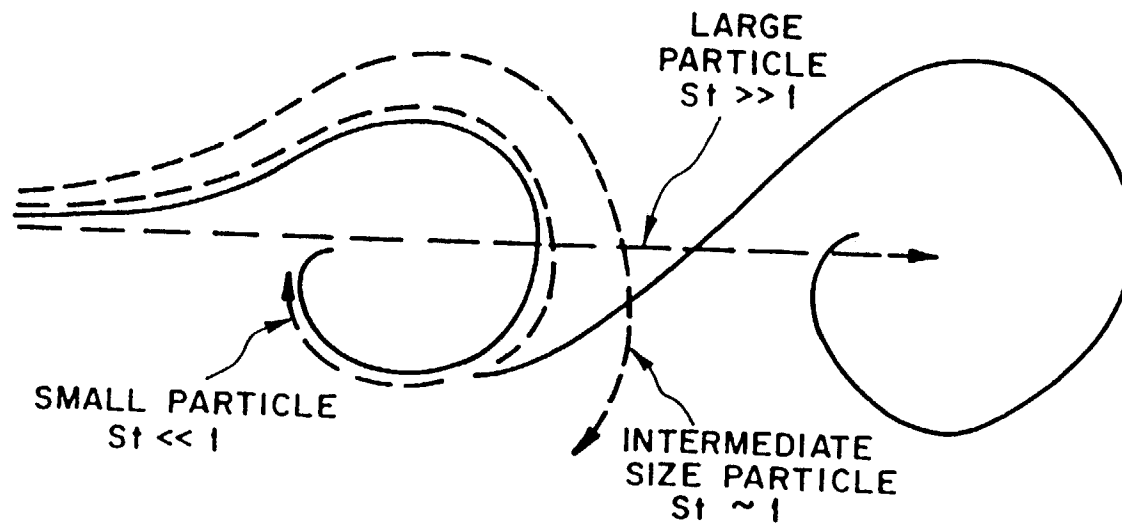St << 1

INTERMEDIATE
SIZE PARTICLE
St ~ 1

Figure 2. Schematic Diagram Illustrating the Effect of Large Scale Structures on
Particle Dispersion
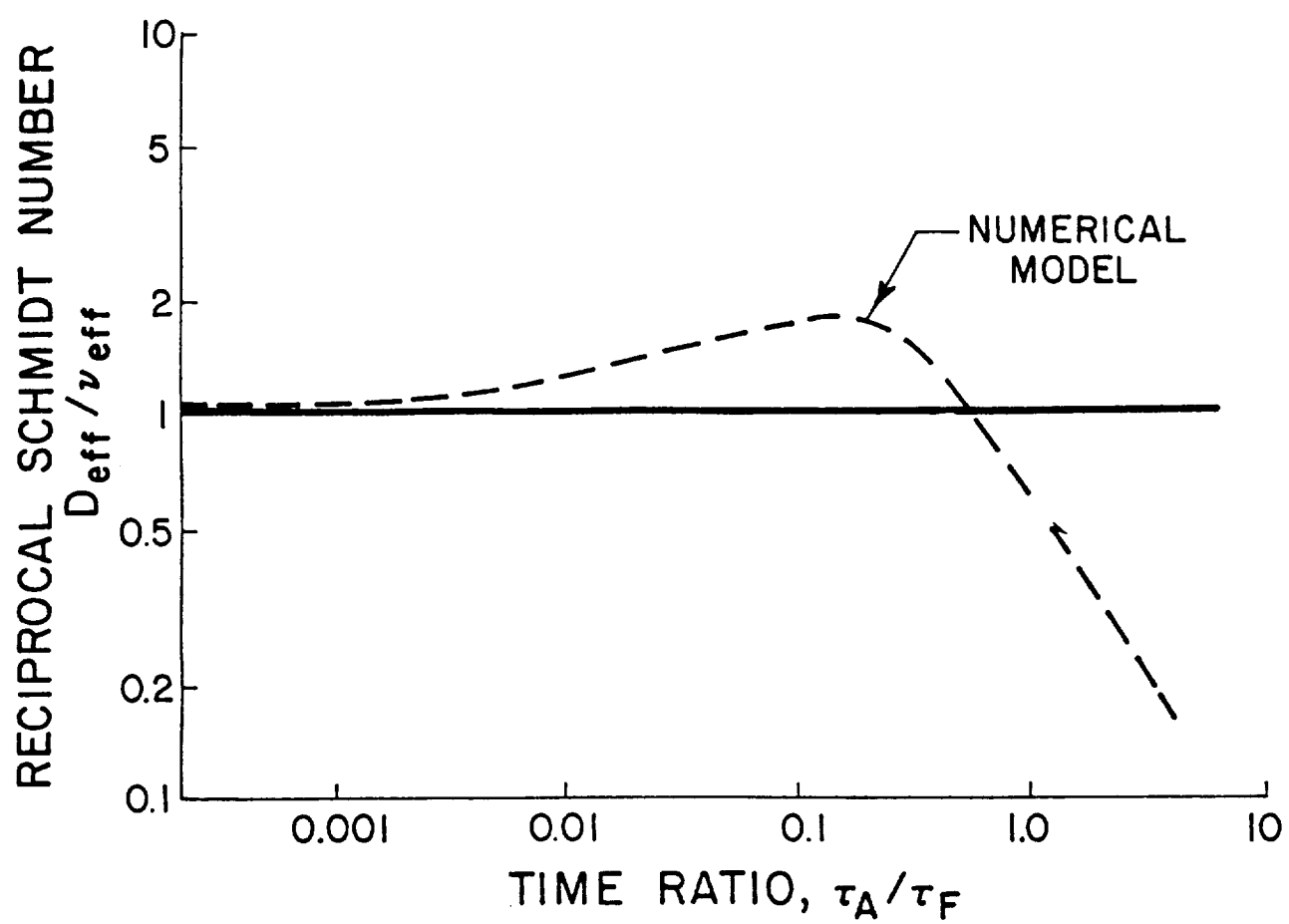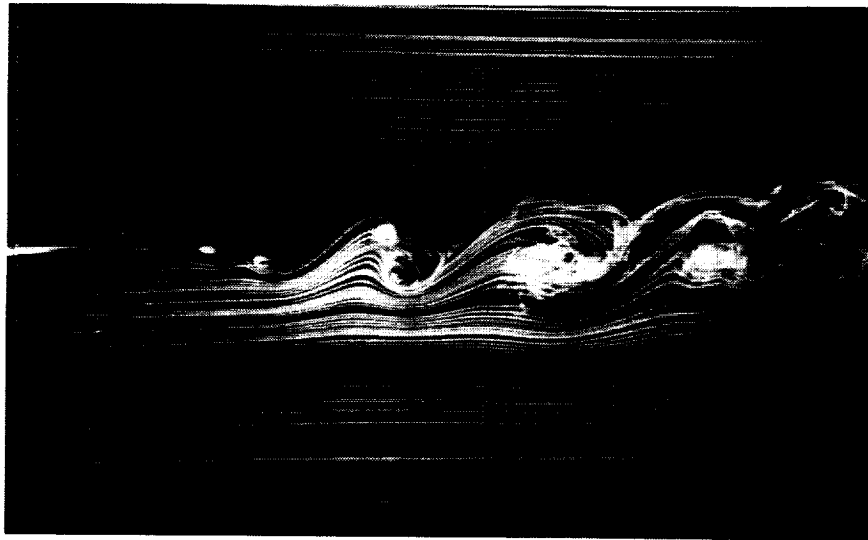
Figure 3. Predicted Particle/Fluid Dispersion Ratio as Function of Stokes Number

Streaklines in **Fluid**

Particle Field

Figure 4. Photographs of Fluid Streaklines and Particles in Large Scale Turbulent
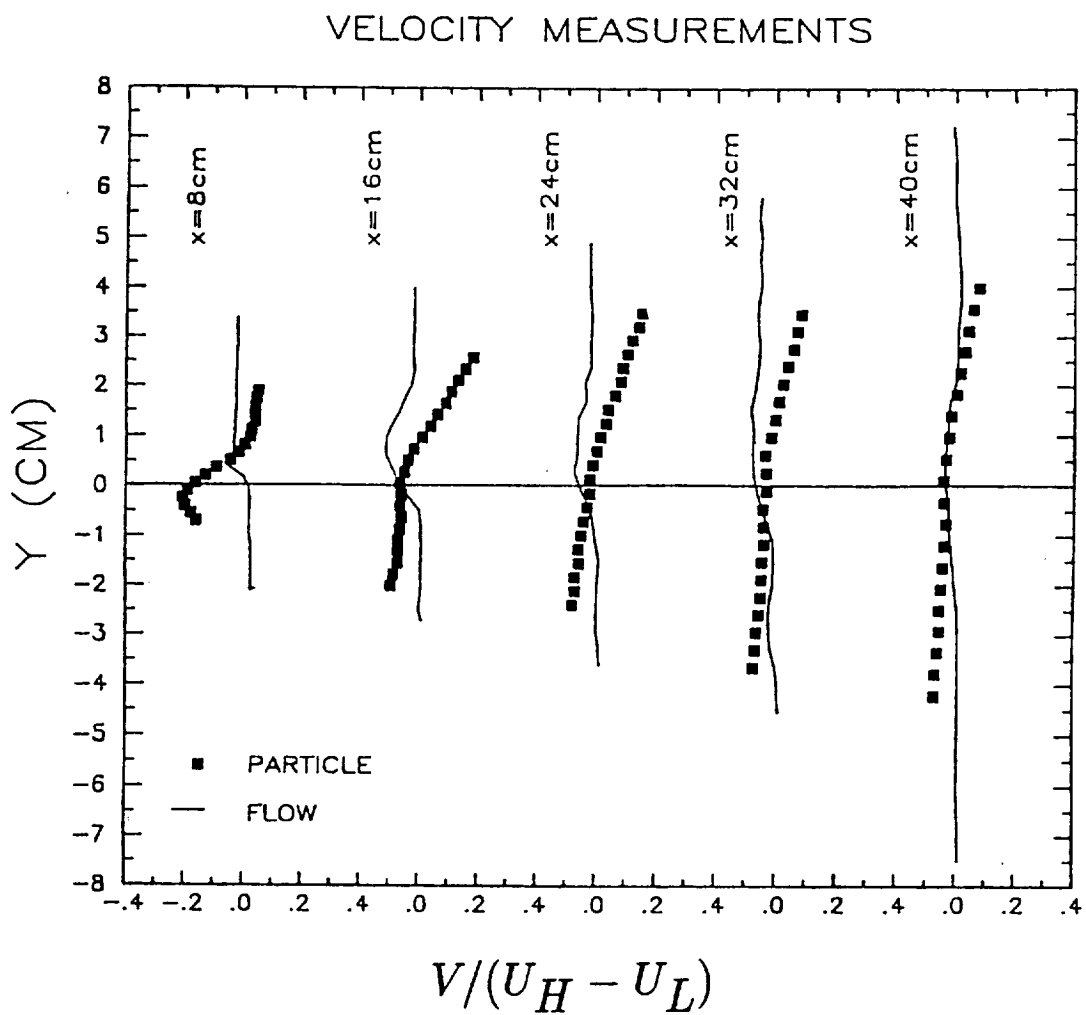Structures (Kamalu *et al.*, 1987)

94

C-2

VELOCITY MEASUREMENTS

Figure 5. Measured Vertical Velocity Component of Fluid and Particles in Mixing Layer (Wen *et al.*, 1987)

NUMERICAL MODELS FOR PARTICLE DISPERSION

Numerical models for fluid-particle flow can be divided into two categories; two-fluid models and trajectory models. A review of these approaches has been provided by Crowe (1982). In the two fluid model, the particulate phase is regarded as another fluid. In the trajectory model, the particle field is established by integrating particle trajectories through the field.

Gradient Transport Models

It is natural in the two fluid model to treat particle dispersion as a gradient transport process and assign a diffusion coefficient to represent particle dispersion due to turbulence. Elghobashi *et al.* (1983) have considered in detail the two-fluid model with the two-equation model for turbulence and applied it to free jets. They recognize that the gradient transport assumption is valid only if the energy containing eddies are much smaller than the length scale for the transport gradient. They suggest a correction term to Ficks law that represents a convective flux due to flow inhomogeneity and which disappears for homogeneous turbulence. The diffusion coefficient is related to the kinematic viscosity through an effective Schmidt number, the value for which is not provided in the paper. The model requires three additional empirical constants above those required for the $k - \epsilon$ model in single phase flows. They apply their model to the prediction flow properties of a jet studied experimentally by Modarress *et al.* (1984) and claim good agreement between measurements and predictions.

Chen and Wood (1985) also use the two-fluid approach to model a jet. They assume that the particle and fluid phase have the same average velocity and justify this assumption on time scale arguments. They also use a gradient transport assumption for particle dispersion due to turbulence and chose an effective Schmidt number of 0.7 which corresponds to the value for diffusion of a passive scalar in a round turbulent jet. Subramanian and Ganesh (1984) measure an effective Schmidt number of 0.47 for the same configuration. Chen and Wood applied their model to experimental studies reported by Modarress *et al.* (1984) and Wood *et al.* (1984) and noted good agreement between predictions and measurements.

The real difficulty in using the gradient transport model for particle dispersion in connection with the two-fluid model is encountered in wall-dominated flows. Here one has to establish boundary conditions for the particle concentration and velocities. The concentration profile will depend on the interaction of particles with the wall. For example, if the particles stick to the wall a different boundary condition must be used than if the particles rebound elastically from the wall. For inelastic collisions, another assumption must be used.

In addition the particle velocity component parallel to the wall is not zero as in a single phase continuum flows. Chen (1986) utilizes concepts from rarefied gasdynamics and calculates a slip velocity which depends on a fluid-particle interaction length. The normal component of velocity is set equal to zero although this would not be true for an inelastic collision. Other ramifications of the two-fluid versus trajectory models are discussed by Crowe (1986).

The advantage of the gradient diffusion model for particle dispersion is that it can be accommodated directly into the two fluid model. It also does not require excessive computational times. The difficulty is the selection of appropriate Schmidt numbers and other empirical parameters for a given application. The relative advantages and

disadvantages of the eulerian and trajectory approaches are discussed by Durst *et al.* (1984).

Monte Carlo Methods

The method most natural to predicting particle dispersion using the trajectory approach is the Monte Carlo method. By this method the turbulent field is represented with a random number generator. The basic idea was first proposed by Hutchinson et al. (1971) and was subsequently used by Gosman and Ioannides (1981) in conjunction with the $k - \epsilon$ turbulence model for sprays. The turbulent fluctuational velocity is selected from a random number generator with a variance proportional to the turbulence energy. The particle motion equation is integrated with this velocity field until it passes from the eddy. The particle-eddy interaction time is established by the characteristic life time of the eddy or by the time for the particle to pass through the eddy. The dissipation length and time scales are chosen as the characteristic size and time and are given by

$$L_e = C_\mu^{3/4} k^{3/2} / \epsilon \qquad 6a)$$

$$T_e = L_e / (2k/3)^{1/2} \qquad 6b)$$

where k is the turbulence energy, ϵ is the dissipation rate and C_μ is an empirical constant arising from the $k - \epsilon$ model. The time to pass through an eddy is approximated by

$$T_p = \frac{L_e}{|U_g - U_p|}$$

where U_p is the particle velocity and U_g is the mean gas velocity. The interaction time is the minimum of the eddy life time and the passage time. If the passage time is small compared to the eddy life time then the crossing trajectory effect is important.

Gosman and Ioannides applied this model as a test case to the experimental study done by Snyder and Lumley (1971) who measured the dispersion of a series of particle types in grid-generated turbulence produced by a vertically oriented wind tunnel. Synder and Lumley found that the heavier copper particles dispersed less than the lighter hollow glass beads. From the current state of knowledge, it is accepted that this trend is due to the crossing trajectory effect. Gosman and Ionaddies report good agreement between the their predictions and Synder and Lumley's results even though their droplet equations do not contain a body force term due to gravity. This was probably an omission in the paper.

The Monte-Carlo technique was used by Chen and Crowe (1984) to model particle dispersion measurements in fully developed pipe flow reported by Arnason and Stock (1984). As with Gosman and Ioannides, they found that the technique worked well for the near isotropic, homogeneous field in Synder and Lumleys experiments. However, it was necessary to tune the model by changing C_μ to achieve the best fit. Applying the model to the pipe flow experiments yielded very poor agreement with the experimental results as shown in figure 6. The model predicted that the larger particles would disperse less than the small particles due to the crossing trajectory effect but the opposite trend was found experimentally. Chen and Crowe rationalized that the turbulence model was too crude for the complex turbulent flow in a pipe. One shortcoming of the model is the

lack of information on the lagrangian length scale which should be used for L_e defined above. The above equations provide, at best, an estimate of the lagrangian length scale.

Faeth *et al.* (Solomon *et al.*, 1983; Solomon *et al*, 1985) have used the Monte-Carlo model extensively with their model for particle and droplet laden jet flows and show good agreement with experimental results. The model is calibrated to fit the analytic results of Hinze (1975) for diffusion of fluid particles from a point source in homogeneous, isotropic turbulence.

The general utility of the Monte-Carlo method for particle and droplet dispersion remains to be established. The Monte Carlo method is attractive because of the minimal empiricism needed to model the flow (provided the stochastic representation of the turbulence is reliable) and the simplicity of handling boundary conditions. The primary problem is the large number of trajectories needed to establish a stationary average in a computational cell.

Another dispersion model which attempts to capture the desirable qualities of the gradient transport and trajectory approaches is the "hybrid" model first proposed by Jurewicz (1976) and subsequently used by others. In this approach the trajectory model is first used to calculate particle concentrations in each cell. Then, a diffusional velocity is added to the particle velocity which is proportional to the concentration gradient and diffusion coefficient. Of course, this model requires selection of a diffusion coefficient.

Nonstationary, nonhomogeneous models

The gradient transport models are inadequate to model particle dispersion by large scale structures. Since particle dispersion appears to be controlled by the large scale motion, the numerical model must represent the essence of these flows. Work in this area is just beginning to appear in the literature.

Chein and Chung (1987) report a report a numerical study of particle dispersion in vortex pairs modeled using discrete vorticies. They found that particles with intermediate Stokes numbers (0.5 to 5) are dispersed more than the fluid particles while at larger Stokes numbers the heavy particles disperse less than the fluid particle.

Chien and Chung (1988) also used the discrete vortex method for generating a time dependent two-dimensional mixing layer. Particles released in this flow field show the same general trend as shown by figure 7. At low Stokes numbers, the particle follow the fluid and disperse as a fluid particle. As the Stokes number is increased the particles disperse more and near a Stokes number of unity the vortex core is almost void of particles as they are centrifuged out. In this regime the particle disperse more than the fluid particle. With further increase in Stokes mumber, the particles become unresponsive to the vortices and move in near rectilinear trajectories. The same trend is noted in a numerical study of jets by Chung and Troutt (1988).

Future work in particle dispersion in large scale structures will witness more advanced fluid mechanic models such as vortex models and pseudo-spectral methods as the computational capability is enhanced by future generation computers.

PARTICLE DRAG COEFFICIENTS

Fundamental to the development of numerical models for gas solids or gas-droplet flows is the particle or droplet equation of motion. In general, there are many forces acting on the disperse phase particle such as the virtual mass force, Basset force, pressure gradient force and the steady state drag force. The most widely accepted formulation for
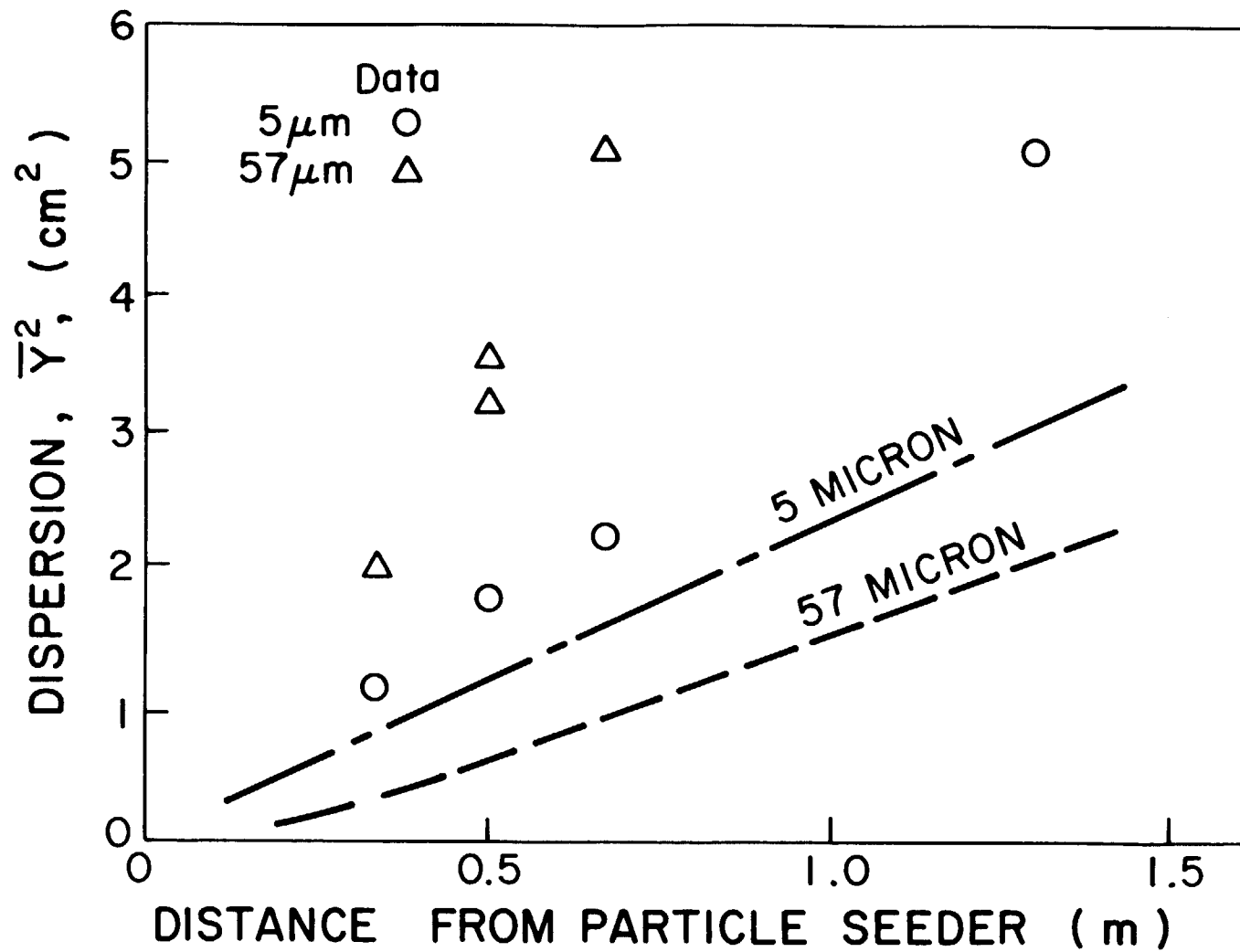
Figure 6. Measured and Predicted Particle Dispersion in Fully Developed Duct Flow (Chen and Crowe, 1984)
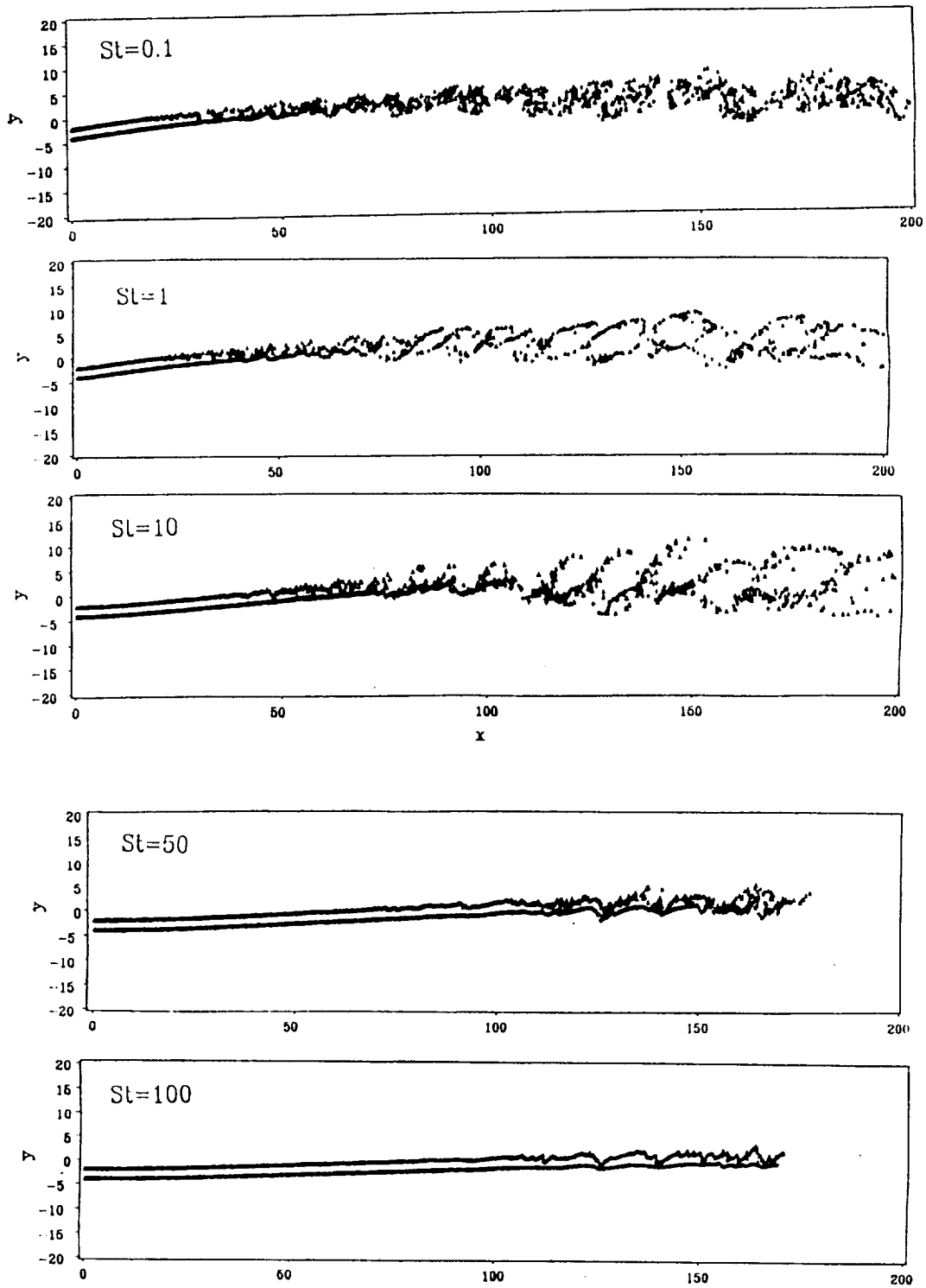
Figure 7. Predicted Particle Field over Range of Stokes Numbers in a Two-Dimensional Mixing Layer (Chien and Chung, 1987)

100

the equation of motion for low Reynolds number flow is that of Maxey and Riley (1983) who derived the equation from basic principles. For gas-solids flows in which the material density of the particle is three orders of magnitude larger than the conveying phase, the primary force is the steady state drag force which is quantified by the value of the drag coefficient, C_D, and related to the steady state drag by.

$$F_D = \frac{1}{2}\rho A_p C_D (U_g - U_p)|U_g - U_p|$$

where ρ is the gas density, A_p is the projected area and $(U_g - U_p)$ is the relative velocity vector between the fluid and the particle.

There is a plethora of literature available on particle drag coefficient. Most of the data have been obtained for single particles or spheres mounted in an airstream. However, in numerical model development, one is more interested in the drag coefficients of particles in a cloud. The particle drag data show significant discrepancies as shown in figure 8.

Ingebo (1956) published a NACA report on particle drag coefficient which he measured by releasing solid particles in an airstream downstream of a grid. The particles were tracked by a rotating mirror camera and the velocity-distance data were reduced to obtain the acceleration and drag force. Ingebo found the drag coefficient was less than the standard value for a sphere and attributed the discrepancy to the acceleration of the particles. Crowe (1962) suggested that the low value could have been due to a critical Reynolds number effect created by the grid upstream of the particle injection location. Arrowsmith (1973) suggested that the local air velocity in the cloud was less than the tunnel speed affecting the calculation of the relative velocity. The discrepancy has yet to be resolved.

Hanson (1952) measured the deceleration of hexane droplets issuing from an atomizer into an air flow. The spray was photographed and the droplet deceleration reduced from the photographs. He assumed that the local gas velocity was constant throughout the chamber. Hanson's results for C_D are very low. Hanson attributed the low drag coefficient to evaporation but this explanation seems unlikely.

Rudinger (1969) injected particles into a vertically oriented shock tube and passed a shock wave through the particle cloud. He used a rotating drum camera to record particle motion. The drag coefficients he reduced were significantly higher than the "standard" curve. Rudinger hypothesized that the turbulence generated by the particles created zig-zag motion which made the particles appear to have an higher "effective" drag coefficient. However the same trend would have been noticed in Ingebo's results.

Crowe (1962) reported measurements on the drag coefficient of burning gun powder. The burning powder was subjected to a shock wave in a vertical shock tube in a manner similar to Rundinger's experiment. Particle motion was measured with a high speed camera. The data lie slightly above the standard curve but well below Rudinger's.

Briffa (1981) has reported on the measurement of droplet drag in sprays. A water spray was photographed to yield a triple exposure of a droplet. The local air velocity was measured by photographing the motion of Lycopodium dust. The reduced drag coefficients were smaller than the standard curve. Briffa attributed this trend to the Basset term in the equation of motion but it is unlikely that the Basset term would be so predominant.
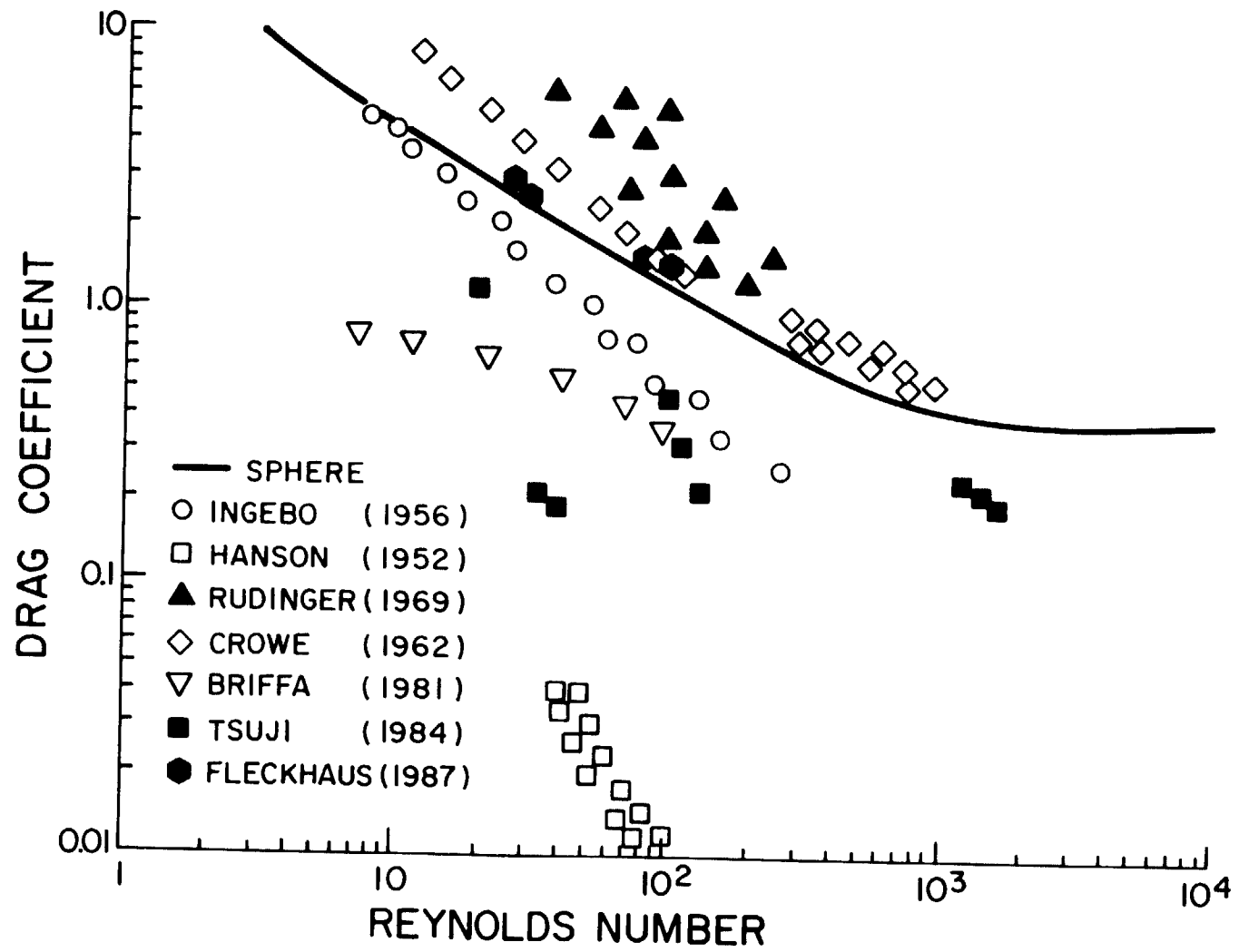
Figure 8. Particle Drag Coefficients for Particles in Gas- Particle Mixtures

Tsuji et al. (1982) generated a stationary array of particles and measured the drag on one particle in the array using the pendulum method. Two configurations were tested; side by side particles and one particle in the wake of another. They found that the drag of the particle in the wake was reduced for separation distances of less than 10 diameters. The difference in drag coefficient does not explain the discrepancies observed in figure 8.

Tsuji et al. (1984) reported on the LDV measurements of particle and air velocities of 200, 500 and 3000 micron particles in a vertical pipe. Small tracer particles were used to measure the gas flow velocity and the signals from the test particles and tracer particles were separated by a special signal discrimination device. The drag coefficients resulting from Tsuji et al.'s experiments have been reduced by Lee (1987). The data fall below the standard drag curve but demonstrate significant scatter. Lee correlates the data with particle volume fraction, Froude number, Reynolds number (based on turbulent fluctuational velocity) and density ratio (particle to fluid material density ratio). By so doing, he was able to fit the data on a single curve. Still, extension of the empirical results to other conditions is tenuous because one would not anticipate that the aerodynamic drag would depend on the density ratio.

Very recently, Fleckhaus et al. (1987) have reported measurements of particle velocities and concentrations in a jet with a two- dimensional LDA system. They also had tracer particles in the jet to obtain the gas-phase velocity. By fitting cubic splines to their velocity measurements, they were able to reduce particle accelerations. The drag coefficients were obtained by knowing the particle (glass beads) size and relative velocity. Their drag data lie above, but close to, the standard curve.

There is a need to establish a valid drag coefficient for particles in a turbulent flow and to resolve the many discrepancies apparent in the data. It would be appropriate to repeat some of the earlier experiments using modern instrumentation to either validate the data or indicate the reason for the observed trends. Until more specific information is available, one is advised to use the standard drag curve for an isolated particle.

ACKNOWLEDGEMENT

REFERENCES

Arrowsmith, A. and Foster, P.J. (1973) The Motion of a Stream of Monosized Liquid Droplets in Air, Chem. Engr. Jnl., 5, 243-250.

Arnason, G. and Stock, D.E. (1984) Dispersion of Particles in Pipe Flow, Gas-Solids Flows, ASME FED- Vol. 10, Energy Resources Technology Conference, Feb. 12-16, 25-30.

Briffa, F.E.J. (1981) Transient Drag in Sprays, Proc. 18th Intl. Symp. on Combustion, 307-319.

Brown, G.L. and Roshko, A. (1974) On Density Effects and Large Structure in Turbulent Mixing Layers, *Jnl. Fluid Mech.* **64**, Part 4, 775-816.

Chen, C.P. and Wood, P.E. (1985) A Turbulence Closure Model for Dilute Gas-Particle Flows, *Can. Jnl. Chem. Engr.*, **63**, 349-360.

Chen, C.P. (1986) Numerical Analysis of Confined Recirculating Gas-Solid Turbulent Flows, *Gas-Solid Flows - 1986*, ASME FED 35, 117-124.

Chen, P.P. and Crowe, C.T. (1984) On the Monte-Carlo Method for Modeling Particle Dispersion in Turbulence, *Gas-Solids Flows*, ASME FED- Vol. 10, Energy Resources Technology Conference, Feb. 12-16, 37-42.

Chien, R. and Chung, J.N. (1987) Effect of Vortex Pairing on Particle Dispersion in Turbulent Shear Flow, *Int. Jnl. Multiphase Flows*, **13**, 785-802.

Chien, R. and Chung, J.N. (1988) Simulation of Particle Dispersion in a Two-Dimensional Mixing Layer, *AIChE Jnl.* (in press).

Chung, J.N. and Troutt, T.R. (1988) Simulation of Particle Dispersion in a Jet, *Jnl. Fluid Mech.* **186**, 199-

Crowe, C.T. (1962) Drag Coefficients for Burning and Non-burning Particles Accelerating in a Gas Stream, PhD Thesis, Univ. of Mich.

Crowe, C.T., Nicholls, J.A. and Morrison, R.B. (1962) Drag Coefficients of Inert and Buring Particles Accelerating in Gas Streams, *Proc. 9th Intl. Symp. Combustion*, 395-402.

Crowe, C.T. (1982) Review: Numerical Models for Dilute Gas- Particle Flows, *Jnl. Fluids Engr.* **104**, 297-303.

Crowe, C.T., Gore, R.A. and Troutt, T.R. (1985) Particle Dispersion by Coherent Strcutures in Free Shear Flows, *Particle Sci. Tech. Jnl.*, **3**, 149-158.

Crowe, C.T.(1986) Two-Fluid versus Trajectory Models; Range of Applicability, *Gas-Solids Flows - 1986* ASME FED 35, 91-96.

Durst, F., Milojevic, D. and Schonung, B. (1984) Eulerian and Lagrangian Predictions of Particulate Two-Phase Flows: a Numerical Study, *App. Math Modeling*, **8**, 101-115.

Elghobashi, S.E. and Abou-Arab, T.W. (1983) A Two-Equation Turbulence Model for Two-Phase Flows. *Phys. Fluids*, **26**, 4, 931-938.

Fleckhaus, D., Hishida, K. and Maeda, M. (1987) Effect of Laden Solid Particles on the Turbulent Flow Structure of a Round Free Jet, *Experiments in Fluids*, **5**, 323-333.

Goldschmidt, V.W., Houserholder, M.K., Ahmadi, G. and Chuang, S.C. (1972) Turbulent Diffusion of Small Particles Suspended in Turbulent Jets, *Prog. in Heat and Mass Trans.*,6, 487-508.

Gore, R.A., Crowe, C.T., Troutt, T.R. and Riley, J.J. (1985) A Numerical Study of Particle Dispersion in Large Scale Structures, ASME Book No. G0034.

Gosman, A.D. and Ioannides, E. (1981) Aspects of Computer Simulation of Liquid-Fuelled Combustors", AIAA-81-0323, 19th Aerospace Sciences Meeting, St. Louis, Jan 12-15.

Hanson, A.R. (1952) The Evaporation of a Fuel Spray in an Airstream and the Effect of Turbulence on Droplet Size Distribution, *Proc. 2nd Midwest Conf. on Fluid Mech.*, 415-428.

Hinze, J.O. (1972) Turbulent Fluid and Particle Interaction, *Prog. in Heat and Mass Trans.*, 6, 433-452.

Hinze, J.O. (1975) *Turbulence*, McGraw-Hill.

Householder, M.K. (1968) Turbulent Diffusion of Small Particles in a Two-dimensional free jet, Ph.D. Thesis, Purdue University.

Hutchinson, P., Hewitt, G.F. and Dukler, A.E. (1971) Deposition of Liquid or Solid Dispersions from Turbulent Gas Streams: a Stochastic Model, *Chem. Engr. Sci.*, 26, 419-439.

Ingebo, R.D. (1956) Drag Coefficients of Droplets or Solid Spheres in Clouds Accelerating in a Gas Stream, NACA TN 3762.

Jurewicz, J.T. and Stock, D.E. (1976) A Numerical Model for Turbulent Diffusion in Gas-Particle Flows, ASME WAM, Paper No. 76-WA/FE-33.

Kamalu, N., Wen, F., Hanle, R., Chung, J.N. and Troutt, T.R. (1987) Visualization of Particle Dispersion in Free Shear Flows, *Bull. Amer. Phy. Soc., Ser. II*, 32, 2066.

Kobayashi, H. Masutani, S.M., Azuhata, S.,Arashi, N., Hishinuma, Y. (1987) Dispersed Phase Transport in a Plane Mixing Layer, *Second Intl. Symp. on Transport Phenomena in "Turbulent Flows"*, Tokyo, Oct. 25-29.

Laats, M.K. and Frishman, F.A. (1970) Scattering of a Inert Admixture of Different Grain Size in a Two-Phase Axisymmetric Jet, *Heat Transfer - Soviet Research*, 2, 6, 7-12.

Lazaro, B.J. and Lasheras, J.C. (1987) Entrainment and Mixing Mechanisms in a Two-phase Flow Plane Free Shear Layer, *Bull. Amer. Phys. Soc. Ser. II*, 32, 2035.

Lee, S.L. (1987) Particle Drag in a Dilute Turbulent Two-Phase Suspension Flow, *Intl. Jnl. Multiphase Flow*, **13**, 2, 247-256.

Lilly, G.P. (1973) Effect of Particle Size on Particle Eddy Diffusivity *Ind. Eng. Chem. Fund.*, **12**, 3, 268-275.

Maxey, M.R. and Riley, J.J. (1983) Equation of Motion for a Small Rigid Sphere in a Non-uniform Flow, *Phys. Fluids* **26**, 4, 883-889.

Modarress, D., Wuerer, J. and Elghobashi, S. (1984) An Experimental Study of a Turbulent Round Two-Phase Jet, *Chem. Engr. Commun.*, **28**, 341-354.

Modarress, D., Tan, H. and Elghobashi, S. (1984) Two- Component LDA Measurement in a Two-Phase Turbulent Jet, *AIAA Jnl.* **22**, 624-630.

Phythian, R. (1975) Dispersion by Random Velocity Fields, *Jnl. Fluid Mech.*, **67**, Part 1, 145-153.

Reeks, M.W. (1977) On the Dispersion of Small Particles Suspended in an Isotropic Turbulent Fluid, *Jnl. Fluid Mech.*, **83**, Part 3, 529-546.

Reeks, M.W. (1981) The Transport of Discrete Particles in Turbulent Shear Flows, Central Electricity Generating Board Rpt. RD/B/5070N81.

Rudinger, G. (1969) Effective Drag Coefficient for Gas-Particle Flow in Shock Tubes" ASME WAM Pap. No. 69-WA/FE 21.

Solomon, A.S.P., Shuen, J-S, Zhang, Q-F and Faeth, G.M. (1985) Structure of Nonevaporating Sprays, Part I: Initial Conditions and Mean Properties, *AIAA Jnl.* **23**, 10, 1548-1555.

Solomon, A.S.P., Shuen, J-S, Zhang, Q-S, and Faeth, G.M. (1985) Structure of Nonevaporating Sprays, Part II: Drop and Turbulence Properties. *AIAA Jnl.* **23**, 11, 1724-1730.

Singamsetti, S.R. (1966) Diffusion of Sediment in a Submerged Jet, *ASCE Proceedings*, HY 2, 153-168.

Synder, W.H. and Lumley, J.L. (1971) Some Measurements of Particle Velocity Autocorrelation Functions for Turbulent Flow, *Jnl. of Fluid Mech.*, **48**, 41-71.

Soo, S.L. (1967) *Fluid Dynamics of Multiphase Systems*, Blaisdell Pub. Waltham, Mass.

Stuart, J.T. (1967) On Finite Amplitude Oscillations in Laminar Mixing Layers, *Jnl. Fluid Mech.* **29**, Part 3, 417-440.

Subramanian, V and Ganesh, R. (1984) Particle-Gas Dispersion Effects in Round Jets, *Can. Jnl. of Chem. Engr.*, **62**, 161-164.

Taylor, G.I. (1921) Diffusion by Continuous Movements, *Proc. London Math. Soc.***20**, 196-211.

Tchen, C.M. (1947) Mean Value and Correlation Problems connected with the Motion of Small Particles suspended in a turbulent fluid.PhD Thesis, Delft.

Tsuji, Y., Morikawa, Y and Terashina, K. (1982) Fluid Dynamic Interaction between Two Spheres, *Intl. Jnl. Multiphase Flows*,**8**, 1, 71-82.

Tsuji, Y., Morikawa, Y. and Shiomi, H. (1984) LDV Measurements of an Air-Solid Two-Phase Flow in a Vertical Pipe, *Jnl. Fluid Mech.*, **139**, 417-434.

Wall, T.F. Subramanian, V. and Howley, P. (1984) An Experimental Study of the Geometry Mixing and Entrainment of Particle Laden Jets up to Ten Diameters from the Nozzle, *Trans. Inst. Chem. Engr.*, **60**, 231.

Wells, M.R. and Stock, D.E. (1983) The effects of crossing trajectories on the dispersion of particles in a turbulent flow, *Jnl. Fluid Mech.*, **136**, 31-62.

Wen, F., Gajdeczko, B., Chung, J.N. and Crowe, C.T. (1987) Particle Dispersion Measurements in Free Shear Layers, *Bull. Amer. Phy. Soc., Ser. II*, **32**, 2036.

Yule, A.J.(1981) Investigations of Eddy Coherence in Jet Flows, *Proc. of the Intl. Conf.; The Role of Coherent Structures in Modelling Turbulence and Mixing*, Ed. J. Jimenez, Springer-Verlag, Berlin, 188-207.

Yuu, S., Yasukouchi, N., Hirosawa, Y. and Jotaki, T. (1978) Particle Turbulent Diffusion in a Dust Laden Round Jet, *AIChE Jnl.*, **24**, 3, 509-519.

Migration Arising From Gradients in Shear Stress: Particle Distributions in Poiseuille Flow

D. T. Leighton, Jr.
University of Notre Dame
Notre Dame, IN 46556

Recent work has demonstrated that the time dependent properties exhibited by concentrated suspensions of non-colloidal spheres when sheared in a conventional Couette viscometer may be explained in terms of shear-induced particle migrations (Gadala-Maria and Acrivos, 1980; Leighton and Acrivos, 1987b). These suspensions were observed to exhibit both a short-term increase in viscosity upon shearing immediately after loading into the Couette device and a subsequent long-term decrease after prolonged shearing, which were used to estimate the effective shear-induced diffusivity for concentrated suspensions both normal to the plane of shear and parallel to gradients in fluid velocity within the plane of shear (Leighton and Acrivos, 1987b).

In this paper the experimental evidence for the existence of shear induced migration processes is reviewed and the mechanism proposed by Leighton and Acrivos (1987b) is described in detail. The proposed mechanism is shown to lead to the existence of an additional shear induced migration in the presence of gradients in shear stress such as would be found in Poiseuille flow, and which may be used to predict the amplitude of the observed short-term viscosity increase. The concentration and velocity profiles which result from such a migration are discussed in detail and are compared to the experimental observations of Karnis, Goldsmith and Mason (1966).

1. Introduction

Particle migrations across fluid streamlines in suspensions may result from a wide variety of mechanisms, ranging from Brownian type diffusive motions to the inertia induced drift mechanisms studied by Ho and Leal (1974) and others. In this paper we are concerned with *shear-induced* particle migrations which have been observed to occur in concentrated suspensions of non-colloidal particles (particles sufficiently large that colloidal forces are unimportant at distances comparable to the particle diameter) and at sufficiently low Reynolds numbers that inertial forces may be neglected. Particle migrations under these conditions have been observed by a number of researchers. Early work by Karnis and Mason (1967) demonstrated that particles tend to accumulate behind an advancing meniscus in flow through a tube, and to be depleted behind a receding meniscus, the magnitude of the phenomenon being a strong function of the particle diameter/tube radius ratio and the concentration, suggesting that the particle migration was the result of some type of wall effect. Leighton (1985) demonstrated that if proper precautions were not taken, this effect can lead to serious errors in viscosity measurements in concentrated suspensions. The coefficient of shear-induced self-diffusion of spheres in a sheared suspension (i.e., the diffusion or dispersion arising from a random walk of particles in a sheared suspension analogous to Brownian diffusion) was examined by Eckstein, Bailey and Shapiro (1977) and later by Leighton and Acrivos (1987a).

The observations of particle migration of primary interest here were initially made by Gadala-Maria and Acrivos (1980) in suspensions of 40μm to 50μm diameter polystyrene spheres in silicone fluids. In the course of viscometric measurements of concentrated suspensions made with a conventional Couette viscometer, Gadala-Maria and Acrivos (1980) found that the suspension viscosity would decrease after prolonged shearing, and eventually reach a steady-state value which was as much as a factor of two below the initially observed value (cf. Figure 1). In
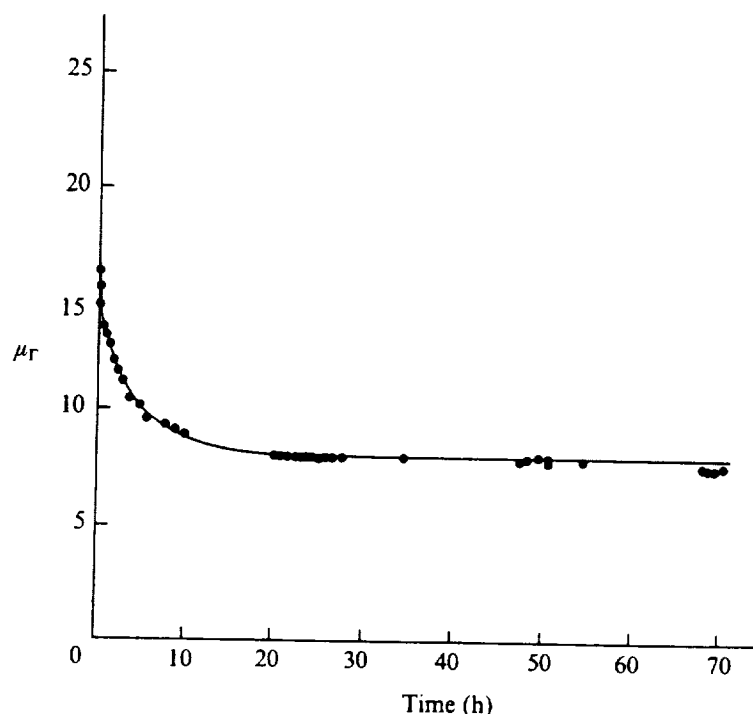
FIGURE 1 Relative viscosity of a $\phi = 0.45$ suspension as a function of the time that it had been sheared in the Couette device at $\dot{\gamma} = 24$ s^{-1}. Polystyrene spheres, 40–50 μm in diameter in a mixture of silicone oils (from Gadala-Maria 1979, figure 33).

subsequent experiments, Leighton and Acrivos (1987b) demonstrated that the viscosity decrease was due to particle migration out of the sheared gap and into the reservoir by sealing the base of the Couette device with a layer of mercury and showing that the phenomenon disappeared. The rate of particle migration was found to be proportional to the shear rate and the square of the particle radius, and was successfully modelled by a one-dimensional diffusion process. The viscosity decrease was thus used to measure the effective diffusivity in the direction normal to the plane of shear for concentrated suspensions. The effective diffusivity was found to be a very strong function of concentration (cf. Figure 2) and to be much larger than the shear-induced coefficient of self-diffusion measured by Leighton and Acrivos (1987a).

During the course of their experiments (also with polystyrene spheres in silicone oils) Leighton and Acrivos (1987b) observed that, upon first shearing the suspension in the Couette device, the viscosity would increase over a total strain of approximately 100, reaching a steady-state value before the subsequent long-term viscosity decrease. Since the long-term viscosity decrease only became significant after a strain of about 10^3 had elapsed, the two phenomena were well separated in time and could be investigated independently. As it is central to the present investigation into concentration distributions in Poiseuille flow, the short term viscosity decrease phenomenon is examined in more detail in the next section, which follows the development by Leighton and Acrivos (1987b).

2. Short-Term Viscosity Increase

The observed timescale appropriate to the initial viscosity increase phenomenon was found to be inversely proportional both to the shear rate $\dot{\gamma}$ and to the square of the ratio of the particle
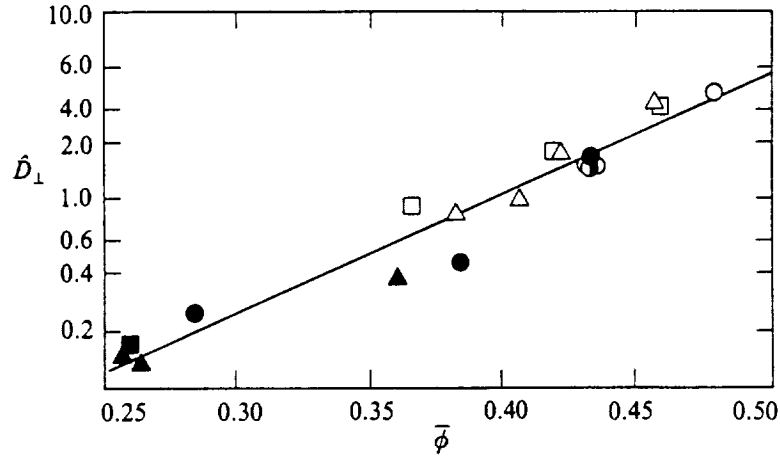
FIGURE 2 Diffusion coefficients calculated from the long-term viscosity decrease experiments: □, 46 μm polystyrene in 0.639 mm gap; ○, 46 μm polystyrene in 1.261 mm gap; △, 87 μm polystyrene in 1.261 mm gap. Shear rates were: filled symbols, 76 s⁻¹; open symbols, 24 s⁻¹; half-filled symbols, 7.6 s⁻¹.

diameter to gap width ratio $\hat{a}$; thus this effect was explained in terms of a shear-induced migration of particles across the width of the Couette gap analogous to the long-term viscosity decrease phenomenon. This could only be the case, however, if the suspension flowing into the gap during the loading procedure acquired a concentration distribution across the gap that was different from the equilibrium profile corresponding to Couette flow. Then, upon shearing, the particle distribution would diffuse into that appropriate for the Couette flow, and thereby induce a change in the observed viscosity. The actual change in the viscosity results from the non-linear dependence of the observed viscosity on the concentration profile. For example, if the concentration profile is only slightly non-uniform and is assumed to be symmetric about the centerline of the gap, then the observed viscosity may be calculated to be:

$$\frac{\mu_{obs}}{\overline{\mu}} - 1 = \frac{1}{\overline{\mu}}\left[\frac{1}{b}\int_0^b \frac{1}{\mu}dy\right]^{-1} = -\left[(\frac{1}{\mu}\frac{d\mu}{d\phi})^2 - \frac{1}{2}\frac{1}{\mu}\frac{d^2\mu}{d\mu^2}\right]\Big|_{\phi}\frac{1}{b}\int_0^b (\Delta\phi)^2 dy + O(<(\Delta\phi)^3>) \qquad (2.1)$$

where the viscosity has been expanded in a Taylor series about $\phi = \overline{\phi}$. In equation 2.1, μ is the viscosity that corresponds to a uniform concentration $\overline{\phi}$, $\Delta\phi = \phi(y)-\overline{\phi}$ is the deviation from the average concentration across the gap, y = 0 denotes the centerline of the gap, and y = ±b the walls. Note that the variation in viscosity is proportional to the average value of $(\Delta\phi)^2$ across the gap for small fluctuations in concentration. The viscosity function in equation 2.1 may be calculated from the dependence of viscosity on concentration observed by Leighton and Acrivos (1987b):

$$\frac{\mu}{\mu_0} = \left[1 + \frac{\frac{1}{2}[\mu]\,\phi}{1 - \phi/\phi_m}\right]^2 \qquad (2.2)$$

an Eiler's equation where ϕ_m is the maximem particle concentration and $[\mu]$ is the intrinsic viscosity. The best fit values for the suspensions used in the experiments discussed here in the

111

range $.3 < \phi < .5$ were $\phi_m = 0.58$ and $[\mu] = 3.0$. From (2.2) it is found that any non-uniformity in concentration leads to a decrease in the observed viscosity, the magnitude of which is a strong function of the average concentration. Since the viscosity was observed to increase upon shearing, it was concluded that the initial concentration profile established upon loading the suspension into the gap was more non-uniform than that corresponding to Couette flow.

2.1. *Diffusion model for the observed short-term viscosity increase*

The viscosity increase phenomenon was modelled by assuming that the diffusion coefficient across the gap was constant throughout the migration. This approximation is acceptable if the variation in concentration is sufficiently small, and in any case the experiment yielded some average value of the diffusion coefficient for the migration. If the initial concentration profile is given by $\phi(0,y)$ and the concentration after a long period of shear is $\bar{\phi}$ (assumed to be constant), the concentration profile at all times is given by:

$$\phi(y,t) = \bar{\phi} + \sum_{n=1}^{\infty} B_n \cos\frac{n\pi y}{b} \exp\left(\frac{-n^2\pi^2 D_{\parallel} t}{b^2}\right) \qquad (2.3)$$

where

$$B_n = \frac{2}{b} \int_0^b \phi(0,y) \cos\frac{n\pi y}{b}\, dy$$

and $D_{\parallel}$ is the diffusivity within the plane of shear parallel to gradients in fluid velocity.

To further simplify the model, equation 2.3 was approximated by its limiting form at long times, i.e. the coefficients were chosen such that:

$$B_1 \neq 0; \quad B_n = 0, \quad n \neq 1 \qquad (2.4)$$

in which case, to obtain accurate values of the diffusion coefficient under this assumption, equation 2.3 was fitted only to data taken after sufficient time has elapsed for the neglected terms to become unimportant. Since these higher-order terms decrease exponentially with a rate constant at least four times that of the leading-order term, this requirement was easily met. Thus the model describing the short-term viscosity increase contains three adjustable parameters: the equilibrium uniform concentration; the amplitude of the initial variation in concentration B_1; and the diffusion coefficient. The first of these was fixed by the equilibrium viscosity corresponding to the concentration of the suspension initially loaded; thus the rate at which the viscosity approached its equilibrium value and the magnitude of the deviation between this and its value at the start of the experiment yielded the diffusion coefficient and the approximate initial concentration variation across the gap

It is important to note that the above development tacitly assumes that the concentration profile is not a function of the distance up the gap. In practice this is unlikely to be true since at the base of the gap the concentration profile will correspond to the entrance region into the gap, while sufficiently far up the gap it should correspond to the steady-state distribution resulting from Poiseuille flow. While this will be discussed in more detail in section 4, it is noted here that while variations in the initial concentration profile up the gap may affect the estimated amplitude of the concentration variation B_1, it should not affect the calculated value of $D_{\parallel}$. This arises from the assumption that the diffusivity is essentially constant within the gap, corresponding to the average concentration which does not vary along the length of the gap, and thus the rate at which the concentration approaches its steady-state distribution is the same at all positions along the gap.

2.2 *Experimental results*

Short-term viscosity increase experiments were performed by Leighton and Acrivos (1987b) with suspensions of 46μm and 87μm polystyrene spheres at concentrations from 30% to 50% in

two mixture of silicone oils with viscosities of 1.22p and 1.07p. The measurements were taken using Couette gap widths of 0.639mm, 1.261mm and 2.513mm. The gap height for all experiments was 4.508cm, and the bob diameter was 4.7498cm.

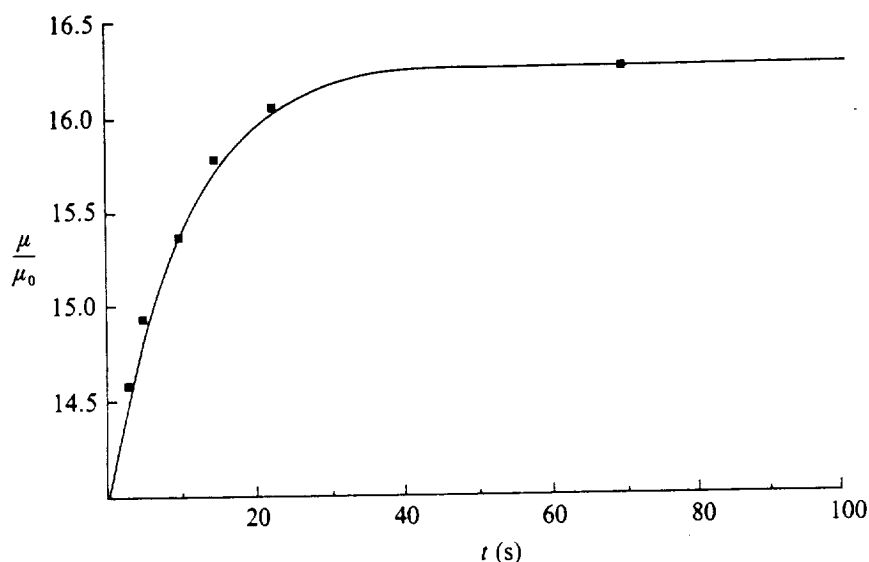The fit of the data to the model was excellent (cf. Figure 3); however, owing to the many

FIGURE 3 Short-term viscosity increase with shearing, 46 μm polystyrene suspension. Model parameters were: $\bar{\phi} = 0.45$, $\dot{\gamma} = 2.4\ s^{-1}$, $\hat{D}_{\parallel} = 1.8$, $B_1 = 0.062$.

assumptions that were necessary in deriving (2.3), the calculated values of the diffusion coefficient and concentration fluctuation across the gap must be considered only approximate. The diffusion coefficient was found to be proportional to $\dot{\gamma}a^2$ and, as in the case of diffusion normal to the plane of shear measured in the long-term viscosity decrease experiments, was a strong function of concentration. A plot of the diffusion coefficient as a function of concentration is given in Figure 4, where the dashed line is the diffusion coefficient normal to the plane of
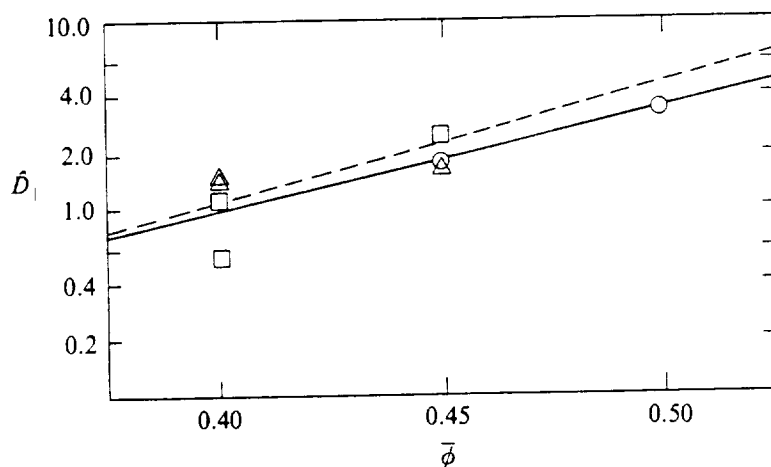

FIGURE 4 Diffusion coefficient observed in the short-term viscosity-increase experiments: ○, 46 μm polystyrene in medium gap; □, 46 μm polystyrene in small gap; △, 87 μm polystyrene in medium gap. Dashed line is the diffusion coefficient observed in the long-term viscosity-decrease experiments.

113

shear. The fact that the measured values of the two diffusion coefficients were almost identical provides us with added confidence that the viscosity increase was interpreted correctly as resulting from a particle migration across the gap width.

The short-term viscosity increase phenomenon was observable only for a narrow range of particle diameters, suspension concentrations and Couette gap widths. This was due in part to the fact that, since the diffusion coefficient was found to be proportional to the square of the particle radius, the total length of shearing necessary to reach steady-state was inversely proportional to $\hat{a}^2$, the square of the ration of the particle diameter to gap width. Thus, for very large values of $\hat{a}$ (such as were obtained for experiments with the 87μm polystyrene spheres in the narrow Couette gap) the strain associated with the migration was sufficiently short that it was not possible to reliably separate fluctuations in the viscosity due to migrations across the gap from those due to the initial equilibration of any short range order in the suspension, first observed by Gadala-Maria and Acrivos (1980). Similarly, the timescale for the viscosity increase was also much too short for experiments with the 46μm spheres in the narrow gap and a 50% concentration, owing to the high value of the dimensionless diffusion coefficient found at this concentration.

At 30% solids concentration, a different experimental difficulty was encountered in that, although the total fluctuation in concentration across the gap may have been the same as that observed for more concentrated suspensions, the resultant variation in the observed viscosity was too small to be accurately measured. From the observed dependence of viscosity on concentration, the same fluctuation in concentration across the width of the gap affects the observed viscosity at an average concentration of 30% by an amount that is less by an order of magnitude than that at 50%.

Finally, for some combinations of concentration, particle diameter and gap width, the short-term viscosity increase effect was not observable. No useable measurements were obtained for tha suspensions of either 46μm or 87μm spheres in the large Couette gap at concentrations of 30% to 45%, and for suspensions of 46μm spheres at 30% to 40% concentration in the medium Couette gap. Possible causes for the absence of a measurable initial increase will be discussed in section 4. Table 1 presents the calculated amplitude of the concentration fluctuation across the channel for those experiments where it was measurable.

Particle diameter (μm)	Gap width (mm)	ϕ	$\hat{D}$	B_1
46	0.639	0.40	1.1	0.131
		0.40	0.54	0.094
		0.45	2.45	0.075
	1.261	0.45	1.7	0.062
		0.50	3.2	0.081
87	1.261	0.40	1.4	0.050
		0.40	1.4	0.075
		0.45	1.6	0.063

TABLE 1. Estimated diffusion coefficient and amplitude of concentration fluctuation for the short-term viscosity-increase experiments

3. Mechanisms leading to shear-induced migration

Thus far, we have presented experimental evidence for the existence of shear-induced particle migrations arising from gradients in concentration and shear stress. To see how these migrations take place we follow the development provided by Leighton and Acrivos (1987b). Let us first examine the case of migration due to gradients in particle concentration.

Consider a single marked sphere of radius a in a suspension of otherwise identical spheres undergoing the viscous linear shear flow $u = \dot{\gamma}y$, where u is the velocity in the x-direction. As the sphere interacts with its neighbors in the shear flow, it will experience a series of displacements in both the y- and z-directions with a characteristic length proportional to a and a frequency proportional to the shear rate $\dot{\gamma}$. In the absence of any gradient in concentration, these displacements will be random with zero mean (i.e. on average the particle will remain on its initial streamline), and thus will constitute a random walk. But, as is well known, in the presence of a concentration gradient such a random walk will lead to a diffusive flux and thus may be characterized by a diffusion coefficient, in this case with the dimensional scaling $\dot{\gamma}a^2$, the same as was observed in the experiments described here. It is important to note that in a dilute suspension the spheres will return to their initial streamlines at the end of all two-particle interactions owing to the linearity of the viscous-flow equations when only viscous forces are present. As a consequence, at least three particles must interact to yield the permanent displacements that lead to a random walk, and therefore, since the reate at which two particles interact with the marked sphere is proportional to $\dot{\gamma}\phi^2$, the diffusion coefficient must be proportional to $\phi^2\dot{\gamma}a^2$ in the dilute limit.

This source of diffusive flux, termed shear-induced self-diffusion, may be measured by examining the random walk of a single marked particle in a homogeneous suspension. Experiments carried out along these lines have been conducted by Eckstein, Bailey & Shapiro (1977), and more recently by Leighton & Acrivos (1987a), and have demonstrated that the diffusion coefficient is indeed proportional to $\dot{\gamma}a^2$. Leighton & Acrivos (1987a) also obtained a dimensionless value of the diffusivity of about $\phi^2/2$ in the dilute limit, in agreement with the scaling predicted by the theory. The measured coefficient of self-diffusion, however, was found to be a much weaker function of concentration and, at a concentration of 40%, had a value nearly an order of magnitude lower than the diffusivity that was calculated from the experiments described earlier in this work. The discrepancy between the observations of self-diffusion and effective diffusivity in the presence of a gradient in concentration suggests, therefore, that the presence of a concentration gradient in some way induces a drift of particles from regions of high to low concentration in addition to that provided by random self-diffusion.

The most likely source of this additional drift is that interparticle interactions in the presence of a gradient in concentration lead to an average displacement of the marked sphere from regions of high to low concentration. It is not clear at this stage whether interactions in the presence solely of viscous forces can lead to such a drift. Direct calculations of the drift for such a suspension would require consideration of interactions involving at least three spheres in a dilute suspension and, in concentrated suspensions where the average interparticle separation distance is very small, the interaction of many spheres would have to be taken into account. Such calculations are far beyond the capabilities of current analytical techniques, and are also quite difficult to deal with numerically owing to the very large number of particles that must be included in any computation.

As we shall presently demonstrate, however, for sufficiently concentrated suspensions of real non-colloidal particles, it is not necessary or even appropriate to consider only the influence of purely viscous hydrodynamic forces because, in such systems, the particles are driven sufficiently close together by the flow that irreversible surface contact will occur as a consequence of surface-roughness effects, thereby destroying the macroscopic reversibility of the purely viscous interactions. In this section we shall therefore discuss both theoretical and experimental evidence for the existance of such irreversible interactions and demonstrate that they may lead to

the diffusivities observed here.

3.1. *Irreversible interactions in concentrated suspensions*

Consider a sphere interacting with a second sphere in a simple shear flow. As the two spheres approach one another, the viscous stresses in the fluid act to drive the spheres together. Under purely viscous conditions, when the interparticle separation distance is very small this approach is resisted by the lubrication layer between the particles, in which the resistance is inversely proportional to the separation distance. Thus although two mathematically smooth interacting spheres may never touch, hydrodynamic theory predicts that, over a certain range of initial configurations, they will approach one another very closely even in a dilute suspension. On the other hand, in the presence of a finite amount of surface roughness on the spheres (as is the case for any real particles), the interaction may be significantly modified. Indeed, Arp & Mason (1977) found that even for two isolated interacting spheres, the existence of a small degree of surface roughness was sufficient to eliminate the closed orbits predicted for purely viscous interactions.

This effect of surface roughness is accentuated for concentrated suspensions. Specifically, since the forces driving spheres together in the flow depend on the bulk fluid stresses, they are proportional to the bulk suspension viscosity, which in turn is a strong function of concentration. In contrast, the lubrication forces resisting this approach remain proportional to the pure-fluid viscosity since the presence of other particles in the suspension does not affect the flow in the narrow gap between particles. This imbalance, combined with some finite surface roughness, implies that in sufficiently concentrated suspensions particles will simply approach one another without any significant displacemtn from the their original streamlines until they come into physical contact, folowing which they will rotate owing to the vorticity of the shear flow, and finally separate. Moreover, since the interaction is no longer reversible owing to the surface contact it will also no longer be symmetric and thus will lead to permanent displacemtns of the particles from their original streamlines at the end of each interaction. A more complete discussion of the evidence for irreversible interactions and thier effect on the rheology of concentrated suspensions is given by Leighton (1985).

3.2 *Particle drift arising from irreversible interactions*

There are several ways in which the irreversible interactions described above can lead to drift in the presence of gradients in concentration or shear stress. To see this, consider a test sphere at the origin which is immersed in a suspension undergoing shear. We shall assume that the bulk flow is in the x-direction with a constant shear stress $\sigma = \sigma_{yx}$ and a linear concentration gradient in the z-direction, normal to the plane of shear. Under these conditions, the viscosity, and hence the shear rate, will be be constant within the plane of shear. Consequently, when the particles are not mathematically smooth, the test sphere will be irreversibly displaced upwards following an interaction with another sphere approaching it from below, and conversely if approached from above. Thus, in the presence of a higher particle concentraiton on one side of the test sphere than on the other, this sphere will experience a drift towards the region of lower concentration since it interacts with more particles on one side than on the other. Moreover, the displacement after each interaction will be proportional to the particle radius; thus since the excess rate of interactions from regions of higher concentration is proportional to $\dot{\gamma}ad\phi/dz$, the particle flux resulting from this source of drift should be proportional to $\dot{\gamma}a^2\phi d\phi/dz$, which is the same scaling expected for shear-induced diffusion.

A second source of drift normal to the plane of shear arises from the gradients in suspension viscosity brought about by gradients in concentration. First we note that in the absence of a gradient in viscosity, two touching spheres in a shear field will rotate about their center of mass (the point of contact). But, in the presence of a viscosity gradient, the center of mass will no longer be the center of rotation and the particles will, on average, be displaced during an interaction from regions of high to low viscosity. The magnitude of this displacement during each irreversible interaction will scale as the relative variation in viscosity across the

116

particle, i.e. it will be proportional to $(a/\mu)d\mu/dz$, multiplied by the particle radius. Since, for small gradients in concentration, the variation in viscosity is linear in the concentration gradient, the above result, when multiplied by the rate of interactions $\dot{\gamma}\phi$, gives the corresponding drift velocity. In turn, when multiplied by ϕ and divided by $d\phi/dz$, the drift velocity leads to an expression for the effective diffusivity arising from this source of drift $D \sim \dot{\gamma}a^2(\phi^2/\mu)d\mu/d\phi$. The total effective diffusivity normal to the plane of shear is then the sum of the two mechanisms outlined above, plus that due to shear induced self-diffusion.

For concentrated suspensions, the function $(1/\mu)d\mu d\phi$ is very large, with a value of about 15 for a 45% suspension; thus drift due to gradients in viscosity is likely to dominate the diffusivity. Recognizing this, we therefore let

$$D_\perp = K_\perp \frac{\phi^2}{\mu} \frac{d\mu}{d\phi} \dot{\gamma}a^2 \qquad (3.1)$$

be the expected form for the effective diffusivity normal to the plane of shear at high concentrations, where $K_\perp$ is a dimensionless parameter whose value will depend on the exact geometry of the interactions. As shown in figure 5, $K_\perp$, as determined from the results of the long-term viscosity experiment, was found to be a relatively weak function of concentration with a value of about 0.7 at 45%. The scatter in the data is, of course, indicative of the simplcity of the model.

The contribution of irreversible interactions to drift within the plane of shear is quite similar to that found above for the case of drift normal to the plane of shear. Again, displacements will lead to random self-diffusion, to drift arising from a higher rate of interactions on one side than on another due to the concentration gradient (assuming a uniform shear rate), and drift from regioins
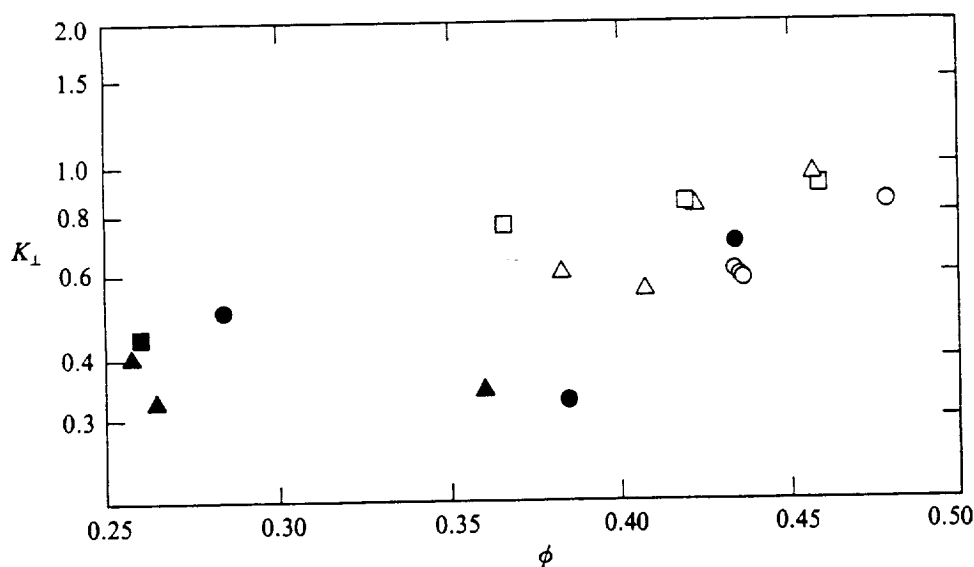

FIGURE 5 Value of $K_\perp$ vs. concentration: $\square$, 46 μm polystyrene in 0.639 mm gap; $\bigcirc$, 46 μm polystyrene in 1.261 mm gap; $\triangle$, 87 μm polystyrene in 1.261 mm gap. Open symbols, $\dot{\gamma} = 24$ s^{-1}; filled symbols, $\dot{\gamma} = 76$ s^{-1}; half-filled symbols, $\dot{\gamma} = 7.6$ s^{-1}.

of high to low viscosity. In addition to these sources of drift, however, variations in viscosity within the plane of shear will, in the case of a uniform applied shear stress, lead to variations in the local shear rate. Thus, in regions of low concentration and low viscosity the shear rate will be greater, with the consequence that a test sphere will, on average, experience a greater number of interactions from the region of lower concentration than would otherwise be the case. Since the shear rate is inversely proportional to the local viscosity for a constant shear stress, the excess rate

of such interactions will be proportional to $(\phi\dot{\gamma}a/\mu)(d\mu/dy)$, which in turn will reduce the drift velocity from regions of high to low concentration by an amount proportional to $(\dot{\gamma}a^2\phi/\mu)(d\mu/d\phi)(d\phi/dy)$, an expression for the drift velocity identical with that due to gradients in viscosity with uniform shear.

Although this drift due to the shear rate gradient effect will certainly reduce the magnitude of the effective diffusivity (the sum of all contributions due to drift and random walk) it appears unlikely that the two terms due to gradients in fluid viscosity will exactly cancel out. Thus, as in the case of diffusion normal to the plane of shear, we obtain for the limiting expression of the effective diffusivity at high concentrations

$$D_\| = K_\| \frac{\phi^2}{\mu} \frac{d\mu}{d\phi} \dot{\gamma}a^2 \qquad (3.2)$$

where the value of $K_\|$ may be determined from the initial-viscosity-increase experiments. The results are shown in Figure 6 from where it is seen that, in spite of the scatter, which again is indicative of the simplicity of the model, $K_\|$ appears to be relatively independent of concentration and approximately equal to 0.6.

The same mechanism due to gradients in shear rate that reduced the effective diffusivity within the plane of shear should also lead to drift from regions of high to low shear stress in a homogeneous suspension. This is because, for the case of uniform particle concentrations and uniform suspension viscosities, the local shear rate is proportional to the local shear stress σ; hence the excess rate of particles interacting with the test sphere from regions of high shear stress is proportional to $(\phi\dot{\gamma}a/\sigma)/(d\sigma/dy)$, yielding a particle flux

$$N_y = -K_\sigma \frac{\phi^2}{\sigma} \frac{d\sigma}{dy} \dot{\gamma}a^2 \qquad (3.3)$$

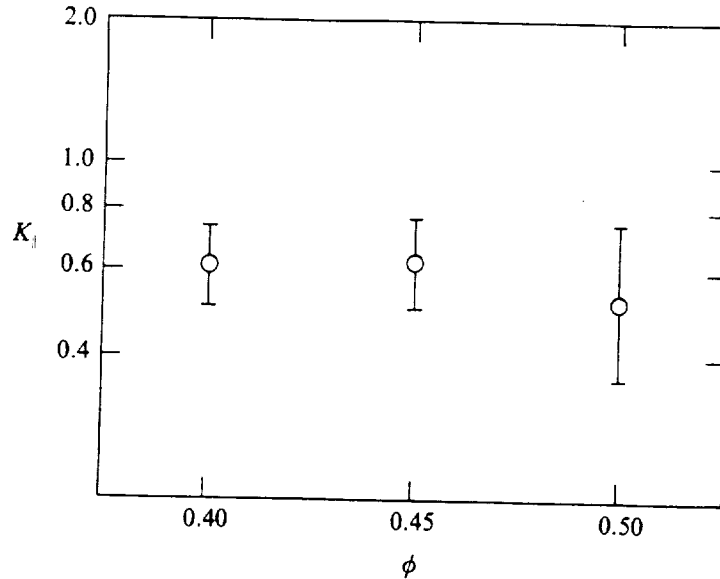where again K_σ is some order-one function of concentration.

FIGURE 6 Average value of $K_\|$ vs. concentration calculated from the data in table 1. Error bars denote one standard deviation as estimated from the scatter in the experimental results.

4. Particle distributions in Poiseuille flow

Using the above analysis it is possible to determine the steady-state concentration distribution acquired by a concentrated suspension undergoing flow in a channel or a tube. Since the shear stress in Poiseuille flow is a maximum at the walls and zero in the center, migration due to the gradient in shear stress will result in a depleted concentration near the walls. At steady-state, this inward migration is balanced by shear-induced diffusive migration outwards, where the net particle flux:

$$N_y = -\left[K_\sigma \frac{\phi^2}{\sigma} \frac{d\sigma}{dy} + K_\parallel \frac{\phi^2}{\mu} \frac{d\mu}{d\phi} \frac{d\phi}{dy} \right] \dot{\gamma} a^2 \qquad (4.1)$$

is set equal to zero. For Poiseuille flow the shear stress is simply proportional to y, hence

$$\frac{1}{\sigma} \frac{d\sigma}{dy} = \frac{1}{y} \qquad (4.2)$$

and therefore we obtain the derivative of the steady-state concentration profile:

$$\frac{d\phi}{dy} = -\frac{K_\sigma}{K_\parallel} \left(\frac{1}{\mu} \frac{d\mu}{d\phi} \right)^{-1} \frac{1}{y} \qquad (4.3)$$

where the viscosity is a known function of concentration. If we assume that the ratio $K_\sigma/K_\parallel$ is approximately constant across the gap, then (4.3) may be directly integrated to yield the viscosity profile:

$$\frac{\mu}{\mu_w} = \left(\frac{b}{y} \right)^{\frac{K_\sigma}{K_\parallel}} \qquad (4.4)$$

where μ_w is the relative viscosity of the suspension evaluated at the concentration at the walls. Using the observed relationship between viscosity and concentration (given by equation 2.2), we may invert equation 4.4 to obtain the concentration profile across the channel:

$$\phi = \phi_m \left(1 + \frac{\frac{1}{2} [\mu] \phi_m}{\left[\mu_w \left(\frac{b}{y} \right)^{\frac{K_\sigma}{K_\parallel}} \right]^{\frac{1}{2}} - 1} \right)^{-1} \qquad (4.5)$$

which is a function only of the ratio $K_\sigma/K_\parallel$ and the concentration at the wall. Note that the concentration distribution given by equation 4.5 applies to both flow through channels and tubes. For a known value of $K_\sigma/K_\parallel$ the wall concentration may be determined from the average concentration by integrating 4.5 across the channel or, in the case of flow through a tube, by integrating the product $\phi 2r dr$. A plot of the expected concentration profile for ϕ as a function of $K_\sigma/K_\parallel$ is given in Figure 7 for $\phi = 0.45$. Note that the predicted concentration approaches the maximum value $\phi = \phi_m$ at y=0. This is a consequence of the singularity in (4.2), and the divergence of the effective diffusivity as the particle concentration approaches its maximum value.

4.1 Estimation of K_σ

We may estimate the value of K_σ from the amplitude of the short-term viscosity increase phenomenon if we examine in more detail the procedure by which suspensions are loaded into the Couette device. As is described in detail by Leighton and Acrivos (1987b), in these experiments the fluid was loaded into the gap by first pouring the suspension into the Couette cup and then lowering the bob, thus displacing the fluid and filling the gap. The flow thus created consists of a converging entrance flow at the base of the gap, followed by channel flow up the gap. While it is unclear what effect, if any, the entrance flow has on the concentration profile, the channel flow up the gap should lead to a migration of the particles from the regions near the walls into the center. The concentration profile in the gap will thus be a function of distance up the gap, but provided that the height of the gap is sufficiently large the concentration profile in the gap will approach the steady-state distribution given by (4.5).
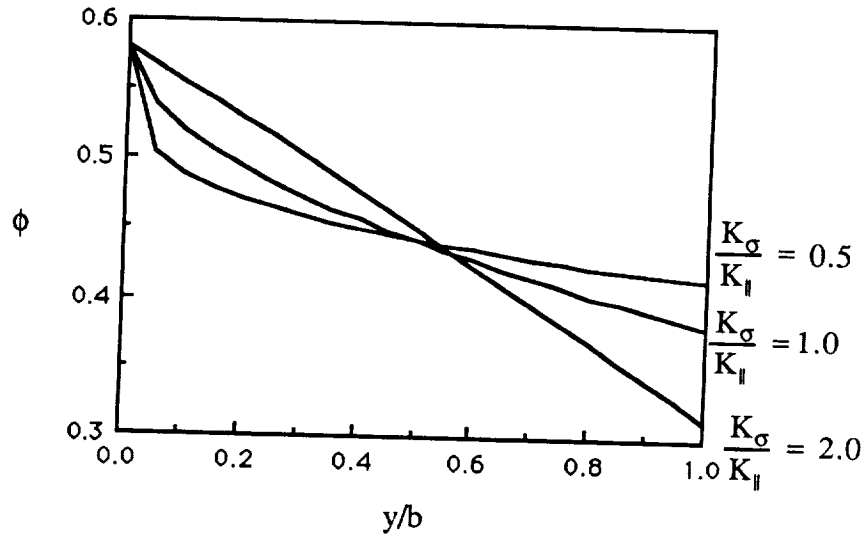
119

Figure 7. Plot of concentration profile across a channel predicted from equation 4.5 for an average concentration of 45%, as a function of $K_\sigma/K_{\|}$.

If we assume that the concentration profile in the gap is indeed due to migrations arising from gradients in shear stress we may estimate the influence of finite gap length on the short-term viscosity increase phenomenon. The concentration distribution in the gap will be governed by the differential equation:

where:

$$u\frac{\partial\phi}{\partial x} = -\frac{\partial N_y}{\partial y} = \frac{\partial}{\partial y}\left\{ \hat{D}_{\|}\dot{\gamma}\,a^2\left[\frac{\partial\phi}{\partial y} + \frac{K_\sigma}{\hat{D}_{\|}}\frac{1}{y}\right]\right\}$$

(4.6)

$$u = u_m\left(1 - \frac{y^2}{b^2}\right) \quad ; \quad N_y\Big|_{y=\pm b} = 0 \quad ; \quad \phi\Big|_{x=0} = \phi_0$$

where, for purposes of estimation, we linearize the problem by assuming the velocity profile to be parabolic and the diffusivity to be constant, and where we have assumed a no-flux boundary condition at the sides of the channel and a uniform concentration at the entrance. The differential equation may be rendered dimensionless using the variables

$$y^* = \frac{y}{b} \quad ; \quad x^* = \frac{2\,x\,a^2\hat{D}_{\|}}{b^3}$$

(4.7)

resulting in the dimensionless equation:

$$(1 - y^{*2})\frac{\partial\phi}{\partial x^*} = \frac{\partial}{\partial y^*}\left\{ |y^*|\left[\frac{\partial\phi}{\partial y^*} + \frac{K_\sigma}{\hat{D}_{\|}}\frac{1}{y^*}\right]\right\}$$

(4.8)

where:

$$\frac{\partial\phi}{\partial y^*}\Big|_{y^*=\pm 1} = \pm\left(-\frac{K_\sigma}{\hat{D}_{\|}}\right) \quad \text{and} \quad \phi\Big|_{x^*=0} = \phi_0$$

which may be solved using separation of variables. Equation 4.8 admits a solution of the form:

120

$$\phi(x^*,y^*) = \phi_\infty(y^*) + \sum_{n=0}^{\infty} A_n \exp(-\alpha_n^2 x^*) \, F_n(y^*) \qquad (4.9)$$

with

$$A_n = \frac{\displaystyle\int_0^1 (1 - y^2) \, F_n(y) \left(\phi_\infty(y) - \phi_0\right) dy}{\displaystyle\int_0^1 (1 - y^2) \, F_n^2(y) \, dy}$$

where the eigenfunctions F_n satisfy the Sturm-Liouville type equation:

$$\left(y^* F_n'\right)' + \alpha_n^2 (1 - y^{*2}) \, F_n = 0 \qquad (4.10)$$

with

$$F_n(0) = \text{finite} \ ; \ F_n'(1) = 0$$

While equation 4.10 does not admit a closed form solution, the leading eigenvalue has been determined numerically to be $\alpha_0 = 2.277795$. As a consequence, the assumption that the concentration distribution in the gap is close to that at steady-state for channel flow will be valid provided

$$\frac{2 \alpha_0^2 \, a^2 \hat{D}_\parallel h}{b^3} \gg 1 \qquad (4.11)$$

where h is the gap height. In the experiments described by Leighton and Acrivos (1987b) where the short-term viscosity increase was observable, the dimensionless parameter given in (4.11) ranged from 1.9 to 14, thus the assumption of steady-state is reasonably good. In contrast, in those experiments where the short-term viscosity increase was not observed, the value of the parameter was less than 1, suggesting that the observed increase was, in fact, due to particle migrations in Poiseuille flow rather than entrance effects.

To estimate the value of K_σ, we may simply substitute the steady-state concentration distribution given by equation 4.5 into the equation for B_1 given in equation 2.3 and integrate. The resulting values of K_σ are given in Figure 8, which, allowing for considerable scatter in the experimental data, indicates that K_σ is a relatively weak function of concentration (not quite constant as we have assumed) with a value of about 0.6 at $\phi = 0.45$.
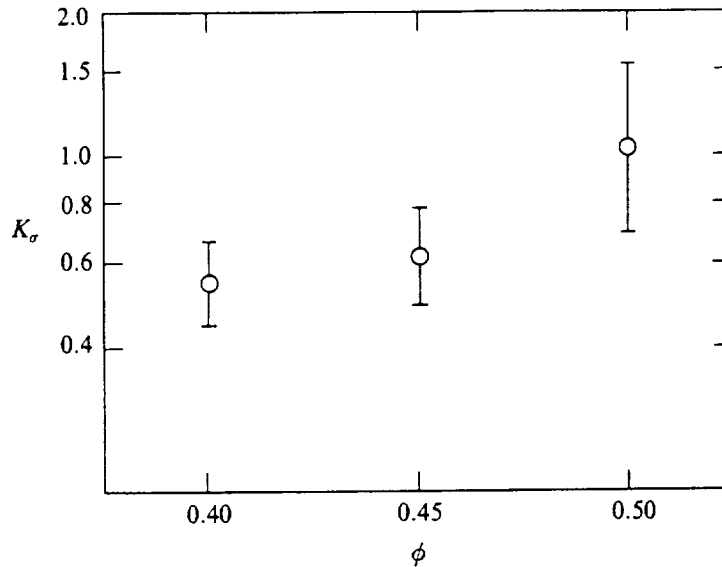

FIGURE 8 Average value of K_σ vs. concentration calculated from the data in table 1. Error bars are one-standard-deviation error estimated from the scatter in the experimental results.

121

4.2 Comparison with other experiments

In a bounded Poiseuille flow (channel or tube), any migration of particles toward the center leads to an increase in the viscosity in this region and hence to a blunting of the parabolic velocity profile that applies for Newtonian fluids. We may calculate the expected velocity profile resulting from the steady-state viscosity distribution given in equation 4.4:

$$\frac{u}{u_m} = 1 - \left(\frac{y}{b}\right)^{2 + K_\sigma/K_\parallel} \tag{4.12}$$

which, surprisingly, is not a function of concentration. Of course, in the development leading up to (4.4) we assumed that the ratio $K_\sigma/K_\parallel$ is independent of concentration. This is certainly not true for dilute suspensions where the mechanisms leading to the shear stress gradient induced migrations would be expected to vanish, and is only approximately correct for concentrated suspensions.

Observations of velocity profiles in concentrated suspensions flowing through tubes were conducted by Karnis, Goldsmith and Mason (1966). Their observations at an average concentration of 38% (the highest concentration for which measurements were reported) and particle/tube diameter ratio of .028 is reproduced in Figure 9 together with the profile predicted by
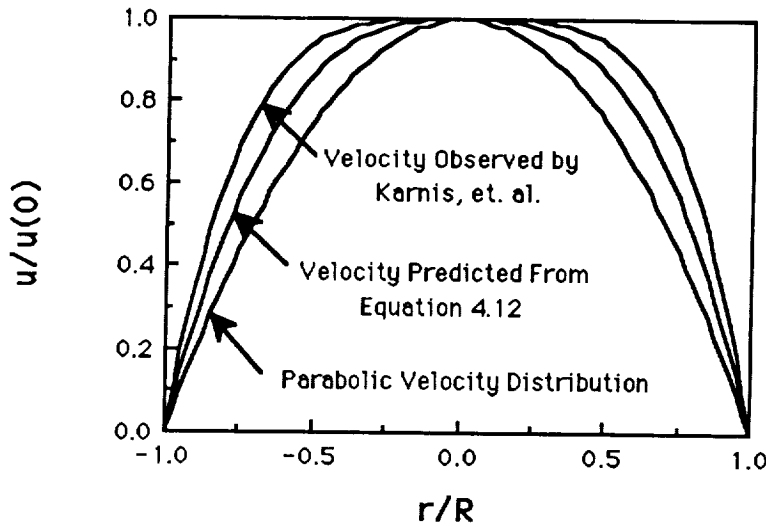

Figure 9. Comparison of the velocity distribution estimated from equation 4.12 with that observed by Karnis, et al. (1966).

equation 4.12 using an observed ratio $K_\sigma/K_\parallel = .912$ estimated from the $\phi = 0.40$ experiments described above. From this comparison it is seen that the velocity profile observed by Karnis, *et al.* is blunter than that predicted here, corresponding to $K_\sigma/K_\parallel \approx 2.1$. While these two values do not greatly differ considering the large degree of scatter in our experiments, at least part of the discrepancy may be accounted for by wall effects. Indeed, Karnis, Goldsmith, and Mason attributed their observed blunting entirely to wall effects, however in view of the small particle diameter / tube diameter used in the experiment depicted here, this seems unlikely. Experiments in the Couette geometry reported by Karnis, *et al.* (1966), showed that wall effects were insignificant at the same concentrations even for particle diameter / gap width ratios over a factor of three larger than that used in the experiments leading to Figure 9.

122

These authors did attempt to measure the concentration profile across a tube, although only at a lower average concentration of 32%. Owing to the statistical nature of their measurement technique, however, their observations had a very large experimental error. Specifically, their measurements involved counting the number of spheres that were present in each of four divisions of the half-width of a tube cross-section, and since only a small fraction of the spheres were marked, their observations were subject to Poisson statistics, which dictate that the one-standard-deviation error in the number of spheres that were counted is equal to the square root of that number. But since the total number of spheres that were counted in each region was rather small (less than 80), the concentrations reported by Karnis *et al.* (1966) had a two standard deviation error of nearly 25%. Their observations, with error estimated as described above, together with the concentration profile predicted using equation 4.5 and a value of $K_\sigma/K_\parallel = .912$ is given in Figure 10. While the concentration observations of Karnis *et al.* do not agree with the predicted concentration profile (which has been extrapolated well beyond the range over which $K_\sigma/K_\parallel$ was estimated), more accurate measurements of the concentration distribution in Poiseuille flow are needed in order to determine the source of the observed blunting of the velocity profiles.
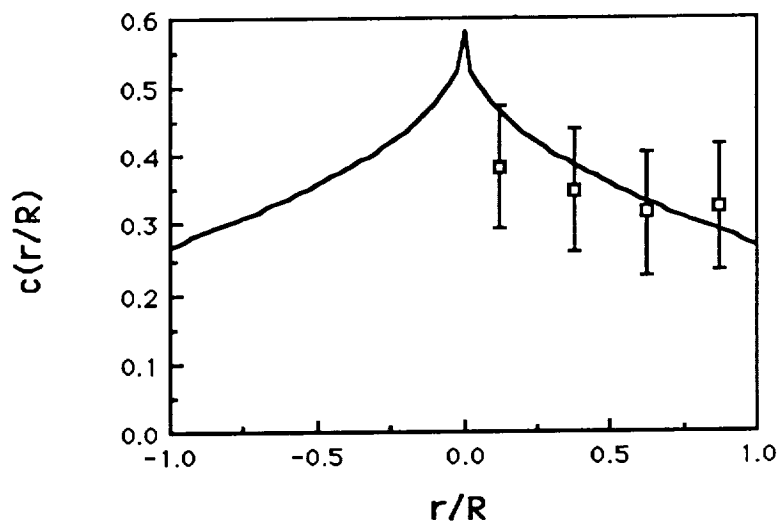

Figure 10. Comparison of concentration distribution estimated from equation 4.5 with particle distribution observed by Karnis, et al. (1966). Error given is 2 standard deviation error calculated by statistical means.

Acknowledgements

References:

Arp, P. A. & Mason, S.G. 1977 The kinetics of flowing dispersions. IX. Doublets of rigid spheres (experimental). *J. Colloid Interface Sci.* **61**, 44.

Eckstein, E. C., Bailey, D. G. & Shapiro, A. H. 1977 Self-diffusion of particles in shear flow of a suspension. *J. Fluid Mech.* **79**, 191.

Gadala-Maria, F. 1979 The rheology of concentrated suspensions. Ph.D. thesis, Stanford University.

Gadala-Maria, F. & Acrivos, A. 1980 Shear-induced structure in a concentrated suspension of solid spheres. *J. Rheology* **24**, 799.

Ho, B. &Leal, L. 1974 Inertial migration of rigid spheres in two-dimensional uni-directional flows. *J. Fluid Mech.* **65**, 365.

Karnis, A., Goldsmith, H. L. & Mason, S. G. 1966 The kinetics of flowing dispersions. I. Concentrated suspensions of rigid particles. *J. Colloid Interface Sci.* **22**, 531.

Karnis, A. & Mason, S. G. 1967 The flow of suspensions through tubes. I. Meniscus effects. *J. Colloid Interface Sci.* **23**, 120.

Leighton, D. 1985 The shear induced migration of particulates in concentrated suspensions. Ph.D. thesis, Stanford University.

Leighton, D. & Acrivos, A. 1987 Measurement of self-diffusion in concentrated suspensions of spheres. *J. Fluid Mech.* **177**, 109.

Leighton, D. & Acrivos, A. 1987 Shear-induced migration of particles in concentrated suspensions. *J. Fluid Mech.* **181**, 415.

J. M. Char,[†] K. K. Kuo,[ς] and K. C. Hsieh[†]
Department of Mechanical Engineering
The Pennsylvania State University
University Park, Pennsylvania 16802

Abstract

Liquid jet breakup mechanisms and processes have been studied extensively over the last one hundred years. However, since the region near the jet injector is too dense and optically opaque, conventional visualization cannot be applied with satisfactory experimental results. To unravel the liquid jet breakup process in the non-dilute region, a newly developed system of real-time X-ray radiography together with an advanced digital image processor and a high-speed video camera was used in this study. Based upon recorded X-ray images, the inner structure of a liquid jet during breakup was observed. The jet divergent angle, jet breakup length, and void fraction distributions along the axial and transverse directions of liquid jets, etc., were determined in the near-injector region. Both wall- and free-jet tests were conducted to study the effect of wall friction on the jet breakup process.

Introduction

Understanding the breakup mechanism of liquid jets in diesel engines, regenerative liquid propellant guns, and many other combustion and propulsion systems is extremely important, since the jet breakup process can strongly affect the jet divergent angle, the distributions of droplet size and velocity, and the mixing and combustion processes. As indicated in a detailed review paper by Arcoumanis and Whitelow,[1] numerous theoretical and experimental attempts have been made to study the stability and breakup phenomena of liquid jets ejected from nozzles. In recent years, Wu, Reitz and Bracco,[2] Birk and Reeves,[3] and Baev et al.[4] conducted intensive studies in the experimental investigation of breakup behavior in the near-injector region. Shimizu et al.[5] studied the breakup length of a high-speed jet by measuring the electrical resistance between a nozzle and a fine wire detector located in a spray jet. They found that breakup length decreases with increase in injection velocity, finally reaching a constant value.

In the theoretical analyses, the growth of initial perturbations on the liquid surface, the effects of liquid inertia, surface tension, viscous and aerodynamic forces on the jet were considered. The earliest development of a predictive model for the jet breakup was initiated by Rayleigh.[6,7] His linear stability analysis of an inviscid cylindrical liquid jet showed that an

axisymmetric disturbance could be stable or unstable, depending upon the magnitude of the wavelength (stable for wavelengths less than the circumference of the jet, and unstable for other cases). Further investigations using linear stability analysis were conducted by Tyler and Richardson,[8] Schweitzer,[9] Merrington,[10] Levich[11], Dombrowski and Hooper,[12] and others. Based on these studies, the jet divergent angle near the injector exit, and jet breakup length and mean drop size near the lateral surface of the jet can be estimated from the Reynolds number, the Weber number, the density ratio of liquid to gas, and several empirical constants. The effect of viscosity was studied by Weber.[13] More recently, the effect of nonlinearity[14-19] has been considered and solved numerically in order to simulate more closely the jet breakup processes.

In the experimental studies, the core of the jet is optically opaque due to the high-density condition in the near-injector region. Hence, observations and measurements of the near-injector region are almost impossible. Consequently, most previous studies focused on the dilute region or on the jet boundary near the injector exit.[2] Due to the lack of quantitative test results in the near-injector region, the theoretical models developed for prediction of jet-core breakup length, mean drop size distribution, etc., have not yet been validated. The estimated jet profiles and characteristics at a given near-injector station were used as initial and/or boundary conditions in order to simulate the atomization and combustion processes in the dilute region; this, in turn, could cause errors and uncertainties in the theoretical predictions of combustion processes.

The purpose of the present study is to achieve a better understanding of the jet breakup process, using a newly developed system of real-time X-ray radiography together with an advanced digital image processor and a high-speed video camera. The specific objectives are: (1) to illustrate the differences between X-ray radiography images and regular high-speed movie films; (2) to measure jet velocity, jet breakup length, and void fraction distributions in the near-injector region; (3) to observe the evolution of the jet breakup and the formation of ligaments and droplets in the near-injector region in order to determine the inner structure of the liquid jets; and (4) to demonstrate the feasibility and advantage of using X-ray radiography in the jet breakup study. In order to study the effect of wall friction on the jet breakup process, both wall- and free-jet tests were conducted.

Experiment Apparatus

In the experimental approach, a test rig has been designed and fabricated to simulate both wall and free jets ejected from a two-dimensional slit with an aspect ratio of 10. The advantage of using a planar two-dimensional jet is to avoid the curvature effect which is inherently associated with circular or annular jets.[3] The side view of

the jet breakup process is much clearer in the planar two-dimensional case than in other cases. The schematic diagram of the test rig is shown in Fig. 1. A photograph of the test setup is shown in Fig. 2. In Fig. 1, the gap of the two-dimensional slit between elements 5 and 7 is 2 mm, and element 5 is an interchangeable piece for providing different lengths of the wall jet. When a piece of element 5 ends at the same location as element 7, the configuration is that of a free jet test case. A pressure transmitting rod is shown as element 4. Prior to the test, this rod was lifted by a vacuum pump. The liquid was then loaded through element 6 into the free volume beneath the rod and the entire slit region. The liquids used in tests were either water or Pantopaque ($C_{19}H_{29}IO_2$), a fluid used in medical X-ray examinations. The physical properties of the two test fluids are presented in Table 1. During the test, a solenoid valve was activated to introduce high-pressure nitrogen gas into the top portion of the test rig (see Fig. 2), thus pushing the rod downward to inject the liquid into the unconfined ambient air. A major portion of the Pantopaque was recovered for further use.
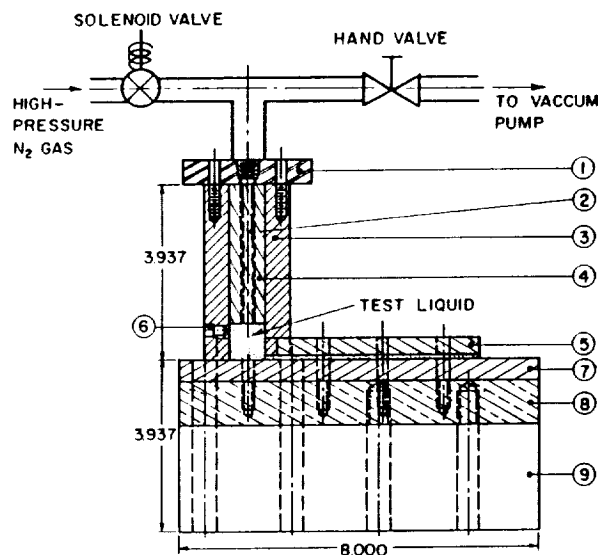

Fig. 1   Schematic Diagram of Test Rig Assembly for Two-Dimensional Wall or Free Jet Breakup Studies (1. top cover, 2. bolts, 3. liquid reservoir, 4. push rod, 5. top plate of slit, 6. liquid feeding hole, 7. base plate of slit, 8 and 9. test rig holder)

Fig. 2   Photograph of the Test Setup

Data Acquisition System

During the test, the instantaneous liquid jet contour was filmed by real-time X-ray radiography. Figure 3 shows the layout of various components of the radiography system. A continuous X-ray was generated from the Phillips MG 321 constant potential X-ray system. Two X-ray tubes [one with a focal spot combination of 0.2 x 0.2 mm/3.0 x 3.0 mm (MCN 167/160 kV), the other with a focal spot combination of 1.2 x 1.2 mm/4.0 x 4.0 mm (MCN 321/320 kV)] were employed to achieve different penetration depths and spatial resolution requirements. A lead diaphragm was installed at the exit port of the X-ray tube head to limit the angle of divergence of the X-ray beam and to confine the beam to the measuring section of the liquid jet test rig. (This also reduced unnecessary radiation exposure.) A second lead diaphragm with a larger opening was placed in front of the image intensifier to reduce scattered X-ray radiation and decrease the noise level on the fluorescent screen.

After passing through the test rig and liquid jet, X-ray signals were transformed to fluorescent light signals on the output screen of a tri-field image intensifier (Precise Optics, Model P1 2400 ATF, 4", 6", or 9" field diameter). The input fluor of the image intensifier was made of cesium iodide with a decay-time constant of 650 ns, and the output fluor was a p20 type with a 85 ns decay-time constant. These time constants are short enough to allow the motion analysis system to operate at its maximum framing rate without generating image blur.

The fluorescent light signal output from the image intensifier was recorded by a Spin Physics 2000 Motion Analysis System. This system can record up to 2000 fully digitized frames per second, or up to 12,000 digitized pictures per second with adjustable playback speed. The motion analysis system consists of the following subsystems:

a) a Spin Physics 2000 video camera with solid-state image sensor. The picture information goes to the console from the camera, and is processed into a frequency-modulated carrier that is recorded on tape.

b) a main electronic bin, which contains record and playback electronics, along with video output circuitry.

c) a tape transport, which drives the half-inch tape cassette at a maximum speed of 250 inches per second.

Digitized data was stored on a high-intensity magnetic recording tape and transferred to the digital image-processing system frame by frame for analysis through an IEEE-488 interface. The digital image-processing system consists of several major components:

a) a Quantex (QX-9210) digital image processor with two pipeline point processors, each with a random access image memory of 480 x 640 x 12 bits. The processors perform real-time image enhancements, including noise reduction, image subtraction, arbitrary contrast control, roam, and zoom. The processor can also be used to conduct such high-speed image analyses as brightness histogram, local contrast stretch, area and point brightness
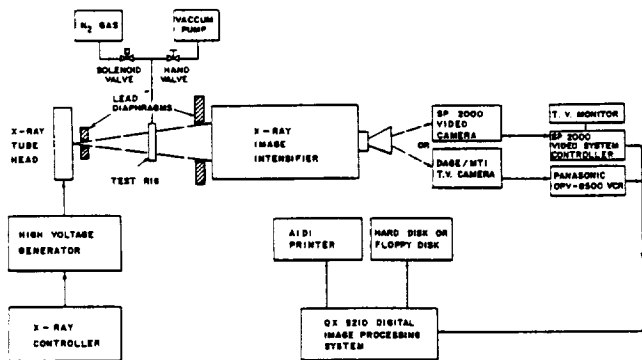
Fig. 3   Real Time X-ray Radiography and Digital
         Image Processing System

IDEAL X-RAY POINT SOURCE

y = CONSTANT

Fig. 4   X-ray Intensity Distribution Across a
         Liquid Jet Under Idealized Conditions

measurements, calibrated length and
area measurements, Sobel edge
enhancement, and so forth.

b)   a mass storage device consisting of
     both a 2.4 MB dual 8" floppy diskette
     drive and a 50 MB hard disk for storage
     of image data.

c)   a high-resolution videograph printer
     (AIDI CT1500) for producing large
     high-quality pictures on hard copies
     with 1660 lines/inch resolution.

Data Reduction Procedure

Besides observing the jet structure directly
from the recorded film (both regular movie and
X-ray films), more detailed and accurate data
could be deduced by analyzing the X-ray intensity
distribution across the jet in horizontal and
vertical directions. Basically, an ideal
radiography image of the liquid jet can be
determined from the assumptions that 1) X-ray
radiation is generated from a point source via an
infinitely small focal spot, 2) X-ray is only
attenuated by photoelectric absorption, and 3)
distribution of X-ray intensity over the input
screen of an image intensifier is uniform. As
shown in Fig. 4, the X-ray intensity distribution
on a y = constant plane can be evaluated by the
following equation:

$$I(x) = I_0 \, EXP \, [-mW(x)] \qquad (1)$$

where m is the linear attenuation coefficient of
photoelectric absorption, and W(x) is the local
sum of the intercepted width of the liquid in the
two-phase jet. Due to the X-ray beam attenuation
across the liquid jet, the following test data can
be obtained using the digital image-processing
system:

a)   Measurement of Radiance or Pixel Value:
     The radiance (or pixel value) of any
     arbitrary point of interest in the jet
     can be obtained by moving the cursor to
     that point. The local radiance and the
     x, y coordinates of the location can be
     displayed on the screen.

b)   Measurement of Area and Pixel Value:
     The software program combines a
     measurement of an area with a
     measurement of the integrated pixel
     values (or total radiance) within the
     area. The calculated average pixel
     value within the area is also displayed
     on the screen. This feature can be used
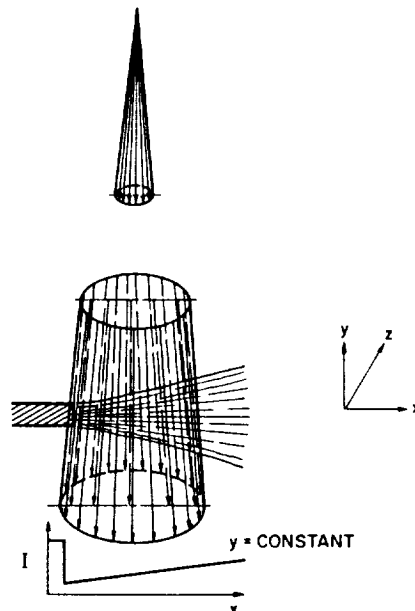   to detect the local void fraction level

from the X-ray radiograph for a
specified jet region (see Fig. 5).

c)   Profile Analysis: Figures 6 and 7 show
     the measurement of the pixel value of
     two scan lines--one parallel and one
     perpendicular to the jet core and head
     regions. Both end at the cursor point.
     From these profiles, the void-fraction
     distribution can be deduced for a
     certain cross-section of the jet.

d)   Histogram Analysis: This procedure
     consists of measuring the frequency of
     occurrence of pixel values within a
     selected boundary of a rectangle. Such
     distributions can be used to detect jet
     breakup phenomena in the core region.
     Keeping the axial length of rectangular
     area constant by varying the width of
     the rectangle, different sets of
     histograms can be obtained. These are
     arranged into a series of histograms
     (see Fig. 8).

e)   Isophote Analysis: Using the data
     reduction program, certain regions of
     the viewing area with the same range of
     pixel values can be replaced by white
     spots. This feature makes it possible
     to observe the contours of different
     radiances. The inner structure of a
     liquid jet can, therefore, be studied by
     selecting different pixel values (see
     Fig. 13, to be discussed later in the
     results section).

Finally, jet-head velocities in both axial
and radial directions can be deduced from the
recorded film by using the elapsed time and
displacement of reticle lines on the monitor of
the Spin Physics Camera System.

Discussion of Results

A series of high-speed motion pictures

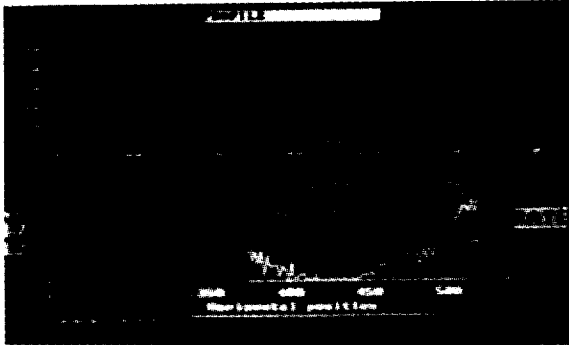Fig. 5 Measurement of Area and Pixel Value of a Liquid Jet

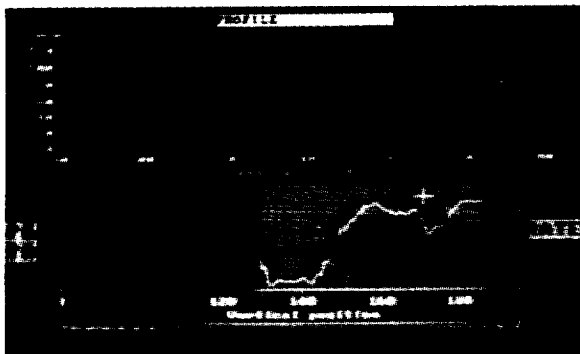Fig. 6 Horizontal X-ray Intensity Profile at the Center Plane of a Liquid Jet

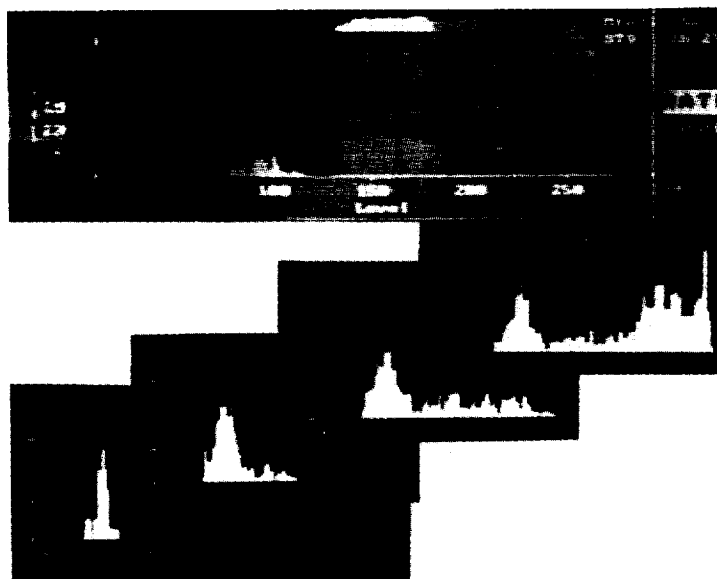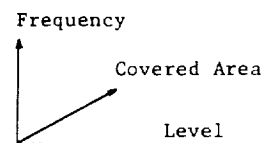Fig. 7 Vertical X-ray Intensity Profile at a Distance from Jet Exit

showing the breakup process of a plane wall jet is given in Fig. 9. Several interesting phenomena of wall jet evolution and breakup can be noted from these photographs. In Fig. 9a, as the liquid jet traveled along the wall surface in the early stage, the head region diverged in the upward direction. A thin sheet of liquid was formed ahead of the main jet, as shown in Fig. 9b. This thin sheet of liquid surface is believed to be caused by shedding phenomena introduced by the inertia of the fast-moving liquid near the free surface of the engulfing wave front. Near the top surface, the velocity of the liquid is much higher than that near the wall, since the viscous force is much smaller at the free surface. As time progressed, this sheet became more evident, and the head region expanded further (see Fig. 9c). In Fig. 9d, the main jet accelerated and merged with part of the thin liquid sheet. In the later stage, the so-called Klystron effect[20] was visible. This effect was introduced by the acceleration of the main jet, which had higher axial momentum to catch up with the precursor jet mass. Due to the coalescence of the fast and slow moving fluids, the width of the jet spread in transverse directions. This spreading also made the jet-head portion more symmetric. In the meantime, several ligaments and numerous droplets were formed as the head region expanded further. Such a breakup process greatly influenced vaporization, ignition, and combustion of liquid sprays.

A set of high-speed photographs for the free jet case is shown in Fig. 10. The jet head was quite symmetric as it expanded in the transverse direction. The shape of the jet head changed from a round cross section to a mushroom-shaped contour. The Klystron effect can also be seen in Figs. 10d, e, and f. The jet head in Fig. 10e became spear shaped with a sharp leading edge. Some ligaments and droplets were formed (see Fig. 10f) near the boundary of the liquid-gas interface.

To demonstrate the differences between conventional high-speed movie film and high-speed X-ray radiography, a set of X-ray movie films showing free jet breakup processes is given in Fig. 11. It is quite obvious that, unlike the conventional high-speed movie film, the radiance of the jet head region is highly nonuniform. The
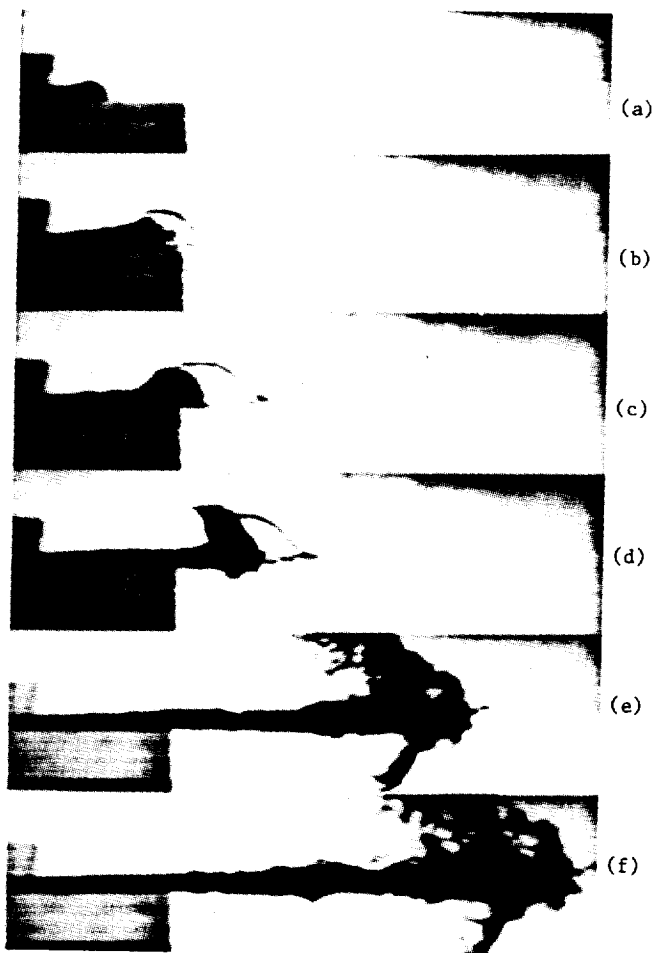

Frequency

Covered Area

Level

Fig. 8 Histogram Analysis on Different Selected Area of a Liquid Jet

Fig. 9   Interesting Phenomena of a Plane Wall
          Liquid Jet Breakup Process (From
          High-Speed Movie Film)

Fig. 10   Evolution of a Plane Free Liquid Jet
           Breakup (From High-Speed Movie Film)

inner structure of the jet can, therefore, be observed and analyzed from these images.

An enlarged photograph of the X-ray radiography, obtained from the zoom feature, is shown in Fig. 12. Figure 13 gives a set of pictures of the same object, but with different levels of radiance. The variation in contour of the isophote shows the detailed structure of the nondilute liquid jet. Although some pulsed X-ray photographs were obtained by Baev, et al.,[4] for liquid jet, the detailed inner structure of a non-dilute jet during the process of breakup has never been observed before, to the best of the authors' knowledge.

Using the Quantex Image Analyzer, the void fraction distribution in the vertical direction (normal to the jet axis) can be deduced for any axial location. Figure 14 shows the void fraction distribution across the widest jet head of photograph 12 (see also Fig. 7 cursor station). Near the centerplane (y = 0), the void fraction is much lower than that at the jet boundary [when y is approximately equal to 4H (gap width of the jet exit)]. The magnitude of the local void fraction is taken to be proportional to the local pixel value, (see Fig. 7) i.e.,

$$\phi(x,y) = |1 + 1/_m L(x,y) \ln I^{(x,y)}/I_0| \qquad (2)$$

where I_G and I_L represent the intensity (pixel value) of pure gas and liquid, respectively. For Pantopaque in air, the values of I_G and $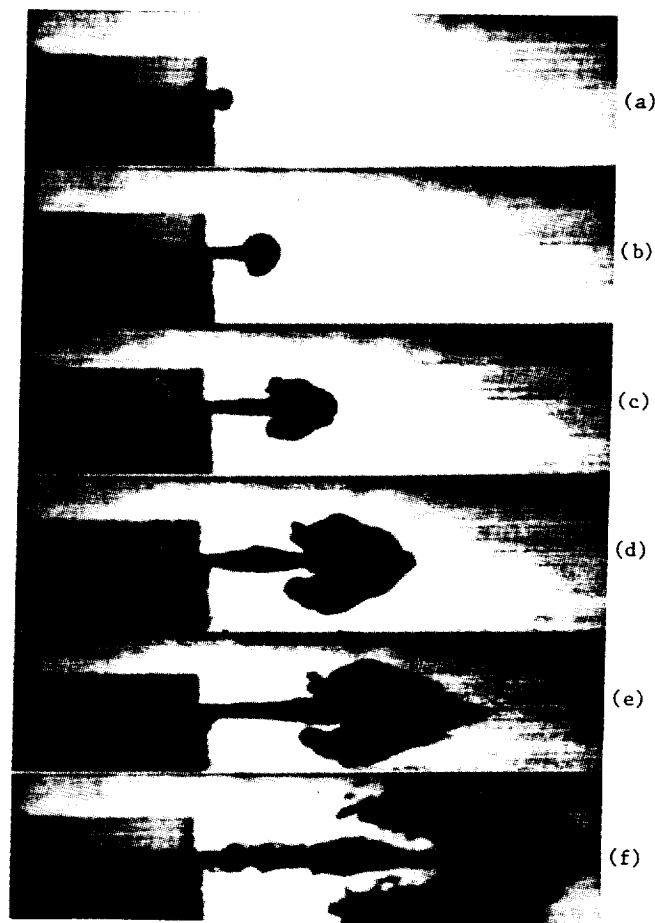I_L$ were 130 and 20, corresponding to the X-ray setting for most tests. It is useful to note that the distance between the X-ray tube head and the image intensifier was held constant during these tests.

A typical void fraction distribution for a wall jet is shown in Fig. 15. It is evident that near the wall (y/H = 0.5) the void fraction was almost zero, while the value of ϕ was quite close to unity near the outer edge of the wall jet.

A question about the effect of diffraction and scattering from multiple interfaces on the accuracy of Eq. (2) has been addressed. Equation (2) essentially assumes that diffraction and scattering from multiple interfaces have no effect on the reduction of void fraction from intensity measurements. To verify the weak dependence of intensity on the number and orientation of interfaces, two strands of rectangular-shaped solid propellant grains from the same batch with equal length were tested. One strand was cut into 10 sections with different angles to the main axis. The other strand remained as an integral piece. The two strands were placed on a platform adjacent to each other and viewed by X-ray from their end surfaces. The local intensity distribution for each strand was obtained and compared. It was found that the intensity of the uncut piece is only 5.80% higher than that of the chopped strand. This implies that the intensity of the X-ray radiography is minimally affected by the number and orientation of the interfaces. The loaded fraction (1-ϕ) deduced from Eq. (2) corresponds to
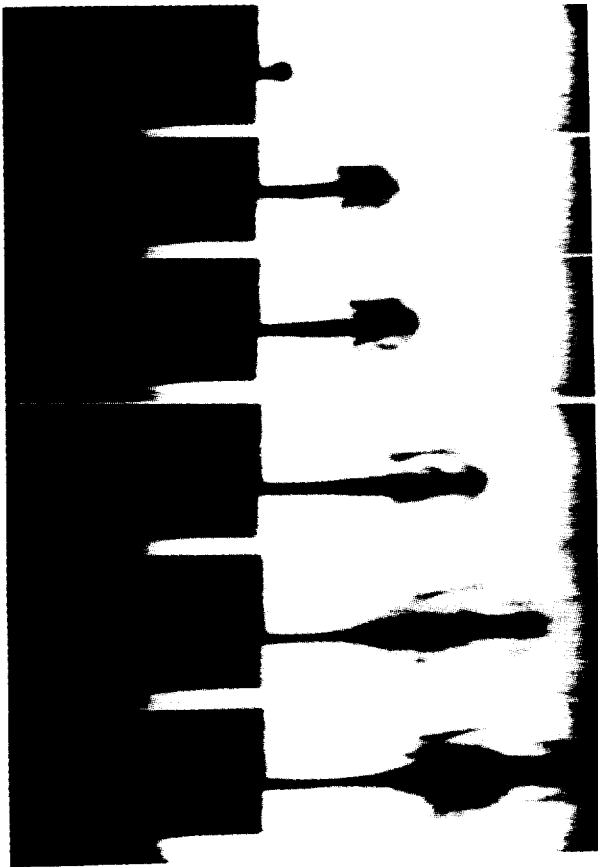
Fig. 11 Evolution of a Plane Free Liquid Jet
Using the X-ray Radiography System

Fig. 13 Isophote Analysis Shows the Inner
Structure of a Liquid Jet Using Different
X-ray Intensity Levels

the total width of the liquid intercepted by the X-ray.

The jet spreading angle in the y direction is of interest in spray combustion. The angle θ can be determined from the instantaneous jet velocities in both x and y directions. The jet head velocities (u and v) in the x and y directions are deduced from the displacements of the vertical and horizontal lines on the Spin Physics monitor. The spread angle is defined as

$$\theta = 2 \tan^{-1} (v/u) \qquad (3)$$
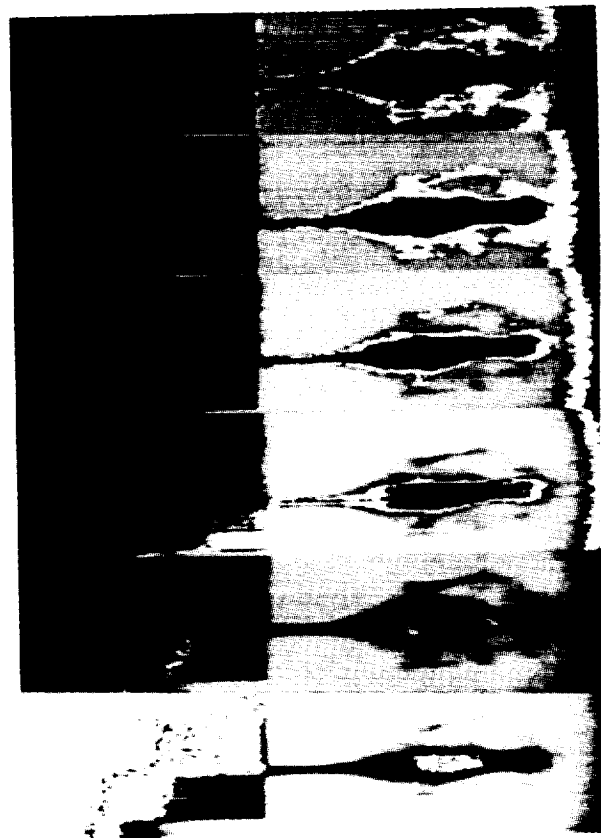
A plot of half spread angle (θ/2) versus jet head

axial velocity (u) is shown in Fig. 16. For both wall- and free-jet experiments, spread angles decrease as jet head velocity increases. This is due to the fact that when a jet has higher axial momentum, the rate of spreading is lower. Based upon the data shown in Fig. 16, the wall jet spread out more than the free jet due to the momentum distribution effect in the wall jet. Near the wall surface, the non-slip condition must be satisfied, and hence the liquid near the free surface has a higher velocity than the free jet case for the same jet head velocity.
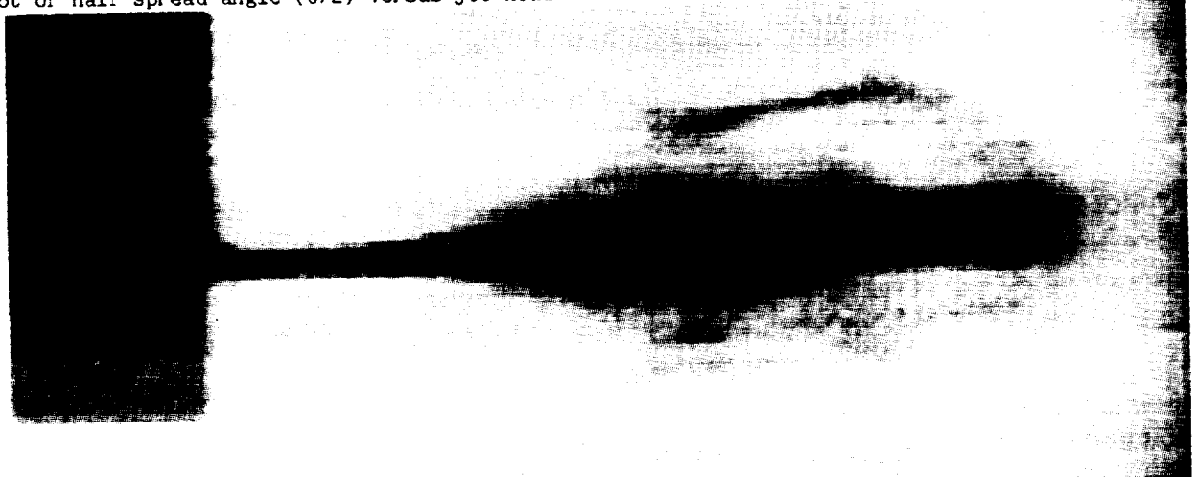

Fig. 12 Enlarged Picture of a Liquid Jet from
X-ray Image

The jet surface breakup distance (L_{SB}) and the jet core breakup distance (L_{CB}) from the exit station are also important in spray combustion. Figure 17 plots these two distances versus jet head velocity. Determination of L_{SB} was based upon the location of the first discernible divergence of liquid from the jet surface. The value of L_{CB} was determined from the abrupt increase of intensity along the axial intensity distribution at the centerplane of the jet. For both wall and free jets, L_{SB} increased with jet head velocity due to the higher inertia of the liquid jet which delays the jet surface breakup. However, L_{CB} decreased while jet head velocity increased for both wall and free jets due to the fact that higher velocity jets may cause droplet collision and coalescence to occur earlier, generating an inhomogeneous axial intensity profile. It should be noticed that the jet core breakup distance used here is different from that used in previous studies. (In earlier studies, L_{CB} is the length beyond which the jet is no longer continuous.) At the same jet head velocity, wall jets have longer L_{SB} and L_{CB} than free jets due to the fact that wall jets, which are affected significantly by the stronger viscous force, retard the core breakup. In comparing surface breakup length, at the same value of jet head velocity, the wall jet has lower momentum than the free jet; hence, breakup length is longer.

Summary and Conclusions

1) The advantages of using real-time X-ray radiography for liquid-jet breakup measurements are summarized below:
   a) X-ray can partially penetrate through the liquid jets, even in the dense regions. Therefore, it is feasible to determine the instantaneous inner structure of the jet in the near-injector region during the jet breakup processes.
   b) X-ray radiography is a nonintrusive technique which does not affect the liquid jet breakup processes and is superior to other methods.
   c) The real-time feature of X-ray radiography gives the entire history of the jet breakup event instead of a few snapshots. The X-ray motion pictures taken during the test event can be played back immediately at a lower speed for detailed flow visualization and analysis.
   d) All data are in digital form and are convenient for recording, analysis, transfer, and storage in computers.
2) Based upon the recorded X-ray images analyzed on a digital image processor, jet divergent angle, jet breakup length, and jet void fraction distributions can even be measured in the near-injector region.
3) The effect of wall friction on the jet breakup process was observed by conducting wall- and free-jet tests. While the spread angle is larger for the same jet head velocity, longer distances are required for the surface and core to break up in the case of wall jet.
4) To understand the jet breakup mechanism, more detailed studies are required. Future tests should be conducted under varied conditions, such as different

pressure and density levels in the gas phase, higher liquid-jet velocity ranges, various test liquids, different jet nozzle geometries, etc. The development of a comprehensive theoretical model for the near-injector region is also necessary. The predicted results should be compared with experimental data for model validation.

References

1. Arcoumanis, C. and Whitelaw, J. H., "Fluid Mechanics of Internal Combustion Engines: A Review," International Symposium on Flows in Internal Combustion Engines - III, Eds., T. Uzkan, W. G. Tiederman, J. M. Novak, ASME FED-Vol. 28, New York, 1985, pp. 1-17.

2. Wu, K.-J., Reitz, R. D. and F. V. Bracco, "Measurements of Drop Size at the Spray Edge Near the Nozzle in Atomizing Liquid Jets," Phys. Fluids, 29, 1986, pp. 914-951.

3. Birl, A. and Reeves, P., "Annular Liquid Propellant Jets - Injection, Atomization and Ignition," BRL Report, February, 1986.

4. Baev, V. K., Bazhaikin, A. N., Buzukov, A. A., and Timoshenko, B. P., "Experimental Study of the Development and Structure of High-Velocity Liquid Jets in Air," Progress in Astronautics and Aeronautics, Vol. 105, 1986, p. 104.

5. Shimizu, M., Arai, M. and Hiroyasu, H., "Measurements of Breakup Length in High-Speed Jets," Bull. of JSME, Vol. 27, No. 230, p. 1709, 1984.

6. Rayleigh, W. S., "On the Instability of Jets," Proc. London Math. Soc., V. X, 1879, p. 4.

7. Rayleigh, W. S., "On the Capillary Phenomena of Jets," Proc. Royal Soc., V. XXIX, 1879, p. 71.

8. Tyler, E. and Richardson, E. G., "The Characteristic Curves of Liquid Jets," Proc. Phys. Soc., V. 37, 1925, p. 297.

9. Schweitzer, P. H., "Mechanism of Disintegration of Liquid Jets," J. Appl. Physics, V. 8, 1937, p. 513.

10. Merrington, A. C. and Richardson, E. G., "The Breakup of Liquid Jets," Proc. Phys. Soc., V. 59, No. 331, 1947, p. 1.

11. Levich, V. G., Physiochemical Hydrodynamics, Prentice-Hall, New Jersey, 1962.

12. Dombrowski, N. and Hooper, P. C., "The Effect of Ambient Density on Drop Formation in Sprays," Chem. Eng. Sci., Vol. 17, 1962, pp. 291-305.

13. Weber, C., "Zum Zerfall eines Flussigkeitsstrables," ZAMM, V. 2, 1931, p. 136.

14. Chaudhary, K. C. and Redekopp, L. G., "The Nonlinear Capillary Instability of a Liquid Jet - Part 1 - Theory," J. Fluid Mech., V. 96, p. 2, 1980.

15. Chaudhary, K. C. and Maxworthy, T., "The Nonlinear Capillary Instability of a Liquid Jet - Part 2 - Experiments on Jet Behavior Before Droplet Formation," J. Fluid Mech., V. 96, 1980, p. 275.

16. Lafrance, P., "Nonlinear Breakup of a Liquid Jet," The Physics of Fluids, V. 17, No. 10, 1974, p. 1913.

17. Lee, H. C., "Drop Formation in a Liquid Jet," IBM J. Res. Develop., V. 18, 1974, p. 364.

18. Nayfeh, A. H., "Nonlinear Stability of a Liquid Jet," The Physics of Fluids, V. 13, No. 4, 1970, p. 841.

19. J. K. Dukowicz, "A Particle-Fluid Numerical Method for Liquid Sprays," J. Comp. Phys., Vol. 35, 1980, pp. 229-253.

20. Fenwick, J. R. and Bugler, G. J., "Oscillatory Flame Front Flow Rate Amplifications Through Propellant Injection Ballistics (The Klystron Effect). Third ICRPG Combustion Conference, CPIA Pub. No. 138, Vol. 1, February, 1967, p. 417.

TABLE 1. PHYSICAL PROPERTIES OF TEST LIQUIDS

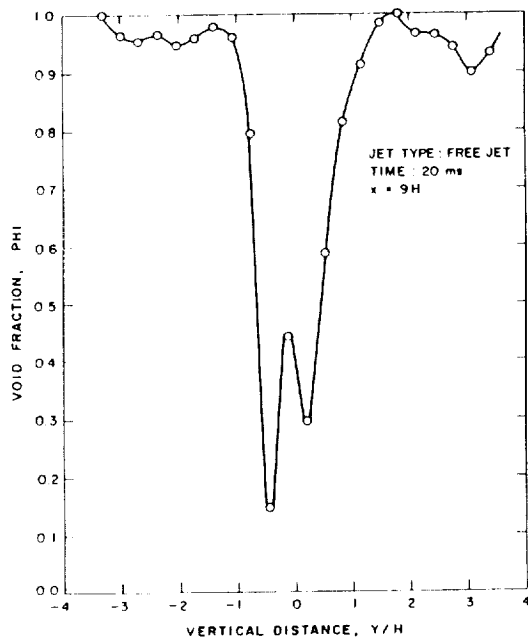| Type	Viscosity (poise)	Density (gm/cm^3)	Surface Tension (dynes/cm)
Water	0.01	1.0	72.7
Pantopaque ($C_{19}H_{29}IO_2$)	0.051	1.259	32.1

Fig. 15 Void Fraction Distribution Across the Wildest Jet-Head Region (Plane Wall Jet Case)
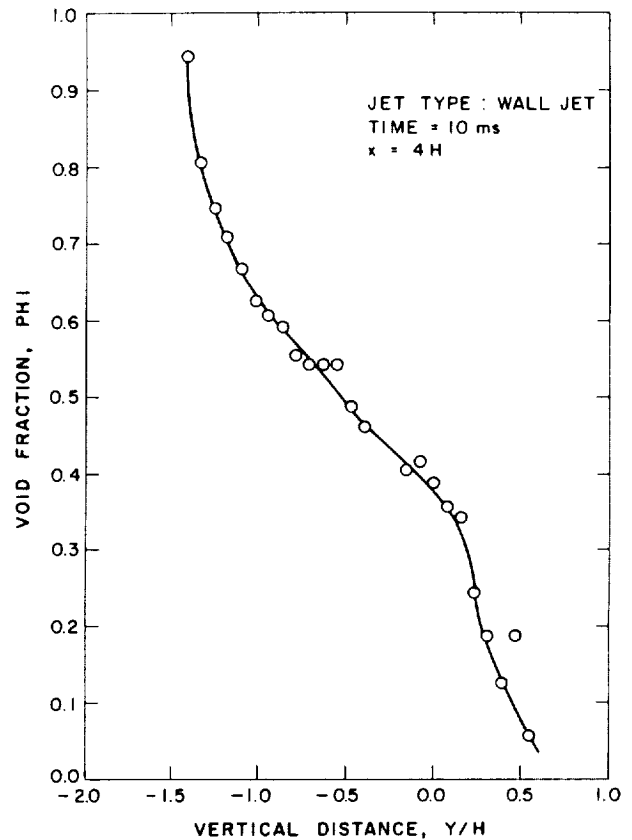

Fig. 14 Void Fraction Distribution Across the Widest Jet-Head Region (Plane Free Jet Case)
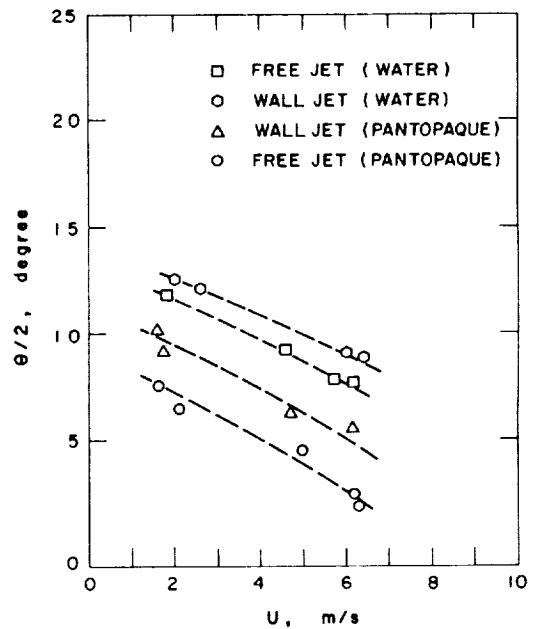

Fig. 16 Liquid Jet Divergent Angle Under Different Jet-Head Velocities
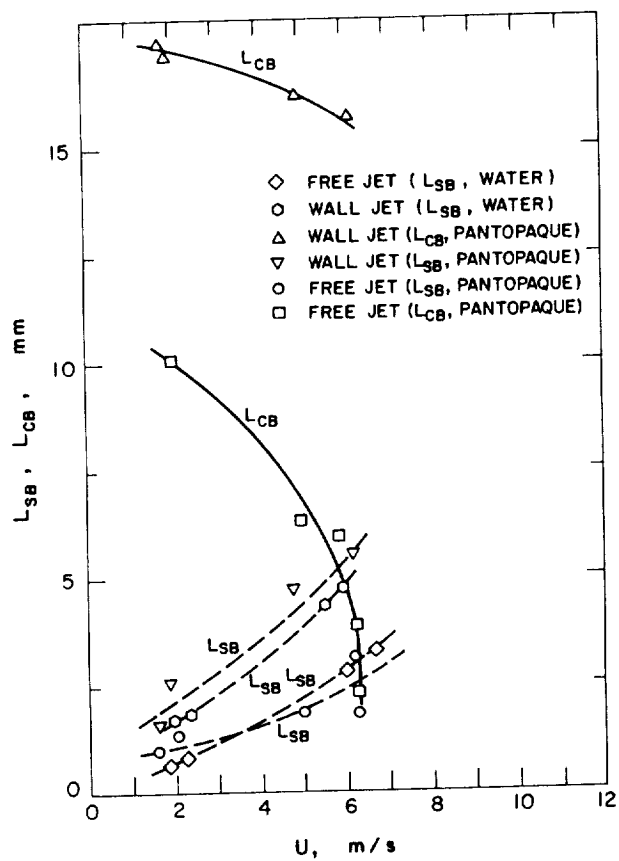
132

Fig. 17 Liquid Jet Breakup Length Under Different
Jet-Head Velocities

Editor's Narrative:

Round-Table Discussion: Physical, Model, Numerical and Experimental Aspects of Mixing and Demixing Processes in Multiphase Flows

At the conclusion of the first day of presentations a discussion was opened in the general areas of physical, model, numerical and experimental aspects of mixing and demixing processes in multiphase flows. Two specific topics became the focus of the discussion. These were the relative merits of the continuum vs. Lagrangian-Eulerian frameworks for developing multiphase flow theories and the accuracy of the turbulence models used within these theories.

By the lack of discussion, it would appear that laminar flow about a single spherical particle, at small or zero Reynolds number, leading to expressions for the drag and migrations in idealized mechanical two-phase flows are not imperative issues. This is despite the fact that most theories of turbulent multiphase flow, whether continuum or Lagrangain-Eulerian in origin, accept aspects of Stokes flow analysis within the models for the phase coupling drag. Hence, the accurate description of the forces on a single particle in various circumstances is important for a wide variety of flows. In addition, there exists a prevailing attitude that the diffusion potentials due to the turbulence of the continuous fluid phase dominates any transverse or migrational motions of the dispersed phase. However, it should be noted that laminar processes resulting in transverse particle migrations may be of consequence within the viscous sublayer of turbulent flows if the particle sizes are small relative to the viscous sublayer thickness. This may be the case for such phenomenon as near wall particle depletion, as observed in turbulent multiphase pipe and channel flows. Lastly, within this same context, it should be noted that there are particle migration processes which may be analyzed by in-the-mean or laminar theory for some scale of 'large' or 'heavy' particles relative to the turbulence. For example, a baseball, by imparting a spin to it can be made to curve (migrate laterally) through the atmospheric boundary layer with apparent disregard for the random diffusion potentials placed on it by the turbulent air.

In the discussion of the relative merits of the continuum vs. the Lagrangian-Eulerian frameworks for developing theories of multiphase flows, one of the shortcomings of the continuum approach was immediately pointed out. Specifically, the continuum approach requires *a priori* acceptance of the assumption that the particles are of a single size category and have identical mechanical properties. Thus, if the particles or droplets are a variety of different sizes or vary in mechanical properties then the 'two-fluid' model has become the 'many-fluid' model. This results in losing one of the original benefits of the continuum theories for two-phase flow, that being computational efficiency. This raised the question as to whether or not the continuum theories are an artifact of the pre-supercomputer era. A conclusion on this question was not reached. In defense of the continuum approach to modeling two-phase flow it was pointed out that a well posed continuum theory does not contain the implicit geometric dependencies that a Lagrangian-Eulerian scheme contains. In addition, continuum theories have been used successfully to provide dispersed phase field variable information in situations where the added complexity of tracking individual particles was not warranted.

Due to the stochastic nature and high frequency of collision between particles or droplets, a consensus was reached that continuum models may provide a more tractable approach than Lagrangian-Eulerian schemes for modeling dense two-phase flows. However, advances within this area will require constitutive relationships for the dispersed phase spherical and deviatoric stress, separate from those of the continuous fluid phase. The development of these relationships will have many of the same problems faced in trying to derive viscosity and strain-displacement relationships from kinetic gas theory. Advantages of the intuitively satisfying Lagrangian-Eulerian approach to multiphase flow theory were discussed. The 'particle tracking' allows for the coupling of the fluid and particle at a level consistent with single particle hydrodynamic analysis. This approach, despite its requirement for increased computational resources can provide a very detailed level of information on field variables, including the spectrum of a stochastic variable at any point in the domain. Since it is usually the average behavior of any given variable, for example particle velocity, that is desired this stochastic response is averaged statistically over an ensemble of realizations. The result is to produce information at the same level as is available from continuum theory, that is, averaged fields. This highlights one of the primary differences between the continuum vs. the Lagrangian-Eulerian approach to multiphase flow modeling. Continuum theories give averaged field information from averaged conservation equations. On the other hand, Lagrangian-Eulerian theories will provide for the calculation of stochastic fields, from an ensemble of 'exact' conservation equations. Averaged information from Lagrangian-Eulerian theories requires the averaging of fields.

The modification or modulation of the turbulence structure of the continuous fluid phase due to the presence of the dispersed phase was discussed. Even at dilute concentrations, the coupling of the phases via drag will result in a modification of the production and dissipation of turbulent kinetic energy. Questions as to whether or not the presence of the dispersed phase will always enhance dissipation of fluid phase turbulent kinetic energy ensued and references to experimental observations were made. This led to the discussion of the models for the turbulent time scales of the dispersed phase and the continuous phase. A passive dispersed phase would have a relaxation time that approaches zero and it would follow the continuous phase turbulent and mean motions exactly. On the other hand, the relaxation time of the dispersed phase may be very large in which case the motion of the dispersed phase would be unaffected by the turbulence of the continuous phase. Unfortunately, in many turbulent multiphase flows of practical interest there exists a spectrum of dispersed phase time and length scales. Further complexity is introduced when it is pointed out that, despite the abundant use of single time and length scale models, single phase turbulent fluid flow is also dominated by a variety of length and time scales over the domain of the flow. Hence, the need for improved models of turbulence, for use in theories of single phase flow as well as multiphase flow was recognized. Concerning an earlier argument, it was pointed out that regardless of the level of physical detail or lack thereof of the continuum or the Lagrangian-Eulerian theory, they both suffer from inadequate turbulence models. Any advantage in accuracy gained from using one theoretical approach over the other may, in some cases, be washed-out by the inaccuracies inherent in the common turbulence model.

The wisdom and desirability of repeating this workshop at sometime in the future was noted in closing.

136

NONGRADIENT DIFFUSION IN PREMIXED TURBULENT FLAMES

Paul A. Libby

University of California San Diego
La Jolla, California 92093

Abstract - We review recent theoretical and experimental results demonstrating the interaction between force fields and density inhomogeneities as they arise in premixed turbulent flames. In such flames the density fluctuates between two levels, the high density in reactants ρ_r and the low density in products ρ_p with the ratio ρ_r/ρ_p on the order of five to ten in flows of applied interest. The force fields in such flames arise from the mean pressure drop across the flame or from the Reynolds shear stresses in tangential flames with constrained streamlines. The consequence of the interaction is nongradient turbulent transport, countergradient in the direction normal to the flame and nongradient in the tangential direction. The theoretical basis for these results, the presently available experimental support therefor and the implications for other variable density turbulent flows are discussed.

INTRODUCTION

The phenomenology of turbulent flows is largely based on gradient transport assumptions proposed over a century ago by de St. Venant and/or Boussinesq. Even in the recently exploited second moment methods of analysis, methods which involve large systems of partial differential equations calling for considerable computational effort, closure is achieved by employing gradient models to eliminate third moment and other quantities. The extension to turbulent flows with variable density of the various gradient models carefully developed and validated for constant density turbulence has unfortunately been casually undertaken with the consequence that much additional research is needed before the phenomenology is well founded for high speed turbulent boundary layers and jets and for turbulent reacting flows, both high and low speed. That new significant processes may be operative in turbulent flows with variable density is suggested by the recent findings in premixed turbulent flames. It is our purpose to review these findings and to discuss their implications.

Exposition is facilitated if we consider a normal premixed turbulent flame as shown schematically in Fig. 1. Cold reactants, a metastable mixture of fuel and oxidizer, with a mean velocity $\bar{u}_o$, a density ρ_r, an intensity of velocity fluctuations characterized by a turbulent kinetic energy k_o and a length scale of the large eddies l_o are consumed within the flame and exit as hot products with these quantities changes to $(1 + \tau)\,\bar{u}_o$, ρ_p, k_∞ and l_∞ respectively. Here τ is a heat release parameter with values of practical interest from five to ten. Figure 1 may be considered an idealization of the flames which occur in internal combustion engines, various propulsion systems involving prevaporized fuels and industrial accidents.

The object of a theory for such flames is the prediction of the turbulent flame speed $\bar{u}_o$ and of the flame structure. The development of such a theory involves two related considerations; one concerns the thermochemistry of the flow, the description of the state of the gas, its density, temperature and composition, while the second relates to fluid mechanics. These two aspects are the aerothermochemistry of the flow.

138

Various parameters can be used to characterize these flames. One system is proposed by Abraham *et al.* (1985) and involves a Damköhler number $Da_\Lambda \equiv (\Lambda/u') (S_L/\delta_L)$ where Λ is a large eddy scale, i.e., l_o introduced earlier, $u' \simeq (3/2\, k_o)^{1/2}$ is a characteristic intensity of the velocity fluctuations and S_L and δ_L are the speed and thickness respectively of an unstrained laminar flame in the chemical system under consideration. A second parameter is a turbulent Reynolds number $R_\Lambda \equiv u'\,\Lambda/\nu$ where ν is a representative kinematic viscosity.* A pair of values, Da_Λ and R_Λ, determines the ratio of two velocities u'/S_L and of two lengths L_K/δ_L where L_K is a characteristic Kolomogoroff length. For premixed turbulent flames within internal combustion engines Abraham *et al.* (1985) determine that $1 < (L_K/\delta_L) < 10^2$. The implication of this finding is that chemical reaction at the molecular level takes place in thin surfaces, laminar flamelets, whose structure is dominated by laminar transport and whose motion is determined by the turbulent velocity field. Similar considerations applied to other premixed turbulent flames indicate that in many, indeed most, applications of applied interest this laminar flamelet description prevails.

The Bray-Moss Model and Some Consequences

Although not restricted to flows involving such flamelets, the Bray-Moss (BM) model simply and with an accuracy suitable for many purposes describes the thermochemistry of premixed turbulent flows (cf. Bray and Moss 1975). According to this description the instantaneous value of a progress variable $c(x,t)$ which has the values zero in reactants, unity in products and intermediate values in gas possibly undergoing chemical reaction determines the entire state of the gas. Thus, for example,

$$\frac{\rho}{\rho_r} = \frac{1}{1+\tau c} \qquad \frac{T}{T_r} = 1 + \tau c \tag{1}$$

where τ is most readily determined from the specialization of the second of these equations to products, i.e., from

$$\frac{T_p}{T_r} = 1 + \tau \tag{2}$$

---

* It should be kept in mind that ν can vary by one to two decades within a flame and thus that there is some ambiguity as to its appropriate value for determining R_Λ.

In averaging the equations for variable density turbulent flows it is useful to employ Favre or mass averaging; to illustrate the notion and notation involved consider the i-th velocity component, namely

$$u_i(\underset{\sim}{x},t) = \frac{\overline{\rho u_i}}{\overline{\rho}}(\underset{\sim}{x}) + u''(\underset{\sim}{x},t) = \tilde{u}(\underset{\sim}{x}) + u''(\underset{\sim}{x},t)$$

All variables except the density and pressure are averaged in this fashion. The great advantage of Favre averaging is that the conservation equations for variable density flows closely resemble those for constant density with exceptions which, as we shall see, indicate special effects associated with the variability of the density. Despite this advantage it should not be assumed without support from experiment that the closure methods applicable to constant density flows can be carried over to variable density cases without modification. Furthermore, although significant only when low turbulence Reynolds numbers must be taken into account, Favre averaging is not adaptable without approximation to the molecular terms in the conservation equations. The definitive discussion of Favre averaging applied to turbulent combustion is given by Jones (1980) while such averaging is emphasized in the monograph on turbulent reacting flows by Libby and Williams (1980). Rubesin and coworkers at the Ames Research Center of NASA apply Favre averaging for the analysis of high speed turbulent boundary layers (cf. Wilcox and Rubesin 1980).

When Favre averaging is applied to Eqs. (1), there results

$$\frac{\overline{\rho}}{\rho_r} = \frac{1}{1 + \tau \tilde{c}} \qquad \frac{\tilde{T}}{T_r} = 1 + \tau \tilde{c} \tag{2}$$

A further important feature of the BM model is an approximation for the probability density function (pdf) of the progress variable. In general for a statistically stationary flow

$$P(c;\underset{\sim}{x}) = \alpha(\underset{\sim}{x})\,\delta(c) + \beta(\underset{\sim}{x})\,\delta(1-c) + \gamma(\underset{\sim}{x})\,f(c;\underset{\sim}{x}) \tag{3}$$

Now if

$$\int_{0^+}^{1^-} dc\, f(c;\underset{\sim}{x}) = 1$$

i.e., if the pdf describing the interior values of the progress variable is normalized, then

$$\alpha(\underset{\sim}{x}) + \beta(\underset{\sim}{x}) + \gamma(\underset{\sim}{x}) = 1 \tag{4}$$

140

The essential approximation in the BM-model is that $\gamma \ll 1$, an approximation which is satisfied when chemical reaction occurs in laminar flamelets as well as in other flow structures, e.g., reaction zones with $\delta_L > L_K$. The implication of this approximation is that the temperature as measured by an idealized thermometer within a premixed turbulent flame possesses essentially two values, T_r within reactants and T_p within products, and that flamelet passages cause the switch from one level to the other.*

An important consequence of the $\gamma \ll 1$ approximation is exposed if $\tilde{c}(x)$ is calculated from Eq. (3). There results

$$\alpha(\underline{x}) = \frac{1 - \tilde{c}}{1 + \tau \tilde{c}} \qquad \beta(\underline{x}) = \frac{(1 + \tau)\,\tilde{c}}{1 + \tau\,\tilde{c}} \tag{5}$$

where Eq. (4) is used to calculate $\alpha(\underline{x})$. We thus see that the strengths of the delta functions is simply related to the mean value of the progress variable which must be considered one of the principal dependent variables in a theory of premixed turbulent flames.

For the present discussion it is useful to consider the intensity of the density fluctuations; from Eqs. (1), (3) and (5) we can compute

$$\frac{\overline{\rho'^2}}{\overline{\rho}^2} = \tau^2 \frac{\tilde{c}\,(1 - \tilde{c})}{1 + \tau} \tag{6}$$

We thus see that the maximum in the relative intensity of the density fluctuations occurs within the flame where $\tilde{c} = 1/2$ and has a value $\tau^2/4(1 + \tau) \approx \tau/4$ for $\tau \gg 1$. Thus for degrees of heat release of applied interest we must expect intense density fluctuations.

Although not essential for the present discussion, it is worth noting that the mean rate of creation of product $\overline{w}(\underline{x})$ in the BM model involves the product γw_{max} where w_{max} is the maximum rate of creation of product, a quantity determined by the chemical kinetics of the system under consideration. In the BM model this product involves a vanishingly small term multiplied by an indefinitely large term and is thus

---

* Extensive studies of the statistics of two valued functions with specific reference to premixed turbulent flames have been carried out in order to develop a model for the mean rate of creation of product (cf. Bray *et al.* 1987).

indeterminant. As a consequence a separate model for $\overline{w}(\underline{x})$ is needed; progress in this direction is described in Bray *et al.* (1987).

The Bray-Moss-Libby Model for the Aerothermochemistry

The notion of bimodality extends to the the description of the velocity components in premixed turbulent combustion and leads to the Bray-Moss-Libby (BML) model of the aerothermochemistry of such combustion. To appreciate this extension consider the bivariate pdf

$$P(u_i, c; \underline{x}) = \alpha(\underline{x})\, \delta(c)\, P(u_i, 0; \underline{x}) + \beta(\underline{x})\, \delta(1 - c)\, P(u_i, 1; \underline{x}) +$$

$$\gamma(\underline{x})\, f(u_1, c; \underline{x}) \tag{7}$$

Figure 2 shows schematically such a joint pdf. If $f(u_i, c; \underline{x})$ is normalized, Eq. (4) again applies and with the approximation $\gamma \ll 1$ the statistical behavior of u_i and c are again dominated by contributions from reactants and products. Note that two of the three pdf's on the right side of Eq. (7) are conditional and describe the velocity within reactants and products. It is possible with current diagnostic techniques to measure with good spatial resolution the temperature and one or more velocity components and thus to determine experimentally the conditional pdf's appearing in Eq. (7) (cf. Moss 1980 and Shepherd and Cheng 1988).

Equation (7) leads to significant results if $\gamma \ll 1$. To illustrate consider the mean *unconditional* velocity component $\tilde{u}_i(\underline{x})$ which is given by Eqs. (5) and (7) as

$$\tilde{u}_i(\underline{x}) = (1 - \tilde{c})\, \overline{u}_{ir} + \tilde{c}\, \overline{u}_{ip} \tag{8}$$

where $\overline{u}_{ir}$ and $\overline{u}_{ip}$ are the *conditional* mean values of the i-th velocity component within reactants and products respectively. We show these values in Fig. 2. Precise definitions of these quantities are as follows:

$$\overline{u}_{ir}(\underline{x}) = \int_{-\infty}^{\infty} du_i\; u_i\, P(u_i, 0; \underline{x})$$

$$\bar{u}_{ip}(x) = \int\limits_{-\infty}^{\infty} du_i \; u_i \; P(u_i, 1;x) \tag{9}$$

According to the BM model the mean turbulent flux of all state variables in the i-th coordinate direction can be determined from the corresponding flux of the progress variable but from Eq. (7) we have

$$\frac{\overline{\rho u_i''c''}}{\bar{\rho}} = \tilde{c}\;(1-\tilde{c})\;(\bar{u}_{ip} - \bar{u}_{ir}) \tag{10}$$

Now a gradient model for this mean flux yields

$$\frac{\overline{\rho u_i''c''}}{\bar{\rho}} = -\nu_T\;\frac{\partial \tilde{c}}{\partial x_i} \tag{11}$$

where ν_T is a positive turbulent exchange coefficient. If in connection with Fig. 1 we let x_i correspond to x, then $\partial \tilde{c}/\partial x > 0$ implying that $\overline{\rho u''c''} < 0$ and if gradient transport applies, then $\bar{u}_p < \bar{u}_r$. But we know from our earlier discussion that the velocity in the product stream downstream of the flame where $\tilde{c} = 1$ is $(1 + \tau)$ times greater than that in the reactant stream. Given this overall increase in mean velocities it does not seem reasonable to expect the conditional velocities in products within the flame to be less than those within reactants. Accordingly, we see a potential difficulty with a gradient model for premixed turbulent flames if, as is the case in flames of practical interest, $\tau \gg 1$.

In Bray *et al.* (1981), Masuya and Libby (1981) and Libby (1985) the BML model with all gradient assumptions avoided is applied to normal and oblique turbulent flames in premixed systems in order to clarify the applicability of the gradient model therein. In the next sections we sketch the analyses involved and review the results from them

APPLICATION TO NORMAL PREMIXED TURBULENT FLAMES

We now consider application of the notions advanced in the previous section to the flame of Fig. 1. The equations needed for the analysis are as follows:

$$\frac{d}{dx}(\bar{\rho}\,\tilde{u}) = 0$$

$$\frac{d}{dx}(\bar{\rho}\,\tilde{u}^2 + \overline{\rho u''^2}) = -\frac{d\bar{p}}{dx} \tag{12}$$

$$\frac{d}{dx}(\bar{\rho}\,\tilde{u}\,\tilde{c} + \overline{\rho u'' c''}) = \bar{w}$$

and

$$\frac{d}{dx}\left[\bar{\rho}\,\tilde{u}\,\frac{\overline{\rho u''^2}}{\bar{\rho}} + \overline{\rho u''^3}\right] + 2\,\overline{\rho u''^2}\,\frac{d\tilde{u}}{dx} = -2\,\overline{u''}\,\frac{d\bar{p}}{dx} - \bar{\chi}_u$$

$$\frac{d}{dx}\left[\bar{\rho}\,\tilde{u}\,\frac{\overline{\rho u'' c''}}{\bar{\rho}} + \overline{\rho u''^2 c''}\right] + \overline{\rho u'' c''}\,\frac{d\tilde{u}}{dx} + \overline{\rho u''^2}\,\frac{d\tilde{c}}{dx} = -\overline{c''}\,\frac{d\bar{p}}{dx} + \overline{u'' w} - \bar{\chi}_{uc} \tag{13}$$

The usual notation applies to Eqs. (12) and (13) which represent the first and second moment equations respectively for one dimensional flames. The quantities $\bar{\chi}_u$ and $\bar{\chi}_{uc}$ describe dissipation effects which for the flames under consideration are due solely to chemical reaction, i.e., are proportional to $\bar{w}$. Similarly the velocity-chemical reaction term $\overline{u'' w}$ can be convincingly described by application of the BML model; it is found to be proportional to $\bar{w}$, models for which are presently under development (cf. Bray *et al.* 1987) but which are not needed for present purposes.*

Some analysis permits Eqs. (12) and (13) to be reduced to two equations with $\tilde{c}$ as the *independent* variable and with a dimensionless velocity intensity $I \equiv \overline{\rho u''^2}/\rho_r\,\bar{u}_o^2$ and a dimensionless turbulent flux $F \equiv \overline{\rho u'' c''}/\rho_r\,\bar{u}_o$ as the two *dependent* variables. In the present discussion the latter variable is of more significance. In this formulation $\bar{w}$ is needed only if subsequent to finding the solutions for $I(\tilde{c})$ and $F(\tilde{c})$ the spatial distributions are sought. However, comparison between theory and experiment is

---

* It is worth noting that in these equations the effects of pressure fluctuations are neglected. In constant density turbulence models for such effects have been painfully and carefully developed over a period of many years but these models do not apply to reacting flows with heat release since combustion induced pressure fluctuations result from volumetric sources, i.e., from an entirely different mechanism. Appropriate models for such fluctuations are not presently available.

conveniently carried out in terms of $\tilde{c}$ so that generally the absence of a model for $\bar{w}$ is not a shortcoming relative to the analysis of one dimensional flames. For premixed turbulent flows in two and three dimensions such a model is needed and research to that end is underway (cf. Bray *et al.* 1987).

In developing the final equations for $I(\tilde{c})$ and $F(\tilde{c})$ the first of Eqs. (2) and (12) permit $\bar{u}$ to be eliminated while the second and third of Eqs. (12) are used to eliminate $d\bar{p}/dx$ and $\bar{w}$ respectively. Closure requires the third moment quantities $\overline{\rho u''^3}$ and $\overline{\rho u''^2 c''}$, $\overline{u''}$, $\overline{c''}$ and the dissipation terms to be expressed in terms of the two dependent and the independent variables but with the exception of some inessential uncertainties in the conditional velocity statistics suitable models for these quantities free of gradient assumptions can be developed. For example, we have

$$\overline{u''} = \tau \frac{\overline{\rho u'' c''}}{\rho_r} \qquad \overline{c''} = \tau \frac{\tilde{c}\,(1 - \tilde{c})}{1 + \tau\,\tilde{c}} \tag{14}$$

In the present discussion two terms in Eqs. (13) are of particular interest; we refer to those involving $d\bar{p}/dx$. If Eqs. (12) and (13) are specialized to constant density flows, e.g., by setting $\tau = 0$, then from Eqs. (14) we see that these terms vanish and indeed the reduction to standard equations for such flows is complete. The implication to be drawn from this consideration is that these pressure gradient terms account for effects operative in variable density turbulence, in particular an interaction between a force field associated with the pressure gradient and density fluctuations associated with heat release. In premixed turbulent flames this interaction is present only within the flame proper since both the force field and the density fluctuations are absent in the reactant and product streams on each side of the flame.

Additional comments on this interaction are indicated. If conventional rather than Favre averaging is used, the interaction is contained within the resulting equations but is obscured by the clutter of a large number of terms involving density fluctuations. In more general variable density flows models for the multipliers of the several pressure gradient terms must be introduced as indicated for nonpremixed combustion by Jones (1980) and for high speed flows by Wilcox and Rubesin (1980).

The final equations for $I(\tilde{c})$ and $F(\tilde{c})$ involve singularities at $\tilde{c} = 0, 1$ as is to be expected since these points correspond to points at infinity in the x-variable but appropriate series expansions permit the numerical solutions to be initiated in the neighborhood of these end points. A shortcoming of the theory

is that $I_o \equiv \overline{u'^2_o}/\overline{u}_o^2$ where $\overline{u'^2_o}$ is the intensity in the reactant stream upstream of the flame must be imposed, i.e., the turbulent flame speed is not calculated. This shortcoming can be turned into a virtue for the purpose of studying the structure of premixed turbulent flames since it can be argued that selection of I_o so as to achieve agreement with experimental results assures that the predicted flame structure corresponds to realistic flames. In our original work we set $I_o = 0.22$ unless we had specific reasons to do otherwise but in recent years our confidence in this value has been reduced by evidence that a wide variety of values is found depending on the geometry of the flames and on the flameholding mechanism employed. The detailed reasons for this ambiguity are unknown.*

Numerical Results for Normal Flames

In Fig. 3 we show the distribution of the turbulent flux in terms of $F(\tilde{c})$ from both theory and from the experiment of Moss (1980). In the open flame studied by Moss $\tau = 6.5$ and $I_o = 0.16$. The two curves represent theoretical predictions based on slightly different models for the conditional statistics, differences which are irrelevant for the present discussion. If it is recalled that gradient transport for these flames implies $F < 0$, we see that the entire flame structure exhibits countergradient diffusion. The explanation for such diffusion resides in the interaction between the pressure drop across the flame and the density fluctuations which from Eq. (6) are seen to involve a relative intensity greater than unity, roughly 1.4. The pressure drop tends to accelerate the light parcels of product relative to the heavy parcels of reactants in the direction of high product concentration, a differential effect contrary to gradient transport.

Several further comments are indicated. Calculations with the pressure gradient terms in Eqs. (13) suppressed yield $F < 0$ for all values of τ. Moreover, as $\tau \to 0$ the theory predicts gradient transport and thus the expected behavior for nearly constant density turbulent flows. These results lend credibility to the explanation of interaction as the cause of countergradient diffusion and to the validity of the theory in general. The notion of countergradient transport in premixed turbulent flames is now widely accepted

---

* A recent study (Libby 1987) removes the shortcoming with respect to I_o by invoking the Hakberg-Gosman condition and discusses in some detail the uncertainties in its value.

and has been observed in a variety of laboratory flames with simple geometries. Later we discuss its more general applicability.

THE OBLIQUE PREMIXED TURBULENT FLAME WITH CONSTRAINED MEAN STREAM-LINES

In Fig. 4 we show schematically a premixed turbulent flame which is oblique to the reactant stream. Such flames can be established by a flameholder, e.g., a cylinder, in a duct carrying reactants. The classic experiment of this nature is due to Wright and Zukoski (1962) while the theoretical description of these flames based on the BML model is given by Masuya and Libby (1981). If we assume that the duct prohibits significant deflection of the mean streamlines both upstream and downstream of the flame, it is reasonable to consider as an idealization an infinite planar flame held at a specified angle θ with undeflected mean streamlines. In this case description of the flow involves an analysis identical with that for purely normal flames and a second, subsequent analysis of the tangential velocity component which involves explicitly the flame angle θ. The treatment of the tangential flow requires determination of the intensity of the fluctuations of the v-velocity component and the tangential flux of the progress variable which in dimensionless form are $I_v \equiv \overline{\rho v''^2}/\rho_r \bar{u}_o^2$ and $F_v \equiv \overline{\rho v'' c''}/\rho_r \bar{u}_o$ respectively. This latter variable is of principal concern in the context of the present discussion and from Eq.) is given by

$$\frac{\overline{\rho v'' c''}}{\bar{\rho}} = \tilde{c} \, (1 - \tilde{c}) \, (\bar{v}_p - \bar{v}_r)$$

(15)

where $\bar{v}_r$ and $\bar{v}_p$ are the conditional tangential velocity components within reactants and products respectively.

Gradient transport indicates that this mean flux is zero since the tangential gradient of the progress variable is zero and thus that the two conditional velocities in the tangential direction are equal. The implication from this result is that parcels of reactants and products have streamlines which differ only by the differences in the normal conditional velocities. However, there is a tangential force field in these flames arising from the x-wise gradient of the Reynolds shear stress $\overline{\rho u'' v''}$; the existence of this forces field can be seen from the mean conservation equation for tangential momentum which yields

$$\frac{d}{dx} \overline{\rho u'' v''} = -\tau \, \frac{\rho_r \, \bar{u}_o^2}{\tan \theta} \, \frac{d\tilde{c}}{dx}$$

(16)

Note that when the heat release and thus the density fluctuations vanish, this force field is absent.

This discussion establishes that oblique turbulent flames in premixed systems involve a tangential force field and density fluctuations. Thus according to our previous argument we can expect nongradient turbulent transport in the tangential direction. Indeed calculations show that $\bar{v}_p > \bar{v}_r$, that $\overline{\rho v''c''} > 0$ and that the parcels of reactants and products follow different mean streamlines with the former exhibiting only small tangential velocity while the latter possesses large tangential velocities. This behavior is shown schematically in Fig. 4. We thus have an example of nongradient transport to add to the previously discussed case of countergradient transport. To date there have been no detailed measurements in oblique flames to assess the validity of this theory.

CONCLUDING REMARKS

We show that when mean force fields and density fluctuations coexist, an interaction leads to turbulent transport which is not described by the usual gradient model. In the simple flow configurations associated with normal and oblique planar flames, the latter with constrained mean streamlines, countergradient and nongradient transport exists. There is no question that the notions suggested by these findings are conceptually important. Moreover, the experimental results of Heitor *et al.* (1987) relative to the complex flow associated with a baffle stabilized premixed turbulent flame establish that nongradient transport exists in complex flow configurations, i.e., in flows of applied interest. Within the context of the present discussion the first few sentences of this paper are worth quoting:

> In turbulent, premixed flames there arise source terms, explicitly set out below, in the conservation equations for the turbulent heat transfer rate and stresses that have no counterparts in non-reacting flows. Analysis (Masuya and Libby 1981; Bray, Libby and Moss 1985; Libby 1985) has shown that at least in the two idealized extremes with the flame either normal or oblique to the approaching reactants, and at practically important levels of heat release, these terms are sufficiently large to cause non-gradient transport of turbulent heat flux. This finding is important because it casts doubt on the applicability of turbulence models that use gradient-transport hypothesis.

From a detailed study of the velocity and temperature fields Heitor *et al.* conclude that the interaction between pressure gradients and density fluctuations results in the largest contribution to the balance of the turbulent heat flux and that that flux is not aligned with the mean temperature gradient.

The importance of nongradient transport on general variable density turbulence remains to be established. With respect to premixed turbulent flames we note that the question arises as to the influence of these processes arising within their structure on their orientation between reactant and product streams remains to be clarified. Answering this question requires further theoretical and computational efforts.*

---

* If the provisional model for $\overline{W}(\chi)$ set forth in Bray *et al.* (1987) is validated, the effort required is largely computational.

Additional research is also required to determine the importance of the interaction under discussion in high speed flows. It would seem obvious that in scramjets with their large gradients of mean pressure and mean turbulent shear stresses this interaction must be operative but whether it plays an important role in the mixing and chemical processes in the flow is unclear. Certainly the present casual, uncritical extension to supersonic chemically reacting flows of the phenomenology of constant density turbulence should raise healthy skepticism concerning the validity of the resulting predictions but unfortunately that skepticism does not appear to be shared by authors, reviewers and editors of current journal articles.** Similar uncertainties would appear to prevail for turbulent boundary layers in high speed flows so that additional research is indicated.

** Occasionally there is a mild rejoinder warning the reader of potential fundamental difficulties. An example from a recent report is as follows: "The turbulence model we we have used is the $k - \varepsilon$ model as described in ... Although Reference ... specifically addresses the question of compressible flows, it should be noted that turbulence models for compressible flows are not well-developed. Hence, the choice of the standard $k - \varepsilon$ model in this situation cannot be regarded as definite."
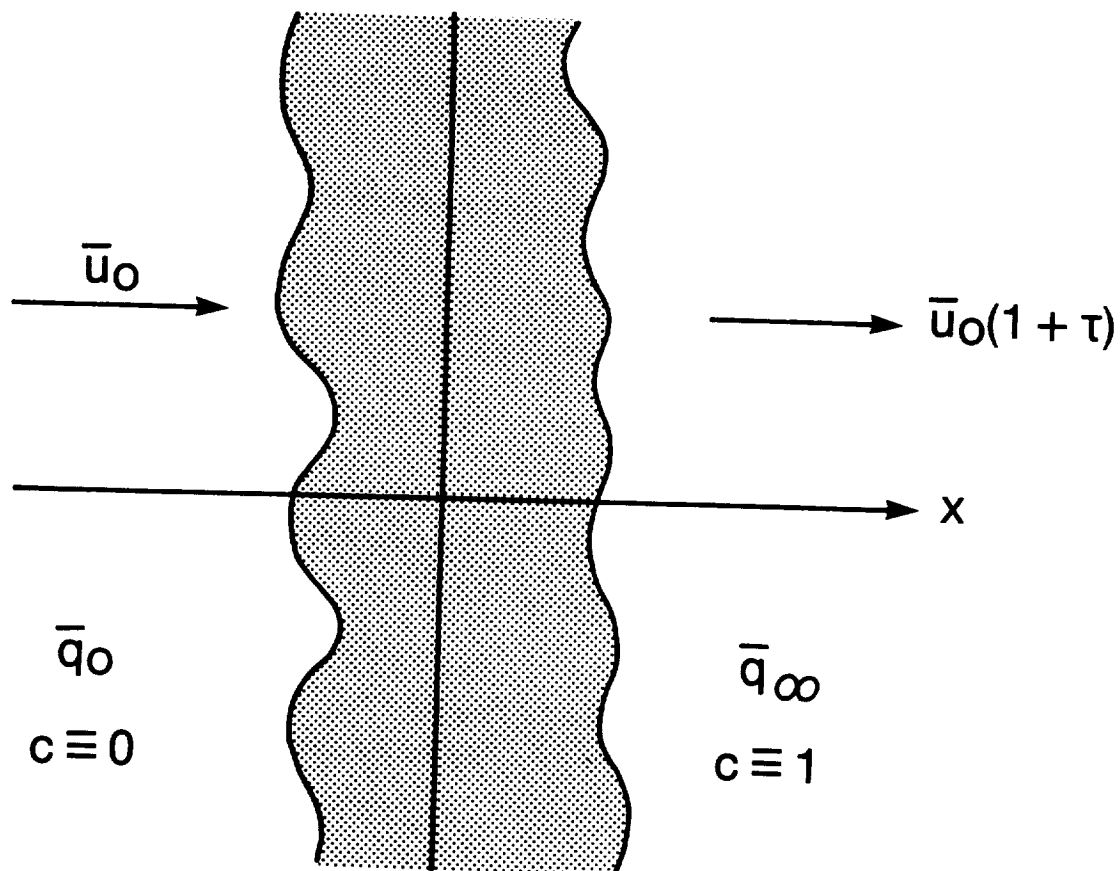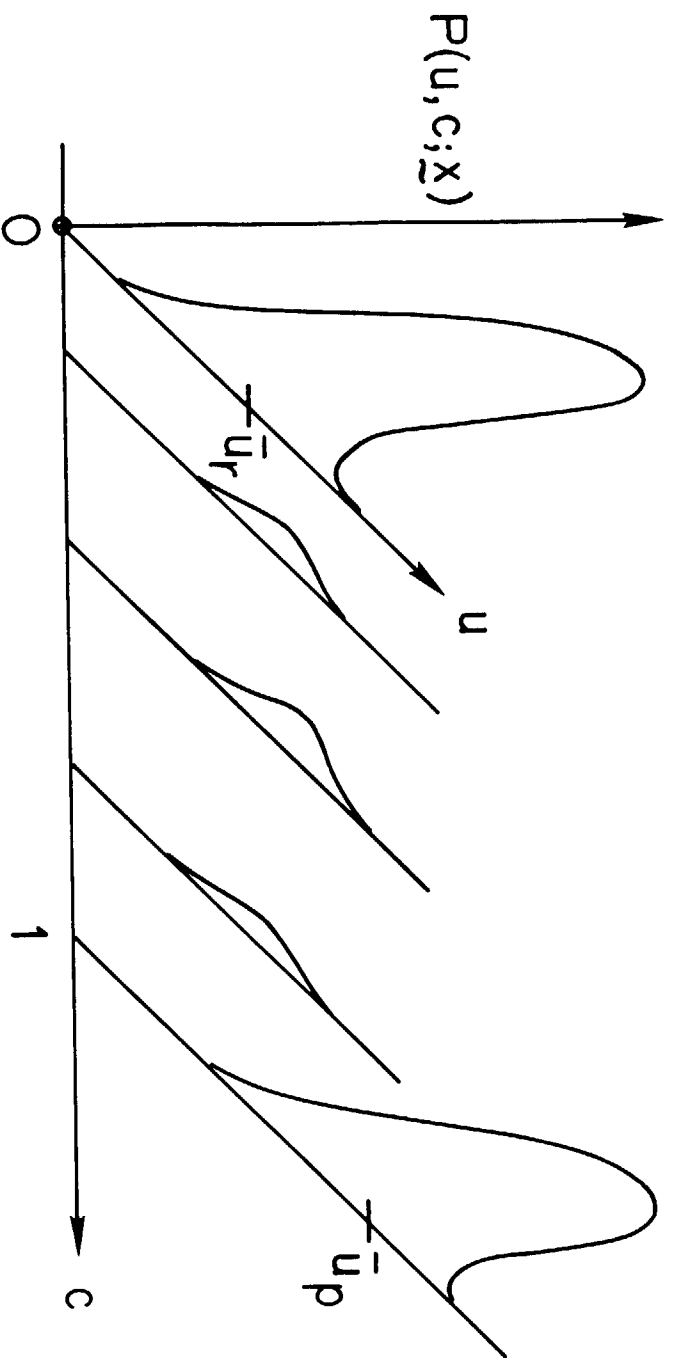
REFERENCES

Abraham, J., Williams, F.A. and Bracco, F. (1985). A discussion of turbulent flame structure in premixed charges, SAE Paper 850345.

Bray, K.N.C. and Moss, J.B. (1977). A unified statistical model of the premixed turbulent flame, *Acta Astronautica* 4:291.

Bray, K.N.C., Libby, P.A., Masuya, G. and Moss, J.B. (1981). Turbulence production in premixed turbulent flames, *Combustion Science and Technology* 25:127.

Bray, K.N.C., Libby, P.A. and Moss, J.B. (1985). Unified modelling approach for premixed turbulent combustion - Part i: General formulation, *Combustion and Flame* 61:87.

Bray, K.N.C., Champion, M. and Libby, P.A. (1987). Mean reaction rates in premixed turbulent flames (Submitted to the Twenty second Symposium (International) on Combustion, The Combustion Institute).

Heitor, M.V., Taylor, A.M.K.P. and Whitelaw, J.H. (1987). The interaction of turbulence and pressure gradients in a baffle-stabilized premixed flame, *Journal of Fluid Mechanics* 181:387.

Jones, W.P. (1980). Models for turbulent flows with variable density and combustion, *Prediction Methods for Turbulent Flows*, (W. Kollmann, Ed.), Hemisphere Publishing Company, Washington, 379.

Libby, P.A. (1985). Theory of normal premixed turbulent flames revisited, *Progress in Energy and Combustion Science*, 11:83.

Libby, P.A. (1987). Theoretical analysis of the effect of gravity on premixed turbulent flames, *Combustion Science and Technology* (Submitted).

Libby, P.A. and Williams, F.A. (1980). *Turbulent Reacting Flows*, Volume 44, Topics in Applied Physics, Springer-Verlag, Berlin.
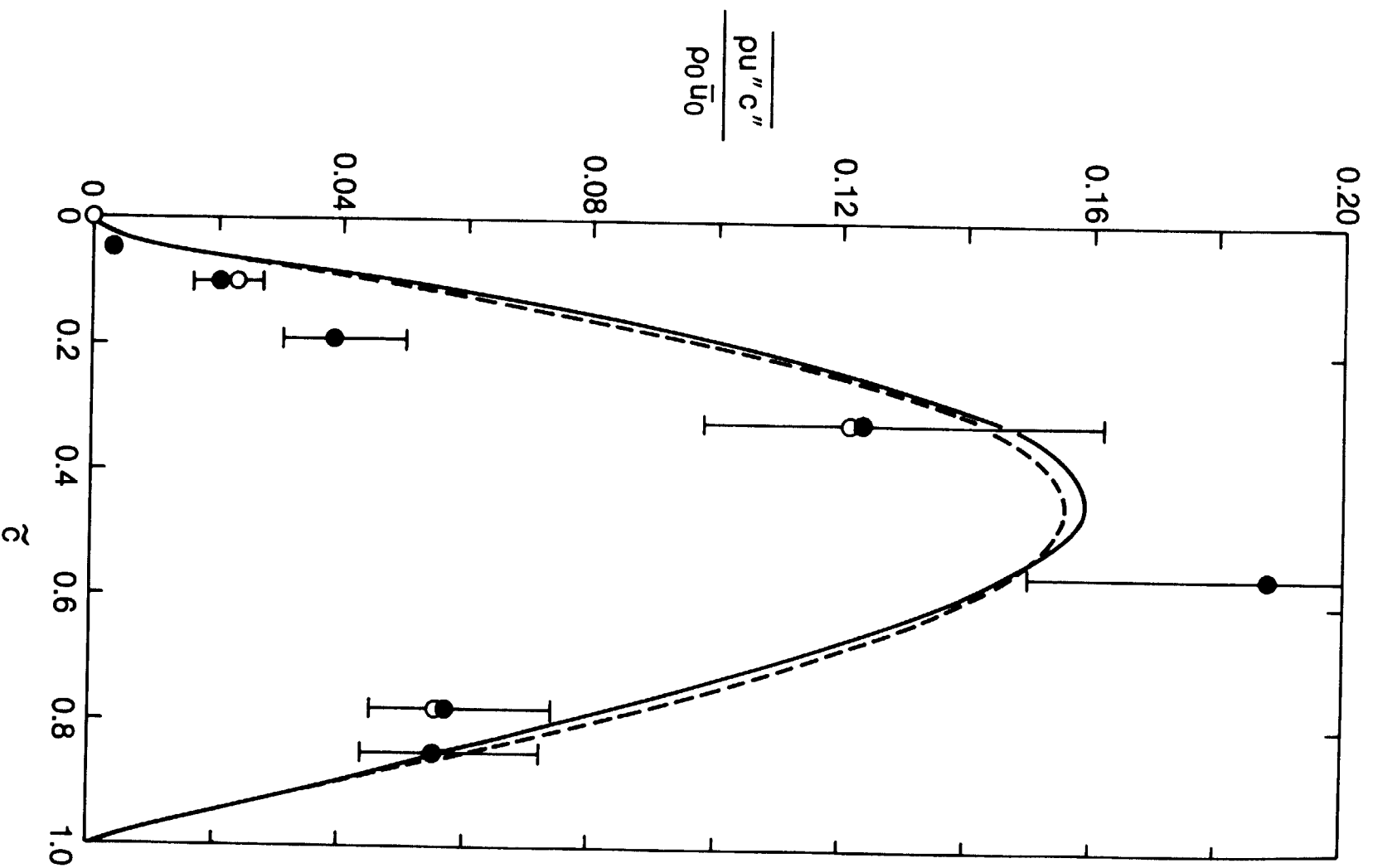
Masuya, G.M. and Libby, P.A. (1981). Nongradient theory for oblique turbulent flames with premixed reactants. *AIAA Journal* **19**:1590.

Moss, J.B. (1980). Simultaneous measurement of concentration and velocity in an open premixed turbulent flame, *Combustion Science and Technology* **22**:119.

Shepherd, I.G. and Cheng, R.K. (1988). An experimental evaluation of the BLM model of the scalar field in turbulent premixed flames, *Combustion Science and Technology* (To appear).

Wilcox, D.C. and Rubesin, M.W. (1980). Progress in turbulence modeling for complex flow fields including effects of compressibility, NASA TP 1517.

Wright, F.H. and Zukoski, E.E. (1962). Flame spreading from bluff body flameholders, *Eighth Symposium (International) on Combustion*, Williams and Wilkens, Baltimore, 933.
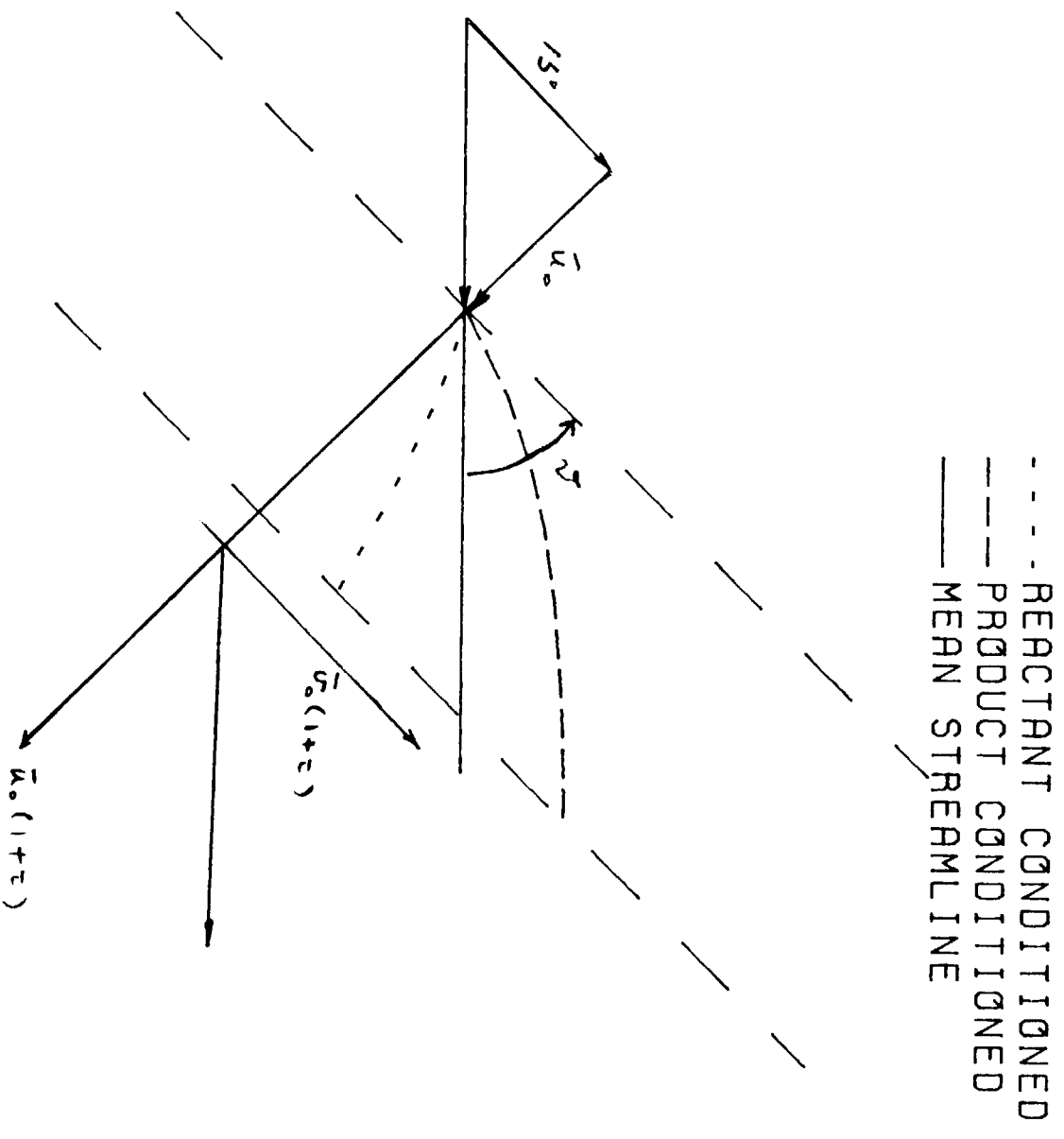
154

LIST OF FIGURES

$$\bar{u}_O \qquad\qquad \bar{u}_O(1 + \tau)$$

$$x$$

$$\bar{q}_O \qquad\qquad \bar{q}_\infty$$

$$c \equiv 0 \qquad\qquad c \equiv 1$$

156

confined oblique flame

- - - - REACTANT CONDITIONED
— — — PRODUCT CONDITIONED
——— MEAN STREAMLINE

15°

$\bar{u}_o$

$\bar{u}_o(1+\tau)$

15°(1+τ)

LA-UR-88-

TITLE: THE TURBULENT HEAT FLUX IN LOW MACH NUMBER FLOWS WITH LARGE DENSITY VARIATIONS

AUTHOR(S): *Peter J. O'Rourke and Lance R. Collins*

Los Alamos

Los Alamos National Laboratory
Los Alamos, New Mexico 87545

PRECEDING PAGE BLANK NOT FILMED

THE TURBULENT HEAT FLUX IN LOW MACH NUMBER FLOWS WITH LARGE DENSITY VARIATIONS

Peter J. O'Rourke and Lance R. Collins
Theoretical Division, Group T-3
Los Alamos National Laboratory
Los Alamos, New Mexico 87545

I. INTRODUCTION: THE DIRECTED ENERGY FLUX

This paper is concerned with a physical effect of fundamental importance for the modeling of turbulence transport in flows with large density variations. The effect occurs because the interaction of pressure and density gradients gives rise to a turbulent heat flux, which we call a directed flux, that is not accounted for in turbulence models for constant density flows. To see how this flux arises, it is perhaps best to consider an example of Rayleigh-Taylor instability, as depicted in Fig. 1. A heavy, cold gas overlays a light, hot gas in a box with a gravitational acceleration in the negative z-direction. The induced hydrostatic pressure gradient accelerates the light gas into the heavy gas and causes the instability and mixing. The velocities averaged across a horizontal plane are in the z-direction, and because the heavy gases are falling, the mass-averaged velocities in the mixing region will be negative. Relative to a surface moving downward with the mass-averaged velocity, there will be a net upward flux of energy. This is because although the mass flux of light gas crossing the surface upward equals the mass flux of heavy gas crossing downward, the light gas, being hotter, carries with it more energy per unit mass.

This upward energy flux is the directed flux. In the example of Fig. 1, this energy flux is in the direction of the negative of the temperature gradient, just as given by the laminar Fourier heat conduction law. If after some time we were to turn the box over so that the light gas overlay the heavy gas, to the extent that the two gases had not already mixed on the molecular level, there would be an unmixing in which the light gas would separate from the heavy gas. In this
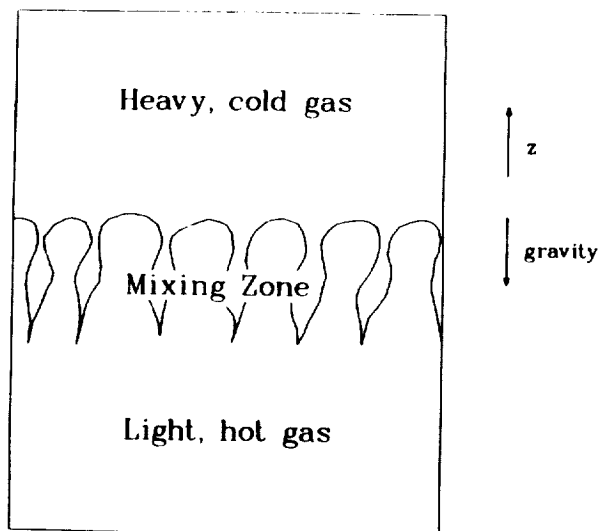

Fig. 1. Schematic depiction of Rayleigh-Taylor instability.

unmixing process, the directed heat flux would be upward, in the direction of the mean temperature gradient and opposite the direction given by the Fourier heat conduction law. This phenomenon has thus been called countergradient diffusion.[1] It cannot be predicted by turbulence models that use gradient transport, or a Fourier-like law, to describe turbulent heat transport. In our example, the turbulent heat flux ϕ^h is in the direction opposed to the pressure gradient, rather than the temperature gradient. We shall see that taking $\phi^h \sim - \nabla p$ is often more realistic for turbulent flows.

Between single-phase, two-density turbulent flows and two-phase flows there is an analogy that we will exploit in our turbulence modeling. This analogy will be used in helping to formulate the equations and in developing closure approximations for some of the terms. In two-phase flow modeling, which has received much attention within the last ten years[2,3] separate mass, momentum, and energy equations are kept for each phase, and these equations are coupled through functions that give the exchange rates of mass, momentum, and energy between the phases. Following Besnard, Harlow, and Rauenzahn,[4] we will use an alternative, analogous formulation. In place of two mass equations, we will keep an equation for the mean density and one for density fluctuations. In place of two momentum equations, we will keep a mean momentum equation and an equation for mean velocity differences associated with fluid elements of differing density. We use this second formulation because it allows for the possibility of modeling not just two-density flows, but the flows with a spectrum of densities that often occur in practical applications.

Two physical examples, one of two-phase flow and one of single-phase flow with density variations, serve to illustrate the analogy and another situation in which countergradient transport can arise. In both examples, pressure gradients are responsible for centrifuging lighter material inward toward the centers of rotating flows. In a two-phase bubbly flow, this effect has been observed in the vortices in the wake of an obstacle.[5] In single-phase flow, it is probably responsible for the experimental results of Wahiduzzaman and Ferguson.[6] The experimenters measured the radial temperature profiles in an axisymmetric swirling flow in a constant volume cylinder. The experimentally measured temperatures are plotted at four different times as the circles in Fig. 2. The lines are computed temperature profiles using the KIVA code[7] with a k-ε turbulence model[8] and gradient heat transport with a turbulent Prandtl number of 0.9. It can be seen that a hot region in the center of the cylinder persists much longer in the experiment than in the calculation, showing the large errors that can arise when a gradient heat transport approximation is used.

The phenomenon of countergradient transport in single-phase flows was recognized seven years ago in research on the structure of turbulent premixed flames.[1] In retrospect, it is easy to see how this phenomenon arises. Figure 3 depicts schematically a planar turbulent premixed flame with velocities shown in the frame of reference of the flame. Mass conservation and the fact that the combustion is nearly isobaric together imply that the hot product gas velocities will be larger than those in the reactants. Momentum conservation then implies that the pressure in the products will be lower than in the reactants. Since the directed heat flux is in the direction opposed to the pressure gradient, this heat flux will be from the colder to the hotter gases; that is, it will be countergradient transport.

Two approaches have been used for modeling turbulent premixed flames -- a single-phase formulation and a two-phase formulation. In the single-phase formulation of Bray, Moss, and Libby[1,9-11] (BML formulation), equations are kept for the mean product gas concentration, the mean momentum, the turbulent fluxes of these quantities, and for the dissipation rate of turbulent kinetic energy.
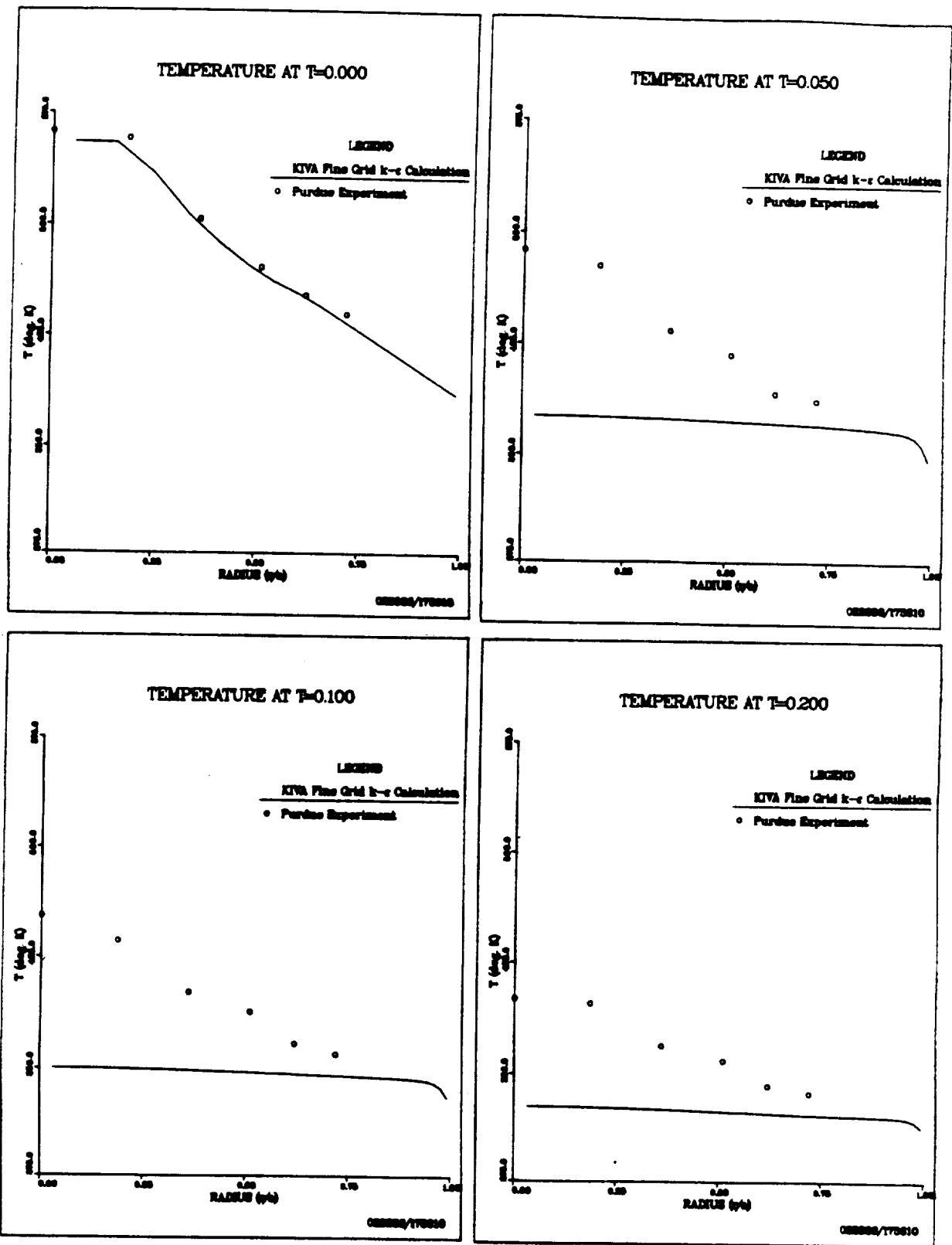
Fig. 2. Experimentally measured (Ref. 6) and computed (KIVA code) radial
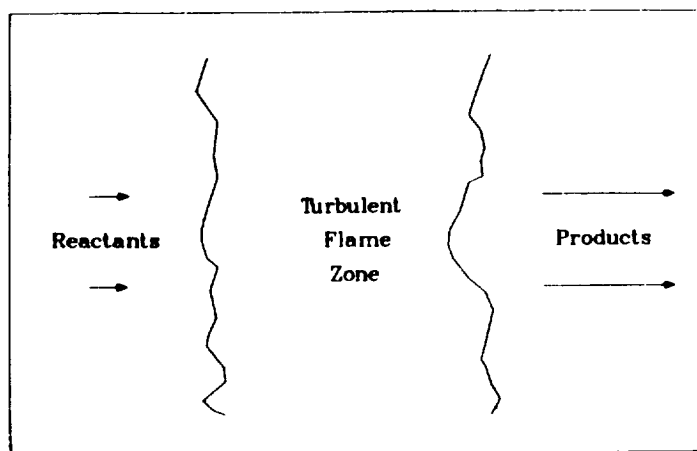temperature profiles at four different times.

Fig. 3. Schematic depiction of a turbulent premixed flame.

Spalding[12] utilizes a two-phase formulation, retaining mass, momentum, and energy equations for each phase. Spalding[12] assumes that the major source of mixing is due to the difference between the mean velocity of the phases and thus ignores the turbulent kinetic energy within each phase. The BML formulation accounts for both sources to the turbulent kinetic energy. In principle, the equations of one formulation should be derivable in terms of those of the other, although to our knowledge such a derivation and comparison have not been made. In this paper some closure approximations are proposed, based on a derivation of the single-phase equations from two-phase equations. Only the BML formulation has been compared with experimental measurements of turbulent flames,[11] and satisfactory agreement was obtained.

In practical applications of turbulent combustion, other physical effects that cause mixing and unmixing are superimposed on the pressure drop across the flame. At Los Alamos, we have been involved for the past twelve years in the numerical modeling of combustion in internal combustion engines.[7,13-16] Figure 4 illustrates some of the complexities of the turbulence/chemistry interaction in an engine burning premixed charges. A turbulent premixed flame is propagating away from an ignitor located near the center of the cylinder head wall. Mach numbers are small, and thus the mean pressure is nearly uniform in space[17] and changing with time due to piston motion, combustion, and wall heat loss. Near the top of its motion, the piston, and the axial flow velocities in the combustion chamber, decelerate. This causes a small positive axial pressure gradient and induces Rayleigh-Taylor instability and mixing where the flame is propagating downward in the axial direction. This same pressure gradient will cause a differential axial acceleration of the hot products and cool reactants and promote Kelvin-Helmholtz instability where the flame is propagating radially. Swirl, a nearly symmetric rotational motion of the burning gases, is introduced by engine designers to promote mixing but will have two competing effects in the engine of Fig. 4. Swirl induced shears will enhance turbulence and mixing, but the radial pressure gradient caused by the swirl will, as in the experiments of Wahiduzzaman and Ferguson,[6] cause countergradient transport and suppress mixing. It is important to point out that among these various turbulence effects, only those associated with shear instability and mixing are accounted for in current engine models.

In predicting turbulence in internal combustion engines and other practical combustors, one cannot use two-phase models or single-phase equations for two density flows. This is because within the reactants and products there will be
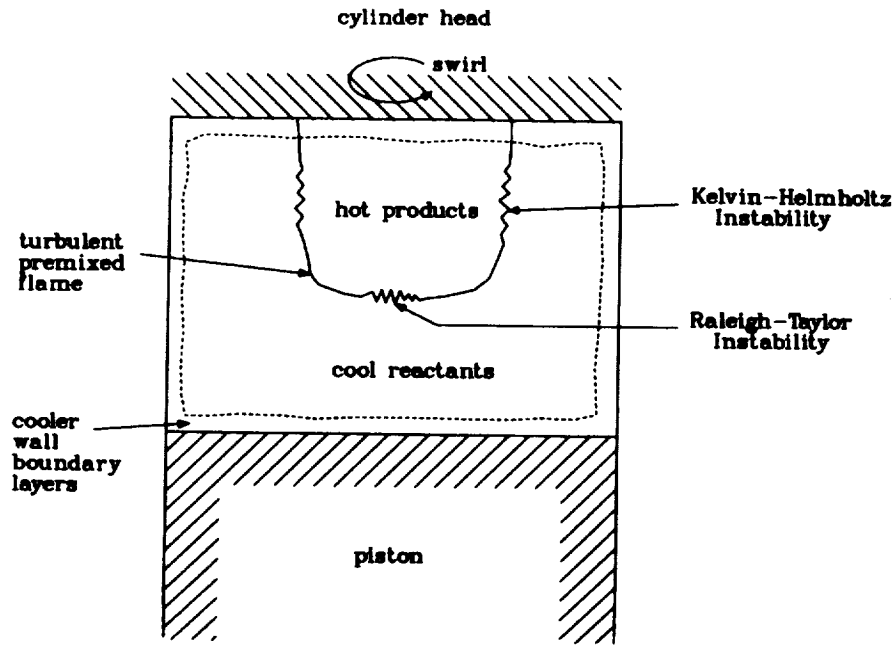
Fig. 4. The turbulence/chemistry interaction in an internal combustion engine.

distributions of density. In the engine of Fig. 4 density differences will arise due to wall heat transfer and due to entropy differences in the product gases of this confined burn.[18] In other combustors density distributions are caused by charge non-uniformity and spray vaporization.

In the next section we derive preliminary equations for a turbulent fluid with large density variations. Our aim is to develop a model that has three attributes:

(1) the model can predict mixing and unmixing due to shear instabilities and pressure-density gradient interactions;
(2) the model can account for a distribution of densities; and
(3) the model equations can be efficiently integrated in two and three dimensions.

The second attribute precludes use of two-phase flow equations, although investigation of the two-density limit will yield valuable information. The third attribute precludes use of the Reynolds stress equations, especially in three dimensions. It seems appropriate to seek a simple one- or two-equation extension of popular two-equation models for turbulent shear flows.

II. THE EQUATIONS

A. Overview

We first derive equations for the average density $\bar{\rho}$ and the Favre-averaged velocity $\tilde{u}$ and enthalpy $\tilde{h}$. Using the low Mach number assumption, we relate the turbulent heat flux ϕ^h to the difference between the average velocity $\bar{u}$ and the Favre-averaged velocity $\tilde{u}$. We denote this difference $\bar{u} - \tilde{u}$ by a, and the transport equation for a is derived and discussed. Closure approximations for terms in the a-equation are postulated based on the analogy between two-phase flows and single-phase, two-density flows. A comparison between the single-phase and two-phase equations suggests that the fluctuating stress terms in the a-equation are primarily associated with the decay of a. We present an algebraic

166

closure approximation for **a** that results in a heat flux that is the sum of contributions due to gradient and directed transport. Our **a**-equation is compared with similar equations in the literature.

B. The Equations of a Low Mach Number Flow with Large Density Variations

For the low Mach number flow of a single component ideal gas with large density variations, the equations are the following:[19]

$$\frac{\partial \rho}{\partial t} + \nabla \cdot (\rho \mathbf{u}) = 0 \ , \qquad (continuity) \qquad (1)$$

$$\frac{\partial \rho \mathbf{u}}{\partial t} + \nabla \cdot (\rho \mathbf{u} \mathbf{u}) + \nabla p = \nabla \cdot \boldsymbol{\sigma} + \rho \mathbf{g} \ , \qquad (momentum) \qquad (2)$$

$$\frac{\partial \rho h}{\partial t} + \nabla \cdot (\rho \mathbf{u} h) = \frac{dP}{dt} + Q \ , \qquad (enthalpy) \qquad (3)$$

$$P(t) M_w = \rho R T \ , \qquad (thermal\ equation\ of\ state) \qquad (4)$$

and

$$h(T) = \int^{T} c_p(\iota) d\iota \ , \qquad (caloric\ equation\ of\ state) \qquad (5)$$

where $\boldsymbol{\sigma}$ is the laminar viscous stress tensor, Q is the volumetric rate of heating due to such sources as chemical reaction or divergence of the laminar heat flux, $P(t)$ is the volume average pressure of the system, $p(\mathbf{x},t)$ is the pressure fluctuation from the mean value $P(t)$, and M_w is the molecular weight of the gas. For low Mach number flows $|p|/P \approx M^2$, where M is the Mach number.[17] From these equations one can derive an equation for the divergence of the velocity field:[19]

$$\nabla \cdot \mathbf{u} = -\frac{1}{\gamma P} \frac{dP}{dt} + \frac{\gamma - 1}{\gamma P} Q \ . \qquad (6)$$

In an open flow system, P is just the ambient pressure; for flow in a closed volume V, an equation for P can be derived by integrating (6) over V:

$$\frac{1}{\gamma P} \frac{dP}{dt} = -\frac{1}{V} \frac{dV}{dt} + \frac{\gamma - 1}{\gamma P} \frac{1}{V} \int_V Q \, dv \ . \qquad (7)$$

C. The Averaged Equations

In our turbulence equations we will use both unweighted averaged quantities and Favre (density-weighted) averaged quantities. The unweighted average and Favre average of a quantity ϕ are defined respectively by

$$\overline{\phi}(\mathbf{x}, t) = \frac{1}{NE} \sum_a \phi_a(\mathbf{x}, t) \qquad (8)$$

and

167

$$\tilde{\phi}(\mathbf{x}, t) = \frac{1}{\bar{\rho}(\mathbf{x}, t)} \frac{1}{NE} \sum_a \rho_a(\mathbf{x}, t) \phi_a(\mathbf{x}, t) \tag{9}$$

where ensemble averages are used, ϕ_a being the value of ϕ in a particular experiment a and NE being the number of experiments in the ensemble. The fluctuations from these averages are denoted by

$$\phi' = \phi_a - \bar{\phi} \tag{10}$$

and

$$\phi'' = \phi_a - \tilde{\phi} , \tag{11}$$

where we drop the subscript a on the fluctuations.

By averaging Eqs. (1)-(5) we obtain the turbulence equations:

$$\frac{\partial \bar{\rho}}{\partial t} + \nabla \cdot (\bar{\rho} \, \tilde{\mathbf{u}}) = 0 , \tag{12}$$

$$\frac{\partial \bar{\rho} \, \tilde{\mathbf{u}}}{\partial t} + \nabla \cdot (\bar{\rho} \, \tilde{\mathbf{u}}\tilde{\mathbf{u}}) + \nabla p = \nabla \cdot \mathbf{R} + \nabla \cdot \bar{\sigma} + \bar{\rho} \, \mathbf{g} , \tag{13}$$

$$\frac{\partial \bar{\rho} \, \tilde{h}}{\partial t} + \nabla \cdot (\bar{\rho} \, \tilde{h}\tilde{u}) = \frac{d \bar{P}}{dt} + \bar{Q} - \nabla \cdot \Phi^h , \tag{14}$$

$$\bar{P} \, M_w = \bar{\rho} R \tilde{T} , \tag{15}$$

and

$$\tilde{h} = \int^{\tilde{T}} c_p(\iota) \, d\iota , \tag{16}$$

where the Reynolds stress $\mathbf{R}$ is given by $- \overline{\rho u'' u''}$ and the turbulent heat flux Φ^h is given by $\overline{\rho u'' h''}$. In deriving Eq. (16) we have assumed that the characteristic temperatures over which significant changes in c_p occur, are much larger than characteristic temperature fluctuations T''.

D.   An Alternative Expression for Φ^h

An alternative expression for the turbulent heat flux can be derived from the averaged and unaveraged equations of state. Subtracting (15) from (4) results in

$$P' M_w = \rho RT - \bar{\rho} R \tilde{T} = \rho RT'' + \rho' R \tilde{T} . \tag{17}$$

We now assume that

$$|P'| / \bar{P} << |\rho'| / \bar{\rho} . \tag{18}$$

168

Under this assumption the left-hand side of (17) can be neglected, and we obtain

$$\tilde{T}'' = - T \frac{\rho'}{\rho} ,$$

(19)

wherein temperature and density fluctuations are directly related.

The assumption (18) requires some discussion. It will certainly be true for an open flow system, because the P is always the ambient pressure and never fluctuates. In a closed system, such as in internal combustion engine cylinder, there can be significant fluctuations in the mean pressure P, primarily due to fluctuations in the chemical heat release rate. In an internal combustion engine these are referred to as cycle-to-cycle variations, and there is currently some debate[20] whether or not these cycle-to-cycle variations should be called turbulence. We recommend that in performing the averages (8) and (9) one should use only experiments for which the mean pressure history $P(t)$ is nearly equal to $\tilde{P}(t)$. When this limited ensemble average is used, the assumption (18) is automatically satisfied.

Subtracting (16) from (5) gives

$$h'' = \int_{\tilde{T}}^{\tilde{T}+T''} c_p(\iota) \, d\iota = c_p(\tilde{T}) \, T'' ,$$

(20)

where again we use the assumption that c_p varies little for temperature changes equal to T''. Using (20) and (19) in the defining formula for ϕ^h gives

$$\phi^h = \overline{\rho u'' h''}$$

$$= -c_p(\tilde{T}) \, \tilde{T} \, \overline{\rho' u''}$$

$$= \overline{\rho} \, c_p(\tilde{T}) \, \tilde{T} \, \mathbf{a}$$

(21)

where

$$\mathbf{a} = \overline{\mathbf{u}''} = \overline{\mathbf{u}} - \tilde{\mathbf{u}} .$$

(22)

Equation (21) is the alternative expression we seek for the heat flux. It says that ϕ^h is proportional to a quantity a that can be loosely thought of as the difference between the volume-averaged and mass-averaged velocities. In a two-density or two-phase system, a is proportional to the difference between the velocities of the two phases. In order to investigate further the nature of the turbulent heat flux, we must derive a transport equation for a.

E. The Transport Equation for a

The transport equation for a is obtained by subtracting the equation for the mass-averaged velocity ũ from that for the volume-averaged velocity ū. The result is

$$\frac{\partial \mathbf{a}}{\partial t} + \overline{\mathbf{u} \cdot \nabla \mathbf{u}} - \tilde{\mathbf{u}} \cdot \nabla \tilde{\mathbf{u}} + \left(\frac{\overline{1}}{\rho} - \frac{1}{\tilde{\rho}}\right) \nabla \overline{p} + \frac{1}{\rho} \overline{\nabla p'}$$

$$= -\frac{1}{\tilde{\rho}} \nabla \cdot \mathbf{R} + \left(\frac{\overline{1}}{\rho} - \frac{1}{\tilde{\rho}}\right) \nabla \cdot \overline{\sigma} + \frac{1}{\rho} \overline{\nabla \cdot \sigma'} \ . \tag{23}$$

As an aid in modeling some of the terms in Eq. (23) we will derive an a-equation for two-phase flows and compare this with Eq. (23). It will turn out that all of the terms in Eq. (23), with the exception of those associated with the fluctuating stresses p' and σ', will be duplicated exactly by terms in the a-equation for two-phase flows. The terms $1/\rho \, \overline{\nabla p'}$ and $1/\rho \, \overline{\nabla \cdot \sigma'}$ are then associated with terms in the two-phase a-equation that arise due to momentum exchange between the phases. With this comparison as a guide we postulate a model for the fluctuating stress terms.

We now briefly introduce the equations for two-phase flow. For more details the interested reader should consult Refs. 2 and 3. For simplicity we restrict ourselves to the flow of two incompressible phases. The continuity equations for each phase are

$$\frac{\partial \rho_1 \alpha_1}{\partial t} + \nabla \cdot (\rho_1 \alpha_1 \overline{\mathbf{u}}^1) = J_{21} \tag{24}$$

and

$$\frac{\partial \rho_2 \alpha_2}{\partial t} + \nabla \cdot (\rho_2 \alpha_2 \overline{\mathbf{u}}^2) = J_{12} = -J_{21} \ . \tag{25}$$

In these equations ρ_i are the microscopic (or conditional) densities, which we assume to be constant; $\overline{\mathbf{u}}^i$ are the average velocities within each phase (where the "i" next to the overbar indicates a conditional average in phase i); a_i are the volume fractions of each phase ($a_1 + a_2 = 1$); and J_{21} is the rate of mass transfer per unit volume from phase 2 to phase 1. The momentum equations for each phase are

$$\frac{\partial \rho_1 \alpha_1 \overline{\mathbf{u}}^1}{\partial t} + \nabla \cdot (\rho_1 \alpha_1 \overline{\mathbf{u}}^1 \overline{\mathbf{u}}^1) + \alpha_1 \nabla \overline{p} = \rho_1 \alpha_1 \mathbf{g} + \alpha_1 \nabla \cdot \overline{\sigma} + \nabla \cdot (\alpha_1 \mathbf{R}_1) + \mathbf{P}_{21} \tag{26}$$

and

$$\frac{\partial \rho_2 \alpha_2 \overline{\mathbf{u}}^2}{\partial t} + \nabla \cdot (\rho_2 \alpha_2 \overline{\mathbf{u}}^2 \overline{\mathbf{u}}^2) + \alpha_2 \nabla \overline{p} = \rho_2 \alpha_2 \mathbf{g} + \alpha_2 \nabla \cdot \overline{\sigma} + \nabla \cdot (\alpha_2 \mathbf{R}_2) - \mathbf{P}_{21} \ . \tag{27}$$

As is commonly done in two-phase flow modeling,[2] we assume here that the phases are in local pressure equilibrium; that is $\overline{p}^1 = \overline{p}^2 = \overline{p}$. The conditional Reynolds stresses $\mathbf{R}_i$ are given by

$$R_i = -\rho_i \overline{(u - \overline{u}^i)(u - \overline{u}^i)}^i .$$

The rate of momentum exchange per unit volume from phase 2 to phase 1 is denoted by P_{21}.

Average flow variables $\bar{f}$ are related to the averages within each phase $\bar{f}^i$ by

$$\bar{f} = a_1\bar{f}^1 + a_2\bar{f}^2 . \tag{28}$$

Thus, for example,

$$\bar{\rho} = a_1\rho_1 + a_2\rho_2 \tag{29}$$

and

$$\bar{\rho}\,\tilde{u} = a_1\rho_1\overline{u}^1 + a_2\rho_2\overline{u}^2 .$$

By using the relations (29) and adding Eqs. (24) and (25) and Eqs. (26) and (27) we obtain the same total mass and momentum equations, Eqs. (12) and (13), that we have previously derived, when it is realized that

$$R = a_1R_1 + a_2R_2$$

$$- \rho_1 a_1 (\overline{u}^1 - \tilde{u})(\overline{u}^1 - \tilde{u})$$

$$- \rho_2 a_2 (\overline{u}^2 - \tilde{u})(\overline{u}^2 - \tilde{u}) . \tag{30}$$

Thus the mass-averaged velocity equation is

$$\frac{\partial u}{\partial t} + \tilde{u}\cdot\nabla\tilde{u} + \frac{1}{\bar{\rho}}\nabla\bar{p} = \frac{1}{\bar{\rho}}\nabla\cdot\bar{\sigma} + \frac{1}{\bar{\rho}}\nabla\cdot R + g . \tag{31}$$

To obtain the a-equation, we will subtract (31) from an equation for $\bar{u}$, which will now be derived. By dividing (26) by ρ_1 and (27) by ρ_2 and summing the results, we obtain

$$\frac{\partial \bar{u}}{\partial t} + \nabla\cdot(a_1\overline{u}^1\overline{u}^1 + a_2\overline{u}^2\overline{u}^2) + \left(\frac{1}{\bar{\rho}}\right)\nabla\bar{p}$$

$$= g + \left(\frac{1}{\bar{\rho}}\right)\nabla\cdot\bar{\sigma} + \nabla\cdot\left(\frac{a_1}{\rho_1}R_1 + \frac{a_2}{\rho_2}R_2\right) + P_{21}\left(\frac{1}{\rho_1} - \frac{1}{\rho_2}\right) . \tag{32}$$

It can be seen that

$$\nabla \cdot \left| a_1 \overline{u}^{-1}\overline{u}^{-1} + a_2 \overline{u}^{-2}\overline{u}^{-2} - \frac{a_1}{\rho_1} \mathbf{R}_1 - \frac{a_2}{\rho_2} \mathbf{R}_2 \right| = \nabla \cdot (\overline{uu}) = \overline{u \cdot \nabla u} + \overline{u\nabla \cdot u} \ . \tag{33}$$

Using (33) in (32) and subtracting (31) yields the two-phase a-equation:

$$\frac{\partial a}{\partial t} + \overline{u \cdot \nabla u} - \overline{\tilde{u} \cdot \nabla \tilde{u}} + \overline{u\nabla \cdot u} + \left(\frac{\overline{1}}{\rho} - \frac{1}{=} \right) \nabla \overline{p}$$

$$= -\frac{1}{=} \nabla \cdot \mathbf{R} + \left(\frac{\overline{1}}{\rho} - \frac{1}{=} \right) \nabla \cdot \overline{\sigma} + \mathbf{P}_{21} \left(\frac{1}{\rho_1} - \frac{1}{\rho_2} \right). \tag{34}$$

Comparing (34) and (23), we see they agree __if__

$$\overline{\frac{1}{\rho} \nabla p'} - \frac{1}{\rho} \overline{\nabla \cdot \sigma'} = \overline{u\nabla \cdot u} + \mathbf{P}_{21} \left(\frac{1}{\rho_2} - \frac{1}{\rho_1} \right). \tag{35}$$

This is the relationship we seek between the fluctuating stress terms and the two-phase momentum transfer terms. To obtain closure we need to postulate a form for $\mathbf{P}_{21}$, and we will investigate expressions employed in two-phase flow modeling.

F.   Expressions for the Momentum Exchange Rate in Two-Phase Flows

For a dispersed phase 2 of equal-sized spherical particles of radius r in a continuous phase 1, an expression for the momentum transfer term is[21]

$$\mathbf{P}_{21} = \frac{3}{8} c_D \frac{\rho_1 a_2}{r} |\overline{u}^2 - \overline{u}^1|(\overline{u}^2 - \overline{u}^1) + J_{21}\overline{u}^2 \ . \tag{36}$$

Thus, $\mathbf{P}_{21}$ has two terms -- one due to aerodynamic drag and one due to mass exchange. This form of the mass exchange term assumes there are no circulation velocities within the particles. Equation (36) has theoretical justification[21] when $\rho_2 >> \rho_1$ and velocities within each phase are sharply peaked near their mean values. It neglects virtual mass effects, Basset history effects, and particle distortions and oscillations.[22]

Motivated by Eq. (36), modelers usually use a similar expression for all two-phase regimes:[2]

$$\mathbf{P}_{21} = K(\overline{u}^2 - \overline{u}^1) + J_{21}\overline{u}^s \tag{37}$$

where K is called the drag function and $\overline{u}^s$ is some average interface velocity. The quantity K is a positive function of $\rho_1, \rho_2, a_1, a_2, |\overline{u}^2 - \overline{u}^1|$, and an entity size r.

If we accept Eq. (37) then one is led to the postulate that the fluctuating stress terms in the a-equation (23) contribute to the decay of $\mathbf{a}$. Indeed one can show that for a two-phase flow

$$\mathbf{a} = \frac{a_1 a_2 (\rho_1 - \rho_2)}{\overline{\rho}} (\overline{u}^2 - \overline{u}^1), \tag{38}$$

and (38), in conjunction with (35) and (37), gives

$$\frac{1}{\rho}\,\boldsymbol{\nabla}\,p' - \frac{1}{\rho}\,\boldsymbol{\nabla}\cdot\boldsymbol{\sigma}' = \overline{\mathbf{u}\boldsymbol{\nabla}\cdot\mathbf{u}} + K'\mathbf{a} + J_{21}\!\left(\frac{1}{\rho_2} - \frac{1}{\rho_1}\right)\!\overline{\mathbf{u}}^{\,s}\,,\tag{39}$$

where

$$K' = \frac{\overline{\rho}}{a_1 a_2 \rho_1 \rho_2}\,K\;.$$

K' has dimensions of a frequency.

G. Final Form of the a-Equation

After substituting (39) in (23) and some rearrangement of terms one obtains

$$\frac{\partial \mathbf{a}}{\partial t} + \boldsymbol{\nabla}\cdot(\tilde{\mathbf{u}}\mathbf{a} + \mathbf{a}\tilde{\mathbf{u}}) + K'\mathbf{a} + J_{21}\!\left(\frac{1}{\rho_2} - \frac{1}{\rho_1}\right)\!\overline{\mathbf{u}}^{\,s} + \tilde{\mathbf{u}}\boldsymbol{\nabla}\cdot\tilde{\mathbf{u}} + \frac{b}{\rho}\,\boldsymbol{\nabla}\,\overline{p}$$

$$= -\frac{1}{\rho}\,\boldsymbol{\nabla}\cdot\mathbf{R} - \boldsymbol{\nabla}\cdot(\overline{\mathbf{u}''\mathbf{u}''}) = \frac{1}{\rho}\,\overline{\mathbf{u}''\mathbf{u}''}\cdot\boldsymbol{\nabla}\,\overline{\rho} + \frac{1}{\rho}\,\boldsymbol{\nabla}\cdot(\overline{\rho'\mathbf{u}''\mathbf{u}''})\;.\tag{40}$$

Here we have introduced the quantity b as a dimensionless measure of the density fluctuations:

$$b = \overline{\rho}\left(\overline{\frac{1}{\rho}}\right) - 1\;.\tag{41}$$

If the density fluctuations are not too large, then b is approximately a self-correlation coefficient for density fluctuations:

$$b \approx \frac{\overline{(\rho')^2}}{(\overline{\rho})^2}\;.\tag{42}$$

In fact, Ref. 4 uses

$$B = \overline{(\rho')^2}\tag{43}$$

as a measure of the density fluctuations. We will develop a transport equation for b in future work.

Three further terms in (40) must be modeled. First we deal with the mass exchange term. One can show from (24) and (25) that

$$\boldsymbol{\nabla}\cdot\overline{\mathbf{u}} = J_{21}\!\left(\frac{1}{\rho_1} - \frac{1}{\rho_2}\right)\tag{44}$$

and hence the fourth and fifth terms on the left-hand side of (40) combine to give

$$\tilde{u}\nabla \cdot \tilde{u} + J_{21}\left(\frac{1}{\rho_2} - \frac{1}{\rho_1}\right)\overline{u}^s = J_{21}\left(\frac{1}{\rho_2} - \frac{1}{\rho_1}\right)(\overline{u}^s - \tilde{u}) - \tilde{u}\nabla \cdot a . \tag{45}$$

We assume that $\bar{u}^s = \tilde{u}$. An assessment of the validity of this assumption must await a precise physical interpretation of the quantity $\bar{u}^s$.

Second, for the tensor $\overline{u''u''}$ one can show that for two-phase flows

$$\overline{u''u''} = -a_1 \frac{R_1}{\rho_1} - a_2 \frac{R_2}{\rho_2} + \left(1 + \frac{(\bar{\rho})^2}{B}\right)aa , \tag{46}$$

where B is defined by (43) and given in two-phase flows by

$$B = a_1 a_2 (\rho_1 - \rho_2)^2 . \tag{47a}$$

For future reference we also note that

$$b = \frac{B}{\rho_1 \rho_2} \tag{47b}$$

in two-phase flows. We define the volume-averaged conditional Reynolds stress r by

$$r = a_1 \frac{R_1}{\rho_1} + a_2 \frac{R_2}{\rho_2} . \tag{48}$$

As a first approximation, and despite experimental evidence to the contrary in turbulent flame experiments,[9] we assume the conditional Reynolds stresses are equal and isotropic. Then

$$\frac{R_1}{\rho_1} = \frac{R_2}{\rho_2} = r = -\frac{2}{3} k'1 \tag{49}$$

where k' is related to the specific turbulent kinetic energy $\tilde{k} = \frac{1}{2}(\tilde{u}'')^2$ by

$$\tilde{k} = k' + \frac{1}{2}\frac{a^2}{b} . \tag{50}$$

A transport equation for $\tilde{k}$ will be developed in future work.

We also use a two-density distribution to model the triple correlation term in Eq. (40). After some algebraic manipulation and use of the assumption (49) one obtains

$$\overline{\rho'u''u''} = -\bar{\rho}\left(1 - \frac{1}{b} + \frac{\bar{\rho}^2}{B}\right)aa . \tag{51}$$

By substituting (45), (46), (49), and (51) in (40) and using the approximation (42) we obtain the final form of the a-equation:

$$\frac{\partial \mathbf{a}}{\partial t} + \tilde{\mathbf{u}} \cdot \nabla \mathbf{a} + \mathbf{a}\nabla \cdot \tilde{\mathbf{u}} + \mathbf{a} \cdot \nabla \tilde{\mathbf{u}} + \nabla \cdot (\mathbf{a}\mathbf{a}) + \frac{b}{\rho} \nabla \bar{p}$$

$$= - K'\mathbf{a} + \frac{\mathbf{a}\mathbf{a}}{b} \cdot \frac{\nabla \bar{\rho}}{\bar{\rho}} + \frac{2}{3}\left(k - \frac{1}{2}\frac{\mathbf{a}^2}{b} \right) \frac{\nabla \bar{\rho}}{\bar{\rho}} . \tag{52}$$

H. An Algebraic Closure Approximation

In numerical computations of multidimensional fluid flows, use of Eq. (52) would require solving two or three additional transport equations for components of **a**. Although this is not an unrealistic task for modern computers, considerable computational efficiency would result if an accurate algebraic closure approximation for **a** could be found. In this section we present such an approximation based on an assumption whose validity must be tested in experimental comparisons. The resulting expression for **a** predicts gradient heat transport, but also contains a contribution that predicts the directed flux arising from the interaction of pressure gradients and density inhomogeneities.

The assumption we make is analogous to the drift flux approximation of two-phase flow modeling.[2] In two-phase modeling this assumption is that the two velocity fields are so tightly coupled through the drag terms that characteristic drag times are much smaller than characteristic flow times. For us the assumption is that

$$K' >> \frac{u_o}{L} , \tag{53}$$

where u_o and L are a characteristic velocity and gradient length for the flow.

Assuming (53) is true, order of magnitude estimates of the terms in (52) show all terms on the left-hand side can be neglected, except the pressure gradient term. On the right-hand side, the dyadic product term **aa** is negligible since Eqs. (38) and (47) show that $\mathbf{a}/b$ is proportional to the velocity difference between fluid elements of different density. The resulting equation for **a** becomes

$$\mathbf{a} = \frac{1}{K'}\left[- \frac{b}{\rho} \nabla \bar{p} + \frac{2}{3}k \cdot \frac{\nabla \bar{\rho}}{\bar{\rho}} \right] . \tag{54}$$

Equation (54) can be put in a more recognizable form if we use

$$\frac{\nabla \bar{\rho}}{\bar{\rho}} = - \frac{\nabla \tilde{T}}{\tilde{T}} :$$

$$\mathbf{a} = \frac{1}{K'}\left[- \frac{b}{\rho} \nabla \bar{p} - \frac{2}{3}k \frac{\nabla \tilde{T}}{\tilde{T}} \right] . \tag{55}$$

In conjunction with (21), Eq. (55) gives a heat flux that is the sum of contributions proportional to $-\nabla \bar{p}$ and $-\nabla T$. The former is the directed flux. It goes to zero in the absence of density fluctuations b.

175

The gradient transport term in (55) looks similar to the gradient heat flux commonly used in turbulence modeling, but there is a difference. The usual form used for the turbulent heat flux[8] is

$$\Phi^h = - \bar{\rho} \, c_p \, \frac{\tilde{k}^2}{Pr_{_T}\tilde{\varepsilon}} \, \nabla \tilde{T}$$

(56)

where $Pr_{_T}$ is the turbulent Prandtl number and $\tilde{\varepsilon}$ the turbulence dissipation rate. Equation (56) agrees with the heat flux contribution obtained from the second term in (55) if the drag time associated with fluid elements of differing density equals the turbulence dissipation time. For the momentum exchange function (36) it can be seen that the drag time is

$$\frac{1}{K'} \approx \frac{\rho_2}{\rho_1} \frac{r}{|\bar{u}^1 - \bar{u}^2|}$$

(57)

when c_D is approximately unity. On the other hand, the turbulence dissipation time is

$$\frac{\tilde{k}}{\tilde{\varepsilon}} \approx \frac{L}{\tilde{k}^{\frac{1}{2}}} \, ,$$

(58)

where L is a turbulence length scale. Equations (57) and (58) agree if $r \approx L$, $\tilde{k}^{\frac{1}{2}} \approx |\bar{u}^1 - \bar{u}^2|$ and $\rho_1 \approx \rho_2$, but when these equalities are violated more accurate heat fluxes could be obtained using a drag time, and not a turbulence dissipation time, to evaluate the heat flux vector.

III. COMPARISON WITH OTHER WORK

In this section we compare our a-equation with two others in the literature. In the BML formulation for turbulent flames,[10] an equation is kept for the turbulent flux of reaction progress variable c. Our quantity a is just a constant times the turbulent flux of c:

$$\overline{\rho u''c''} = \frac{\rho_r \rho_p}{\rho_r - \rho_p} \, \mathbf{a} \, ,$$

(59)

where ρ_r and ρ_p are the reactant and product densities. Two differences are observed between the a-equation one derives from the BML formulation and ours. First, in the BML formulation it is not assumed that the conditional Reynolds stresses within each phase are equal and isotropic. An equation for the unconditional Reynolds stress R is retained, and the difference between the conditional Reynolds stresses is modeled using R. Accordingly, the double and triple correlation terms on the right-hand side of (40) are modeled in a more detailed fashion, although the authors observe[10] that "this modeling is generally not found to be too critical to the predictions of first- and second-moment unconditional quantities."

The second difference is in the modeling of the fluctuating stress terms. The authors follow Launder[23] and model

$$\overline{\frac{1}{\rho}\frac{\partial p'}{\partial x}} = 2c_{1_c}\frac{\tilde{\varepsilon}}{\tilde{k}}\mathbf{a} - c_{2_c}\mathbf{a}\cdot\nabla\mathbf{u} \tag{60}$$

where c_{1_c} and c_{2_c} are empirical constants. Comparison with Eq. (39) shows that these models have in common the decay of **a** term and that these would be the same if

$$K' = 2c_{1_c}\frac{\tilde{\varepsilon}}{\tilde{k}} \ . \tag{61}$$

Besnard, Harlow, and Rauenzahn[4] keep equations for both the turbulent heat flux and the quantity $\mathbf{A} = \overline{\rho'\mathbf{u}'}$, which is related to **a** by

$$\mathbf{A} = -\,\bar{\rho}\,\mathbf{a}\ , \tag{62}$$

since they are interested in more complicated equations of state in which the relation (19) does not hold. Their a-equation differs from ours in several respects. An equation for the Reynolds stress is retained and used in modeling the first term on the right-hand side of (40). The triple correlation is broken into two terms

$$\overline{\rho'\mathbf{u}''\mathbf{u}''} = -2\,\bar{\rho}\,\mathbf{aa} + \overline{\rho'\mathbf{u}'\mathbf{u}'}\ , \tag{63}$$

and the latter term is modeled by a gradient diffusion of **a**. There is a decay of **a** that arises solely from the viscous stress terms.

IV. SUMMARY AND FUTURE WORK

We have derived a transport equation for the quantity **a**, which is the difference between the volume- and mass-averaged velocities and is simply related to the turbulent heat flux ϕ^h. Using this equation and an assumption analogous to the drift flux approximation of two-phase flow modeling, we have obtained an algebraic closure relation for ϕ^h that exhibits fluxes due to directed transport proportional to $-\nabla\bar{p}$ and due to gradient transport proportional to $-\nabla T$.

Much work remains to be done before the model can be used in predictive calculations of low Mach number flows with large density variations. The equation for **a** involves an additional scalar b that is a measure of the density fluctuations. An equation for b must be derived and terms in it modeled. We hope to use the a - and b-equations in conjunction with a k - ε turbulence model. The k- and ε-equations must be reexamined to see what modifications are needed when the flows have large density variations. When mass transport is important, such as in many combustion problems, expressions for the turbulent mass flux must be developed.

In an effort to test some of the modeling assumptions we are currently writing a one-dimensional code that solves the turbulence equations of this paper. Computed results will be compared with experimental measurements of Rayleigh-Taylor instability, turbulent premixed flames, and flows with centrifuging and density variations. These results and extensions of the model will be reported in future publications.

177

REFERENCES

1. Libby, P. A. and Bray, K. N. C., *AIAA J.* 19, 205 (1981).

2. Stewart, H. B. and Wendroff, B., *J. Comput. Phys.* 56, 3, 363 (1984).

3. Anderson, T. B. and Jackson, R., *I and EC Fundamentals* 6, 4, 527 (1967).

4. Besnard, D., Harlow, F. H., and Rauenzahn, R., "Conservation and Transport Properties of Turbulence with Large Density Variations," Los Alamos National Laboratory report LA-10911-MS (1987).

5. Cook, T. L. and Harlow, F. H., *Int. J. Multiphase Flow* 12, 1, 35 (1986).

6. Wahiduzzaman, S. and Ferguson, C. R., Eight International Heat Transfer Conference, Paper # 86-IHTC-253, August 1986.

7. Amsden, A. A., et al., "KIVA: A Computer Program for Two- and Three-Dimensional Fluid Flows with Chemical Reactions and Fuel Sprays," Los Alamos National Laboratory report LA-10245-MS (1985).

8. Launder, B. E. and Spalding, D. B., *Computer Methods in Applied Mechanics and Engineering* 3, 269 (1974).

9. Bray, K. N. C., et al., *Combustion Science and Technology* 25, 127 (1981).

10. Bray, K. N. C., Libby, P. A., and Moss, J. B., *Combustion and Flame* 61, 87 (1985).

11. Libby, P. A., *Prog. Energy Combust. Sci.* 11, 83 (1985).

12. Spalding, D. B., Oral presentation to the Conference on Combustion and Nonlinear Phenomena, Les Houches, France (1985).

13. Rivard, W. C., Farmer, O. A., and Butler, T. D., "RICE: A Computer Program for Multicomponent Chemically Reactive Flows at All Speeds," Los Alamos Scientific Laboratory report LA-5812 (1975).

14. Butler, T. D. et al., "CONCHAS: An Arbitrary Lagrangian-Eulerian Computer Code for Multicomponent Chemically Reactive Fluid Flow at All Speeds," Los Alamos Scientific Laboratory report LA-8129-MS (1979).

15. Butler, T. D. et al., *Prog. Energy Combust. Sci.* 7, 293 (1981).

16. Cloutman, L. D. et al., "CONCHAS-SPRAY: A Computer code for Reactive Flows with Fuel Sprays," Los Alamos National Laboratory report LA-9294-MS (1982).

17. Williams, F. A., *Combustion Theory*, (Benjamin/Cummings Publishing Co., Menlo Park, California, 1985).

18. Bracco, F. V., "Modeling of Two-Phase, Two-Dimensional, Unsteady Combustion in Internal Combustion Engines," Institution of Mechanical Engineers Conference on Stratified Charge Engines, London (1976).

19. O'Rourke, P. J., "The Acoustic Mode in Numerical Calculations of Subsonic Combustion," in *Combustion and Nonlinear Phenomena*, ed. P. Clavin, B. Larrouturou, and P. Pelce (Les Editions de Physique, Les Ulis, France, 1985).

20. Fraser, R. A. and Bracco, F. V., "Cycle-Resolved LDV Integral Length Scale Measurements in an I.C. Engine," SAE paper 880381 (1988).

21. O'Rourke, P.J., "Collective Drop Effects on Vaporizing Liquid Sprays," Los Alamos National Laboratory report LA-9069-T (1981).

22. Clift, R., Grace, J. R., and Weber, M. E., *Bubbles, Drops, and Particles* (Academic Press, New York, 1978).

23. Bradshaw, P. (ed.), *Turbulence*, Topics in Applied Physics Vol. 12 (Springer-Verlag, Berlin, 1976).

MODELING OF COMBUSTION PROCESSES OF STICK PROPELLANTS
VIA COMBINED EULERIAN-LAGRANGIAN APPROACH.

K. K. Kuo, K. C. Hsieh, M. M. Athavale
Department of Mechanical Engineering
The Pennsylvania State University
University Park, Pennsylvania

This research is motivated by the improved ballistic performance of large-caliber guns using stick propellant charges. A comprehensive theoretical model for predicting the flame-spreading, combustion , and grain deformation phenomena of long unslotted stick propellants is presented. The formulation is based upon a combined Eulerian-Lagrangian approach to simulate special characteristics of the two-phase combustion processes in a cartridge loaded with a bundle of sticks. The model considers five separate regions consisting of the internal perforation, the solid phase , the external interstitial gas phase, and two lumped parameter regions at either end of the stick bundle. For the external gas-phase region, a set of transient one-dimensional fluid-dynamic equations using the Eulerian approach is obtained; governing equations for the stick propellants are formulated using the Lagrangian approach. The motion of a representative stick is derived by considering the forces acting on the entire propellant stick. The instantaneous temperature and stress fields in the stick propellant are modeled by considering the transient axisymmetric heat-conduction equation and dynamic structural analysis. For the internal perforation region, a set of one-dimensional transient fluid-dynamic equations is formulated with a coordinate system attached to the moving stick. Major distinctions between the present and the conventional formulations for interior ballistic simulation are delineated.

I. Introduction

Recently, there has been an increasing interest in the use of stick propellant charges in large-caliber gun systems. Stick propellants offer many advantages over conventional randomly packed multi-perforated granular propellant charges. The regular geometry of stick propellants allows a higher loading density, flexibility in charge design, and easier charge loading. The higher charge density is preferable for low vulnerability ammunition (LOVA) propellants, which require a higher propellant mass to produce an equivalent performance. It has been observed by Robbins et al. (1,2) that flow resistance through the charge of a stick propellant bundle is lower than that through packed beds of granular propellants, thus enabling faster and more reproducible flame spreading through the stick propellant charge. The lower flow resistance also reduces considerably the phenomena of high pressure gradients and severe pressure waves in the gun tube, as indicated by Minor (3).

A number of studies (1-10) on various aspects of stick propellant combustion have been reported to date. The NOVA code, developed by Gough (11,12) for ballistic performance of granular charges, was used with some modifications (1,4) to predict the performance of a stick propellant charge. Results obtained were in good agreement with experimental data for multiperforated granular NACO propellants and single-perforated slotted stick bundles (1). However, the same is not true for the case of single-perforated, unslotted stick propellants.

The structure mechanics consideration in the continuum modeling of unslotted stick charge combustion of the modified NOVA code (4) is rather crude, due to the application of a steady-state relationship between radial and hoop stresses and internal and external pressures. Although pressure distributions in the internal perforation were calculated, only the external pressure was used in evaluating the axial stress component, which is in turn related to the intra-granular stress. Grain deformation and fracture of unslotted long sticks are mainly due to the radial expansion and attainment of a critical hoop stress.

Rupture of stick propellants during combustion in a gun barrel was observed by Robbins and Horst (2). Grain fracture can lead to high peak pressures due to increase in total burning surface area. The pressure difference across the web of a stick propellant can cause the grain to deform prior to fracture and alter the flow-channel width and the distance between opposite burning surfaces, thereby changing the combustion process. Hence, the prediction of grain deformation and rupture should be given due importance in the overall interior ballistic cycle.

The proposed model is based on a relatively new method, previously applied to two-phase reacting flow problems such as spray combustion of liquid droplets (14). In the separated-flow approach, the continuous phase (gas phase) is treated by a Eulerian approach, while the condensed phase media (stick propellants) are divided into several representative groups and tracked, using a Lagrangian approach, as they move in the continuous phase. The interstitial gas-phase region in the present problem is treated in a similar fashion to the continuous phase in spray combustion, while the internal gas-phase regions in the grain perforations are treated separately. The flame-spreading and combustion phenomena inside the perforation are similar to those in a cylindrical side-burning rocket motor grain. The ignition transient analysis developed by Peretz et al. (15) is therefore adapted to model the flame spreading and combustion processes in the perforation. This two-phase separated flow approach is convenient because the

stick propellants have identical dimensions and
symmetry about their own axes as well as a central
axis. The number of representative sticks in a
stick propellant bundle is relatively low, there-
fore making it possible to study some of the
detailed flow and combustion phenomena of these
representative stick propellant grains.

All of the gun interior ballistic codes and
analyses developed so far do not consider the dis-
tribution of chemical species (16-18). The heat
release is assumed to occur at the same location as
that of pyrolysis of the propellant. However, for
LOVA or other types of modern propellants, some
chemical species could be pyrolyzed from the pro-
pellant surface, be carried by the flow during the
ignition transient interval, and then react at some
downstream location. Therefore, in general, the
heat release could occur at a different position
than the site of initial pyrolysis. These complic-
ated phenomena, which were simplified in previous
analyses, are included in the present model.

Objectives of the current research are to for-
mulate a combined Eulerian-Lagrangian model for the
combustion of a bundle of stick propellants inside
a gun chamber. It is intended to cover many as-
pects of realistic simulation of stick propellant
combustion characteristics so that the model is ca-
pable of predicting the phenomena of ignition,
flame spreading, and combustion of stick propel-
lants. Development of the model is also intended
to help explain the experimental observations from
test firings being conducted by the authors in a
simulated gun system. The data to be obtained will
be used for model validation.

II. Method of Approach

1. Physical Model

Figure 1 shows a bundle of stick propellants
loaded in the combustion chamber of a gun. For the
present model, only unslotted long stick propellant
grains are considered. In the theoretical formul-
ation, the combustion chamber is divided into five
separate regions: 1) lumped parameter region near
the base pad; 2) internal perforation region; 3)
external interstitial gas-phase region; 4) solid
propellant region; and 5) lumped parameter region
near the base of the projectile. Although the
solid propellant region consists of many stick pro-
pellants, only a few representative sticks are
required to be modeled due to the similarity of the
sticks in the same family. Each region has a sep-
arate set of governing equations which are coupled
through various boundary conditions. The erosive
burning of the stick propellants under cross-flow
conditions is also taken into account. Since frac-
ture phenomena of stick propellants under dynamic
loading conditions are under investigation, the
present model is limited to the time period before
one or more stick propellants rupture as a result
of high pressure differential across the web of the
stick propellant. After the onset of rupture, a
stick propellant could become partially slotted,
broken, and/or highly deformed. It is then diffi-
cult to distinguish the internal versus external
surface. These phenomena are beyond the scope of
the present model.

2. Mathematical Formulation

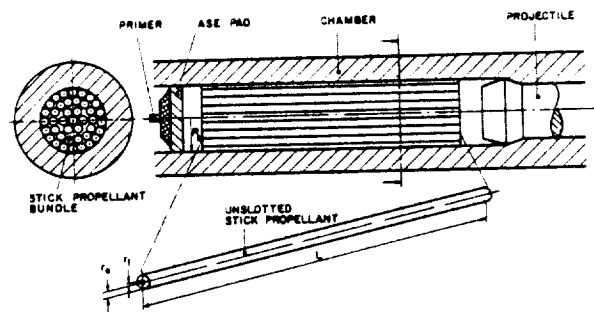#### A. Basic Assumptions:

Fig.1 Stick propellant Charge in a Cartridge
of a Large Caliber Gun.

(1) All the stick propellants have the same
initial geometry and physical conditions. Further-
more, it is possible to divide the stick bundle
into a few families so that the calculations can be
performed for only a few representative sticks. To
simplify the mathematical formulation, the combus-
tion of sticks in a bundle is represented by a
single stick. The mathematical format can be read-
ily extended to multiple families of sticks.

(2) Assumptions used in the gas-phase regions
are:

a. no body forces;
b. bulk viscosity μ' is negligible;
c. Soret and Dufour effects are negligi-
ble;
d. gases obey Noble-Abel equation of
state;
e. all binary diffusion coefficients are
equal;
f. Fick's law of diffusion is valid;
g. flow is one-dimensional transient
(properties are uniform in r and θ di-
rections);
h. total flow area in the external gas-
phase region is assumed to be $\phi_e A$
[Dupuit Forchheimer hypothesis (19)];
and
i. turbulence correlations of flow proper-
ties in the axial direction are consid-
ered negligible in comparison with the
product of their mean flow properties.
However, turbulence effects in the
transverse direction are embedded in
the empirical correlations.

(3) Assumptions used for the solid propellant
are:

a. burning in the inner and outer surfaces
of a stick is axisymmetric;
b. density of the solid is constant;
c. any subsurface heat release occurs very
close to the surface and therefore can
be lumped onto the surface;
d. torsion and rotation are negligible;
e. each stick propellant is locally axi-
symmetric;
f. burning at the end surfaces is uniform;
g. end surfaces are perpendicular to the
axis of the stick; and
h. propellant material behaves as a linear
viscoelastic material in shear and
elastic material in bulk deformation.

B. Overall Structure of the Mathematical
Model

182

Overall Model

External gas phase
- Basic assumptions
- Governing equations (based upon Eulerian coordinate system)
  - Transport equations for flow variables ρ_{ge}, u_{ge}, $(Y_i)_e$, T_{ge}
    - Thermal properties
    - Gas-phase reaction kinetics
    - Transport properties
  - Initial and boundary conditions
- Empirical correlations
  - Propellant burning rate
  - Heat transfer between gases and solid surfaces
  - Viscous drags between gases and solid surfaces

Solid phase
- Governing equations (based upon Lagrangian coordinate fixed to the moving stick)
  - Mass, momentum equations for M and u_s
  - Dynamic structural analysis for grain deformation
    - Constitutive relationship
    - Mechanical properties
  - Energy equation
    - Conduction equation
    - Radiation transport equations
  - Initial and boundary conditions
- Empirical correlations and constants
  - Ignition criterion
  - Thermal properties
  - Burning rate law

Internal gas phase
- Basic assumptions
- Governing equations (based upon Eulerian coordinate fixed to the stick propellant)
  - Transport equations for flow variables ρ_{gi}, V_{gi}, $(Y_i)_i$, T_{gi}
    - Thermal properties
    - Gas-phase reaction kinetics
    - Transport properties
  - Equation of state
  - Initial and boundary conditions
- Empirical correlations
  - Propellant burning rate
  - Convective heat transfer coefficient
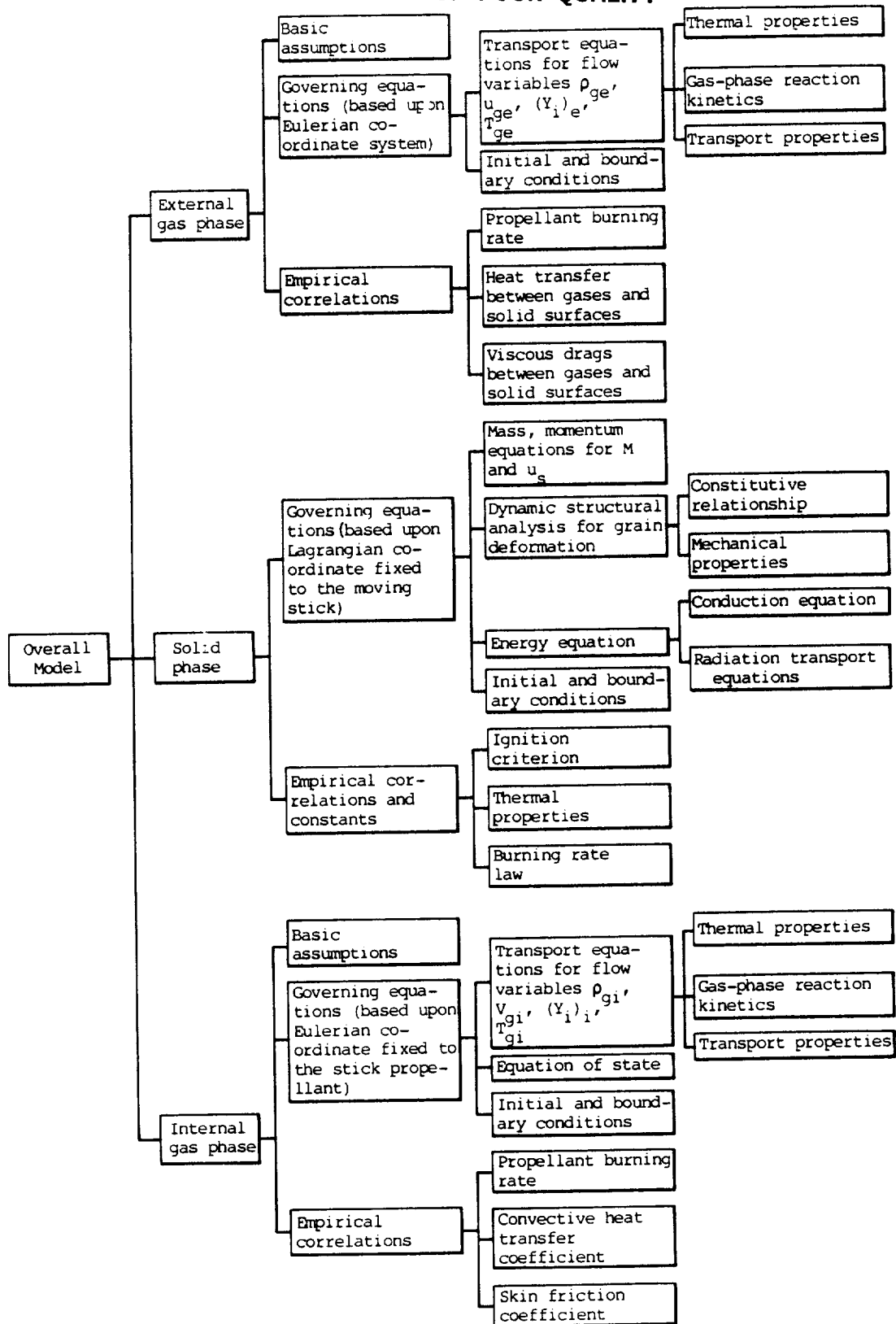 - Skin friction coefficient

Fig.2 Overall Structure of the Theoretical Model

183

In order to give an overview of the structure of the mathematical model, Fig. 2 was constructed. It shows the major components and subcomponents of the formulation for each region in the physical model. To simplify the diagram, the cross-coupling lines between each region are not shown. However, it is important to note that the physicochemical processes in these regions are closely coupled. Mathematical representations of each component and subcomponent are given in the following sections.

C. Governing Equations for the External Gas-Phase Region

The external gas-phase region occupies the whole interstitial space in the cartridge, excluding the shaded region shown in Fig. 3. By using the control volume analysis (reference to Eulerian coordinate), the following governing equations are obtained.
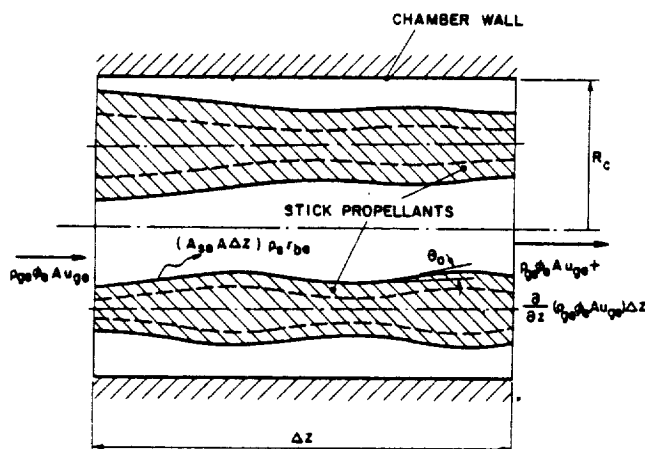

Fig.3 Schematic Diagram Showing the Mass Fluxes Entering and Leaving the External Gas-Phase Region (Unshaded and Multiply Connected Region).

Continuity Equation:

$$\frac{\partial(\rho_{ge}\phi_e)}{\partial t} + \frac{\partial(\rho_{ge}\phi_e u_{ge})}{\partial z} = \frac{2}{R_c^2} \sum_{j=1}^{N} r_{o_j} \rho_s r_{be} \qquad (1)$$

where ϕ_e is the void fraction of the external gas-phase region and is defined as

$$\phi_e = 1 - \frac{1}{R_c^2} \sum_{j=1}^{N} r_{o_j}^2 \qquad (2)$$

Momentum Equation:

$$\frac{\partial(\rho_{ge}\phi_e u_{ge})}{\partial t} + \frac{\partial(\rho_{ge}\phi_e u_{ge}^2)}{\partial z} =$$

$$-\phi_e \frac{\partial P_e}{\partial z} + \frac{\sum_{j=1}^{N} r_{o_j}}{R_c^2} \rho_s r_{be}(u_s - V_{ge}\sin\theta_o)$$

$$-\frac{\sum_{j=1}^{N} r_{o_j}}{R_c^2}(D_{ve} + \underbrace{\frac{\partial}{\partial z}(\phi_e P_e \frac{\partial u_{ge}}{\partial z})}_{small}) - \frac{2\tau_w}{R_c} \qquad (3)$$

where $V_{ge}\sin\theta_o$ is the horizontal component of the gasification velocity normal to the solid propellant surface. The second term in the right-hand side represents the momentum transfer from solid propellant to the external gas-phase region due to burning.

Energy Equation:

$$\frac{\partial(\rho_{ge}\phi_e E_e)}{\partial t} + \frac{\partial(\rho_{ge}u_{ge}\phi_e E_e)}{\partial z} + \frac{\partial(P_e u_{ge}\phi_e)}{\partial z}$$

$$= \frac{2\sum_{j=1}^{N} r_{o_j}}{R_c^2} \rho_s r_{be}\left[\sum_{i=1}^{M} Y_{ie}h_{ie} + \frac{1}{2}\left(\frac{\rho_s r_{be}}{\rho_{ge}}\sin\theta_o + u_s\right)^2\right]$$

$$- \frac{2\sum_{j=1}^{N} r_{o_j}}{R_c^2} \bar{h}_{te}(T_{ge}-T_{se}) - \frac{2\sum_{j=1}^{N} r_{o_j}}{R_c^2} D_{ve}u_s - P_e\frac{\partial\phi_e}{\partial t}$$

$$+ \underbrace{\frac{\partial}{\partial z}(k_{ge}\phi_e\frac{\partial T_{ge}}{\partial z})}_{small} + \underbrace{\frac{4}{3}\frac{\partial}{\partial z}(u_{ge}\phi_e P_e\frac{\partial u_{ge}}{\partial z})}_{small} - 2\dot{Q}_w/R_c \qquad (4)$$

where h_i is the enthalpy of the ith species defined as

$$h_i = \Delta h_{f,i}^o + \int_{T_o}^{T_s} C_{p,i}dT \qquad (5)$$

and E_e is the sum of the internal and kinetic energy of the gas phase in the control volume. The energy transfer due to molecular species diffusion has been neglected because of a high degree of turbulence.

Species Continuity Equation:

$$\frac{\partial(\phi_e\rho_{ge}Y_{ie})}{\partial t} + \frac{\partial(\phi_e\rho_{ge}u_{ge}Y_{ie})}{\partial z} =$$

$$\frac{\partial}{\partial z}(\phi_e\rho_{ge}D\frac{\partial Y_{ie}}{\partial z}) + (\dot{\omega}_i)_e \qquad (6)$$

where the source term $(\dot{\omega}_i)_e$ consists of contributions cause by surface pyrolysis and gas-phase reactions, i.e.

$$(\dot{\omega}_i)_e = (\dot{\omega}_i)_{e,s} + (\dot{\omega}_i)_{e,g} \qquad (7)$$

where the surface pyrolysis part can be expressed as

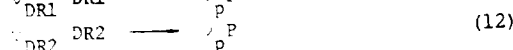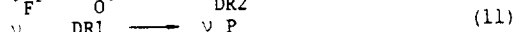$$(\dot{\omega}_i)_{e,s} = r_{be}\rho_s A_{se}Y_{is}^* \qquad (8)$$

where Y_{ie}^* represents the mass fraction of the ith species pyrolyzed from the solid propellant before mixing with ambient gases. Following the flame model proposed by Wu et al. (20) in their study of erosive burning of homogeneous propellants, the solid propellant pyrolyzes into three groups of species:

Solid Propellant ———— Oxidizer-rich gases (O)
                +
                Fuel-rich gases (F)
                +
                First group of species
                with delayed reaction (DR)
$$(9)$$

Under low cross flow conditions, the flame structure adjacent to a burning homogeneous propellant

surface exposed to a large cavity can be assumed to have three stages, as shown in Fig. 4a. This flame structure is based upon the erosive burning study in a rocket motor by Wu et al. (20). In the case of large-caliber guns densely loaded with stick propellants, the void spaces adjacent to burning surfaces are relatively small, and the species pyrolyzed from the surface can be entrained by the high-velocity gases flowing along the axis. The heat release in the final flame generated by the chemical reaction of pyrolyzed species from a specific location occurs at a downstream location, as shown in Fig. 4b. To determine the gas phase reaction rate and heat-release rate, the same chemical reaction mechanism, proposed in Ref. 20, is adopted. This mechanism can be represented by three overall chemical steps:

$$\nu_F F + \nu_O O \longrightarrow \nu_{DR2} DR2 \tag{10}$$

$$\nu_{DR1} DR1 \longrightarrow \nu_p P \tag{11}$$

$$\nu_{DR2} DR2 \longrightarrow \nu_p P \tag{12}$$

Oxidizer-rich gases (O) can be regarded as NO_2 species, fuel-rich gases (F) as a group of aldehydes (CH_2O), and other species generated by surface pyrolysis as one group of delayed reaction species (DR1). Based upon the work of Fifer (21) and Kubota (22), chemical reaction in the Fizz zone is largely due to the reaction involving reduction of NO_2 to NO. After the delay in the dark zone, the reactions in the final flame can be assumed to occur at high activation energies, associated with reactions (11) and (12) to form the final products from DR1 and the second group of delayed reaction species (DR2). In the dark and final flame zones, chemical reactions result in oxidation of CO, and perhaps some H_2 by NO. More detailed discussions of kinetic parameters and mechanisms are given in Ref. 20-22.

It is useful to point out that the chemical reaction mechanism proposed in Ref. 20 can be followed for highly turbulent cross-flow situations. The O and F species pyrolyzed from the solid propellant originate at the same place, and flow together in a torturous path to form DR2 and final products (P). The delayed reaction species of DR1 can also be considered to flow together in the process to form product species P. Gases in the cross-flow can transfer heat to these species and alter the delay times required to form product species P. The stoichiometric coefficients ν_F, ν_O, ν_{DR1}, and ν_{DR2} are therefore functions of propellant ingredients only. The method for calculating these parameters is based upon the original molecular structure of the propellant and is discussed in Ref. 20.

In Ref. 20, the rate of production of species "i" was based upon the chemical reaction rate as well as the eddy-break-up rate (23) controlled by the turbulence intensity and concentration gradient. Turbulence intensity is so high in the gun situation because of base-pad ignition and combustion of propellants that the species diffusion term can be regarded as extremely short. Therefore, the rate of consumption or production of species is determined solely from chemical reaction time.

The rate of chemical reaction of species F, DR1, O, and DR2 are given below in the same form as in Ref. 20.

$$(\dot{\omega}_F)_{e,g} = - A_F \exp(-E_{a,F}/R_u T_{ge})\rho_{ge}^2 (Y_F Y_O)_e/W_F \tag{13}$$

$$(\dot{\omega}_{DR1})_{e,g} = - A_{DR1} \exp(-E_{a,DR1}/R_u T_{ge})\rho_{ge}^2 Y_{DR1_e}^2/W_{DR1} \tag{14}$$

$$(\dot{\omega}_O)_{e,g} = (\dot{\omega}_F)_{e,g} \frac{\nu_O W_O}{\nu_F W_F} \tag{15}$$

$$(\dot{\omega}_{DR2})_{e,g} = - A_{DR2} \exp(-E_{a,DR2}/R_u T_{ge})\rho_{ge}^2 Y_{DR2_e}^2/W_{DR2} - (1 + \nu_O W_O/\nu_F W_F)(\dot{\omega}_F)_{e,g} \tag{16}$$
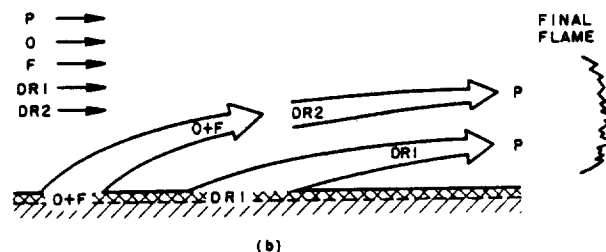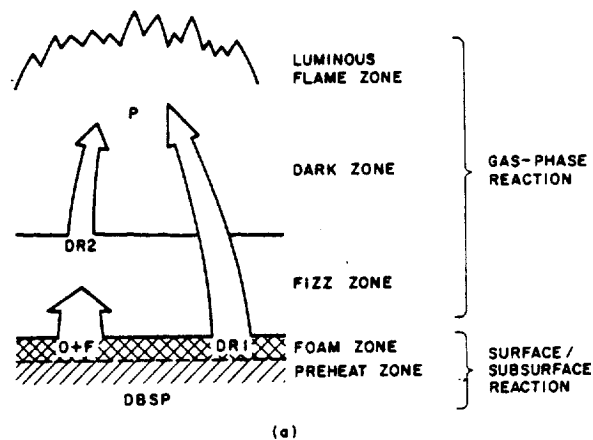

Fig.4 Flame Structure of a Homogeneous Solid Propellant (a) Two-dimensional Structure under Low Cross-Flow Velocities, (b) Distorted Flame under Extremely High Cross-Flow Velocities (Nearly One-Dimensional Structure).

Equation of State:

The Noble-Abel dense gas law is used.

$$P_e(\frac{1}{\rho_{ge}} - b) = RT_{ge} \tag{17}$$

The initial and boundary conditions as well as empirical correlations for the external gas-phase region are given in a later section.

D. Governing Equations for the Stick Propellant

The following governing equations for a representative stick are derived based upon the Lagrangian coordinate.

1) Mass and Momentum Equations:

The instantaneous mass of the representative stick can be calculated from

$$M_s(t) \equiv \int_{-L(t)/2}^{L(t)/2} \rho_s \pi [r_o^2(t,\xi) - r_i^2(t,\xi)] d\xi \quad (18)$$

The instantaneous values of stick propellant length, $L(t)$, and the local inner and outer radii, $r_i(t,\xi)$ and $r_o(t,\xi)$, are determined by integrating the following first order differential equations.

$$\frac{\partial r_i(t,\xi)}{\partial t} = r_{bi}(t,\xi) + V_{sr_i}(t,\xi) \quad (19)$$

$$\frac{\partial r_o(t,\xi)}{\partial t} = -r_{be}(t,\xi) + V_{sr_o}(t,\xi) \quad (20)$$

$$\frac{dL(t)}{dt} = -r_{b_{LB}}(t) - r_{b_{RB}}(t) + V_{SRB}(t) - V_{SLB}(t) \quad (21)$$

where V_{sr_i} and V_{sr_o} represent the radial velocities of the inner and outer surfaces of the stick propellant due to mechanical deformation with respect to the centerline of the stick. V_{SRB} and V_{SLB} represent the rate of mechanical deformation of the right and left boundary surfaces with respect to the geometric center of the stick. The equation of motion is formulated according to the following momentum balance principle.

$$\frac{d(M_s u_s)}{dt} = \Sigma F_\xi + \text{(net rate of momentum flux flowing into the control volume encompassing the stick propellant)}$$
$$(22)$$

which gives (see Fig. 5)

$$\frac{d}{dt}(M_s u_s) = -2\pi \int_{-L/2}^{L/2} [P_i \sin\theta_i - \tau_i \cos\theta_i] r_i d\xi - (F_{pp} + F_{pw})$$
$$+ 2\pi \int_{-L/2}^{L/2} [P_o \sin\theta_o + \tau_o \cos\theta_o] r_o d\xi$$
$$+ 2\pi \rho_s^2 \int_{-L/2}^{L/2} \left[\frac{r_{be}^2 r_o \sin\theta_o}{\rho_{ge}} - \frac{r_{bi}^2 r_i \sin\theta_i}{\rho_{gi}} \right] d\xi$$
$$- \pi \left[(r_o^2 - r_i^2)(P + \frac{\rho_s^2 r_b^2}{\rho_g}) \right]_{\xi = \frac{L}{2}}$$
$$+ \pi \left[(r_o^2 - r_i^2)(P + \frac{\rho_s^2 r_b^2}{\rho_g}) \right]_{\xi = -\frac{L}{2}} \quad (23)$$

where F_{pw} represents the net force acting between the stick propellant and chamber wall, and F_{pp} is the force between adjacent propellants.
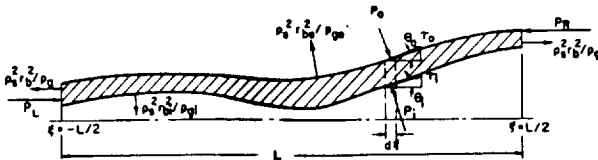

Fig.5 Momentum fluxes and Pressure Forces Acting on the Entire Surface of a Single Perforated Stick Propellant.

2) Transient Heat Conduction Equation:

To determine the instantaneous temperature distribution in the stick propellant, a heat conduction equation must be considered. The equation, which takes into account the subsurface radiation absorption for translucent propellants, has the following form.

$$\rho_s \frac{\partial(C_s T_s)}{\partial t} = \frac{1}{r} \frac{\partial}{\partial r}(r k_s \frac{\partial T_s}{\partial r}) + \frac{\partial}{\partial \xi}(k_s \frac{\partial T_s}{\partial \xi})^{\text{small}}$$
$$+ a \left[(I_r - E_b) + (J_r - E_b) \right] \quad (24)$$

where E_b is the black-body emissive power evaluated as σT_s^4, and "a" represents the flux absorption coefficient of the propellant. This equation is based upon a two-flux model which assumes that the radiation fluxes are dominant in the radial directions (inward and outward). The source terms represent the net rate of energy absorbed due to radiant energy fluxes. The outward and inward radiant fluxes, I_r and J_r, can be determined from the following flux-transport equations.

$$\frac{d(rI_r)}{dr} = -(s+a)rI_r + arE_b + J_r + \frac{1}{2}sr(I_r + J_r) \quad (25)$$

$$\frac{d(rJ_r)}{dr} = (s+a)rJ_r - arE_b + J_r - \frac{1}{2}sr(I_r + J_r) \quad (26)$$

These two equations were used by Gosman and Lockwood.(24)

3) Dynamic Structural Analysis

As a result of the different ignition and flame spreading processes occuring in the internal perforation and external gas-phase regions, a pressure differential exists across the web of a representative stick. A finite element analysis is needed to compute the resulting transient viscoelastic deformation of the stick propellant and to predict the attainment of a critical condition for grain fracture. Regression of the boundary as a result of pyrolysis and burning should also be taken into account. Furthermore, the mechanical properties of the stick propellant must be specified.

The propellant material can be considered as linear viscoelastic in shear and elastic in bulk deformation. This is a commonly accepted practice for solid propellant (25, 26). The elastic bulk behavior is assumed to follow

$$\sigma_i^i = 3K\varepsilon_i^i \quad (27)$$

where K is the bulk modulus. The deviatoric behavior is taken as

$$S_{ij} = \int_o^t G_1(t-t') \frac{\partial e_{ij}(t')}{\partial t'} dt' \quad (28)$$

where the shear relaxation modulus $G_1(t)$ is assumed to be of the form

$$G_1(t) = G_\infty + (G_o - G_\infty)e^{-\beta t} \quad (29)$$

where G_∞ is the long-time shear modulus, G_o is the short-time shear modulus, and β is the decay constant. Since a closed-form solution for the axisymmetric dynamic problem is not possible, a well-established finite element code "HONDO-II" (26) is employed for computations of grain deformation. The code utilizes the principle of virtual work for the solution. It states that at all the points along the path of motion, the differential virtual work, $\delta\pi$, must vanish for all variations δx_k satisfying the imposed displacement boundary conditions (26). $\delta\pi$ is defined as

$$\delta\pi = \int_V \rho\ddot{x}^k \delta x_k \, dv + \int_V \sigma^{km}\delta x_{k,m} \, dv - \int_V \rho f^k \delta x_k \, dv$$
$$- \oint_S \tau^k \delta x_k \, ds \qquad (30)$$

where τ^k is surface traction and σ^{km} is Cauchy stress tensor. The stick propellant is divided into a number of elements over the cross-sectional area of the web. The HONDO-II code uses four node bilinear isoparametric elements. The basic equation of motion, viz., the minimization of virtual work, is then considered for each of the nodes in the stick propellant. Thus, the equation of motion for a node becomes

$$\delta\pi = \sum_{n=1}^{N} \left\{ \int_{V_n} \rho\ddot{x}^k \theta_{\sim k}^\ell \, dv + \int_{V_n} \sigma^{km}\theta_{\sim k,m}^\ell \, dv \right.$$
$$\left. - \int_{V_n} \rho f^k \theta_{\sim k}^\ell dv - \oint_{S_n} \tau^k \theta_{\sim k}^\ell ds \right\} = 0 \qquad (31)$$

where $\theta_{\sim k}^\ell = [\phi_k^1, \phi_k^2, \phi_k^3, \phi_k^4] \Big|_{V_n}$

and ϕ_k^ℓ are the bilinear interpolation functions. In Eq. (31), N is the total number of elements surrounding the node in question. The calculations are carried out on an element-by-element process to get the final equations of motion. The time integration of these equations gives the positions of nodes at the new time step. A central difference method is used for time integration in the HONDO-II code.

E. Governing Equations for the Internal Gas-Phase Region

Conservation equations for the control volume in the perforation of a stick propellant are similar to those given in Ref. 15.

Continuity Equation:

$$\frac{\partial(\rho_{gi}A_p)}{\partial t} + \frac{\partial(\rho_{gi}A_p V_{gi})}{\partial \xi} = r_{bi}\rho_s P_b \qquad (32)$$

where ξ is the distance measured from the center of the stick, and V_{gi} is the velocity of the gas relative to the velocity of the stick propellant. V_{gi} is related to the absolute velocity u_{gi} by

$$V_{gi} = u_{gi} - u_s \qquad (33)$$

Momentum Conservation Equation:

$$\frac{\partial(\rho_{gi}V_{gi}A_p)}{\partial t} + \frac{\partial(\rho_{gi}V_{gi}^2 A_p)}{\partial \xi} = -A_p \frac{\partial P_i}{\partial \xi} - D_{Vi}P_b$$
$$+ \underbrace{\frac{\partial(\tau_{\xi\xi}A_p)}{\partial \xi}}_{small} + \underbrace{\frac{\rho_s^2 r_{bi}^2}{\rho_{gi}}\frac{\partial A_p}{\partial \xi}}_{small} \qquad (34)$$

Energy Conservation Equation:

The energy conservation equation written for the stored total energy (internal and kinetic) per unit mass, E_{gi}, is

$$\frac{\partial(\rho_{gi}A_p E_{gi})}{\partial t} + \frac{\partial(\rho_{gi}A_p V_{gi}E_{gi})}{\partial \xi} = \frac{\partial}{\partial \xi}\underbrace{\left(k_{gi}A_p \frac{\partial T_{gi}}{\partial \xi}\right)}_{small}$$
$$- \frac{\partial(A_p P_i V_{gi})}{\partial \xi} - \frac{\partial}{\partial \xi}(\tau_{\xi\xi}A_p V_{gi}) - \bar{h}_{ti}(T_{gi}-T_{si})P_b$$
$$+ \rho_s r_{bi}P_b \left[\sum_{j=1}^{M} Y_j^* h_j(T_{si})\right]_i \qquad (35)$$

Species Continuity Equation:

The species continuity equation for the internal gas-phase is similar to that for the external gas-phase, with the void fraction taken as one and the absolute velocity replaced by the relative velocity.

$$\frac{\partial[\rho_{gi}(Y_i)_i]}{\partial t} + \frac{\partial[\rho_{gi}V_{gi}(Y_i)_i]}{\partial \xi}$$
$$= \frac{\partial}{\partial \xi}\underbrace{\left[\rho_{gi}D\frac{\partial(Y_i)_i}{\partial \xi}\right]}_{small} + (\dot{\omega}_i)_i \qquad (36)$$

where the source term $(\dot{\omega}_i)_i$, similar to $(\dot{\omega}_i)_e$ in Eq. (7), consists of contributions due to surface pyrolysis and gas-phase reactions. The flame model for the internal gas-phase region is the same as that given earlier for the external gas-phase region.

F. Heat Losses to the Walls of the Combustion Chamber

In order to consider heat losses from the combustion zone to the cartridge chamber, the gun tube, and the projectile, temperature profiles in these metal components are required. For a test rig with a blowout diphragm and short barrel, the transient ignition and combustion phenomena occur in an extremely short time interval and the heat loss to the surrounding walls can be considered negligible. However, if the simulation is made for the full ballistic cycle occurring in a long gun barrel, the loss to the walls must be considered. The heat conduction to the gun tube can be given as

$$\rho_w \frac{\partial(C_w T_w)}{\partial t} = \frac{\partial}{\partial z}\left(k_w \frac{\partial T_w}{\partial z}\right) + \frac{1}{r}\frac{\partial}{\partial r}\left(k_w r \frac{\partial T_w}{\partial r}\right) \qquad (37)$$

The transient heat conduction equation for the wall on the breech end will follow the one-dimensional form:

$$\rho_w \frac{\partial(C_w T_w)}{\partial t} = \frac{\partial}{\partial z}\left(k_w \frac{\partial T_w}{\partial z}\right) \qquad (38)$$

The equation for the projectile is:

$$\rho_w \frac{D(C_w T_w)}{Dt} = \frac{\partial}{\partial z}\left(k_w \frac{\partial T_w}{\partial z}\right) \qquad (39)$$

The solution of these equations are coupled to the external gas-phase region through the boundary conditions on the wall surfaces.

G. Initial and Boundary Conditions

For each of the above governing equations, there is a set of boundary and/or initial conditions required to complete the formulation. The initial conditions can be specified readily, since the gas and stick propellant velocities are zero and the pressure and temperature of gas in the cartridge is at room conditions. The stick propellant charge with known geometry and its surrounding chamber are also at room temperature. Since the amount of air in the initial loading of the cartridge is extremely small in comparison with the gases generated from combustion, it can be treated as any one of the five species discussed above. In view of the fact that air contains oxygen, it is treated as oxidizer-rich gas (O).

A number of important boundary conditions are given in the following.

1). Boundary Conditions for the stick Propellant

The boundary condition for Eq.(24) at outer surface of the stick propellant can be written as

$$k_s \frac{\partial T_s}{\partial r}\bigg|_{r_o^-} = \bar{h}_c(T_{ge}-T_{se}) + \rho_s r_{be}(Q_s)_{chem} + (\dot{q}_{rad})_e$$
$$+ \rho_s r_{be}(C_s-C_{pge})T_{se} + (\dot{Q}_{CPIP})_e \qquad (40)$$

where $(\dot{Q}_{CPIP})_e$ represents the rate of energy input due the deposit of condensed phase igniter products onto the external surface and $(\dot{q}_{rad})_e$ the net radiative heat flux to the surface can be expressed as

$$(\dot{q}_{rad})_e = J_r\bigg|_{r=r_o^+} + \varepsilon_s I_r\bigg|_{r=r_o^-} - \varepsilon_s E_b T_{se} \qquad (41)$$

Similarly, the boundary condition for the inner surface of the stick propellant can be written as

$$-k_s \frac{\partial T_s}{\partial r}\bigg|_{r_i^+} = \bar{h}_c(T_{gi}-T_{si}) + \rho_s r_{bi}(Q_s)_{chem} + (\dot{q}_{rad})_i$$
$$+ \rho_s r_{bi}(C_s-C_{pgi})T_{si} + (\dot{Q}_{CPIP})_i \qquad (42)$$

where

$$(\dot{q}_{rad})_i = I_r\bigg|_{r=r_i^-} + \varepsilon_s J_r\bigg|_{r=r_i^+} - \varepsilon_s E_b T_{si} \qquad (43)$$

The pressure distributions along the internal perforation and external interstitial regions solved from the gas-phase equations are used as boundary conditions · for the solid-phase dynamic structural analysis.

2). Boundary Conditions for the External and Internal Gas-Phase Regions

For simplicity in expressing the boundary treatments, only one representative group of stick propellants is considered, then each stick propellant has the identical instantaneous velocity and length. Therefore, the governing equations for the left lumped-parameter region (see Fig. 6) or called left control volume (LCV) can be readily derived and written as follows.

Mass balance:

$$\frac{d\rho_{g_{LCV}}}{dt} = -\rho_{g_{LCV}} \frac{(u_s+r_{b_{LB}})}{z_L}$$
$$+ \frac{\left[1-\psi_s - \frac{\rho_{g_{LCV}}}{\rho_{ign}}\phi_{LCV}\right]\dot{m}_{ign}-\dot{m}_{oute}-\dot{m}_{outi}}{\pi R_c^2 \phi_{LCV} z_L} \qquad (44)$$

where z_L is the length of the left lumped-parameter region and can be calculated from

$$z_L = z_{L_o} + \int_0^t (u_s+r_{b_{LB}})dt + \int_0^t \frac{\dot{m}_{ign}}{\pi R_c^2 \rho_{ign}} dt \qquad (45)$$

and

$$\dot{m}_{oute} = \phi_e \pi R_c^2 \rho_{pg}[u_{ge} - (u_s+r_{b_{LB}})]\bigg|_{\xi=-L/2} \qquad (46)$$

$$\dot{m}_{outi} = N\pi r_i^2 \rho_{gi}[u_{gi}-(u_s+r_{b_{LB}})]\bigg|_{\xi=-L/2} \qquad (47)$$

Momentum balance:

$$\frac{du_{g_{LCV}}}{dt} = \frac{1}{M_{g_{LCV}}}\left\{ u_{g_{LCV}}[\dot{m}_{oute}+\dot{m}_{outi} - (1-\psi_s)\dot{m}_{ign}] \right.$$
$$+ \frac{(\dot{m}_{ign})^2}{\rho_{g_{LCV}}\pi R_c^2 \phi_{LCV}} - (\dot{m}_{oute}u_{ge})_{LB}$$
$$- (\dot{m}_{outi}u_{gi})_{LB} - N\pi(r_o^2-r_i^2)\bigg|_{\xi=-\frac{L}{2}}$$
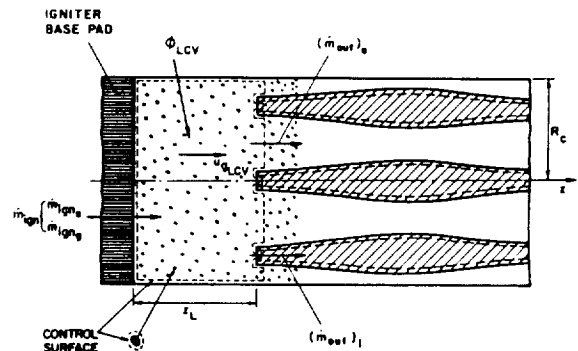$$\left. \cdot (\rho_s^2 r_{b_{LB}}/\rho_{g_{LCV}}) - 2\pi R_c z_L \tau_w \right\} \qquad (48)$$

Fig.6 Control Volume Considered for Deriving Governing Equations in the Left Lumped-Parameter Region.

Energy balance:

$$
\frac{dT_{g_{LCV}}}{dt} = \frac{1}{(C_v M_g)_{LCV}} \left\{ C_{v_{LCV}} T_{g_{LCV}} [\dot{m}_{oute} + \dot{m}_{outi}] \right.
$$
$$
- (1-\psi_s)\dot{m}_{ign}] + (1-\psi_s)\dot{m}_{ign} C_{P_{LCV}} T_{f_{ign}}
$$
$$
- \dot{m}_{oute}(C_{P_{LB}} T_{ge_{LB}} + u_{ge_{LB}}^2/2)
$$
$$
- \dot{m}_{outi}(C_{P_{LB}} T_{gi_{LB}} + u_{gi_{LB}}^2/2) - \dot{Q}_w 2\pi R_c z_L
$$
$$
\left. - N\pi(r_o - r_i^2)\Big|_{\zeta=-L/2} \dot{\rho}_s r_{b_{LB}} C_{Pg_{LCV}} T_f \right\} \quad (49)
$$

Equation of state:

$$
P_{LCV} = \frac{RT_{g_{LCV}}}{\dfrac{1}{\rho_{g_{LCV}}} - b} \quad (50)
$$

The void fraction in the left lumped-parameter region, ϕ_{LCV}, can be evaluated from the continuity equation of the condensed-phase products of the igniter which is given as follows.

$$
\frac{d\phi_{LCV}}{dt} = \frac{1}{z_L} \left\{ (1-\phi_{LCV}) \left[u_s + r_{b_{LB}} + \frac{\dot{m}_{ign}}{\pi R_c^2 \rho_{ign}} \right] - \right.
$$
$$
\frac{\dot{m}_{ign}\psi_s - (1-\phi_{LCV})[\rho_{ign_s} A\phi_e u_{ge_{LB}} + \rho_{ign_s} N\pi r_i^2 u_{gi_{LB}}]}{\pi R_c^2 \rho_{ign_s}} \right\}
$$

$$(51)$$

The boundary values of velocity, density, pressure, and temperature on the left hand side of both internal and external gas-phase regions can be solved from a number of relationships coupled with Eqs. (44) and (48)-(51). Depending upon the flow directions at left boundary of the internal and external regions, three different cases are identified. In the first case, the flow velocities at stick perforation and the interstitial regions are both in the positive z direction, it can be assumed that the pressure at LCV is equal to those at the left boundary of the stick perforation and the external gas-phase region. Also, the stagnation temperature of the gas in LCV can be assumed to be the same as those on the left boundary. One compatibility relation along the characteristic line in each gas-phase region is used together with the aforementioned equations for solving the flow properties in the LCV and the left boundary.

In the second case, the flow velocity at the left opening if the stick perforation is negative, but the bulk velocity at left boundary of the interstitial void region is still positive. In this case, one additional compatibility relationship can be used for the stick perforation region. Only the pressure at the opening of the stick perforation is considered to be equal to that in the LCV. The treatment for the left boundary of the interstitial

region remains the same as that in the first case.

In the third case, the flow velocities at the left boundary of both the perforation region and the interstitial regions are negative. Therefore, two additional compatibility relationships are available. In this case, both the internal and external gas-phase boundaries are treated in a similar fashion as that for the internal perforation region in the second case.

The void region between the right end of the stick propellants and the projectile base is a lumped-parameter region, which could contain either a base pad with powders of igniter material or an ullage space. In the case of base pad, a set of equations similar to Eqs. (44)-(51) are derived. The right control volume (RCV) is considered to move with the projectile and the left surface of RCV coincides with the right boundary of the stick bundle. A detailed discussion on the compatibility relation mentioned above is given in Ref. 27-28.

H. Empirical Correlations and Constants

Several empirical correlations are used in the model. For the internal gas-phase region, these comprise of the correlations for the burning rate law including erosive burning effect, the convective heat-transfer coefficients, and viscous drag coefficient. The latter two correlations are same as those used in Ref. 15. New erosive burning correlation being developed by authors and coworkers in parallel to this study will be used. For the external gas-phase region, correlations for the convective heat-transfer coefficient, and viscous drag coefficient between the gas-phase and solid surfaces are needed. These correlations are similar to those for the internal perforation region except the fact that they are based on a hydraulic diameter D_H defined as

$$
D_H = \frac{2(R_c^2 - Nr_o^2)}{R_c + Nr_o} \quad (52)
$$

The burning rate law for the external region will be the same as that for the internal perforation region.

For the stick propellants, correlations for F_{pp} and F_{pw}, the ignition criterion, and mechanical and thermal properties are needed. At the present time, not all of this information is available; especially F_{pp} and F_{pw} need to be characterized.

4. Summary of Differences Between the Present and Conventional Formulation

In order to bring out the major differences between the present formulation and the conventional interior ballistic predictive models (4), a summary table is given below.

As summarized by Robbins and Einstein (29), there are differences between the measured and calculated pressures from the NOVA code or its extensions for long unslotted stick propellants. Also, the measured muzzle velocities are higher than those calculated for slotted stick propellants. A number of improvements and considerations suggested in the workshop (29) are incorporated in the present model.

189

Table I

Differences Between the Present Formulation and the
Conventional Interior Ballistic Formulation

Subject under Consideration	Present Formulation	Convential formulation (4)
Typical grain configuration	* Simulation of a number of typical full-length grains in a bundle of stick propellants. * Each stick is modeled as separate tube with deformable and combustible walls.	* Simulation of an average grain in a spatial location along a packed bed of granular propellants. * Each bundle is modeled as a continuum characterized by the velocity and stress in the sticks.
Averaging of flow properties	* The external flow properties are averaged over the cross-sectional flow area of interstitial voids, while the internal flow properties are averaged over the flow area of each stick propellant.	* Flow properties in both external and internal regions are averaged over their respective flow areas.
Grain deformation and fracture	* Simulated by the unbalanced pressure forces between the internal perforation and external interstitial void region. * Linear viscoelastic constitutive law is used. * Employs dynamic finite-element structure mechanics computational code.	* The process of grain deformation and fracture are not addressed, except the longitudinal stresses are considered in the solid-phase momentum equation. * Linear elastic constitutive law is used. * Employs a steady-state relationship between stresses (radial and hoop) and pressures (internal and external)
Grain displacement and acceleration	* The kinematics of the full-length grain is determined from the summation of all forces exerted on the grain.	* The bulk properties of the grains are determined from local momentum balance.
Radiative heat transfer	* Subsurface radiation penetration is allowed and treated by a two-flux model.	* No subsurface radiation penetration is considered.
Type of formulation and frame of reference	* Kinematics and grain deformation are formulated by following the stick (Lagrangian approach) while the gas-phase properties for internal and external regions are determined from a fixed frame of reference (Eulerian approach).	* Both the gas-phase and solid-phase properties are all determined from the conservation equations formulated based upon a fixed frame of reference (Eulerian approach).
Species distribution and location of heat release	* Five groups of species are considered. * Heat release does not have to occur at the site of pyrolysis.	* Gas phase is made of combustion products from ignition and propellant. * Heat release occurs locally at the site of pyrolysis.

190

Nomenclature

Letter Symbols

a — flux model absorption coefficient, m^{-1}

A — cross-sectional area of the gun barrel, m^2

A_i — preexponential factor of the ith species, $m^3/kmol\text{-}s$

A_p — cross-sectional area of the perforation, m^2

A_s — specific area of the external surfaces of the stick propellant, m^{-1}

b — covolume of the Noble-Abel equation of state, m^3/kg

C_p — constant pressure specific heat, J/kg-K

C_s — specific heat of stick propellant, J/kg-K

C_v — constant volume specific heat, J/kg-K

DR1 — group of species pyrolyzed from propellant surface having delayed reactions

DR2 — delayed reaction species generated from O and F species

D_v — viscous drag force per unit area, N/m^2

$\mathcal{D}$ — binary diffusion coefficient, m^2/s

e_{ij} — deviatoric strain

E — total stored energy (internal plus kinetic) per unit mass, J/kg

E_a — activation energy, J/kmol

E_b — black-body emissive power, $= \sigma T^4$, $J/m^2\text{-}s$

f^k — body force per unit volume in k^{th} direction, N/m^3

F — fuel rich species pyrolyzed from propellant

F_ξ — external force exerted on the solid propellant in the axial direction, N

h — specific enthalpy, J/kg

$\bar{h}_c$ — convective heat-transfer coefficient, $W/m^2\text{-}K$

h_j — specific enthalpy of the jth species, J/kg

h_{t_0} — total heat-transfer coefficient, $W/m^2\text{-}K$

$\Delta h_{f,i}^0$ — standard enthalpy of formation of the ith species, J/kg

I_r — outward radiation flux in the positive radial direction, W/m^2

J_r — inward radiation flux in the negative radial direction, W/m^2

k — thermal conductivity, W/m-K

K — bulk modulus of the propellant material, N/m^2

M_g — total mass of gas in control volume, kg

M_s — instantaneous total mass of a single stick propellant, kg

O — oxidizer species pyrolyzed from propellant

P — pressure, N/m^2

P — final product species

P_b — perimeter of the internal perforation, m

$\dot{q}_{rad}$ — radiative heat flux per unit time absorbed by the solid propellant surface, W/m^2

$Q_{s_{chem}}$ — surface heat release due to pyrolysis, J/kg

$\dot{Q}_w$ — rate of heat loss to the tube wall, W/m^2

r_b — propellant burning rate, m/s

r_i — inner radius of the perforation, m

r_o — outer radius of the stick propellant, m

R — gas constant, J/kg-K

R_c — radius of the combustion chamber, m

R_u — universal gas constant, J/kmol-K

s — flux-model scattering coefficient, 1/m

S_{ij} — deviatoric stress tensor, N/m^2

S — surface, m^2

t — time, s

T — temperature, K

T_f — adiabatic flame temperature of the solid propellant, K

u — absolute velocity, m/s

V_g — gas velocity relative to the solid propellant, m/s

V — volume, m^3

W_i — molecular weight of the ith species, kg/kmol

x_k — coordinate axis in k^{th} direction, m

$\ddot{x}_k$ — acceleration in k^{th} direction, m/s^2

$\delta x_{k,m}$ — deformation gradient tensor

Y_i — mass fraction of ith species, i could represent F, O, DR1, DR2, or P

z — axial coordinate in Eulerian coordinate system, m

Greek Symbols

ε_{kk} — dilatory strain

ε_s — surface emissivity of solid propellant

θ_i — angle measured ccw from axis to the tangent to the inner surface of the stick propellant, rad

θ_o — angle measured ccw from axis to the tangent to the outer surface of the stick propellant, rad

μ — dynamic viscosity of the gas, $N\text{-}s/m^2$

ν_i — number of kmoles of ith species

ξ — Lagrangian axial coordinate, m

π — virtual work, J

ρ — density, kg/m^3

σ_{km} — Stefan-Boltzmann constant, $W/m^2\text{-}K^4$

σ — stress tensor, N/m^2

τ — viscous shear stress, N/m^2

τ^k — surface traction in k^{th} direction, N/m^2

τ_w — tube wall shear stress, N/m^2

$\tau_{\xi\xi}$ — normal viscous stress, N/m^2

ψ_s — mass fraction of combustion product in the condensed phase from the igniter

$\dot{\omega}_i$ — rate of production of ith species, $kg/m^3\text{-}s$

Subscripts

e — external interstitial region

g — gas-phase, internal or external region

i — internal perforation region

ign   igniter
LB   left boundary of the stick propellant bundle
LCV   left lumped-parameter region in the cartridge
RB   right boundary of the stick propellant bundle
s   solid propellant or surface

Acknowledgements

REFERENCES

1. Robbins, F. W., Kudzal, J. A., McWilliams, J. A., and Gough, P.S., "Experimental Determination of Stick Charge Flow Resistance, " Proceedings of the 17th JANNAF Combustion Meeting, CPIA Publication 329, Vol.II, 1980, pp. 97-118.

2. Robbins, F. W., and Horst, A. W., "A Simple Theoretical Analysis and Experimental Investigation of Burning Processes for Stick Propellant," Proceedings of the 18th JANNAF Combustion Meeting, CPIA Publication 347, Vol. II, 1981, pp. 25-34.

3. Minor, T. C., "Ignition Phenomena in Combustible-Cased Stick Propellant Charges," Proceedings of the 19th JANNAF Combustion Meeting, CPIA Publication 366, Vol. I, 1982, pp. 555-567.

4. Gough, P. S., "Continuum Modeling of Stick Charge Combustion," Proceedings of the 20th JANNAF Combustion Meeting, CPIA Publication 383, Vol. I, 1983, pp.351-363.

5. Gough, P. S., "Modeling of Rigidized Gun Propelling Charges," Contract Report ARBRL-CR-00518, 1983.

6. Horst, A. W., "A Comparison of Barrel-Heating Processes for Granular and Stick Propellant Charges," Memorandum Report ARBRL-MR-03193, 1983.

7. Horst, A. W., Robbins, F. W., and Gough, P. S., "Multi-Dimensional, Multiphase Flow Analysis of Flamespreading in a Stick Propellant Charge," Proceedings of the 20th JANNAF Combustion Meeting, CPIA Publication 383, Vol. I, 1983, pp. 365-386.

8. Keller, G. E., "The Competition Between Tube Heating and Muzzle Velocitiy in Stick Propellant Gun Charges," Proceedings of the 20th JANNAF Combustion Meeting, CPIA Publication 383, Vol. I, 1983, pp. 387-391.

9. Chiu, D., Grabovsky, A., and Downs, D., "Closed Vessel Combustion Studies of Stick Propellants," Proceedings of the 20th Combustion Meeting, CPIA Publication 383, Vol. I, 1983, pp.393-402.

10. Robbins, F. W., "Continued Study of Stick Propellant Combustion Processes," Proceedings of the 19th JANNAF Combustion Meeting, CPIA Publication 366, Vol. I, 1982, pp. 443-459.

11. Gough, P. S., "The Flow of a Compressible Gas Through an Aggregate of Mobile, Reacting Particles," Ph. D. Thesis, McGill University, 1974.

12. Gough, P. S., "The NOVA Code - A User's Manual," Final Report, Task I, Contract N00174-79-C-0082, PGA-TR-79-5.

13. Gough, P. S., "Two-Dimensional, Two-Phase Modeling of Multi-Increment Bagged Artillery Charges," Contract Report ARBRL-CR-00503.

14. Faeth, G. M., "Evaporation and Combustion of Sprays," Progress in Energy and Combustion Science, Vol. 9, 1983, pp. 1-76.

15. Peretz, A., Kuo, K. K., Caveny, L. H., and Summerfield, M., "The Starting Transient of Solid-Propellant Rocket Motors With High Internal Gas Velocities," AIAA Paper No. 72-1119, Nov.-Dec. 1972.

16. Kuo, K. K., "A Summary of the JANNAF Workshop on Theoretical Modeling and Experimental Measurements of the Combustion and Fluid Processes in Gun Propellant Charges," Proceedings of the 13th JANNAF Combustion Meeting, CPIA publication 281, Vol. I, 1976, pp. 213-233.

17. East, J. L., Jr., "Ignition and Flamespreading Phenomena in Granular Propellant Gun Charges," in Interior Ballistics of Guns (H. Krier and M. Summerfield Eds.), AIAA Progress in Astronautics and Aeronautics, Vol. 66, 1979.

18. Krier, H., and Summerfield, M., Eds., "Interior Ballistics of Guns," AIAA Progress in Astronautics and Aeronautics, Vol. 66, 1979.

19. Scheidegger, A. E., "The Physics of Flow Through Porous Media," University of Toronto Press, 1974, Ch. 6, pp. 123-151.

20. Wu, X., Kumar, M., and Kuo, K. K., "A Comprehensive Erosive-burning Model for Double-Base Propellants in Strong Turbulent Shear Flow," Combustion and Flame, Vol. 53, 1983, pp. 49-60.

21. Fifer, R. A., "Chemistry of Nitrate Ester and Nitramine Propellants," in Fundamentals of Solid Propellant Combustion (K. K. Kuo and M. Summerfield Eds.), AIAA Progress Series in Astronautics and Aeronautics, Vol. 90, 1984.

22. Kubota, N., "Survey of Rocket Propellants and Their Combustion Characteristics," in Fundamentals of Solid Propellant Combustion (K. K. Kuo and M. Summerfield Eds.), AIAA Progress Series in Astronautics and Aeronautics, Vol. 90, 1984.

23. Spalding, D. B., "Mixing and Chemical Reactions in Steady Confined Turbulent Flames," Thirteenth Symposium (International) on Combustion, The Combustion Institute, 1965, pp. 1405-1411.

24. COSMAN, A. D., AND LOCKWOOD, F. C., "Incorporation of a Flux Model for Radiation into a Finite-Difference Procedure for Furnace Calculations," Fourteenth (International) Symposium on Combustion, The Combustion Institute, 1973, pp. 661-671.

25. Chang, T. Y., Chang. J. P., Kumar, M., and Kuo, K. K., "Structural Interaction In a Viscoelastic Material," Research in Nonlinear Structural and Solid Mechanics, NASA Conference Publication 2147, 1980, pp. 67-90.

26. Key, S. W., Beisinger, Z. E., and Krieg, R. D., "HONDO II A Finite Element Computer Program for the Large Deformation Dynamics Response of Axisymmetric Solids," Sandia Report SAND78-0422, 1978.

27. Koo, J. H., and Kuo, K. K., "Transient Combustion in Granular Propellant Beds. Part I : Theoretical Modeling and numerical Solution of Transient Combustion Processes in Mobile Granular Propellant Beds," Final Report, U. S. Army Research Office , Contract Number DAAG 29-74-G-0116, 1977.

28. Chen, D. Y., Yang, V., and Kuo. K. K., "Boundary Condition Specification for Mobile

Granular Propellant Bed Combustion Processes,"
AIAA Journal, vol. 19, Number 11, 1981, pp.
1429-1437.

29. Robbins, F., W., and Einstein, S. I., "Workshop
Report: Stick Propellant Combustion Processes,"
to be presented at the 21st JANNAF Combustion
Meeting, Applied Physics Laboratory, Laurel,
MD, Oct. 1-5, 1984.

Editor's Narrative:

Round-Table Discussion: Propulsion Applications of Mixing and Demixing Processes of Multiphase Flows

Several points were made either explicitly or implicitly in the presentations and discussions on the second day concerning mixing processes in multiphase systems and the modeling of these systems. First, there are situations where transport in turbulent flows can be in a direction other than along the gradient of the property being transported. This comes about through coupling of density inhomogenieties with pressure gradients, the former being a consequence of the large temperature differences in combustion environments. Hence, in turbulent flames, some transport processes are "counter gradient" or more correctly, "non-gradient" in nature. Errors due to neglect of these processes are not understood, but could possibly be significant in some combustion systems. Modelers are in the process of learning to incorporate these ideas into practical codes.

Second, the weakest element in modeling of turbulent multiphase flows is probably the turbulence modeling itself. The treatment of the coupling between the turbulence and the non-continuously distributed dispersed phase is also a critical area and includes the question of whether, for numerical purposes, to treat the dispersed particulate (or droplet) phase as a continuum or as an assembly of separate particles.
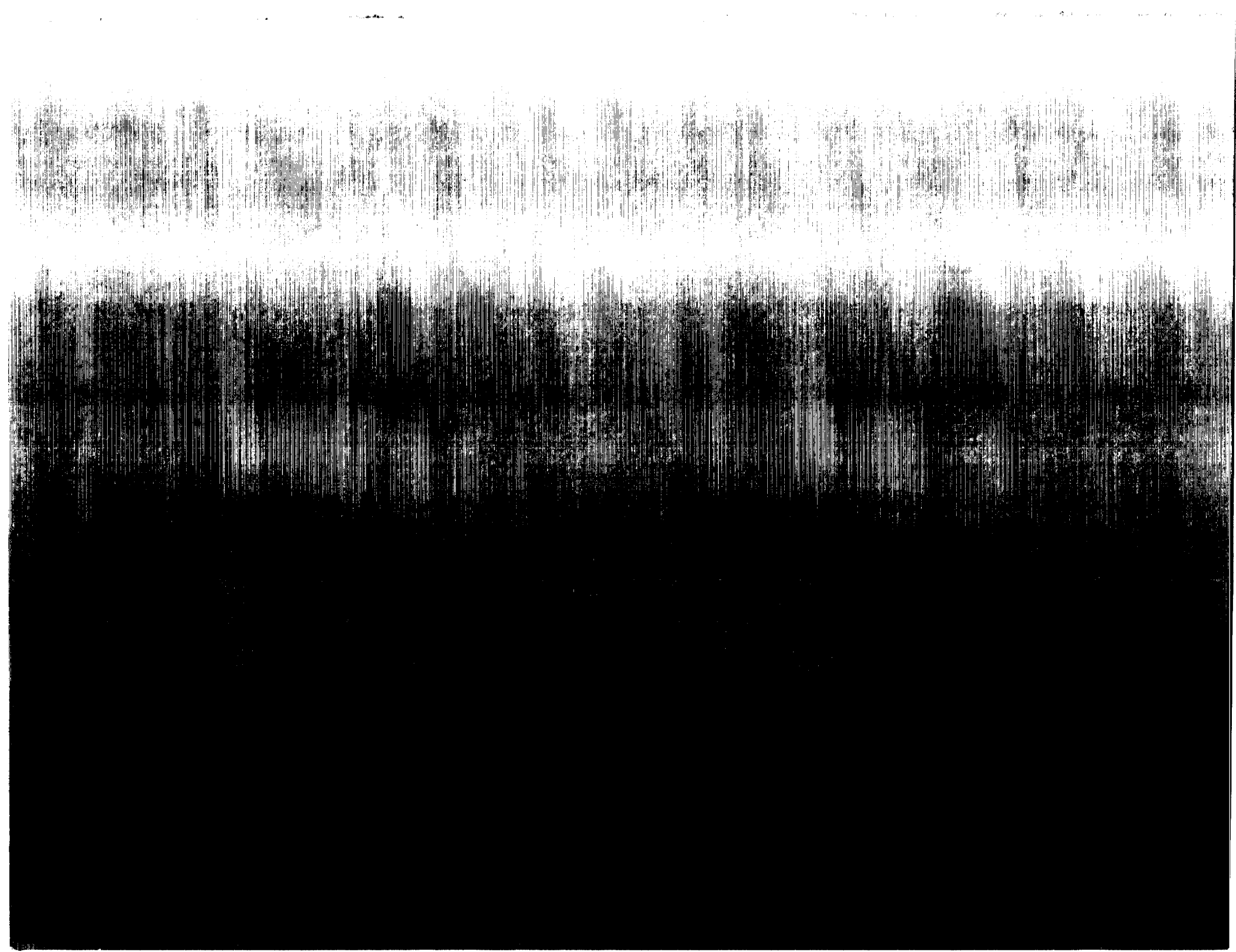
Third, it is possible to treat a very complex problem in great detail by using appropriate levels of approximation and by coupling separate regions together which are best treated with different models or with different levels of approximation.

Fourth, while continuum approaches to multiphase flow calculations are not particularly illuminating in revealing details of the physical processes at work (due to the necessity of averaging quantities before solving the governing equations), there are cases where they can provide useful results for a given problem. The two-fluid approach works best where the dispersed particulate phase is monodisperse, and where the flows are non-reacting.

Sixth, advantages and disadvantages of Favre averaging approaches were discussed. An advantage is that the conservation equations for variable density with Favre averaging are much like the standard constant density equations. Disadvantages are that there is some difficulty in obtaining molecular terms and computed and measured quantities are more difficult to compare.

Finally, physical situations for which multiphase flow models are appropriate generally contain a very broad range of length and time scales within the same problem. This means that when computational approaches to these problems are used, some levels of approximation will need to be made in order to deal with these large ranges of scale. The point in the analysis at which approximation is made is a key difference between a two-fluid model and an Eulerian-Lagrangian model of a dispersed particulate phase in a fluid phase.

1. REPORT NO. NASA CP-3006	2. GOVERNMENT ACCESSION NO.	3. RECIPIENT'S CATALOG NO.
4. TITLE AND SUBTITLE Mixing and Demixing Processes in Multiphase Flows With Application to Propulsion Systems		5. REPORT DATE July 1988
		6. PERFORMING ORGANIZATION CODE
7. AUTHOR(S) Edited by Rand Decker* and Charles F. Schafer		8. PERFORMING ORGANIZATION REPORT #
9. PERFORMING ORGANIZATION NAME AND ADDRESS George C. Marshall Space Flight Center Marshall Space Flight Center, Alabama 35812		10. WORK UNIT NO. M-591
		11. CONTRACT OR GRANT NO.
12. SPONSORING AGENCY NAME AND ADDRESS National Aeronautics and Space Administration Washington, D.C. 20546		13. TYPE OF REPORT & PERIOD COVERED Conference Publication
		14. SPONSORING AGENCY CODE

15. SUPPLEMENTARY NOTES

Prepared by Structures and Dynamics Laboratory, Science and Engineering Directorate.

*NRC Associate

16. ABSTRACT

A workshop on transport processes in multiphase flows was held at the Marshall Space Flight Center on February 25 and 26, 1988. This document provides the program, abstracts, and text of the presentations made at this workshop. In addition, the content of two open discussion sessions are presented in narrative form. The objective of the workshop was to enhance our understanding of mass, momentum, and energy transport processes in laminar and turbulent multiphase shear flows in combustion and propulsion environments.

17. KEY WORDS Multiphase Flow, Transport Processes, Turbulence, Continuum Models, Lagrangian-Eulerian Models, Drag, Lift, Particle Migration	18. DISTRIBUTION STATEMENT Unclassified — Unlimited Subject Category: 34		
19. SECURITY CLASSIF. (of this report) Unclassified	20. SECURITY CLASSIF. (of this page) Unclassified	21. NO. OF PAGES 202	22. PRICE A10